

Closed-loop Temperature Control of Friction Stir Welding

by

Raymond Peter Pothier, BEng. Mechatronics

Submitted in compliance with the requirements for the
Magister in Ingeniaria (Mechatronics Engineering) Degree
to be awarded at the Nelson Mandela Metropolitan University

April 2015

Department of Mechatronics
Engineering, Built Environment and Information Technology
eNtsa

Supervisor: Prof. D.G. Hattingh
Co-Supervisor: Prof. T.I. van Niekerk

Copyright Statement

The copy of this dissertation has been supplied on the condition that anyone who consults it is understood to recognise that its copyright rests with the Nelson Mandela Metropolitan University and that no extracts from the dissertation or information derived from it may be published without the author's prior consent.

I, Raymond Peter Pothier hereby declare that:

- At no time during the registration for the degree of Magister in Ingeniaria have I been registered for any other university degree.
- The work done in the dissertation is my own.
- This dissertation has not been previously submitted in full or partial fulfilment of the requirements for an equivalent or higher qualification at any other educational institution; and
- All sources used or referred to have been documented and recognised.

R. P. Pothier

Date: 9 January 2015

Abstract

This study develops and presents a friction stir weld (FSW) quality assurance tool based on control of weld zone temperature. Apart from correct tool geometry, tool tilt angle, traverse speed and forge force during welding, one important requirement is that the weld material be sufficiently plasticised (softened). The level of plasticisation is related to weld zone temperature which is primarily dependent on spindle speed, traverse speed and forge force. When all other conditions are correct, sufficiently plasticised material flows around and consolidates behind the tool without the production of voids in the weld. Typically, weld temperature varies along the weld length which may result in variations in weld quality. Weld zone temperature control makes constant weld zone temperature possible. In this study, thermocouple sensors were embedded in the FSW tool and a weld zone temperature control algorithm was developed. Spindle speed was the actuating mechanism for controlling weld temperature. The system was modelled and controllers were designed using Matlab tools. The system was simulated and the performance was compared to the system performance during welding. The control system ensures that the weld zone temperature can be maintained irrespective of the presence of thermal disturbances. Tensile testing was conducted which confirmed a range of temperature in which the welds resulted in consistent strength.

Keywords: Friction Stir Welding (FSW); Closed-loop; Temperature Control; System modelling; Controller design; Controller tuning; PID; Aluminium Alloy 6082

I would like to acknowledge the following persons for their contributions to this study:

- The Lord Jesus Christ for providing me with the intellectual ability, strength and the opportunity.
- My supervisors; Prof. Danie Hattingh and Prof. Theo van Niekerk for their continual support and guidance.
- My family, especially my parents; Richard Pothier and Sharon Pothier for their support, encouragement, love and my educational foundation prior to commencement of this study.
- My friends for their support and encouragement in this study as well as the good recreation in the breaks.
- My fellow researchers at eNtsa, NMMU for their support, constructive criticism and guidance.
- The entire eNtsa team for their support, research facilities and the amazing aura in the group which made every day enjoyable.

Table of Contents

List of Figures	iv
List of Tables	vii
Abbreviations	viii
Glossary	ix
Chapter 1 Introduction	1
1.1. Aim.....	3
1.2. Objective	4
1.3. Significance of Research.....	4
1.4. Problem Statement.....	4
1.4.1. Temperature Fluctuation.....	4
1.4.2. Force and Position Control Effects	5
1.4.3. Heat Dissipation into the Surrounding Material.....	5
1.4.4. Work-piece Clamps	5
1.5. Sensor Positioning	6
1.6. Hypothesis	6
1.7. Delimitations.....	6
1.8. Organisation of Dissertation	9
1.9. Summary.....	10
Chapter 2 Relevant Literature	11
2.1. Temperature Response to Spindle Speed and Traverse Speed Changes... 11	
2.2. Temperature Control Model	14
2.3. Weld Temperature at Various Positions in the Weld Area.....	15
2.4. Temperature Control of Friction Stir Welding	18
2.5. Controller Derivative Filtering	21
2.6. Ziegler Nichols Tuning Method.....	21
2.7. Tool Designs	22

2.8. Tensile Strength	24
2.9. Summary.....	25
Chapter 3 Research Methodology and Experimental Setup	26
3.1. Research Methodology	26
3.2. Tool Design	28
3.3. Telemetry System	31
3.3.1. Power Supply.....	31
3.3.2. Sensor Data Transmission	31
3.4. MTS Platform	34
3.5. Process Development System (PDS).....	35
3.6. Weld Geometry and Setup	37
3.7. Summary.....	39
Chapter 4 Machine Control	40
4.1. PDS Platform Systems Control	40
4.2. Z-force Measurement and Z-force Control	41
4.3. Feed Rate Control.....	42
4.4. Summary.....	44
Chapter 5 Temperature Control Design and Verification	45
5.1. Establishment of the Process Window	45
5.2. Temperature Response to Spindle Speed Changes	51
5.3. Algorithm Development.....	58
5.3.1. Control System Layout	59
5.3.2. Control Algorithm	60
5.3.3. Ziegler Nichols Tuning Method ^[3]	62
5.4. Algorithm Performance Testing.....	65
5.5. Process Model (MATLAB).....	81
5.5.1. System Transfer Function Identification.....	81
5.5.2. Bode Diagram Frequency Design.....	88

5.5.3. Simulink PID Tuning	98
5.6. Thermal Disturbance Welds	100
5.6.1. Heat Sink Disturbance	102
5.6.2. Heat Source Disturbance.....	107
5.7. Tensile Testing and Analysis.....	111
5.8. Summary.....	119
Chapter 6	122
6.1. Future Research	124
Bibliography	125
Appendix A	A-1
Appendix B	B-1
Appendix C	C-1
Appendix D	D-1
Appendix E	E-1
Appendix F	F-1
Appendix G	G-1
Appendix H	H-1
Appendix I	I-1
Appendix J	J-1
Appendix K	K-1
Appendix L	L-1

List of Figures

Figure 1.1.	Friction stir weld process geometry ^[1]	1
Figure 2.1.	Section diagram of the thermocouple pocket in the FSW tool ^[5]	11
Figure 2.2.	Aluminium alloy weld temperature response to varying machine parameters ^[5]	13
Figure 2.3.	Simplified dual loop temperature control block diagram ^[6]	14
Figure 2.4.	Temperature control system block diagram	15
Figure 2.5.	Thermocouple positions ^[7]	16
Figure 2.6.	Comparison of a FSW temperature model and actual thermocouple experimental results at 2 mm depth ^[7]	16
Figure 2.7.	Comparison of a FSW temperature model and actual thermocouple experimental results at 4 mm depth ^[7]	17
Figure 2.8.	Comparison of a FSW temperature model and actual thermocouple experimental results at 8.13 mm depth ^[7]	17
Figure 2.9.	Tensile strength below and above the critical temperature ^[8]	19
Figure 2.10.	Voids ^[8]	19
Figure 2.11.	Fehrenbacher, et al. closed-loop temperature control of FSW ^[8]	20
Figure 2.12.	Tool design for AA6061-T6 4.95 mm plate ^[12]	23
Figure 3.1.	FSW tool	29
Figure 3.2.	FSW tool mock-up.....	29
Figure 3.3.	Telemetry rotor	32
Figure 3.4.	Antenna (left front), compact power unit (left rear) and demodulation unit (right)	33
Figure 3.5.	Demodulation unit rear	33
Figure 3.6.	MTS FSW platform.....	34
Figure 3.7.	MTS FSW machine head with attached telemetry components	35
Figure 3.8.	PDS Platform	36
Figure 3.9.	PDS spindle head setup.....	37
Figure 3.10.	Bead on plate FSW	38
Figure 4.1.	One of four of the PDS bed load cells	41

Figure 4.2.	Forge force control system diagram	42
Figure 4.3.	Feed-rate control system diagram.....	43
Figure 5.1.	Forge forces of weld 1 and weld 2	46
Figure 5.2.	Position control weld 5	47
Figure 5.3.	Weld 1.4.....	48
Figure 5.4.	FSW tool FEA analysis.....	49
Figure 5.5.	FEA thermocouple section view	50
Figure 5.6.	Full weld temperature plot.....	52
Figure 5.7.	Increased spindle speed in stage 2.....	53
Figure 5.8.	W2.1. Spindle energy input rate, torque and temperature versus time	55
Figure 5.9.	Decreased spindle speed in stage 2	55
Figure 5.10.	Low spindle speed comparison of inverted weld stages.....	57
Figure 5.11.	High spindle speed comparison of inverted weld stages.....	57
Figure 5.12.	Control system diagram	60
Figure 5.13.	PID flow diagram.....	61
Figure 5.14.	Weld AT_2	64
Figure 5.15.	Weld AT_3	64
Figure 5.16.	Weld AT_4	68
Figure 5.17.	Weld AT_5	69
Figure 5.18.	Weld AT_7	70
Figure 5.19.	AT_7 maximum rate of temperature change.....	74
Figure 5.20.	Derivative filter responses	75
Figure 5.21.	Weld AT_8	76
Figure 5.22.	Modified filtered derivative response	78
Figure 5.23.	Weld AR_1	79
Figure 5.24.	Weld AT_10	80
Figure 5.25.	AT_10 Region 4 oscillation.....	80
Figure 5.26.	Weld 3.2.....	81
Figure 5.27.	Second order model fit	83
Figure 5.28.	Transfer function conversion	84
Figure 5.29.	Simulink control system model.....	85

Figure 5.30. Simulink simulation of FSW control step command	86
Figure 5.31. Weld AT_7 temperature response extract.....	86
Figure 5.32. Open-loop bode and closed-loop step response.....	90
Figure 5.33. Moved bode diagram and corresponding system step response	91
Figure 5.34. Bode diagrams and step response after PI control design	92
Figure 5.35. Final placement of PI and PD design zeros	93
Figure 5.36. Final controller by frequency design.....	94
Figure 5.37. Simulink model of bode frequency design versus Ziegler Nichols design	96
Figure 5.38. Ziegler Nichols PID design output versus bode frequency PID design output	97
Figure 5.39. Simulink tuned PID performance versus Ziegler Nichols PID performance	99
Figure 5.40. Simulink tuned PID (positive D) performance versus Ziegler Nichols PID performance	100
Figure 5.41. Dry ice and methanol heat sink	103
Figure 5.42. Dry ice container placement.....	104
Figure 5.43. Disturbance heat extraction rate versus temperature.....	105
Figure 5.44. Temperature control engaged/disengaged heat sink welds	106
Figure 5.45. Weld 3 added for comparison with weld 1 and weld 2.....	106
Figure 5.46. Spindle speed of weld 1, weld 2 and weld 3.....	107
Figure 5.47. Heated block disturbance close view	108
Figure 5.48. Heated steel block disturbance position relative to the weld setup	109
Figure 5.49. Temperature control engaged/disengaged heat source welds.....	110
Figure 5.50. Spindle speed of weld 3, weld 4 and weld 5.....	110
Figure 5.51. Tensile samples	111
Figure 5.52. Tensile sample positions	112
Figure 5.53. Tensile yield strength comparison between weld sets 4.1 and 4.2.....	115
Figure 5.54. Ultimate tensile strength comparison between weld sets 4.1 and 4.2	116

List of Tables

Table 2.1.	Machine parameters for experiment 1 and experiment 2 ^[5]	12
Table 5.1.	Weld 2.1 traverse power data for stage 1 and stage 2	54
Table 5.2.	Weld stage speeds (inverted welds).....	56
Table 5.3.	AT_7 region 2 and region 4 statistics	71
Table 5.4.	AT_7 control data	72
Table 5.5.	Filter parameters	78
Table 5.6.	Weld and simulation comparison	85
Table 5.7.	Damping ratios	87
Table 5.8.	Disturbance weld matrix	101
Table 5.9.	Heat sink weld plate temperatures	102
Table 5.10.	Heat source weld plate temperatures.....	107
Table 5.11.	Tensile results of temperature controlled, heat sink disturbance welds (4.1).....	113
Table 5.12.	Tensile results of constant spindle speed, heat sink disturbance welds (4.2).....	113
Table 5.13.	Yield strength t-test results.....	115
Table 5.14.	Ultimate strength t-test results.....	117
Table 5.15.	Yield tensile strength standard deviations	118
Table 5.16.	Ultimate tensile strength standard deviations.....	119

Abbreviations

AA	Aluminium Alloy
ASTM	American Society for Testing and Materials
EDM	Electric Discharge Machine
FSW	Friction Stir Weld/Friction Stir Welding
HAZ	Heat affected Zone
HMI	Human Machine Interface
PDS	Process Development System
PID	Proportional Integral Derivative (controller)
PLC	Programmable Logic Controller
SID	System Identification (Tool)
TMAZ	Thermo-Mechanically Affected Zone
USB	Universal Serial Bus (connection)
UTS	Ultimate Tensile Strength

Glossary

Backing plate	The plate which supports the weld material from the bottom.
Bed	In the context of this study, the machine's bed is the support area on which the weld is conducted.
Critically damped	A critically damped system ($\zeta = 1$) achieves the set-point in the shortest amount of time with zero overshoot of the set-point.
Damping	An effect on the system which limits the rate at which the controlled variable of the process can change.
Damping ratio	The ratio (ζ) of the amount of actual damping of the system to the amount of damping at the point of critical damping $\left(\frac{\text{damping}}{\text{critical damping}}\right)$.
Dry ice	Carbon dioxide in its solid form (at a temperature of approximately -78.5°C). Typically in the form of pellets which resemble ice.
Dynamic recrystallisation	Recrystallisation of the material's grain structure caused by the deformation of the material (not heat treatment).
EtherCAT	A computer communication network technology.
Filter	A filter attenuates certain undesired frequencies from a signal. In the case of this study, digital filters are utilised

which take the form of mathematical calculations executed by the machine controller.

Force control	A friction stir weld can be programmed to execute in force control mode in which case the forge force (vertical direction) is maintained at the operator set-point. The vertical position of the tool is allowed to vary according to mechanical influences such as machine bed deflection.
Forge force	The downward force applied by the machine which is supported mainly by the tool shoulder. The force consolidates the material exiting from the rear of the tool.
Fuzzy logic	A control strategy based on rules applied to feedback signals. The importance of the rules (or action taken on a specific feedback signal) can be set using weighted coefficients.
Genetic algorithm	A genetic algorithm is given an objective. In control systems the algorithm modifies the input to the system (actuator(s)), measures the output and continually modifies controller gains in the direction of achieving the objective. The algorithm effectively learns the process which it is controlling.
Linearity	A control system is considered linear if a change in the input variable (actuator(s)) has the same effect on the output variable when the system is at any point in the operating range of the system output.
Load cell	A force sensor or transducer.

Natural frequency	A system will tend to oscillate at its natural frequency if a driving force on the system precisely cancels out any damping force on the system.
Negative damping	A negatively damped system ($\zeta < 0$) will begin to oscillate with growing amplitude (caused by the driving force of the system) which increases indefinitely. The system is considered unstable.
Over aging	As the material age hardens, its strength increases to a peak. Aging of the material beyond this point is considered over aging in this study. The process of over aging requires a large amount of time at room temperature. It is possible to drastically accelerate the process by artificially aging the material using heat. This is what occurs in the heat affected zone of the weld for the material used in this study.
Over damped	An over damped control system ($\zeta > 1$) does not overshoot the set-point although the rise time is larger than for a critically damped system.
Over plunge	In the context of this study, over plunging is when the FSW weld material is unable to support the forge force (the temperature of the material or the forge force is too high) and the tool collides with the backing plate.
Parent material	The portion of the weld plate which is unaffected by the heat of the weld and is considered to have approximately

identical mechanical properties after welding as before welding.

Percentage overshoot	As a control system is driven towards the set-point, it often overshoots the set-point value. The amount by which the control system overshoots the set-point as a percentage of the step command size is the percentage overshoot.
Tilt angle	During a FSW, the tool is tilted from the vertical by a few degrees such that the majority of the forge force is applied at the rear of the tool in order to consolidate the material exiting from underneath the rear of the tool shoulder.
Plunge	The plunge stage is at the beginning of the weld. The rotating welding tool is forced downward into the weld material.
Plunge depth	The distance from the surface of the weld material to the tip of the tool pin.
Position control	The weld tool position is maintained at the operator set plunge depth. The forge force during the weld is allowed to vary according to influences such as deflection of the machine bed.
Quality	The tensile strength of the weld is a representation of the weld quality in this study.

Ramp up	The initial stage during the weld after the plunge stage is complete, in which the weld slowly accelerates up to welding speed. The weld is in position control mode in this stage prior to the weld going into force control mode if the weld is programmed to be a force control weld. For this study the ramp up stage is 20 mm in length.
Rise time	The time taken for the control system to drive the output variable from 10% to 90% of the size of the step command applied to the set-point.
Run-on tab	A sacrificial plate placed at the beginning of the weld on which the plunge and ramp up stage can occur before the weld travels onto the weldment. The run-on tab allows for the FSW to be conducted for the full length of the weldment because a FSW cannot be plunged on the edge of the weldment.
Servo drive	The controller which manages the spindle servo motor parameters such as torque and speed regulation according to the requirements received from the machine PLC via an EtherCAT connection. The servo drive also manages spindle motor power supply.
Settling time	The time required for a control system to stabilise to within 5% of the set-point (for the final occurrence) after a step command change is made to the set-point.
Set-point	The desired position of the output of the control system (temperature in the context of this study), programmed by the operator, which the control system strives to achieve.

Spindle power	The product of spindle torque and spindle angular velocity (units of W or kW).
Spindle speed	The rate at which the spindle rotates (units of rev/min in terms of spindle speed or rad/s in terms of angular velocity).
Spindle torque	The rotational force which the spindle applies to the FSW tool.
Stable zone	Theoretically, the stable zone is the area of the weld in which the weld zone temperature is approximately constant. The study shows that typically the temperature continues to rise from the beginning to end of the weld although the temperature rising rate is relatively small after the ramp up stage.
Steady-state error	When a control system is maintaining constant system output, the error between the system output value and the desired set-point is the steady-state error.
Step command	An instantaneous change in control system set-point, programmed by the operator.
Transfer function	A mathematical equation representing the dynamics of the control system. The transfer function of the process is considered a mathematical model of the system in the context of this study.

Traverse speed	The rate at which the weld is travelling along the weld path. Equivalently, traverse speed can be referred to as feed rate or travel speed in FSW studies.
Ultimate tensile strength	The maximum stress (after the yield point) which the tensile sample is able to withstand prior to fracture.
Undamped	An undamped system (damping ratio $\zeta = 0$) has insufficient damping to diminish oscillation amplitude of the output yet the output oscillation amplitude does not increase indefinitely (the system is on the border of stable/unstable).
Underdamped	An underdamped system ($0 < \zeta < 1$) is stable and percentage overshoot ranges from high to low as ζ moves from zero towards unity. The rise time is shorter than for a critically damped system although overshoot occurs.
Welding tool	The non-consumable tool which applies the frictional and stirring forces to the weld zone during the production of a FSW.
Weldment	The work-piece which is welded or undergoing welding.
Weld nugget	The portion of the weld zone through which the tool pin traverses.
Weld setup	The entire physical setup of backing plate, weld plate(s), welding tool, clamping mechanisms and the FSW welding machine.

Weld zone	The area of the weldment underneath the welding tool during the production of a FSW.
Wind-up	The integral term of the PID controller is a summation over time. Should the error between the set-point and the process feedback be of one sign for a specific amount of time, the integral term will wind-up for that amount of time.
Wind-up limit	In order to prevent excessive wind-up, a wind-up limit is often placed on the integral term.
x-force	The force applied by the x-axis hydraulic cylinder during the production of a FSW (in the welding direction in the context of this study).
y-force	The force applied by the y-axis hydraulic cylinder during the production of a FSW (transverse to the weld direction and is regulated in order to maintain y-axis position in the context of this study).
Yield strength	The stress at the point when the load on the sample causes it to begin plastic deformation.
z-force	The force applied by the z-axis hydraulic cylinder during the production of a FSW (see forge force).

Chapter 1

Introduction

Friction stir welding (FSW) is a solid-state joining process. During process execution, the temperature does not reach the solidus point (or the liquidus point) of the material. Frictional heat is generated between the non-consumable welding tool and the work-piece in order to heat the material to the point of plasticisation. The plasticised material is concurrently stirred and forged by the tool into a joint.

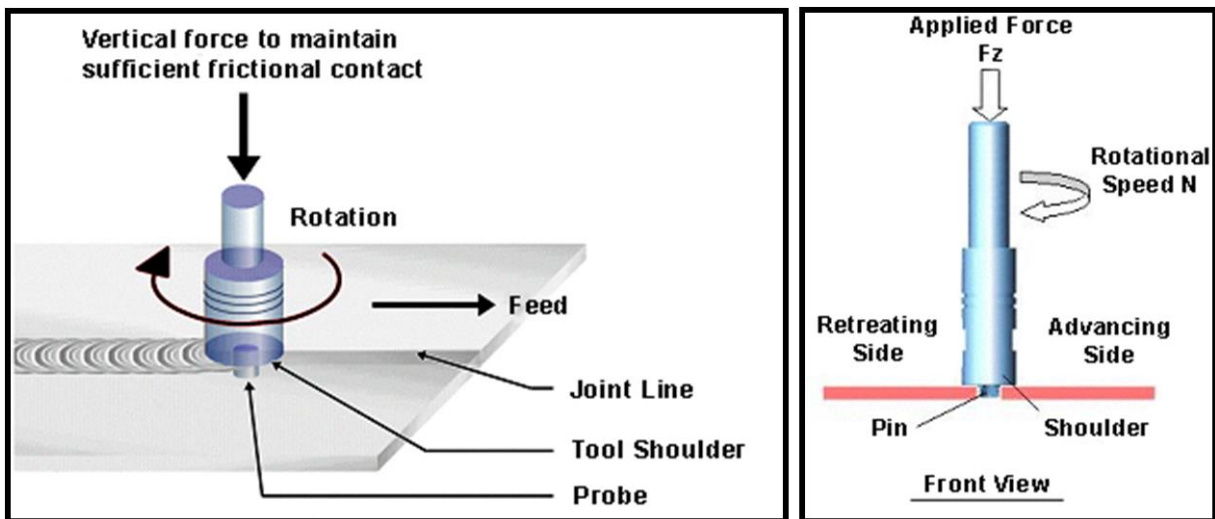


Figure 1.1. Friction stir weld process geometry ^[1]

The friction stir weld tool consists of a shoulder and a pin (see tool design in Section 3.2). The process begins by plunging the rotating tool into the material until the pin reaches the required plunge depth. This depth is usually as close to the backing plate surface as possible. At this point, the tool shoulder comes into contact with the surface of the material. The tool shoulder supports the majority of the forge force (labelled: “Vertical force/Applied force” in Figure 1.1). This force, together with the relative motion between the rotating tool and the weldment generates the frictional heat responsible for plasticising the material. As the material temperature rises, the material plasticises, reducing the spindle torque and hence the spindle power (for

constant spindle speed). The rising rate of the material temperature then decreases because of the reduction of energy input rate and increasing thermal diffusion into the surrounding material. The process stabilises at a specific temperature range. The FSW process is self-regulating in this sense. The weld temperature is typically not constant for the duration of the weld. FSW is an asymmetric process because the rotation of the tool causes the material on one side of the pin to move in the same direction as the welding direction (advancing side) while the material on the opposing side moves in the opposite direction to the welding direction (retreating side).

In order to produce a good quality FSW, which has consistent mechanical properties for the entire length of the weld, certain process conditions need to exist during the execution of the weld. Most of these conditions, such as spindle speed, weld traverse speed, forge force and tool tilt angle can be selected by the operator. During the weld, the machine controls these parameters in order to maintain their values according to the operator's weld program. The temperature of the material in the weld zone is dependent on these parameters as well as process conditions occurring during welding which are specific to the weld setup. The weld temperature is seldom constant because of changes in the amount of heat dissipated from the weld zone at different positions along the weld path. At a specific temperature or temperature range, the material in the weld zone will be optimally plasticised for the process to occur successfully and produce a good quality weld joint. This temperature is referred to as the optimal plasticisation temperature (OPT) in this study. Since the temperature of a typical FSW varies along the weld length, the material in the weld zone is not guaranteed to be at the OPT.

In this study, a temperature control algorithm was developed which was able to control weld zone temperature at various operator set-points. The control system alters spindle speed in order to control the weld zone temperature (which needed to be realistic for the specific weld setup). This control system created the possibility for the operator to conduct a weld with constant weld zone temperature. Selecting the

weld temperature set-point as the OPT (for the particular weld setup) was therefore made possible.

The control system was developed on aluminium alloy 6082-T6 in this study. The system needed to be able to measure the weld zone temperature in the range of room temperature to approximately the material liquidus temperature (as safe limits). This generated the feedback signal for the control system.

The project produced an integrated temperature control system on an operational friction stir welding platform. The controller performance was tested and compared to the performance of various computer generated controllers in a simulated model.

The controller disturbance rejection was also tested by introducing a heat sink disturbance and then a heat source disturbance. Welds were conducted at constant temperature through the disturbance area. Tensile tests were done to investigate the weld quality consistency of these welds.

1.1. Aim

Develop a closed-loop temperature control system for friction stir welding which alters spindle speed in order to maintain the operator's set-point temperature for the plasticised material in the weld zone. The control system needs to exhibit good disturbance rejection.

1.2. Objective

Develop a prototype temperature control system for friction stir welding which will assist with quality control during welding. Determine the contribution of constant weld temperature to joint quality consistency along the weld length.

1.3. Significance of Research

This study provides industry (as well as eNtsa) with a tool to control the temperature of a FSW. The temperature of the weld can be maintained within a specific range (determined by the response capability of the system) of a specific set-point. Constant weld temperature could improve the consistency of the weld quality along the weld length because the material is maintained at a reasonably consistent plasticised state (optimal or not for the material being processed). Preferably, the operator would then select the OPT for the weld material and the weldment would contain the qualities of optimised strength and consistency along the weld length. The system provides the FSW industry with a tool which assists in the production of consistent quality welds.

1.4. Problem Statement

1.4.1. Temperature Fluctuation

The temperature of a FSW fluctuates as the weld progresses due to various influences which change the heat dissipation from the weld. For the weld setup used in this study, it was found that the weld temperature would continue to rise as the weld progresses; if the temperature control algorithm was not engaged. Temperature variation could affect weld quality if the material is not maintained at the OPT.

1.4.2. Force and Position Control Effects

The vertical position (z-axis) of the FSW tool is typically controlled by either position control or force control. Either the z-position or the z-force is kept constant and the other varies as the weld progresses. Force control was the strategy used in the experiments conducted in this study. Typically the weld traverse speed and spindle speed are selected and are maintained constant throughout the duration of the weld. Fluctuation of either of these parameters would cause a change in the frictional forces between the tool and the work-piece; causing the machine to alter its spindle torque and/or welding feed force (x-force in this study) in order to maintain constant spindle speed and traverse speed. This could cause a temperature fluctuation in the weld.

1.4.3. Heat Dissipation into the Surrounding Material

In the proximity of a point in the middle of the weldment, the plate material volume (heat sink) is higher than a position closer to the edges of the weldment. Theoretically, the temperature of the weld zone therefore decreases as the tool moves towards the centre of the weldment, and increases as the tool moves away from the centre of the weldment. If the weld is sufficiently long, there exists a stable zone starting from a certain position after the beginning of the weld length and ending at a certain position before the end of the weld length. In this zone, heat dissipation into the surrounding material can be considered approximately constant. Temperature change outside of the stable zone must be compensated for.

1.4.4. Work-piece Clamps

The clamps which hold the weldment to the bed of the machine are fabricated from steel. These clamps are therefore thermally conductive. Heat is dissipated from the weldment, through the clamps. Weld temperature therefore theoretically increases as the weld tool moves away from one clamp and decreases as it approaches the next clamp. This influence is small and could be considered negligible.

1.5. Sensor Positioning

The sensors which measure the weld zone temperature need to be placed in the optimal position relative to the weld zone. The optimal position is a position anywhere on the tool, work-piece or backing plate which has the least thermal resistance between it and the hottest plasticised material in the weld zone. This position will be at a temperature which represents the temperature of the weld zone. The optimal position will allow a change in temperature to be detected with minimum delay after the moment in which the change occurred. This will allow the system to respond in the minimum amount of time to changes in weld zone temperature in order to achieve minimal temperature fluctuation.

1.6. Hypothesis

Closed-loop temperature control of a friction stir weld can be developed and implemented as a weld quality assurance tool. Upon successful implementation of a closed-loop temperature control system, online process control of weld quality is made possible which will aid in process efficiency regarding cost and quality.

1.7. Delimitations

- This study was intended to develop the temperature control system and show its contribution to weld strength consistency. Once the temperature of the FSW was controllable and the tensile tests were completed, the project was complete. The weld strength consistency was investigated in this study, although the optimisation of the weld quality regarding the influences made by weld zone temperature (determining the OPT of the material) was not within the scope of this study.
- The development of the system was conducted on AA 6082-T6. The reasons for this are that aluminium and the welding tool material (W302 tool steel) are

relatively inexpensive. In addition to this, FSW of aluminium does not require a shielding gas to protect the weld from the atmosphere (oxidation prevention) as would be the case for FSW of steel or titanium. This simplifies the weld setup. Both steel and titanium FSW would require FSW tools manufactured from a material which would not substantially degrade at the welding temperatures of steel or titanium (e.g. Tungsten Rhenium ^[2] which is relatively expensive in comparison to tool steel used for welding aluminium).

- The welds conducted in the development process were bead on plate welds.
- A single tool design was used throughout the project. The hottest point in the weld zone was determined from literature and this position was used in the tool thermocouple pocket design.
- Weld length is 585 mm (maximum allowable x-axis stroke on the PDS FSW platform). This allows for investigation of temperature changes induced by spindle speed alterations in as much of the stable zone as possible. In addition to this, the Ziegler Nichols tuning method ^[3] requires that the tuner increase the controller proportional gain term until the system oscillates with constant amplitude. The tuner will therefore require maximum weld length and hence time for completing the task.
- The parameters selected as a starting point for welding aluminium alloy 6082-T6 are:
 - Traverse speed: 200 mm/min ^[4]
 - Spindle speed: 560 rpm ^[4]
 - Tilt angle: 1° ^[4]
- The FSW temperature control system must have good disturbance rejection. Some examples of these disturbances include the heat conductivity between

the weldment and the clamps as well as changes in heat conductivity between the weldment and the backing plate. The significance of such influences is difficult to quantify. Thermal disturbances, including dry ice as well as heated steel blocks, were introduced to the system in order to test the temperature control algorithm's disturbance rejection. The control system is tuned in such a way that if the temperature of the weld zone were to change due to any influence, the system will make appropriate machine spindle speed adjustments to compensate. These adjustments are made according to the predicted manner in which the temperature of the material responds to changes in spindle speed.

- The greater the error between the temperature set-point and the actual process temperature, the more aggressive the changes in spindle speed are in order to compensate for the error. Proportional, Integral and Derivative (PID) control was implemented. Ziegler Nichols PID tuning method^[3] was conducted in order to tune the control system. Performance of the control algorithm was then tested and compared to the performance of the simulated process model.
- The system components added to the FSW platform include:
 - A telemetry system which allows the sensors to be mounted on the rotating tool and the data transmitted wirelessly to the controller.
 - A tool containing embedded thermocouples.
 - The control algorithm was written and added to the machine control program which executes on the machine's programmable logic controller (PLC). The algorithm tasks include:
 - Acquire sensor data (feedback input)
 - Acquire operator set-point (operator input)
 - Perform necessary control calculations (internal processing)
 - Set the updated machine spindle speed (output)

- Welds were conducted in force control mode in order to maintain approximately constant frictional forces between the tool and the weldment. Undesirable fluctuation of forge force would be experienced in welds conducted in position control mode. Force control mode ensured that the forge force was a control variable for the weld experiments conducted in this study.

1.8. Organisation of Dissertation

Chapter 2 presents relevant scientific documents which support this study in terms of tool design as well as algorithm implementation and tuning.

Chapter 3 details the tool design; explains the research method executed; outlines the FSW machines utilised in the study; explains the method by which temperature data is transmitted from the rotating tool (telemetry system) to the machine controller and discusses the weld setup and geometry.

Chapter 4 discusses the FSW machine control systems which were implemented on the machine prior to the initiation of this study which were utilised in the experiments conducted in this study.

Chapter 5 forms the main body of the dissertation. The chapter includes the design, implementation, tuning and verification of the temperature control system. The performance of the control system regarding response to step command changes as well as disturbance rejection was tested. In addition to this, tensile tests were conducted in order to investigate the influence which weld temperature has on weld quality.

Chapter 6 formulates conclusions from the experimental data generated by this study and provides suggestions for future research which would build on the knowledge generated by this study.

1.9. Summary

This chapter introduced FSW basic concepts and principles necessary for understanding the method by which a typical FSW joint is produced. In addition to this, the concept of the material OPT was introduced. This study is based on optimisation of a control system designed to maintain the weld zone temperature which contributes to good consistency of weld quality. It is thus possible to maintain the material OPT along the weld path using this control system. In addition to this, the control system is able to maintain weld zone temperature in the presence of thermal disturbances. The significance of this study to industry and eNtisa is the possibility of ensuring the consistency of FSW quality through the use of this temperature control tool.

The problem statement outlines causes of weld zone temperature fluctuations. These causes include heat dissipation into the plate being welded (changes according to position on the weld path), heat dissipation into the various physical weld setup components and frictional force changes according to the welding mode (position or force control).

The selection method for the temperature sensor (thermocouple) position relative to the weld zone is described.

The delimitations of the study including project scope; material choice; weld parameters selected as a starting point; weld setup details; tool design; details about the temperature control algorithm development, testing and comparison with simulated models; components added to the existing FSW platform necessary for this study and the reason for the selection of force control mode for this study are clarified.

Chapter 2

Relevant Literature

This chapter highlights relevant knowledge contributions and sections from scientific publications which supports this study. The information from relevant literature made it possible to perform certain tasks in the development of the control system without the need to perform additional experiments to generate the information.

2.1. Temperature Response to Spindle Speed and Traverse Speed Changes

“Towards Process Control of Friction Stir Welding for Different Aluminium Alloys”^[5] investigated the weld temperature change induced by varying spindle speed (whilst maintaining constant traverse speed) as well as the temperature change induced by varying traverse speed (whilst maintaining constant spindle speed). A thermocouple was placed in the shoulder of the tool as shown in Figure 2.1.

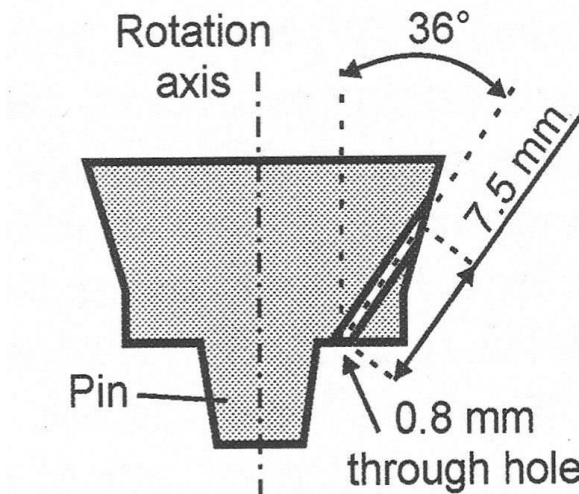


Figure 2.1. Section diagram of the thermocouple pocket in the FSW tool^[5]

The study was carried out on 2xxx, 5xxx, 6xxx and 7xxx series aluminium alloys. During the experiment, the parameter being varied was changed at a frequency of 0.1 Hz in order to allow sufficient time for the weld temperature to change in reaction to the parameter change. The researcher utilised a nominal spindle speed and traverse speed for each alloy which would have been acquired from previous experimentation. As the varying parameter changed (at 0.1 Hz), the amplitude of the change was a percentage of the nominal value of that parameter.

For each alloy, three experiments were conducted and the weld temperature range logged:

1. Maintain constant nominal traverse speed and vary spindle speed (amplitude = 20% of nominal)
2. Maintain constant nominal spindle speed and vary traverse speed (amplitude = 20% of nominal)
3. Maintain constant nominal spindle speed and vary traverse speed (amplitude = 80% of nominal)

The parameter values used in experiment 1 and experiment 2 are shown in Table 2.1.

Alloy	Nominal		20 % Amplitude of Nominal		Feed (mm/rev)		
	Spindle Speed (rev/min)	Travel Speed (mm/min)	Spindle Speed (rev/min)	Travel Speed (mm/min)	Varying Spindle Speed	Varying Travel Speed	
2024-T3	1100	75	220	15	0.085	0.082	Max
					0.057	0.055	Min
5083-H116	1300	150	260	30	0.144	0.138	Max
					0.096	0.092	Min
6061-T6	1300	200	260	40	0.192	0.185	Max
					0.128	0.123	Min
7075-T6	1300	75	260	15	0.072	0.069	Max
					0.048	0.046	Min

Table 2.1. Machine parameters for experiment 1 and experiment 2^[5]

The results of the experiments are shown in Figure 2.2.

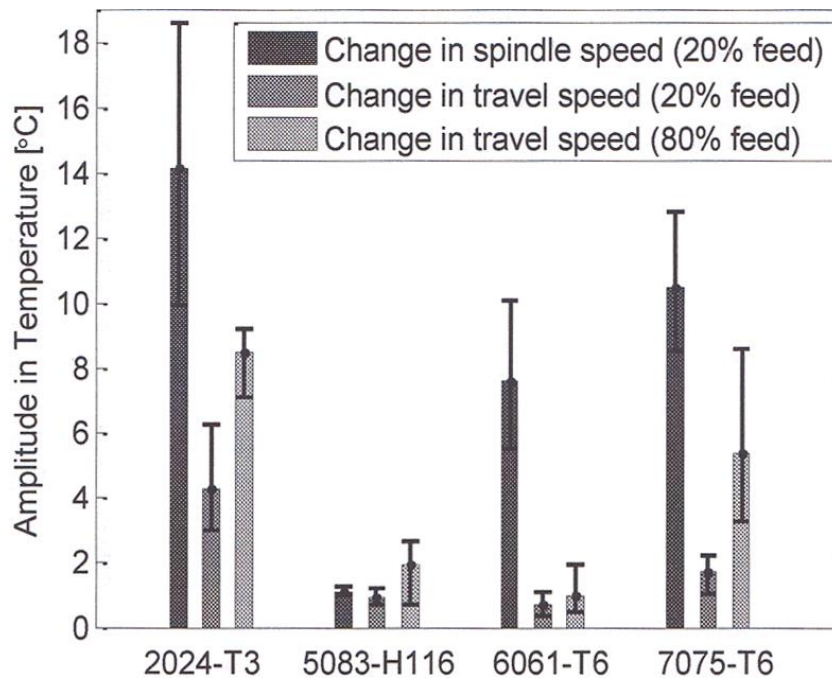


Figure 2.2. Aluminium alloy weld temperature response to varying machine parameters^[5]

The results show that varying the spindle speed resulted in the greatest reaction amplitude in the weld temperature with the exception of the 5xxx series aluminium alloys. Therefore it is more desirable to control weld temperature via variation of spindle speed. The project will therefore involve temperature control via spindle speed changes although there is a limit to the amount of change which can be made to spindle speed. This is based on the spindle speed limits for the weld setup. The machine which was used for conducting the preliminary welds was eNtsa's MTS I-stir FSW platform. The machine used for the implementation of the temperature control algorithm was eNtsa's Process Development System (PDS).

2.2. Temperature Control Model

“Investigation of Methods to Control Friction Stir Weld Power with Spindle Speed Changes” [6] proposed a closed loop temperature control strategy model. The strategy incorporated an inner and an outer control loop.

The outer loop obtains the operator set-point and the temperature feedback signal. From there the controller calculates the required spindle power. The temperature feedback is measured by means of a thermocouple sensor.

The inner loop uses the calculated power value (the outer loop output) as a set-point for spindle power. This set-point, together with the power feedback, is used to calculate the spindle speed command. The spindle power feedback is calculated by measuring the spindle angular velocity and spindle torque by means of a tachometer and a dynamometer respectively and then performing the calculation of power is equal to the product of torque and angular velocity. The control diagram is shown in Figure 2.3.

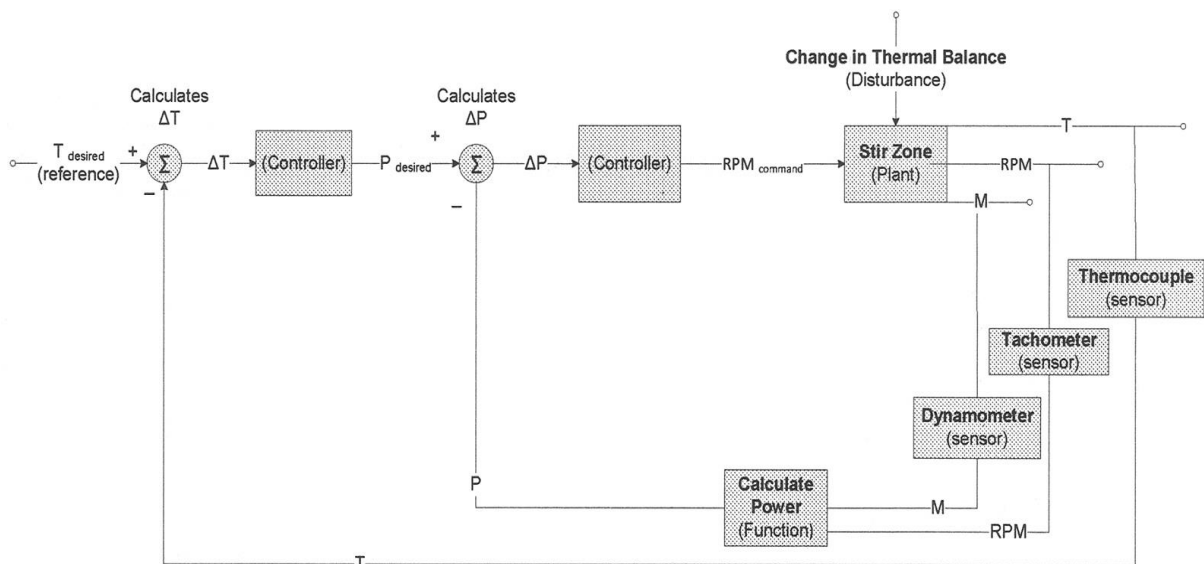


Figure 2.3. Simplified dual loop temperature control block diagram [6]

The spindle speed and spindle torque sensors are incorporated in the MTS I-stir and PDS FSW platforms. The control system which is implemented on the machine controls the spindle speed. Spindle power output is a result of this control because the spindle drive adjusts the spindle torque in order to control spindle speed. This corresponds to a certain power value and the only importance which this value has is that it is below the capability of the spindle motor and drive setup. The control model for this study therefore differs from the model in Figure 2.3 and is shown in Figure 2.4.

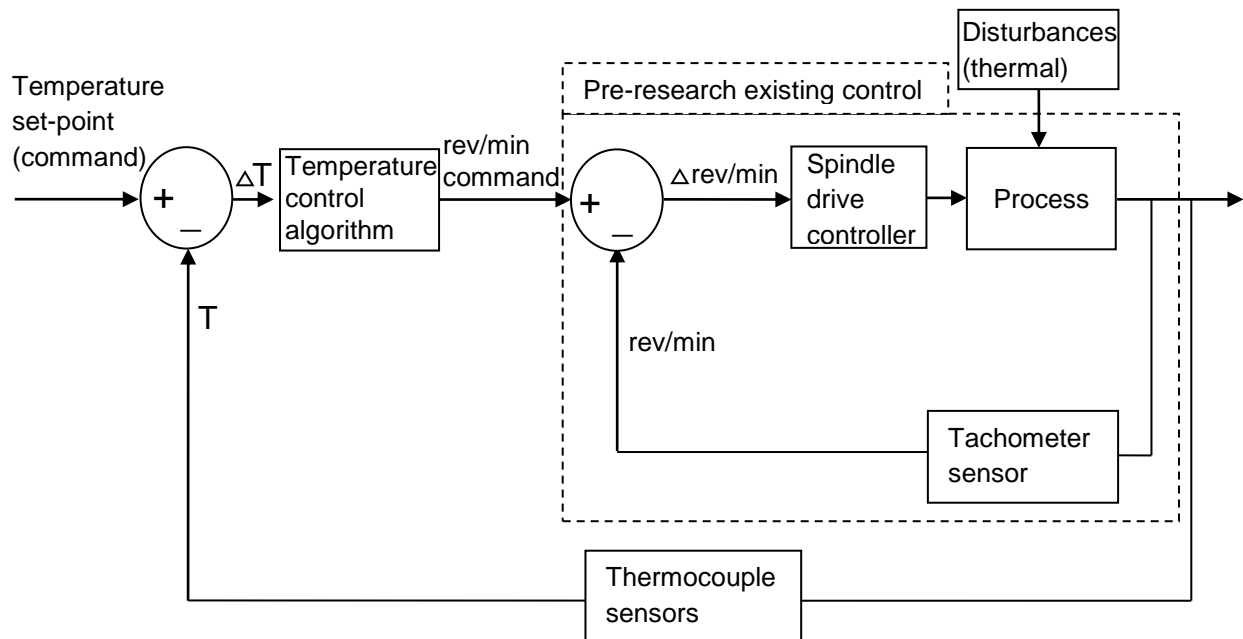


Figure 2.4. Temperature control system block diagram

2.3. Weld Temperature at Various Positions in the Weld Area

“Heat Transfer in Friction Stir Welding-Experimental and Numerical Studies” [7] investigated the temperature at various positions relative to the weld zone. In addition to this, a FSW temperature model was developed and the theoretical results obtained from the model (using the same parameters as used for the physical welds conducted). Temperature data from the simulation was plotted together with the data obtained from the physical welds conducted for comparison. The thermocouples were placed at various positions relative to the weld zone as shown in Figure 2.5.

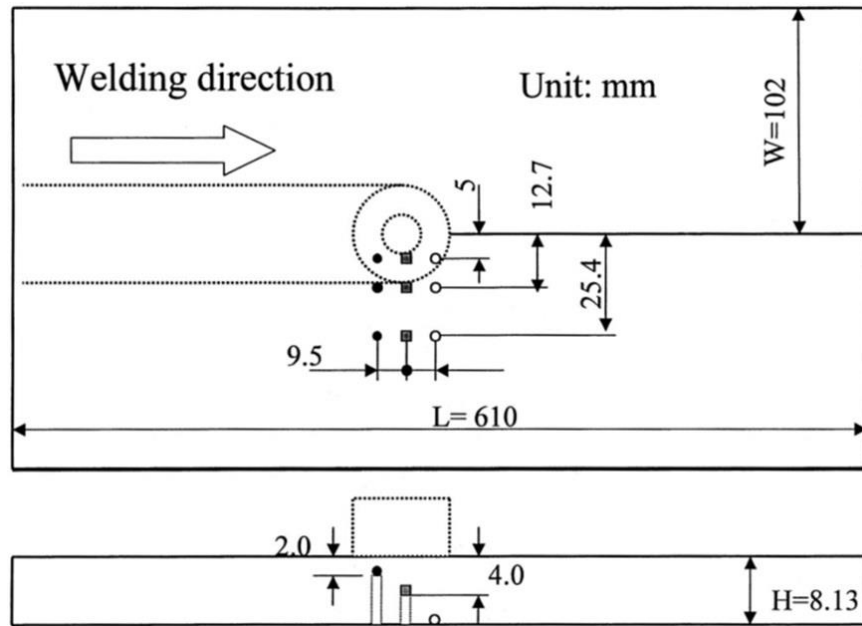


Figure 2.5. Thermocouple positions ^[7]

Figure 2.6, Figure 2.7 and Figure 2.8 show the comparison of the thermocouples at 2 mm (top), 4 mm (middle) and 8.13 mm (bottom) from the weld plate surface respectively.

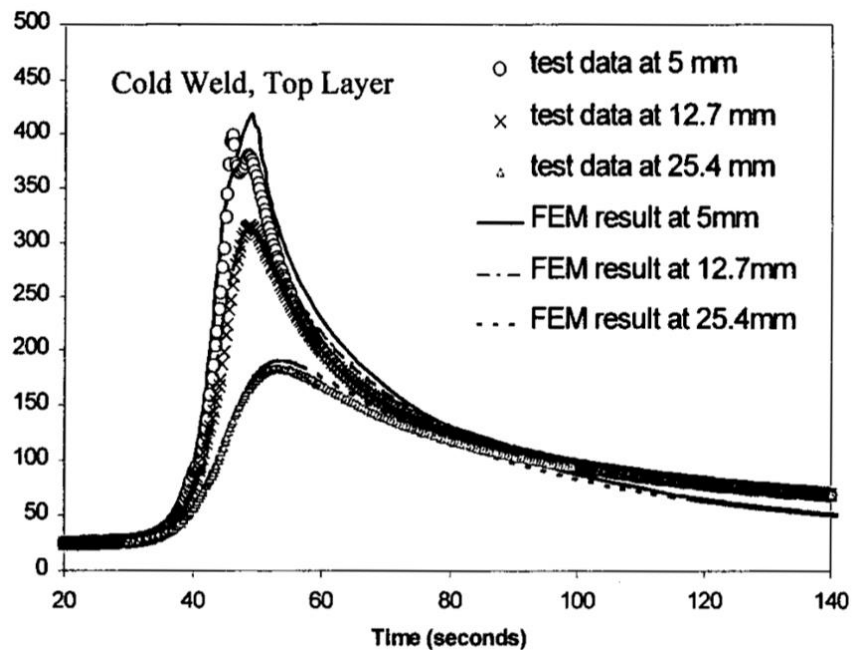


Figure 2.6. Comparison of a FSW temperature model and actual thermocouple experimental results at 2 mm depth ^[7]

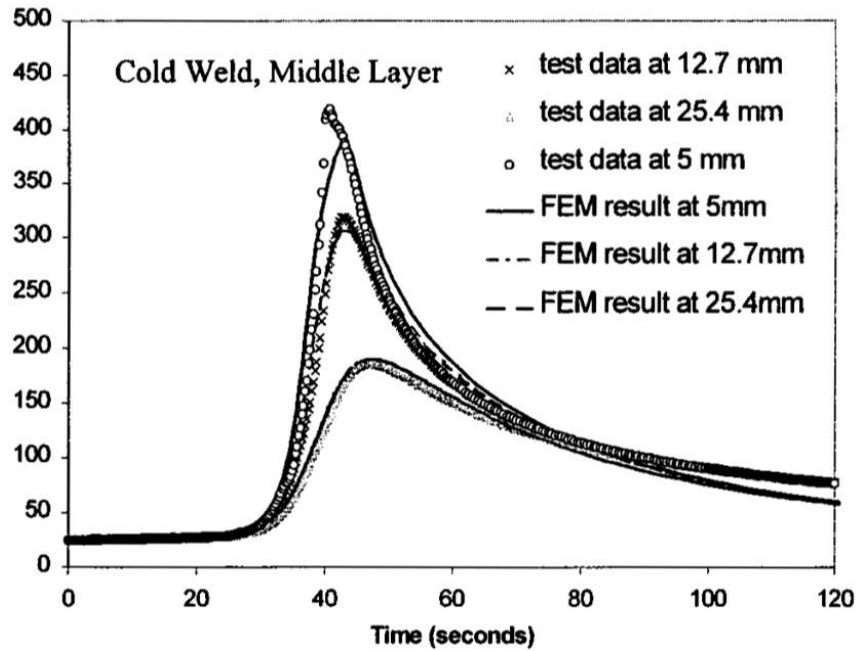


Figure 2.7. Comparison of a FSW temperature model and actual thermocouple experimental results at 4 mm depth [7]

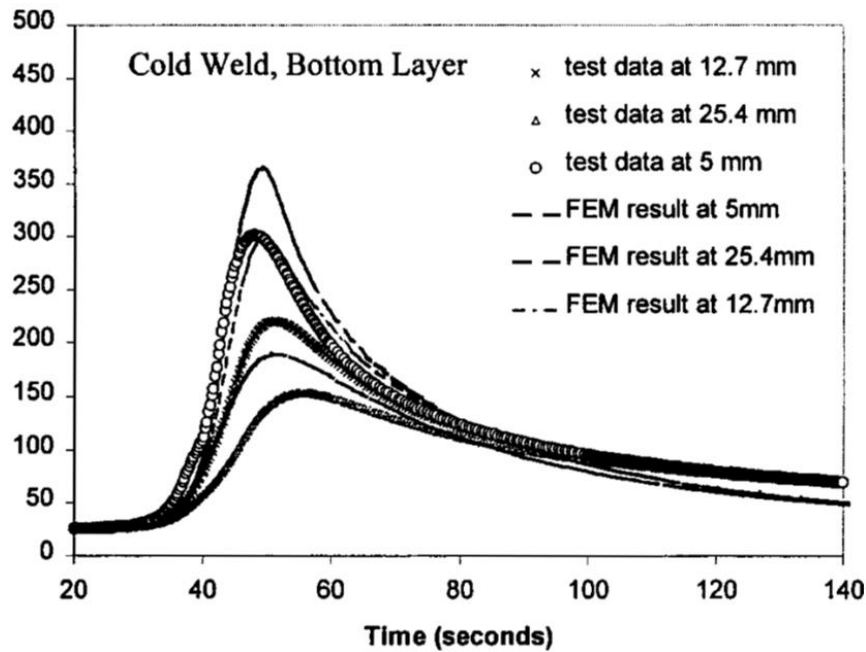


Figure 2.8. Comparison of a FSW temperature model and actual thermocouple experimental results at 8.13 mm depth [7]

From the graphs it can be seen that the FSW finite element model (FEM) and experimental results approximately agree.

Within each of the three graphs, it can be seen that the hottest position in the transverse direction is consistently at 5 mm from the weld centreline (nearest to the tool pin) and gets cooler as temperature is measured further from the weld centreline (at 12.7 mm and 25.4 mm). The hottest position regarding depth is the top surface.

It was decided that for this study, the thermocouples embedded in the tool would be located in the pin and nearest to where the shoulder meets the tool pin. This ensures measurement of the hottest area of the weld zone which would induce the fastest thermocouple response.

2.4. Temperature Control of Friction Stir Welding

“Effects of Tool-Workpiece Interference Temperature on Weld Quality and Quality Improvements Through Temperature Control in Friction Stir Welding” ^[8] investigated weld quality dependence on weld tool to weldment interface temperature. The study was conducted on various aluminium alloys including AA 6061 which is similar to the alloy utilised in this study (AA 6082). The study found that a critical temperature of 515°C exists for the AA 6061 plate and the particular weld setup (see Figure 2.9), below which voids begin to form in the weld and failure occurs in the weld area (not in the heat affected zone (HAZ) or the parent material). The graph identified by the circle (—⊖—) in Figure 2.9 is constructed from welds which were executed with traverse speed of 200 mm/min which is the same as the traverse speed selected for the welds conducted in this study.

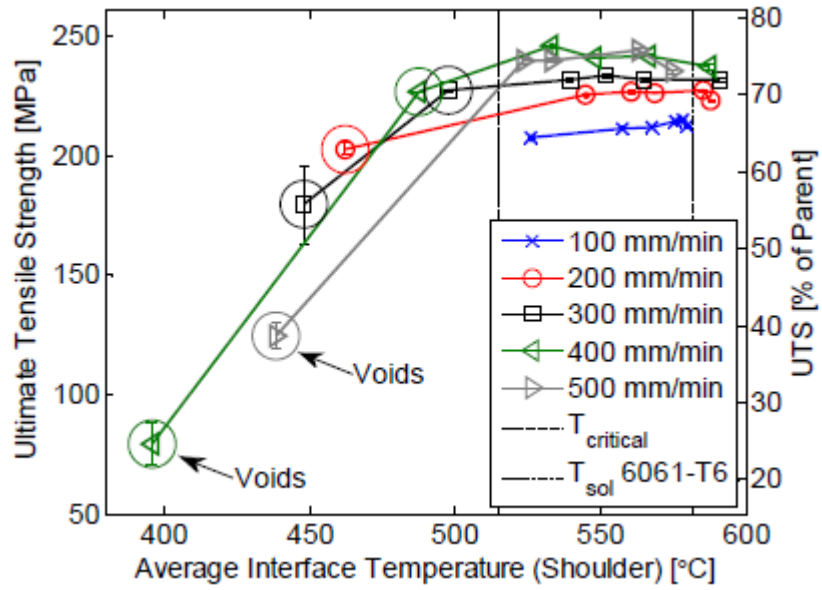


Figure 2.9. Tensile strength below and above the critical temperature [8]

An example of the voids which begin to form are shown in the weld cross section of Figure 2.10. The shoulder to weldment average interface temperature was 439°C in this case.

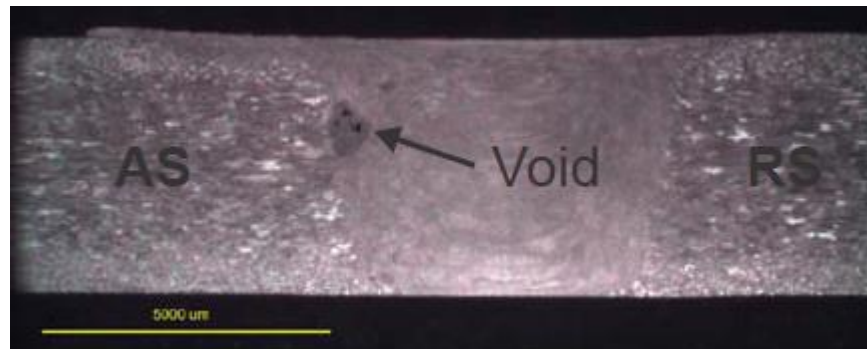


Figure 2.10. Voids [8]

Above the critical temperature in Figure 2.9, the weld strength is seen to be approximately constant for a specific traverse speed.

A dynamic process model was generated using the Matlab system identification tool. It was found that a first order model with a time delay was a good representation of the input data (spindle speed) to output data (process temperature) relationship.

A closed loop temperature control system was implemented and tested on 4.76 mm thick AA 6061-T6 plate by introducing step command changes to the controller set-point. The response obtained is shown in Figure 2.11.

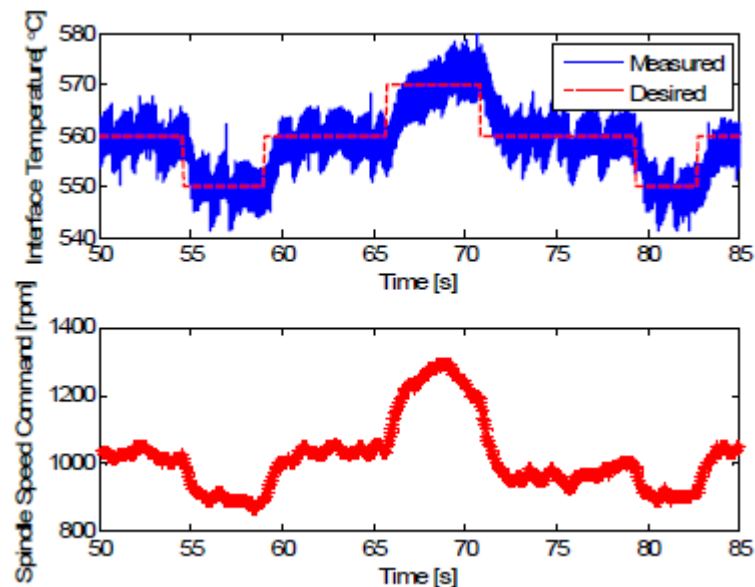


Figure 2.11. Fehrenbacher, et al. closed-loop temperature control of FSW^[8]

The following statement which is made in the study is important to this study: “The data also shows that for the parameter window chosen, varying the spindle speed results in a larger variation in interface temperature than varying the travel speed, which is an important result for developing closed-loop temperature control for FSW.”^[8]. This compliments the findings in Section 2.1.

2.5. Controller Derivative Filtering

In Section 10.5 of “Feedback Systems An Introduction for Scientists and Engineers”^[9], a statement is made that the derivative term of a PID controller typically has high gain for high frequency signals. Typically, the high frequency signal is a result of noise introduced into the system on the sensor feedback signal to the controller. This is a drawback of the controller as it could cause the actuating mechanism (controlled by the PID controller), which drives the system, to oscillate unnecessarily. This could possibly lead to undue wear on the system and a waste of energy. A derivative filter design is suggested in Section 10.5 of “Feedback Systems An Introduction for Scientists and Engineers”^[9]. The filter is designed as a modified calculation for the derivative term of the PID controller which attenuates controller derivative gain for high rates of change of the process variable under control (leading to a high rate of change of the error signal, typically associated with high frequency noise on the feedback signal). The filter is implemented by replacing the equation which calculates the derivative term of the PID controller with Equation 5.12 on page 55.

2.6. Ziegler Nichols Tuning Method

J.G Ziegler and N.B Nichols developed a controller tuning method outlined in “Optimum Settings for Automatic Controllers”^[3]. The method allows the controller tuner to monitor a number of process characteristics and calculate the approximate optimum controller settings without the need to apply excessively complex mathematic calculations regarding the system dynamics. The method could produce controller settings which are closer to optimum than if excessively complex mathematic calculations regarding the system were carried. The reason for this being that the method takes into account all system properties which are difficult to quantify mathematically in the dynamic model. An example of such a property is bearing friction at various operating speeds.

The method begins by setting P, I and D controller gains to zero. With the system operating and the controller set-point set to the position at which the controller is to be tuned, the proportional gain is increased slowly from zero until the system begins to oscillate with constant amplitude. The proportional gain at this point is considered the ultimate gain. The period of the oscillation is measured. From the ultimate gain and the oscillation period, the approximately optimum controller P, I and D gains can be calculated from the Ziegler Nichols equations (see Section 5.3.3 on page 63).

2.7. Tool Designs

A number of sources were referred to during the design of the FSW tool used in this study and relevant details of each are outlined in the following paragraphs:

For FSW of 6.35 mm thick 6061-T6 aluminium alloy in the study titled: “Tool Forces Developed During Friction Stir Welding”^[10], the tool consisted of a shoulder diameter of 19.2 mm, a threaded pin with diameter of 6.35 mm and pin length of 5.83 mm. The tool tilt angle utilised during welding was 1° and the tool rotation direction was such that the thread direction displaces the plasticised material downwards. Pushing the plasticised material downwards compliments the data found in Section 2.3 which shows that the material is at a higher temperature near to the tool shoulder. Pushing this material downward would assist in ensuring that the material at the bottom of the weld zone is sufficiently plasticised in order to avoid flaws at the bottom of the weld.

Friction stir welding of 5 mm thick aluminium alloy 6061 plate was reported in literature titled: “Friction Stir Welding of Al 6061 Alloy”^[11]. The tool consisted of a shoulder diameter of 25 mm, a pin height of 4.8 mm and the tool tilt during welding was 2°.

Friction stir welding of aluminium alloy 6061-T6 plate of thickness 4.95 mm was reported in literature titled: “Tensile Properties and Constitutive Modeling of Friction

Stir Welded AA6061-T6 Butt Joints”^[12]. The tool design utilised in the study is shown in Figure 2.12. A tool tilt angle of 3° was utilised in the study.

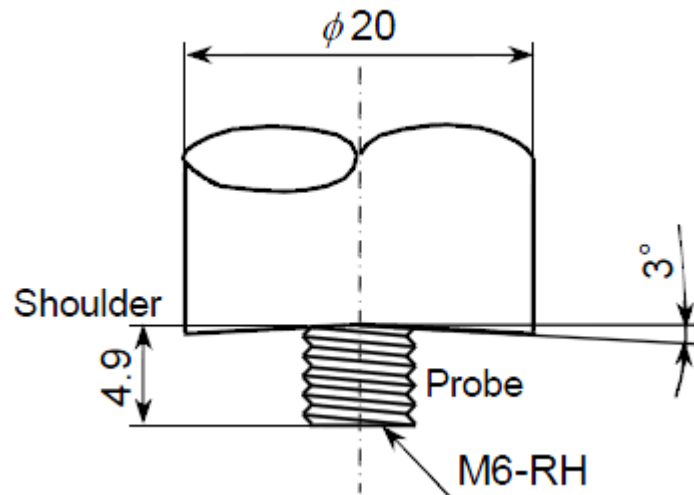


Figure 2.12. Tool design for AA6061-T6 4.95 mm plate^[12]

Tool geometry was investigated in the study titled: “Study of Tool Geometry in Friction Stir Welding Applications”^[13]. The study suggested that the material suitable for FSW welding aluminium between 0.5 mm and 50 mm in thickness is a hot worked tool steel which complies with the AISI H13 standard. This material was suggested for its properties of strength, toughness, hardness and wear resistance at the welding temperature of aluminium FSW. W302 tool steel (which was available for this study) complies with the AISI H13 standard. “Study of Tool Geometry in Friction Stir Welding Applications”^[13] also suggests a tool pin length of 3.85 mm for welding AA6061 plate of 4.00 mm thickness.

“The Influence of Thread Form on Refilling Friction Stir Welding of 2219 Aluminium Alloy Sheets”^[14] investigates the effects of tool pin thread pitch on material flow velocity by means of simulation. The study investigated thread pitch of 0.6 mm and 1.2 mm. The spindle speed was 83.8 rad/s (approximately 800 rev/min) and the tool traverse speed was 3.33 mm/s (approximately 200 mm/min). The study concluded that the thread pitch can increase the material downward flow by more than 20 percent in order to fill any voids which may begin to form in the weld zone.

FSW of 6 mm thick AA 7039 plate was studied in literature titled: “Tool Design Effects for FSW of AA7039”^[15]. Various tool dimensions were tested including shoulder diameters of 16 mm, 19 mm and 22 mm as well as pin diameters of 6 mm, 7 mm and 8 mm. The study found that increasing the tool pin diameter beyond 7 mm caused a reduction in weld cross-sectional area and tensile strength. The study also found that a shoulder diameter of 19 mm was the most suitable. The study utilised a vertical milling machine which was converted to conduct FSW. The setup produces a FSW which is essentially conducted in position control mode (vertical position of the spindle head determines the plunge depth). A further study was conducted (written by some new authors as well as some of the authors of “Tool Design Effects for FSW of AA7039”^[15]) titled: “Effect of Tool Shoulder and Pin Probe Profiles on Friction Stirred Aluminium Welds – a Comparative Study”^[16]. The study made the following statement which was valuable in the design of the FSW tool utilised in this study: “Apart from initial high vibration of the machine, the straight cylindrical tool exhibited good weld surface finish and overall acceptable welds.”^[16]. In the study it was once again found that it was detrimental for weld quality to utilise a FSW tool which exhibits a straight, cylindrical tool exhibiting a pin diameter exceeding 7 mm^[15].

2.8. Tensile Strength

“Tensile Properties and Constitutive Modeling of Friction Stir Welded AA6061-T6 Butt Joints”^[12] reported tensile strength of between 72 percent and 74 percent of parent material. The relevance between this information and this study is that both studies were carried out on 6xxx aluminium alloy in the T6 condition (heat generated during welding causes over aging of the heat affected zone) and the results are comparable. Tensile test results obtained from this study are shown in Section 5.7 of this document.

“Heat Transfer in Friction Stir Welding-Experimental and Numerical Studies”^[7] investigates FSW temperature of AA2195-T8 which is a heat treatable aluminium

alloy (as is the case for AA6082-T6, which is utilised in this study). According to the study, a tensile strength of greater than 66 percent of the parent material is considered a good FSW for heat treatable aluminium alloys^[7].

2.9. Summary

This chapter outlined and discussed information from various literature sources which is of particular relevance to this study. Literature which investigated temperature response to spindle speed and traverse speed changes showed that variation of spindle speed affected weld zone temperature more significantly than variation of traverse speed. A temperature control model for friction stir welding was proposed in the study titled: "Investigation of Methods to Control Friction Stir Weld Power with Spindle Speed Changes"^[6] and there were similarities between the control system diagram in the study and the control system diagram of the control system developed in this study. The study in which temperature was measured at various positions relative to the weld zone assisted with the selection of the positioning of the thermocouples embedded in the FSW tool utilised in this study.

A study was presented which investigated temperature control of friction stir welding and the effects which weld temperature has on weld quality. A particular type of controller derivative filter was presented in literature which was implemented and modified in this study. The purpose of the filter is to reduce undesirable oscillation of the control system actuator's output variable (spindle speed in this study). The Ziegler Nichols PID tuning method^[3], which was used to tune the control system in this study, was outlined. The method is a practical procedure used to determine the approximately optimal controller gains for a control system based on recorded system behaviour. Tool design specifications were collected from relevant studies detailing FSW tool geometry for 2xxx, 6xxx and 7xxx series heat-treatable aluminium alloys. The information assisted with the choice of tool geometry utilised in this study. Typical information (collected from two sources) regarding FSW tensile strength for heat treatable aluminium alloys relative to the parent strength was discussed.

Chapter 3

Research Methodology and Experimental Setup

This chapter explains the research method undertaken in order to investigate and produce an acceptable FSW tool design for the material being welded. The principle by which the telemetry system transmits the temperature data from the rotating tool to the machine controller is explained. The MTS FSW platform used for the preliminary welds and the PDS platform used for the main experimental welds in this study are outlined. The chapter also outlines the experimental setup used for conducting the experimental welds. Details regarding the physical weld geometry and weld setup are explained in the final section of this chapter.

3.1. Research Methodology

Initially a literature survey was completed. A foundation of understanding of the FSW process and weld zone temperature was generated. Information from the survey assisted with tool design including geometry and thermocouple pocket design.

The tool was designed and manufactured according to Section 3.2. The temperature measurement hardware (thermocouples and telemetry system) was fitted to the FSW platform and interfaced with the machine controller.

The process window was established (see Section 5.1). The tool tilt angle was selected appropriately to supply adequate forging force to the material at the rear of the tool whilst producing a good surface finish. Forge force, maximum spindle speed and minimum spindle speed were determined. The tool travel speed (after the ramp up stage) was constant for the entire study and all the welding was done in force control mode, except for the position control mode welds conducted during the establishment of the process window.

In the preliminary welds (see Section 5.2), the relationship between spindle speed and temperature was investigated. This work provided the researcher with a better understanding of the process temperature response and provided data which was used in generating the mathematical model of the process. This mathematical model was later used in simulations of various temperature PID controllers (generated through various methods, see Section 5.5) which were compared to the response of the implemented (real) weld temperature controller response.

The temperature control algorithm was developed and tested (See Section 5.3). The control system measures the temperature of the weld zone via thermocouple temperature sensors located in the non-consumable weld tool. If the temperature is below the set-point, the algorithm increases spindle speed to compensate. If the temperature is above the set-point, the controller decreases spindle speed to compensate. Limits were placed on the amount by which the controller was allowed to alter machine spindle speed. If a limit is reached, the spindle speed is set to that limit and if the system does not reach the set-point temperature, the set-point was set to an unsuitable value for the process setup. These limits protect the equipment because insufficient spindle speed introduces the risk of the weld material cooling excessively which could lead to tool seizure and/or fracture. On the opposite limit, excessive spindle speed would lead to excessive plasticising of the weld material which would cause the tool to over plunge and collide with the backing plate, damaging it and/or the weld tool. The system was tuned using the Ziegler Nichols PID tuning method ^[3].

Matlab's system identification tool was used to generate a mathematical relationship (transfer function) between the spindle speed and weld zone temperature. Matlab's controller design tools (ACSYS and Simulink PID tuner) were used to design PID controllers. These controllers were connected to the transfer function in Matlab Simulink and the responses of each were simulated in comparison to the response of the real control system. See Section 5.4 and Section 5.5.

The disturbance rejection of the system was tested (see Section 5.6). Heat energy sink and heat energy source disturbances were placed on the weld plate. The control system compensated for these disturbances by increasing or decreasing spindle speed in order to maintain the desired weld zone temperature.

Tensile testing was conducted on the welds obtained from the welds completed in Section 5.6 in order to test the weld strength consistency. See Section 5.7 for the discussion about the tensile testing.

3.2. Tool Design

A typical FSW tool consists of a shoulder and a pin. The pin is plunged into the material to the required plunge depth and at this depth; the shoulder comes into contact with the material surface. The shoulder may be concave, flat or consist of some sort of machined pattern intended to improve frictional heat generation and/or material flow. The pin design may consist of a straight or tapered design, flutes, threaded or a combination of these designs. A FSW tool does not typically contain thermocouple pockets unless specifically required for the intended use of the tool.

The FSW tool used in this study was manufactured from W302 tool steel and then through hardened to 54 on the Rockwell C scale. The tool design consists of a 22 mm diameter, 6° concave shoulder, with a straight, threaded (0.8 mm pitch), 7.9 mm diameter pin which is 5.77 mm in length from the lowest point on the shoulder. The FSW tool is shown in Figure 3.1.



Figure 3.1. FSW tool

Two J-type thermocouples of 1.5 mm diameter are located in the tool in order to measure weld zone temperature during the welding process. J-type thermocouples were selected based on their operating range of 0°C to 750°C ^[17] since AA 6082-T6 has a liquidus temperature of approximately 660°C ^[18] and the weld process is executed below this value. These thermocouples provide the sensory feedback necessary for closed-loop temperature control. The thermocouple tips are located with 180° separation, inside the tool pin near the shoulder as shown by the tool mock-up shown in Figure 3.2.

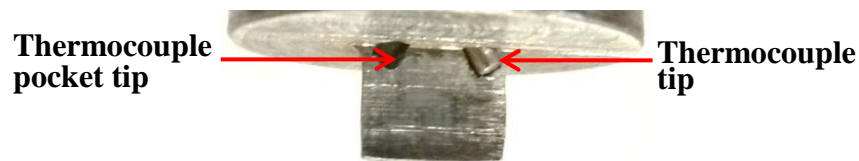


Figure 3.2. FSW tool mock-up

Regarding the weld tool which has the thread machined onto the pin, the thermocouple tip is separated from the weld zone material by approximately 0.2 mm of tool material. The thermocouple pockets are approximately 50 mm in depth. In order to achieve sufficient accuracy of the bottom of the pocket, an Electric Discharge Machine (EDM) die sink with 1.5 mm diameter copper electrodes was used for

machining the pockets. The arc length in the machining process creates the clearance for the thermocouple sheaths.

The thermocouples were calibrated by utilising a furnace and the FSW platform's PLC for the telemetry output signals. The J-type thermocouple specification for temperature versus thermoelectric voltage was plotted and suggests the thermocouples respond linearly in the range achieved by the welds in this study. Refer to **Appendix A** for the calibration data.

The telemetry system provides gain and zero set-point adjustments for each channel. These were adjusted in order to utilise the range of the process and achieve good resolution. Channel 7 and channel 8 of the telemetry system were utilised. The gain and zero set-point for each channel are adjusted by means of turning set screws. The two channels were adjusted to approximately the same setting although it is difficult to set them to the exact identical setting by means of turning a set screw. For this reason there are slightly different calibrations for channel 7 and channel 8. Before welding commenced, it was decided that because the system will never exceed 700°C (which is above the material's liquidus temperature) and the telemetry output is ± 10 V, the gain and zero were set such that 700°C measured by the thermocouple generates approximately +10 V output on the telemetry system output. An initial calibration was done over a broad range of temperatures in order to be able to measure weld temperature. Welds were conducted with this calibration in order to log the temperature range of the particular weld setup. The thermocouples were later re-calibrated for the range of temperature which is experienced by the weld setup used in this study. This eliminates error of the calibration data outside of the process temperature range caused by any possible non-linearity of the thermocouples outside of the process temperature range. The operating range of temperature achieved by the welds conducted in this study was found to be between 450°C and 540°C. The thermocouples were re-calibrated in this range. This makes the thermocouple data as accurate as possible for the experiments conducted thereafter. The measured data and resulting calibration curves can be seen in **Appendix A**. The error of the

temperature measurement system, including the thermocouples, telemetry system and PLC data acquisition was calculated. The combined error for channel 7 was calculated as 1.119% (95% confidence) and the combined error for channel 8 was calculated as 1.823% (95% confidence). See **Appendix A, page A-5 and page A-9** for the error calculations executed with Microsoft Excel.

3.3. Telemetry System

The thermocouple temperature data is transmitted from the rotating tool wirelessly via the telemetry system. The telemetry system communicates the temperature data with the machine controller in order to generate the weld zone temperature feedback signal used by the temperature control algorithm.

3.3.1. Power Supply

The circuitry attached to the rotating spindle head (contained in the telemetry rotor) is powered inductively by the antenna coil as the primary coil and the rotor coil as the secondary. The AC power generated in the rotor coil is rectified to DC power in order to power the rotating circuitry.

3.3.2. Sensor Data Transmission

The circuitry in the rotor amplifies the sensor signals and transforms the data by generating a frequency subcarrier for each sensor channel (different frequencies). The mixer then mixes the subcarriers into one signal (this signal thus contains all sensor channel frequencies and is called the subcarrier mixture signal). The radio frequency modulator (RF modulator) uses the subcarrier mixture signal to modulate the main carrier frequency which is transmitted from the rotor to the receiver via the antenna system. This signal is called the RF signal. The telemetry rotor is shown in Figure 3.3.



Figure 3.3. Telemetry rotor

On the receiver side, the reverse process is done in order to obtain voltage signals for each sensor channel. The demodulation unit (see Figure 3.4) is plugged into a 220 V single phase power supply. It in turn powers the compact power generator which in turn powers the telemetry rotor via the antenna. The RF demodulator (contained in the compact power generator) generates the subcarrier mixture signal (combined sensor data) and sends it to the demodulation unit via the coaxial cable seen in the figure.

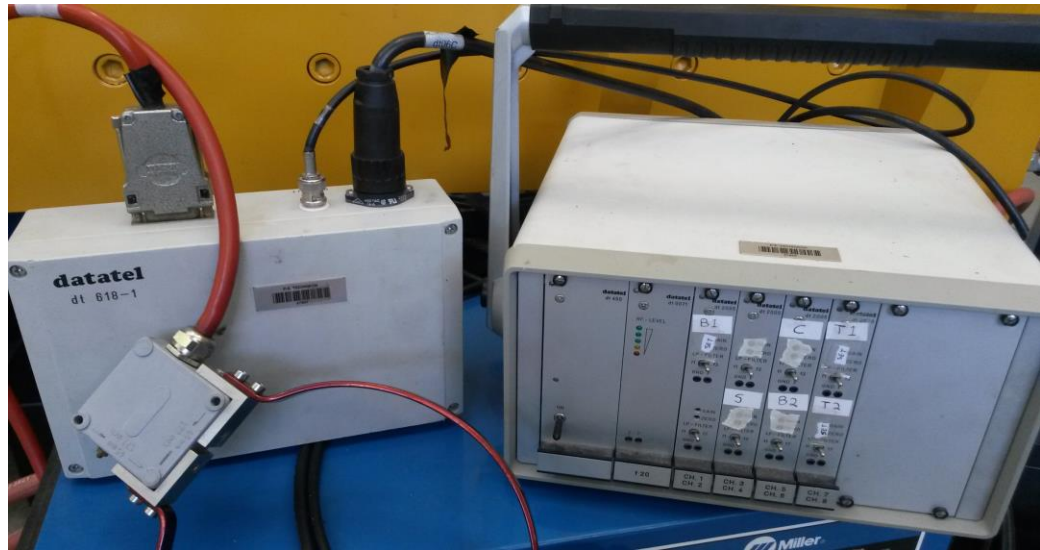


Figure 3.4. Antenna (left front), compact power unit (left rear) and demodulation unit (right)

The demodulator demodulates the signal into the separated subcarrier signals for each channel and converts the data from frequency defined to voltage defined. The voltage signals are amplified to ± 10 V analog outputs for each channel shown at the rear of the demodulation unit (see Figure 3.5). These signals are connected to the controller analog input card.



Figure 3.5. Demodulation unit rear

3.4. MTS Platform

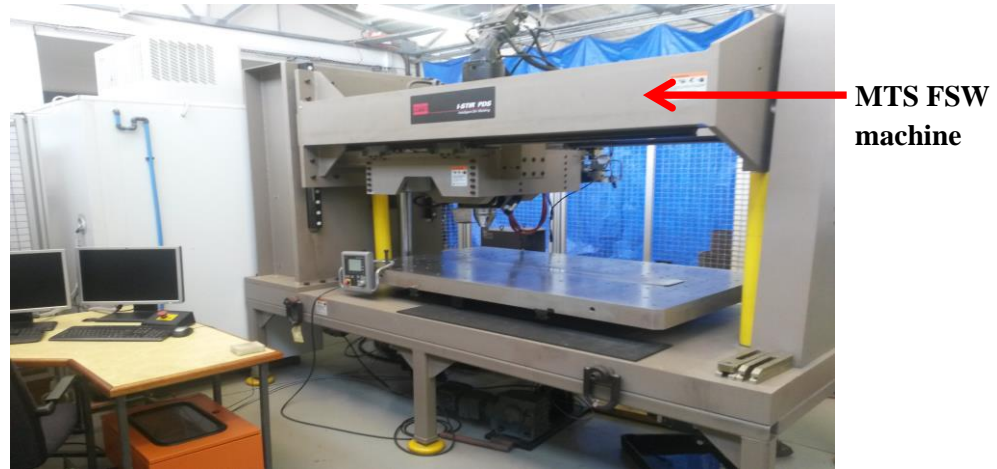


Figure 3.6. MTS FSW platform

The preliminary work for this study was carried out on the MTS FSW platform at eNtsa (a technology station at Nelson Mandela Metropolitan University). The FSW machine is shown in Figure 3.6. This work involved establishment of the process parameter window and investigation of weld zone temperature response to spindle speed step changes of 100 rev/min (see Section 5.1 and Section 5.2). The FSW machine spindle setup is shown in Figure 3.7.

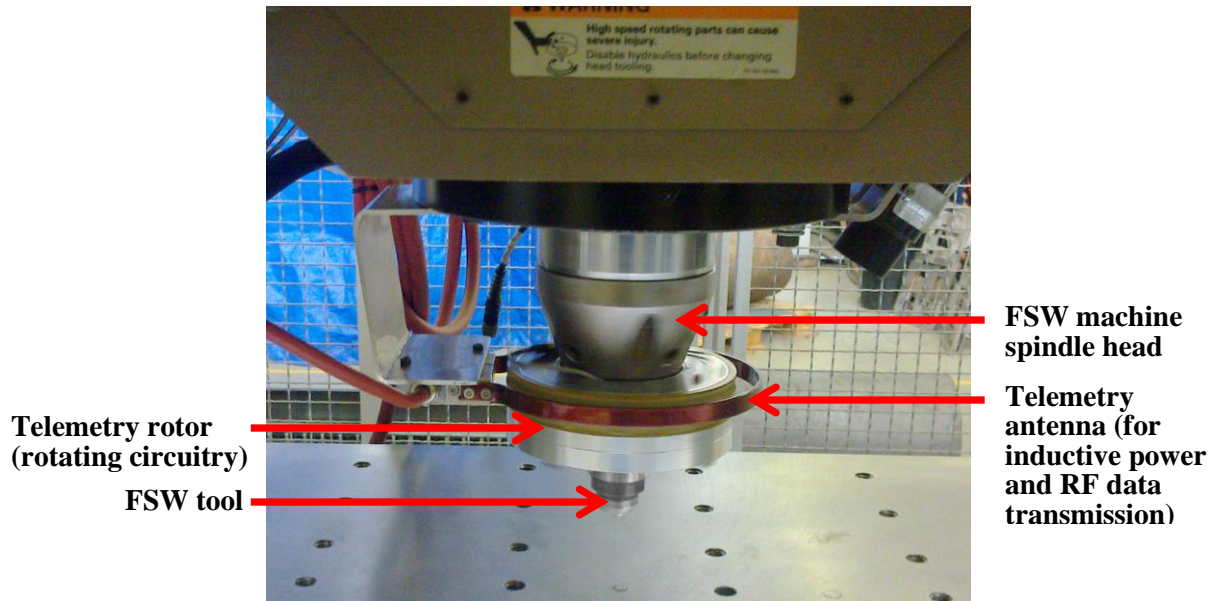


Figure 3.7. MTS FSW machine head with attached telemetry components

3.5. Process Development System (PDS)

The PDS platform (see Figure 3.8) was developed by eNtsa at NMMU. The machine consists of four axes (x, y, z and b which is the tilt axis). The platform is versatile and is capable of performing many types of friction processes such as FSW, friction hydro pillar processing (FHPP) and friction taper stud welding (FTSW). The platform is also able to perform machining operations in a similar manner to a CNC milling machine.

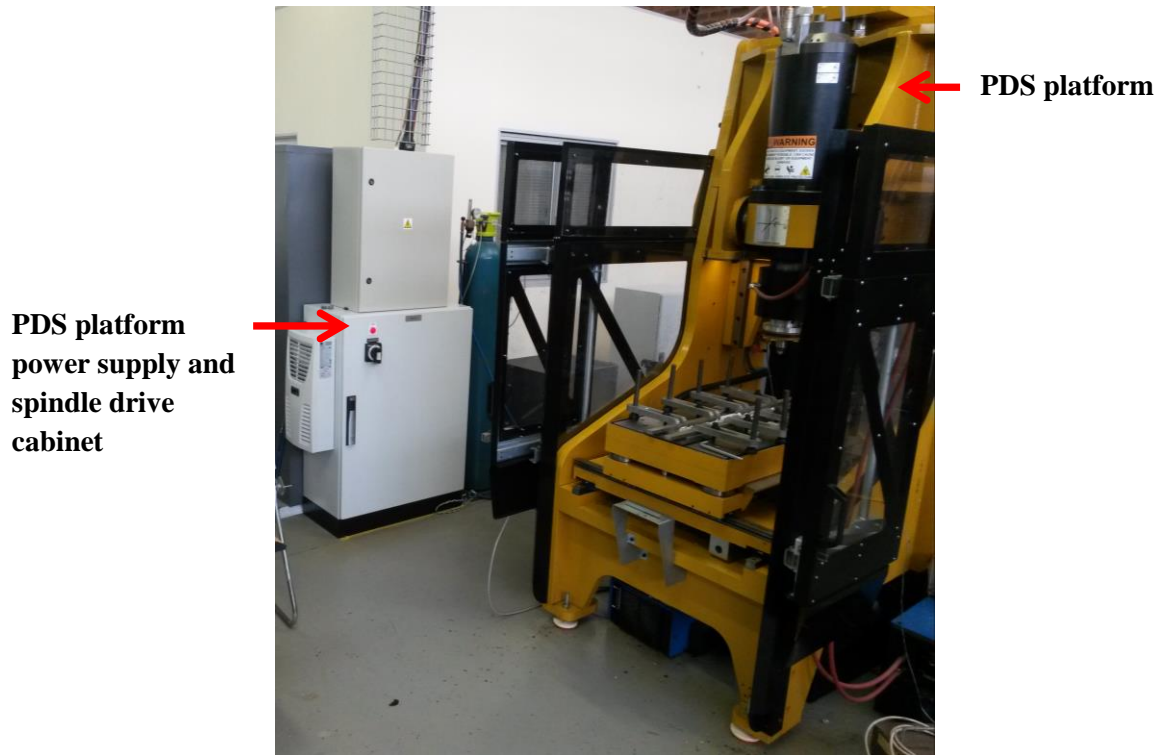


Figure 3.8. PDS Platform

The researcher has full access to the machine control program. Closed-loop control of temperature using analog inputs for the feedback signals and the spindle motor as the actuator was therefore possible. The closed-loop temperature control algorithm was developed and tested; and the experimental welds investigating weld consistency were conducted on this platform (see Section 5.3 to Section 5.6). The FSW tool setup with telemetry system for the PDS platform is shown in Figure 3.9.

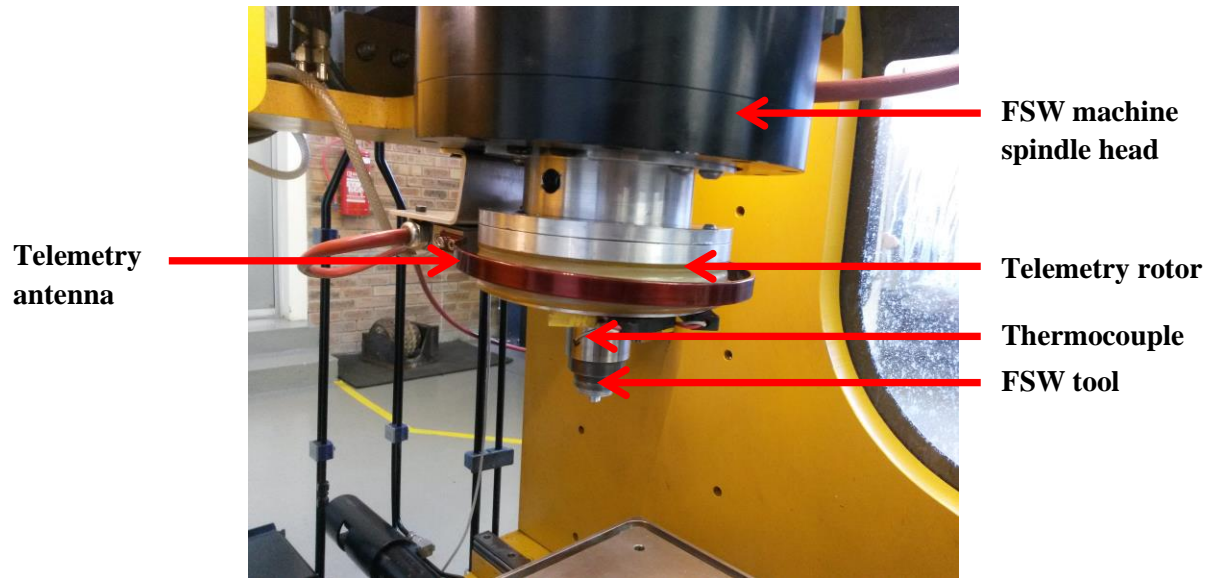


Figure 3.9. PDS spindle head setup

3.6. Weld Geometry and Setup

Experimentation in this study was conducted on Aluminium Alloy 6082-T6 with the following dimensions and backing plate material:

- Plate dimensions: 750 mm x 100 mm x 6.1 mm
- Backing plate material: 17-4 PH stainless steel

The development of the temperature control system was conducted on FSW bead on plate welds as opposed to FSW butt welding. This reduces weld preparation and reduces the number of controlled variables which need to be maintained consistent in order to avoid undesirable influences of the experimental results. For a specific material type and plate thickness, the welding parameters for bead on plate welding and FSW butt welding are approximately identical.

There are three main reasons for the reduction in weld preparation: butt welds require milling of the joining edges in order to ensure that the two edges are perfectly parallel to each other and the joint gap is constant; removal of the aluminium oxide from the

butting edges immediately prior to welding is required because the surface oxide could have a reducing effect on weld quality; a butt weld requires extra clamping in order to prevent the two plates from separating during welding. Controlled variables which are removed from the experiment include: plate gap variation; effectiveness of the aluminium oxide removal procedure; time delay between oxide removal and weld execution during which oxide begins to reform. The weld setup is shown in Figure 3.10.



Figure 3.10. Bead on plate FSW

Weld length conducted on the MTS platform was 650 mm. Maximum weld length on the PDS platform was limited by the stroke of the x-axis. The PDS platform allowed for a maximum weld length of 585 mm (which is the length of the weld shown in Figure 3.10).

3.7. Summary

The research methodology followed in conducting this study outlined the steps taken to develop the temperature control system and verify the resultant PID controller. The FSW tool design was explained and thermocouple pocket machining on the tool verified. The verification of the pocket machining process ensured that the thermocouple tips are located correctly relative to the tool geometry.

The telemetry system was outlined in this chapter. The theory behind supplying the rotating circuitry with power and the transmission of the thermocouple data from the rotating tool to the machine controller was explained.

The chapter shows the FSW setup on the MTS platform (used for the process window establishment (see Section 5.1) and the preliminary welds conducted (see Section 5.2)). The chapter shows the FSW setup on the PDS platform (used for temperature control algorithm development and testing (see Section 5.3, Section 5.4 and Section 5.6)). The physical weld geometry and setup is explained in the final section of this chapter.

Chapter 4

Machine Control

This chapter discusses the control mechanisms of the PDS platform (existing prior to the initiation of this investigation) which are utilised during; and are necessary for executing the experimental welds conducted in this study. See Section 5.3.1 (page 60) and Section 5.3.2 (page 61) for the discussion about implementation of the temperature control system.

4.1. PDS Platform Systems Control

The PDS platform contains a central PLC (Beckhoff TwinCAT) which performs the majority of the calculations necessary for machine control. A human machine interface (HMI) is connected to the PLC. All weld programs are programmed and executed through this interface. The weld data is viewed and/or extracted from the PLC memory via the HMI and a universal serial bus (USB) port. A servo motor drives the machine spindle. The PLC controls the spindle by generating a spindle speed or spindle torque command which is communicated to the servo motor drive via an EtherCAT connection. The servo motor drive contains internal control loops designed to control spindle torque and spindle speed according to the command which it receives from the PLC.

The x, y, z and b axes are driven by hydraulic cylinders. The hydraulic pressure for each cylinder is regulated by servo-valves which are controlled by the PLC. The positions of the axes are measured by means of MTS Temposonic displacement sensors (R series). A PID control loop (similar to the force control loop in the control system diagram of Figure 4.2) controls each axis.

4.2. Z-force Measurement and Z-force Control

The bed of the PDS platform is mounted on four load cells, one of which is shown in Figure 4.1.

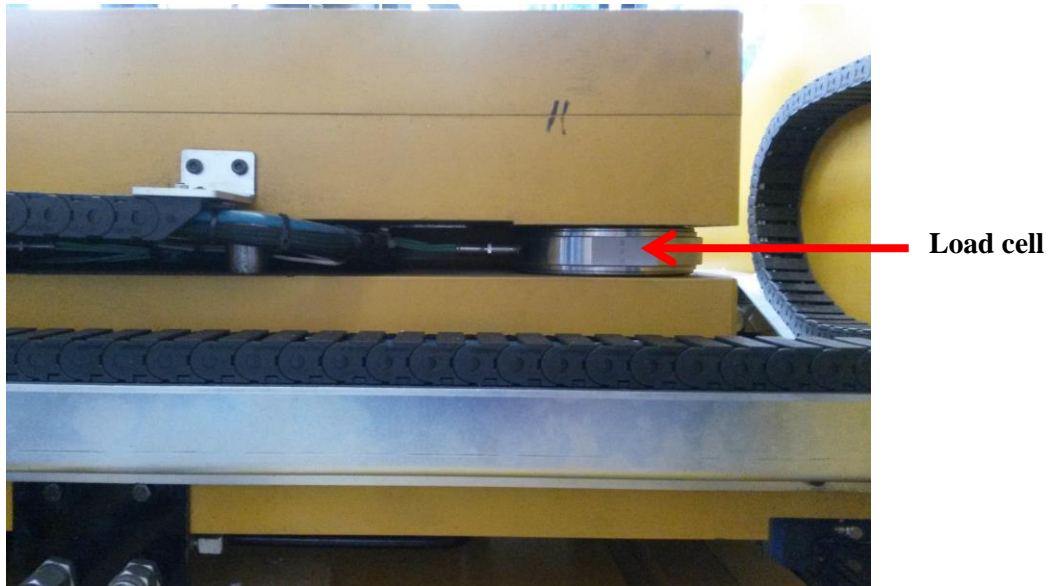


Figure 4.1. One of four of the PDS bed load cells

The load cells measure force along three axes. The force measurements from the four load cells are used to calculate the resultant x-force, y-force and z-force applied to the bed and weldment by the weld tool. All forces are logged by the machine during a weld for the purpose of data analysis. The forge force (z-force) control system diagram (see Figure 4.2) defines the interaction of the system components.

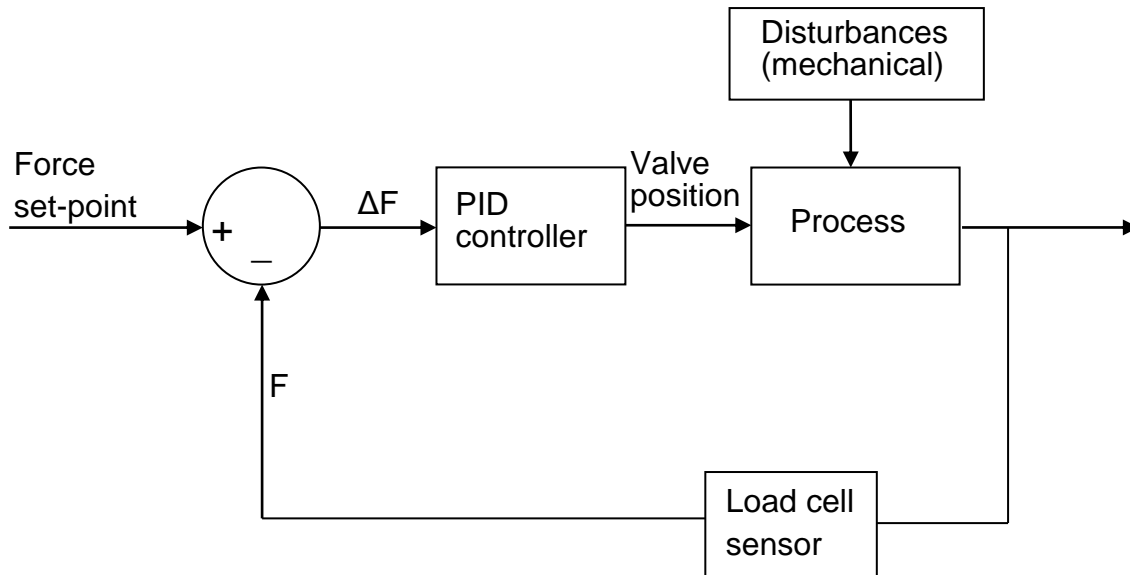


Figure 4.2. Forge force control system diagram

The operator programs a force set-point into the weld program, the load cells provide the forge force feedback signal and the error signal (ΔF) is then used by the PID control algorithm in order to perform necessary control calculations based on the dynamics of the system. The PID output provides a command signal for the z-axis hydraulic servo-valve position. The valve is controlled such that it regulates the hydraulic pressure appropriately in order to maintain the forge force set-point. Mechanical disturbances affecting the process (forge force in this case) such as deflection of the machine bed are accounted for by the PID controller because the controller gains have been set such that the system exhibits good disturbance rejection.

4.3. Feed Rate Control

The control system diagram (see Figure 4.3) for controlling weld traverse speed (x-velocity or feed rate) defines the interaction of the system components.

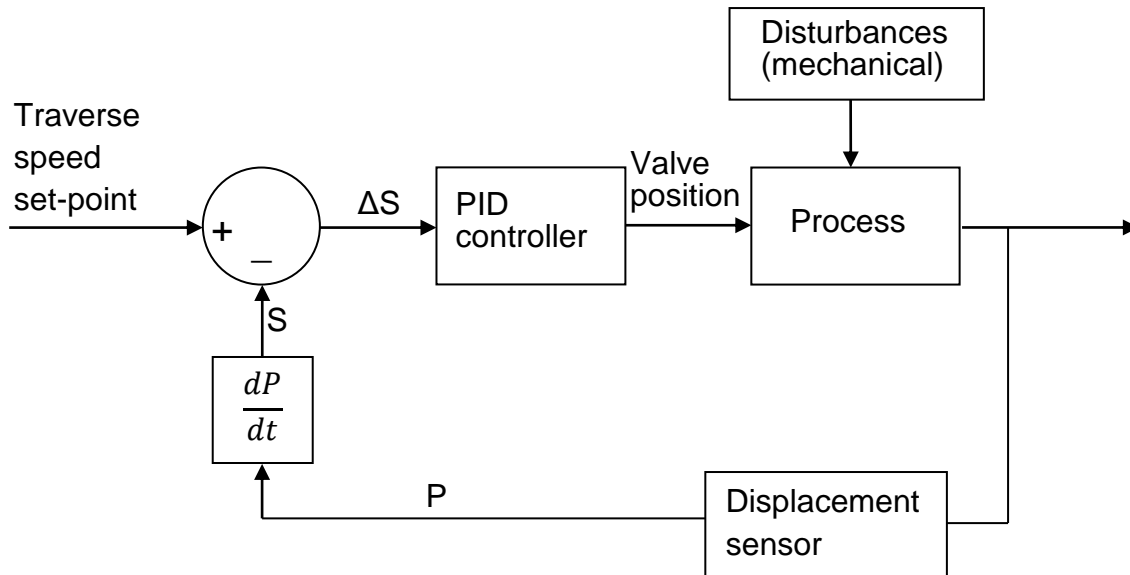


Figure 4.3. Feed-rate control system diagram

The operator programs the traverse speed requirement into the weld program which is the traverse speed set-point. The PLC calculates the derivative of the x-axis displacement position sensor output (P) which results in the x-axis velocity (S) feedback signal. The error signal (ΔS) is then used by the PID controller in order to perform necessary control calculations based on the dynamics of the system. The PID output provides a command signal for the x-axis hydraulic servo-valve position. The valve is controlled such that it adjusts the hydraulic pressure (and hence x-force) appropriately in order to maintain the traverse speed set-point. Mechanical disturbances affecting the process, such as variations in the resistance of the material in front of the tool are accounted for by the PID controller because the controller gains have been set such that the system exhibits good disturbance rejection.

4.4. Summary

This chapter defines various machine control components which were implemented on the machine prior to the initiation of this study. These components include: the main controller for the PDS platform and how it interfaces with the operator; the driving mechanisms for the machine axes and the spindle as well as their respective controlling devices; the force sensors and the manner in which they are laid out on the machine. The control loop for force control and the control loop for weld traverse speed control were outlined in this chapter.

Chapter 5

Temperature Control Design and Verification

This chapter explains in detail the manner in which the experiments were conducted and the results of this study acquired. The procedure followed in the development and testing of the temperature control system is covered in detail. A mathematical model of the relationship between FSW temperature and machine spindle speed was generated using Matlab. The weld temperature response was compared to the response of the model; both of which using the PID controller gains determined from the Ziegler Nichols tuning method ^[3] (see Section 5.3.3). In addition to this, alternative PID controllers were generated using two Matlab controller development tools. The response of each controller was simulated (in Matlab Simulink) on the same scope as the model which was simulated with the PID controller gains found from the Ziegler Nichols tuning method ^[3]. A clear comparison can therefore be seen as the responses are on the same set of axes (see Section 5.5). Experimental welds, which introduce a thermal disturbance between the middle work-piece clamps, were conducted. The data from the experiments is analysed and the behaviour of the control system discussed in this chapter. Furthermore, tensile testing was conducted on these experimental welds in order to generate an indication of the weld quality along the weld length. Weld strength consistency is discussed in this chapter.

5.1. Establishment of the Process Window

The initial set of welds conducted in the establishment of the process parameter window consisted of five welds. These welds were conducted on the MTS FSW platform in position control mode because the forge force requirement for the particular weld setup was unknown. Setting the forge force too high (in a force control mode weld) for a particular weld setup would cause the tool to over plunge, into the backing plate. This could cause damage to the tool and/or the backing plate.

The machine sensor data is automatically logged by the machine during a weld. From the data logs of “Weld 3”, “Weld 4” and “Weld 5”, the process forge force and weld zone temperature was plotted in order to determine the maximum forge force required (and allowed at a given weld zone temperature) for the welds conducted in the remainder of this study (welds which were conducted force control mode). The reactive forge force applied by the machine, which was required to maintain the vertical position of the tool, can be seen from the graphs (see “Weld 5” in Figure 5.2). For the full set of weld graphs, see **Appendix B**.

“Weld 1” and “Weld 2” were conducted with 1° and 2° of tool tilt respectively. As a starting point, spindle speed was 600 rev/min which was slightly above the spindle speed suggested by literature for a weld traverse speed of 200 mm/min^[4]. “Weld 1” rendered a good surface finish and “Weld 2” rendered a rough surface finish. A higher forge force was experienced by the material in “Weld 2” than the material in “Weld 1” which can be seen in Figure 5.1.

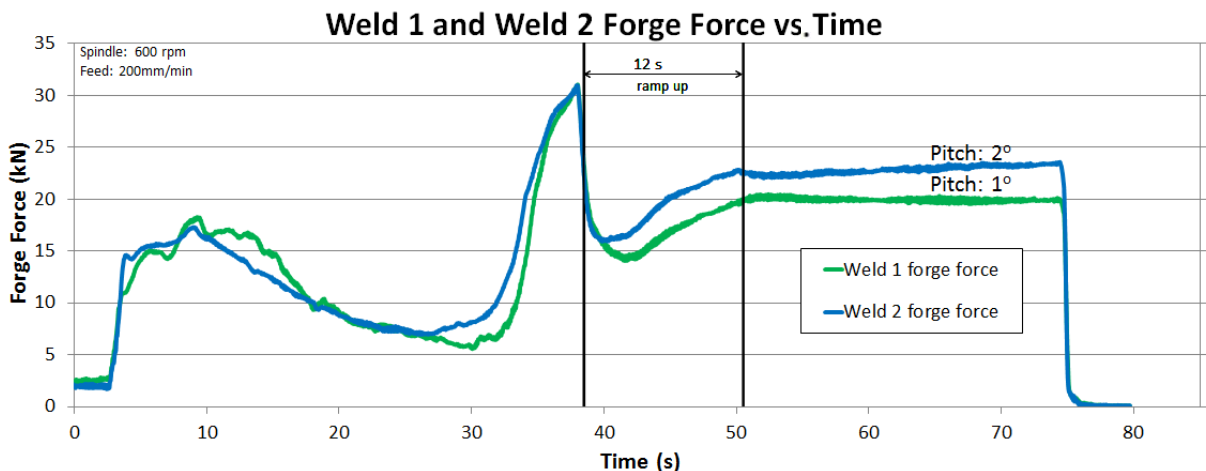


Figure 5.1. Forge forces of weld 1 and weld 2

The researcher thus decided to make a compromise between good surface finish and high forge force by utilising 1.5° of tool tilt for the remaining welds in this study. Various other conditions have an effect on weld surface finish such as temperature

(evident in welds done by the researcher) although investigation of surface finish does not form part of the scope of this study.

“Weld 3” and “Weld 4” introduced spindle speed increases in order to determine the approximate upper limit of the process window regarding spindle speed. “Weld 3” and “Weld 4” were conducted with spindle speed of 700 rev/min and 800 rev/min respectively. Welds conducted with higher spindle speed experienced a lower reactive forge force generated by the machine. The higher spindle speed applies a higher energy input rate to the weld zone which causes the weld zone material temperature to rise, which becomes softer and is therefore displaced by the tool at a lower forge force. “Weld 4” and “Weld 5” (800 rev/min) were the only welds which experienced less than 20 kN forge force for the majority of the weld length after the ramp up stage. The forge force in “Weld 5” reached 20 kN near the end of the weld, which also corresponds to the hottest area of the weld. This suggests that it is safe to run a weld of this particular setup with 800 rev/min spindle speed and 20 kN forge force without the risk of over plunging (into the backing plate). The graph showing temperature and reactive forge force versus time is shown in Figure 5.2.

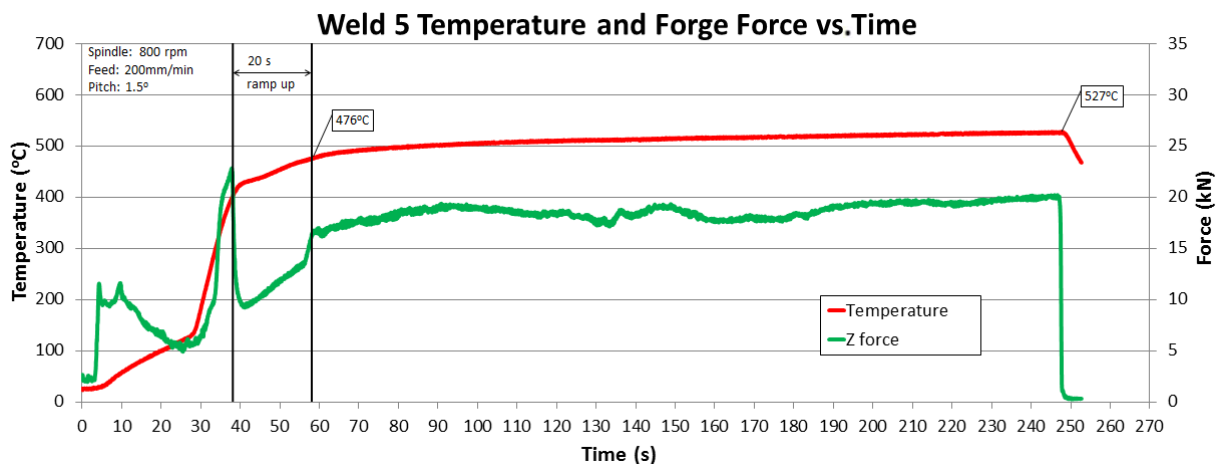


Figure 5.2. Position control weld 5

The researcher thus decided that the forge force of 20 kN would be used for the remaining welds in this study. It was also decided that 800 rev/min would be the preliminary upper limit for the spindle speed. A further six welds were conducted in

force control in order to confirm the maximum spindle speed and determine the minimum spindle speed. See **Appendix C** for the full set of weld graphs. These welds were numbered 1.1 to 1.6 and were force control mode welds (20 kN forge force). The upper limit for spindle speed was confirmed by “Weld 1.4” (800 rev/min spindle speed). For “Weld 1.4”, the region where the tool reached its maximum plunge depth, faint tool marks could be observed for a short distance on the backing plate, meaning that the tool skimmed the backing plate lightly in this region. This meant that the spindle speed could not be increased further (confirming the upper spindle speed limit). The graph for this weld can be seen in Figure 5.3.

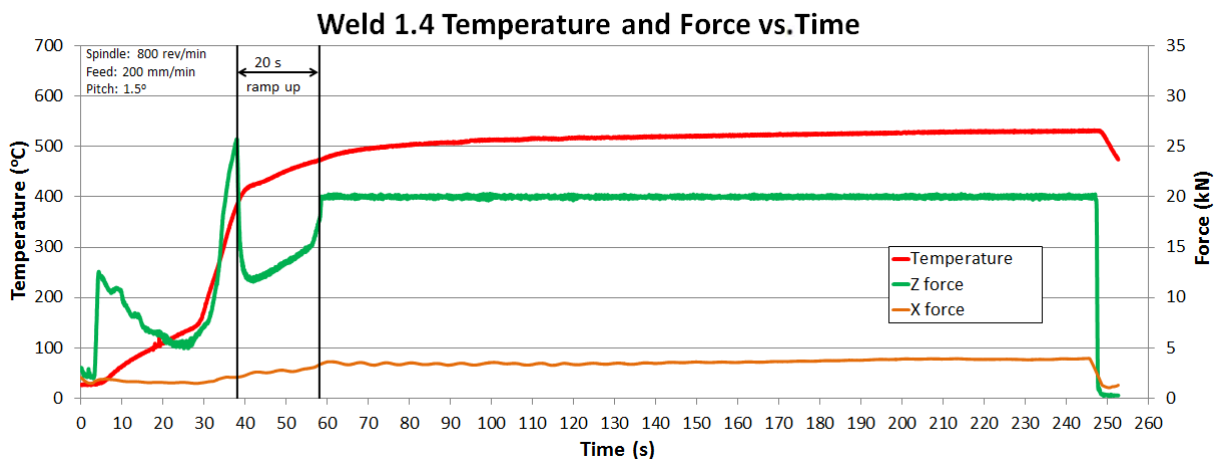


Figure 5.3. Weld 1.4

The next objective was to determine the lower limit for spindle speed. This procedure was the process of most risk in the study. Decreasing spindle speed decreases the plasticised state of the material (lower energy input rate allows cooler weld zone material), causing the machine to apply an increase of x-force (in the traverse direction). The machine does this in order to maintain the weld traverse speed set by the operator (200 mm/min). Decreasing the spindle speed excessively could cause tool seizure or failure (the tool pin may fracture).

A finite element analysis was done on the tool in order to determine the limit of x-force which could be applied to the pin. In reality, the x-force applied by the machine is taken up partially by the tool shoulder (caused by the plunge depth and tool tilt angle)

and the remainder is distributed along the tool pin. In addition to this, the weld zone material is cooler near the bottom (evidenced by Section 2.3) which implies that a greater amount of the x-force (supported by the tool pin) is supported by the lower portion of the tool pin. The proportion of the x-force supported by the pin is unknown for this particular weld setup. For the analysis, the worst case scenario is therefore used and assumes that the entire x-force is supported by the pin tip. See Figure 5.4.

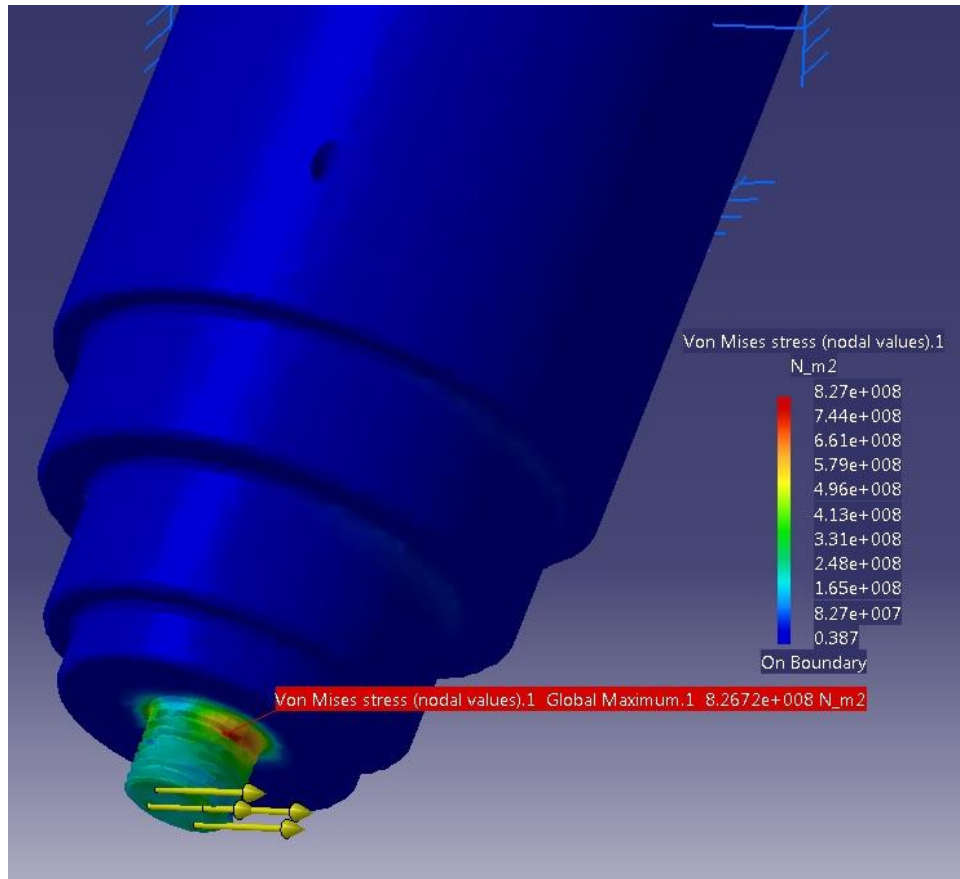


Figure 5.4. FSW tool FEA analysis

The tool analysis showed that for an x-force of 5 kN applied to the pin, the area of maximum bending moment (in combination with a stress concentration caused by the thread) experienced a maximum stress of approximately 827 MPa. A section view revealed that the material at the bottom of the thermocouple pockets experienced approximately 575 MPa as shown in Figure 5.5.

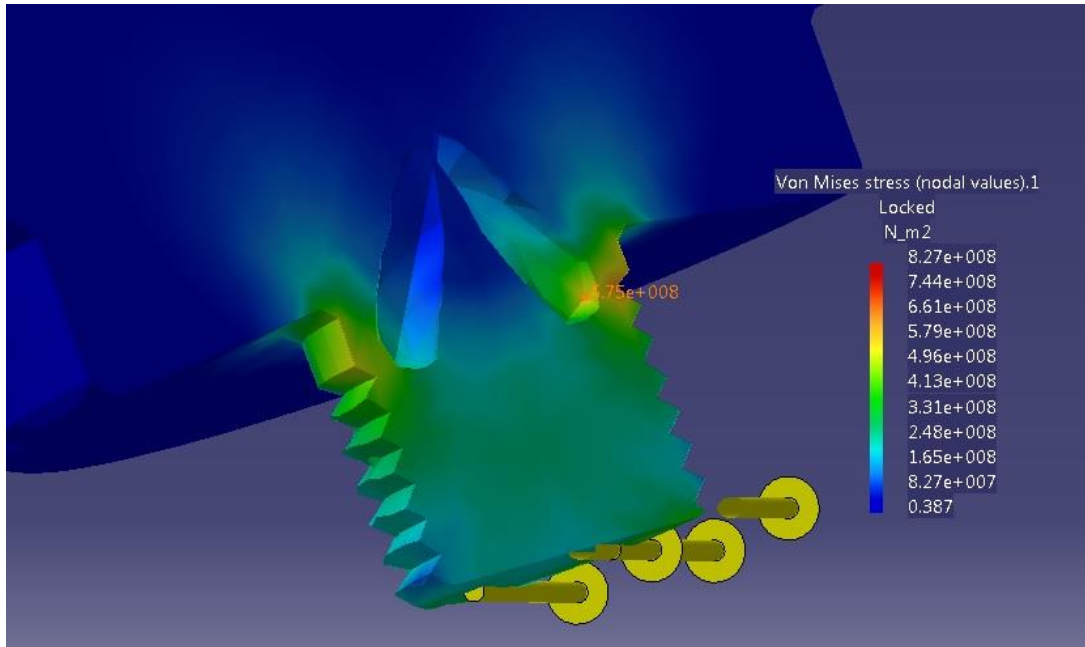


Figure 5.5. FEA thermocouple section view

The Bohler datasheet for W302 tool steel shows material strength after hardening (approximately 54 HRC) for various operating temperatures. Specifically, the 0.2 percent proof stress at 500°C (corresponding to weld temperature in this study) is 900 MPa. The safety factor if the tool were to experience the extreme case modelled in the FEA analysis would be 1.09 which would not be very safe as 1.5 would be desirable. Considering that a portion of the x-force is supported by the tool shoulder and the remaining x-force is distributed along the pin length in reality, it was decided that 5 kN would be a relatively safe limit for x-force when determining the lower spindle speed limit.

For “Weld 1.5”, spindle speed was 400 rev/min. The x-force was checked from the weld log data. The graphs of x-force for “Weld 1.1” to “Weld 1.6” in **Appendix C** show smoothed force data by means of a moving average for clarity of the graphs. The oscillation of the x-force could be attributed to the inevitable small amount of run-out of the tool. This was evident by the frequency of the force oscillation matching the frequency of the spindle rotation. The z-force graphs, however, are plotted from raw

force data. The maximum x-force recorded in “Weld 1.1”, “Weld 1.5” and “Weld 1.6” are as follows:

- “Weld 1.1” (spindle speed: 500 rev/min): 4.55 kN
- “Weld 1.5” (spindle speed: 400 rev/min): 4.97 kN
- “Weld 1.6” (spindle speed: 300 rev/min): 5.57 kN

The spindle speed was not decreased further than 300 rev/min, as it would risk tool failure and the spindle speed lower limit was therefore set at 300 rev/min. The graph of “Weld 1.6” shows that the average x-force is less than 5 kN.

Process parameters for the welds conducted in the remainder of the study:

- Forge force: 20 kN
- Traverse speed: 200 mm/min
- Spindle speed range: 300 rev/min to 800 rev/min

5.2. Temperature Response to Spindle Speed Changes

Preliminary work was carried out on the MTS FSW platform (see Section 3.4). The work investigated weld zone temperature response to changes of spindle speed whilst all other weld parameters, including weld traverse speed and weld forge force, were maintained constant. The weld consisted of five regions which include plunge, ramp up, spindle speed stage 1 (referred to as simply stage 1), spindle speed stage 2 (referred to as simply stage 2) and spindle speed stage 3 (referred to as simply stage 3). The plunge region is the portion where the rotating tool pin is plunged into the material until the tool shoulder comes into contact with the surface of the plate to be welded. The ramp up region is the portion of the weld where the tool begins to move in the traverse direction. The tool is in position control until the end of this region. The tool accelerates slowly (to build up the temperature of the weld zone) over 20 mm and reaches the weld traverse speed at the end of this region. The weld then

enters stage 1 where it stops accelerating (traverse speed is constant at 200 mm/min from this point to the end of the weld) and goes into force control mode (set to 20 kN forge force). The spindle speed is the same in all regions except for stage 2. The spindle speed in this stage is either increased or decreased by 100 rev/min relative to the other regions of the weld.

The temperature graphs of two welds are shown in Figure 5.6. The axis limits are set in order to show the temperature of the weld zone from the beginning to the end of the weld. The temperature change in stage 2 is small relative to the range of temperature of the entire weld and Figure 5.6 is shown in order to put this temperature change into perspective. Subsequent figures show smaller axis ranges in order to make the temperature changes of stage 2 clearer. The legend of each graph is labelled with the spindle speed for each of the three spindle speed stages.

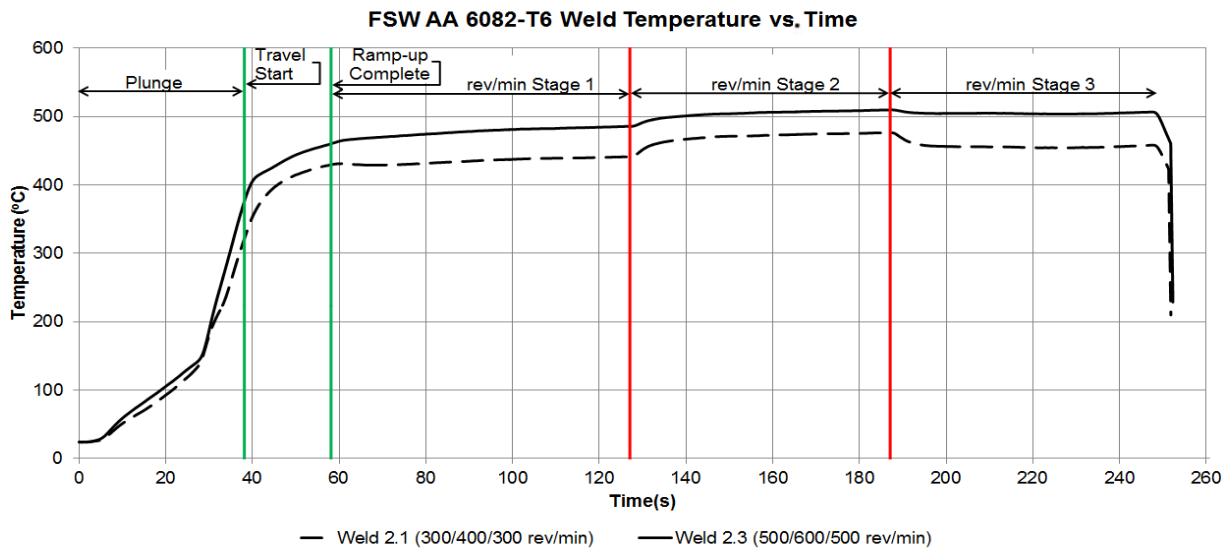


Figure 5.6. Full weld temperature plot

The graphs in Figure 5.7 show that for the low average spindle speed welds (e.g. “Weld 2.1”), the spindle speed increase, of 100 rev/min in stage 2, results in a larger temperature increase than for the higher average spindle speed welds (e.g. “Weld 2.3”). There are two reasons for this. The first is because the material which is at a higher temperature is more plasticised (softer) which results in lower torque between

the tool and the weldment. The 100 rev/min increase in spindle speed therefore results in a smaller increase of energy input rate for the higher temperature welds. The second reason is that the weld zone temperature is higher for the high average spindle speed welds which results in a larger temperature gradient between the weld zone material and the surrounding material. The heat is therefore conducted away from the weld zone at a higher rate for the higher temperature welds.

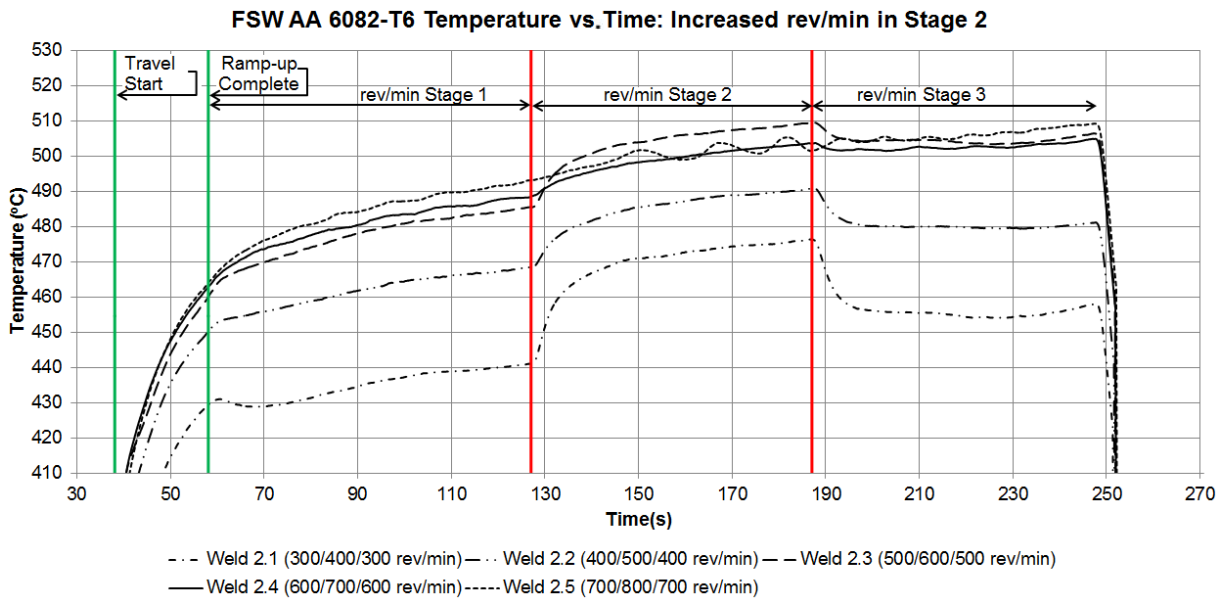


Figure 5.7. Increased spindle speed in stage 2

The graph of “Weld 2.1” (see Figure 5.7 and Figure 5.8) indicates that the increase of spindle speed (300 rev/min to 400 rev/min) in stage 2 causes a weld zone temperature increase, a spindle torque decrease and a spindle energy input rate increase. The total energy input rate of the weld is equal to the sum of spindle power and traverse axis power (rate of work done in the welding direction).

The weld is conducted at constant traverse speed (200 mm/min) which means that in stage 2, when the material temperature rises and the material softens, the traverse force (x-force) decreases, causing a decrease of traverse energy input rate into the weld. In order to quantify this amount, the traverse power decrease from stage 1 to stage 2 was calculated. The x-force average of “Weld 2.1” was taken between 100

seconds and 120 seconds for stage 1 and between 140 seconds and 160 seconds in stage 2. The power for each stage is calculated using Equation 5.1.

$$P_t = f_x \times \frac{t_s}{60} \quad \text{Equation 5.1}$$

where

P_t	is the traverse power (J/s)
f_x	is the force in the welding direction (kN)
t_s	is the weld traverse speed (mm/min)

Equation 5.1 is derived from the law that energy (work done) is equal to the product of force and displacement. The results of the power calculations are shown in Table 5.1.

Stage	Data range (s)	Average x-force (kN)	Average traverse power (J/s)
1	100 to 120	4.27	14.23
2	140 to 160	3.88	12.93

Table 5.1. Weld 2.1 traverse power data for stage 1 and stage 2

From stage 1 to stage 2, the traverse energy input rate decreased by 1.3 J/s. This decrease is small relative to the increase of spindle energy input rate in stage 2 of the weld. The change in total energy input rate introduced in stage 2 of weld 2.1 (see Figure 5.8) can therefore be approximated by the change of spindle energy input rate.

The spindle power is equal to the product of spindle torque and spindle angular velocity. In stage 2, the increase of angular velocity outweighs the decrease of torque in the product calculation resulting in an overall increase in spindle power (spindle energy input rate).

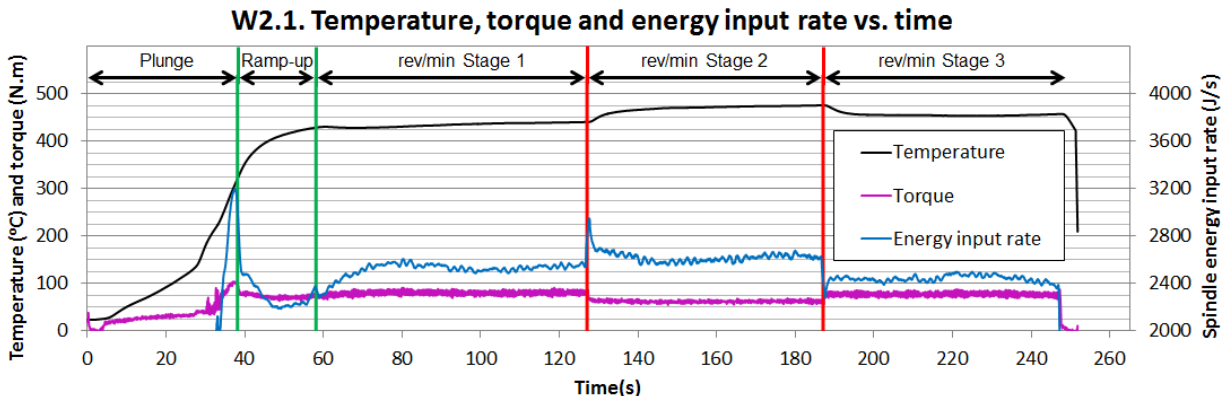


Figure 5.8. W2.1. Spindle energy input rate, torque and temperature versus time

For closer inspection of the weld zone temperature behaviour of “Weld 2.1”, refer to Figure 5.7.

The graphs in Figure 5.9 show that for low spindle speed welds, the spindle speed decrease of 100 rev/min in stage 2 results in a larger temperature decrease than for the higher spindle speed welds. The reasoning is the same as for increasing spindle speed in stage 2 (see the discussion around Figure 5.7). The spindle torque at low weld zone temperature is larger than for high weld zone temperature. This results in a larger energy input rate decrease for a set amount of spindle speed decrease (100 rev/min in this case).

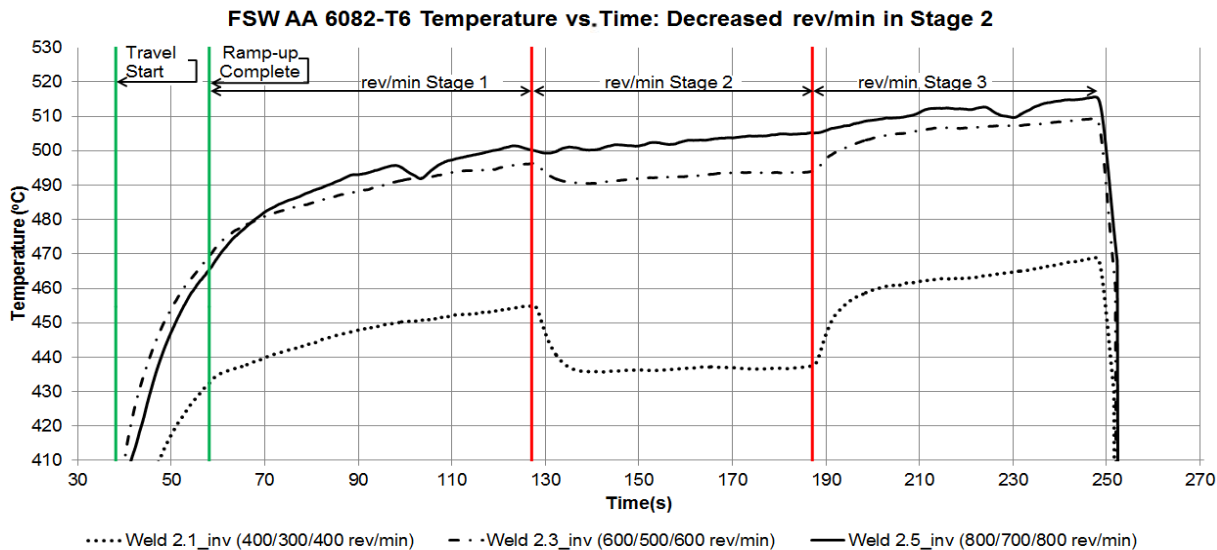


Figure 5.9. Decreased spindle speed in stage 2

The following two figures (Figure 5.10 and Figure 5.11) show a comparison of welds executed with inverted spindle speed stages as per Table 5.2.

Weld number	Spindle speed stage 1 (rev/min)	Spindle speed stage 2 (rev/min)	Spindle speed stage 3 (rev/min)	Figure showing weld temperature
2.1	300	400	300	Figure 5.10
2.1_inv	400	300	400	
2.3	500	600	500	Figure 5.11
2.3_inv	600	500	600	

Table 5.2. Weld stage speeds (inverted welds)

“Weld 2.1” achieved a considerably higher temperature than “Weld 2.1_inv” in stage 2. From the weld graphs it is clear that this would remain the case if “Weld 2.1_inv” did not experience the decrease of spindle speed in stage 2. The effect is explained by the positive energy input rate spike at the beginning of stage 2 of “Weld 2.1” which can be seen in Figure 5.8. At the end of stage 1, the spindle torque is approximately constant. The moment at which the spindle speed is increased, the energy input rate (product of torque and angular velocity) spikes because the spindle torque is high (from stage 1) and the spindle speed suddenly increases (to the value for stage 2). The temperature of the material then increases causing a decrease of spindle torque. The energy input rate therefore decreases as the weld progresses in stage 2.

The same principle applies for “Weld 2.1_inv” which experiences a spike decrease in energy input rate as it enters stage 2. The spindle torque is low due to the higher temperature in stage 1 and the sudden decrease of spindle speed (to the value for stage 2) causes the spike decrease in energy input rate. The material therefore cools dramatically. This causes an increase of spindle torque and the energy input rate therefore increases after the spike decrease.

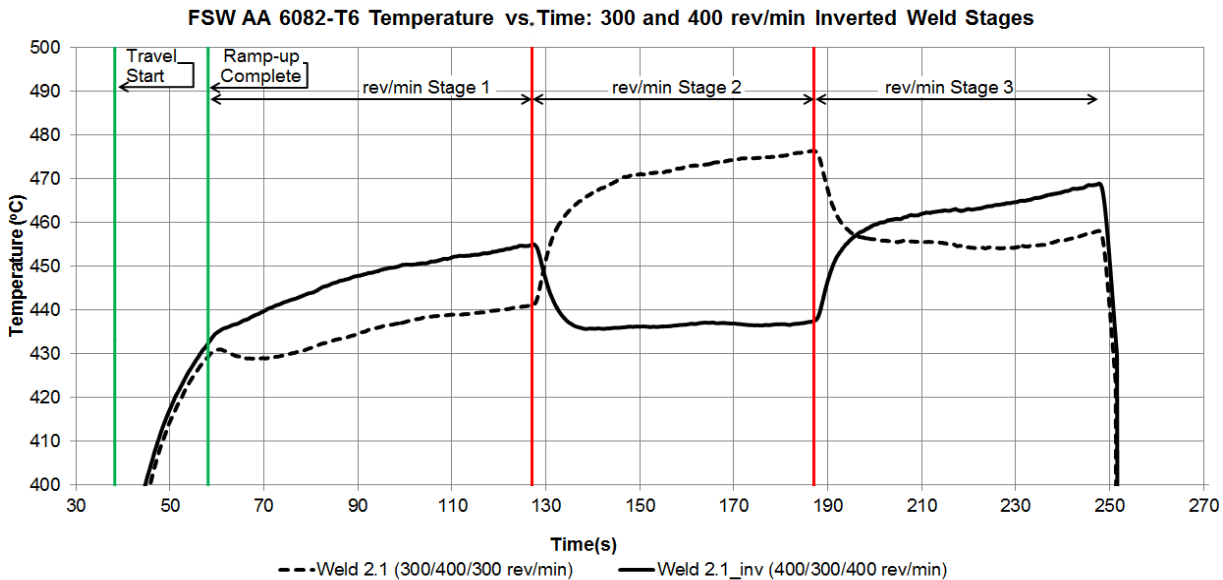


Figure 5.10. Low spindle speed comparison of inverted weld stages

“Weld 2.3” and “Weld 2.3_inv” (see Figure 5.11) are conducted at higher spindle speeds than “Weld 2.1” and “Weld 2.1_inv”. The effect observed in the comparison of “Weld 2.1” and “Weld 2.1_inv” is evident in the comparison of “Weld 2.3” and “Weld 2.3_inv”, although the magnitude of the temperature changes in stage 2 are smaller. The main cause is the smaller spindle torque difference between these two welds due to their higher weld zone temperatures (relative to “Weld 2.1” and “Weld 2.1_inv”).

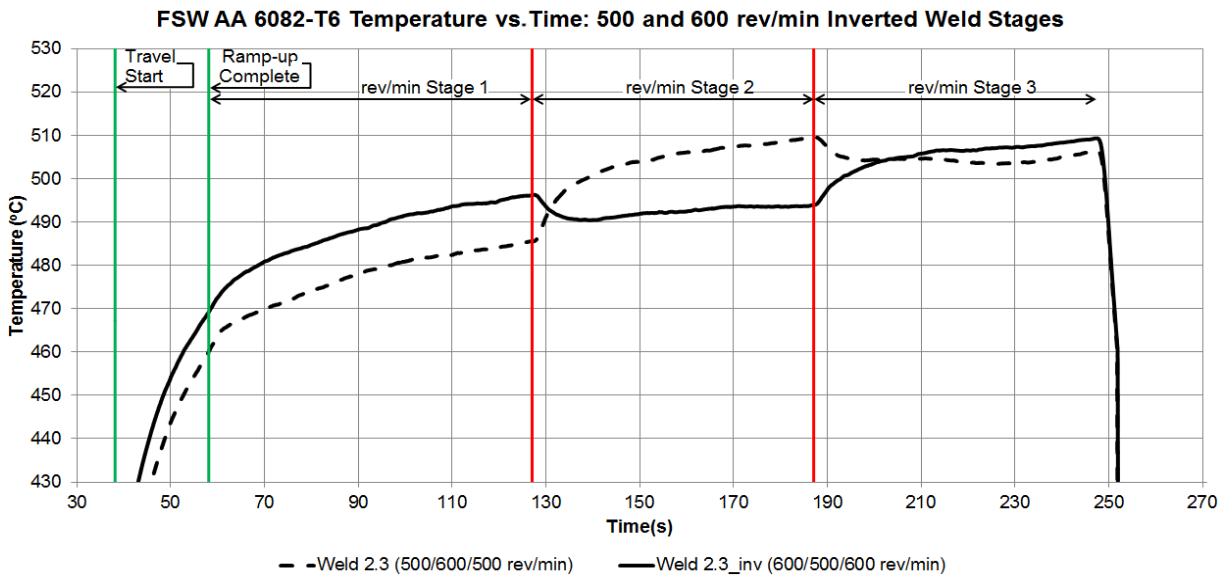


Figure 5.11. High spindle speed comparison of inverted weld stages

The effect observed in Figure 5.10 and Figure 5.11 suggests that the temperature dynamics of FSW are not linear. The full set of weld graphs for this section can be seen in **Appendix D**.

5.3. Algorithm Development

The control architecture implemented in this study for temperature control of FSW consisted of a “Proportional Integral Derivative” (PID) controller. The system was tuned at a certain temperature (492°C). The performance of the control system was assessed at various welding temperatures ranging from 480°C to 530°C. Should the control architecture have been found to be unsuitable for FSW because of non-linearity of FSW temperature dynamics, a modified PID control architecture would have been implemented. This architecture would consist of scheduled gains where the system is tuned at various welding temperatures. The P, I and D gains obtained from the tuning would be placed in a matrix of controller gains versus temperature. According to the operating point of the system, linear interpolation is executed and the appropriate controller gains are selected for the controller as the control algorithm is executed. Should this architecture have been insufficient for FSW, alternative control structures would have been tested such as fuzzy logic and genetic algorithms.

PID control is considered by various researchers as insufficient control for FSW temperature because PID control requires that the dynamics of the system which it is controlling are approximately linear, which is not the case for weld zone temperature of FSW as shown in Section 5.2. Temperature of FSW relies on many process conditions. These conditions include spindle speed, traverse speed, forge force, the specific characteristics of the material being welded, heat dissipation into the backing plate, heat dissipation into the weldment clamps, heat dissipation into the tool and spindle head and other thermal disturbances. For the experiments conducted in this study, the traverse speed was kept constant at 200 mm/min, the forge force was constant at 20 kN, the material being welded originated from one aluminium sheet. The plate and clamp setup was identical for all welds being compared and the tool

geometry was not changed. Variations in external thermal disturbances were eliminated as far as possible and the thermal disturbances in the welds which specifically tested the control algorithm's disturbance rejection were maintained as consistent as possible. For these welds, thermal source and thermal sink disturbances were tested.

5.3.1. Control System Layout

The FSW process and temperature controller are shown in a control system diagram in Figure 5.12. The area demarcated by the dotted outline includes the physical FSW process together with all thermal disturbances, the thermocouple sensors, telemetry rotor and spindle drive (which receives the spindle speed command from the machine PLC and controls the servo motor accordingly). The process output regarding this study is weld zone temperature. The temperature measurements are sent from the rotating tool via the telemetry system which generates a 0 V to 10 V analog signal (for each thermocouple sensor). This analog signal is converted to a digital value via the PLC analog input card. The control algorithm is demarcated by the solid red outline in Figure 5.12. The algorithm was written on the FSW machine's main PLC. The temperature control algorithm uses the operator's temperature set-point (as well as a nominal spindle speed setting) command and the temperature feedback signal to generate a temperature error. This error is used in the PID control calculations (together with the PLC cycle time and various other parameters stored in memory) to calculate the spindle speed command required to drive the system towards zero error between the set-point and the feedback signal.

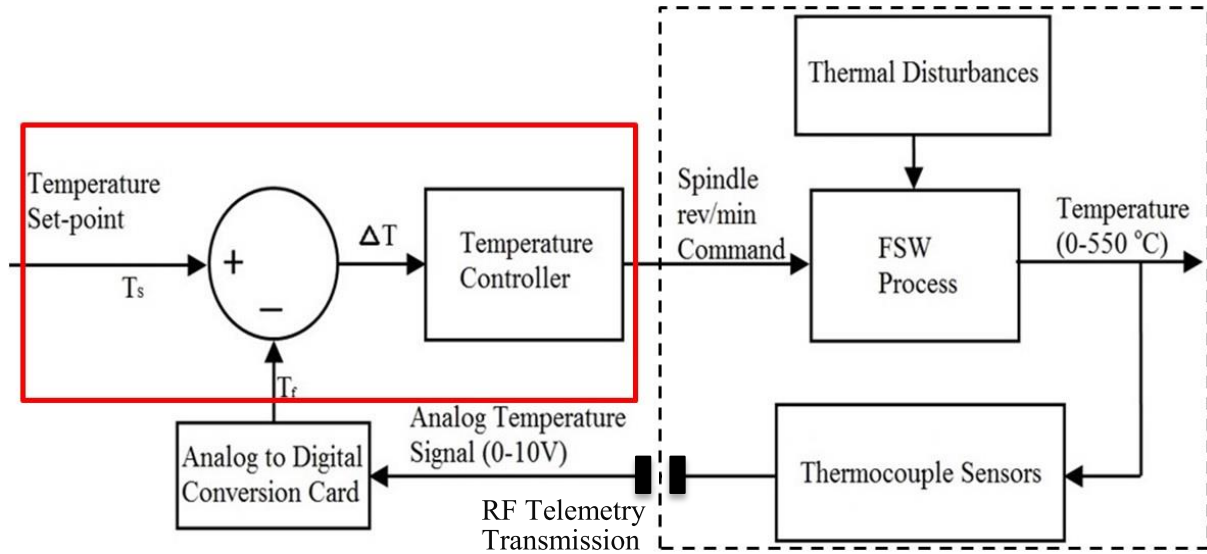


Figure 5.12. Control system diagram

The digital values (generated by the analog to digital conversion cards) representing the temperature feedback signal voltages are converted to temperature values according to their individual curve fit equations found from the thermocouple calibration process (see **Appendix A**).

5.3.2. Control Algorithm

Refer to the PID algorithm flow diagram shown in Figure 5.13, bearing in mind that the procedure is executed every program cycle of the PLC (one millisecond). The temperature control algorithm calculates the error term by subtracting the temperature feedback signal (average of the two thermocouples) from the operator set-point. The proportional term is calculated as the error term multiplied by the proportional gain (K_p). The integral term is a summation over time and is calculated by adding the product of the integral gain (K_i), PLC cycle time (dt) and the error term to the integral sum as it was after the previous program cycle. The derivative term is usually calculated as the rate of change of the error term although a sudden change in set-point will cause a spike in the derivative term. In this study, the derivative term is calculated as the rate of change of the temperature feedback signal. The only difference is that the rate of change of the temperature feedback signal is opposite in

sign to the rate of change of the error term and a sudden change in set-point will not generate a derivative spike. The derivative term is calculated as the difference between the temperature feedback signal and what the temperature feedback signal was in the previous program cycle, divided by the time over which the change took place (which is the PLC cycle time dt) and the quotient is multiplied by the derivative gain (K_d). The spindle speed command sent to the spindle drive is calculated as the sum of the nominal spindle speed value (estimated by the operator for the particular temperature set-point), the proportional term and the integral term; and the derivative term is subtracted from the sum (subtracted because of its sign which is determined as previously explained in this paragraph).

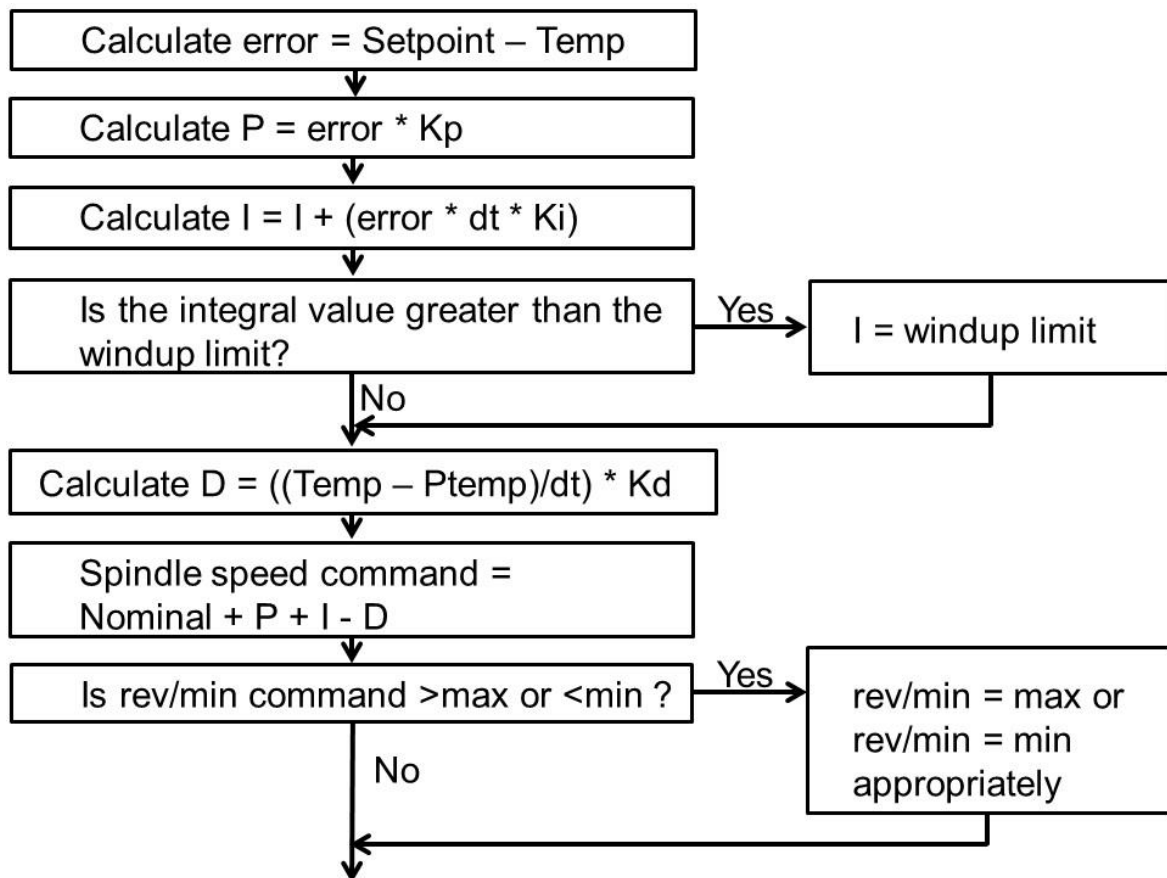


Figure 5.13. PID flow diagram

Should the error term be large and the system require a large amount of time to reach the set-point, the integral term could wind-up to a large value which would require a

large amount of time to unwind after the system overshoots the set-point. This would magnify the amount which the system overshoots the set-point and the amount of time which is required to return the system to the set-point. A wind-up limit is therefore employed after the calculation of the integral term. If the integral term exceeds the wind-up limit (in either direction), the integral term is set equal to the wind-up limit which it exceeded. The nominal spindle speed value could be made unnecessary if the wind-up limit is set sufficiently large although this would degrade the system performance regarding set-points for which the system requires a relatively large amount time to realise. It is also important to avoid setting the wind-up limit too low. The main purpose of the integral term is to eliminate steady state error. Setting the limit too low could cause the system to be unable to eliminate any steady-state error. For this study, each unit of the integral term corresponds to 1 rev/min in the spindle speed command. The wind-up limit which worked well was 150 rev/min (in either direction depending on the sign of the error term). This meant that the nominal value set by the operator for the particular temperature set-point needed to be within 150 rev/min of the actual spindle speed required to maintain the set-point temperature. See **Appendix E, page E-1 to page E-4** for the PLC code.

5.3.3. Ziegler Nichols Tuning Method^[3]

Refer to **Appendix E** for the set of algorithm tuning weld graphs. In order to determine appropriate K_p, K_i and K_d gains for the control system, the Ziegler Nichols tuning method^[3] was utilised. The procedure is conducted in the following manner^[3]:

1. Set K_p, K_i and K_d gains to zero.
2. Begin a weld with a specific temperature set-point (492°C was used).
3. Slowly increase K_p until the ultimate gain value (K_u) reached, where the system output (temperature) oscillates with constant amplitude.
4. Measure the oscillation period (T_u).
5. Calculate PID controller gains according to Equation 5.2 to Equation 5.4.

$$K_p = 0.6K_u$$

Equation 5.2 ^[3]

$$K_i = (2K_p) / T_u$$

Equation 5.3 ^[3]

$$K_d = (K_p \times T_u) / 8$$

Equation 5.4 ^[3]

Step 3 increases the proportional gain until the system becomes undamped. Damping of a PID controlled system originates from two components of the system: the physical damping of the process being controlled and the damping added by the derivative term of the controller. The Ziegler Nichols tuning method ^[3] identifies sufficient system characteristics necessary to calculate appropriate controller gains. The inverse of the output oscillation period is equal to the natural frequency of the system and the critical gain is the maximum controller gain which can be set before the actuator (spindle in this case) would drive the system into an unstable condition. Increasing the proportional gain (with K_i and K_d gains equal to zero) effectively adds driving force to the system which overcomes the physical damping of the process (because zero derivative gain infers that the controller does not add any damping to the system). When the system reaches constant oscillation, the physical damping of the system is effectively cancelled by the driving force generated by the proportional component of the controller. This critical value for the proportional gain is therefore representative of the physical damping in the system.

The live view of temperature was monitored on the machine's human machine interface (HMI) for step 3. After step 1, step 2 and step 3, the weld data was plotted, which is shown in Figure 5.14.

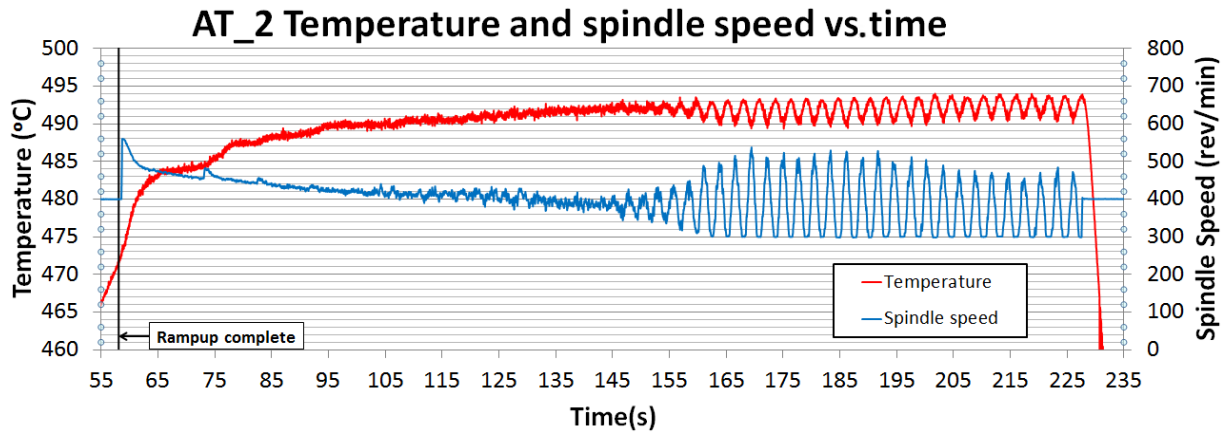


Figure 5.14. Weld AT_2

Close to constant oscillation was observed near the end of “Weld AT_2”. “Weld AT_3” was begun with the proportional gain set as it was at the end of “Weld AT_2”. This second tuning weld was conducted so that the researcher could obtain the critical gain more accurately. The graph for “Weld AT_3” is shown in Figure 5.15.

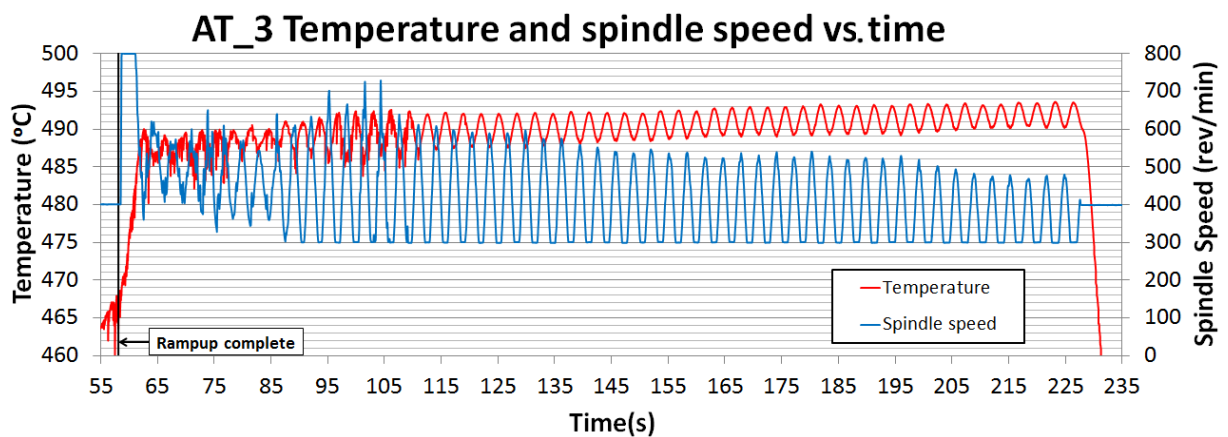


Figure 5.15. Weld AT_3

The ultimate gain (K_u) was found to be 63.5 and from the graph, the period of the oscillation (T_u) was found to be 3.2059 s. The PID gains were calculated according to the Ziegler Nichols equations:

$$K_p = 0.6K_u = 0.6 \times 63.5 = 38.1 \quad \text{Equation 5.5}^{[3]}$$

$$K_i = (2K_p) / T_u = (2 \times 38.1) / 3.2059 = 23.769 \quad \text{Equation 5.6}^{[3]}$$

$$K_d = (K_p \times T_u) / 8 = (38.1 \times 3.2059) / 8 = 15.268 \quad \text{Equation 5.7}^{[3]}$$

5.4. Algorithm Performance Testing

The parameters determined by the Ziegler Nichols tuning ^[3] were implemented in the control algorithm. “Weld AT_4” was done to test the performance of the control system given step input changes which include a rise to 491°C, after stabilisation, another step change to 541°C is introduced. This tests the heating to a set-point response of the system. The set-point then steps back down to 491°C in order to test the cooling to a set-point response of the system. The integral wind-up limit was initially set high in order to allow the integral to behave approximately as it would have if there were no wind-up limit employed (set to 800 rev/min).

In Figure 5.16, it can be seen that for increasing temperature, the temperature control algorithm utilised maximum allowed spindle speed for both the low and high temperature set-points although the system required more time to achieve the higher set-point than the lower set-point. This is related to the rate of transfer of heat energy into and from the weld zone. Energy input rate depends on a number of process conditions. Three important factors include material plasticised condition (hard/soft affecting spindle torque), the spindle speed and the rate of heat conduction from the weld zone into the surrounding material. Regarding the low temperature set-point, the material is relatively cool, corresponding to high spindle torque required to maintain spindle speed. Increasing the spindle speed to the maximum limit at this temperature corresponds to a high energy input rate, allowing the weld zone temperature to approach the set-point at a high rate of change of temperature. On the contrary regarding the high temperature set-point, when the material is at a higher temperature, the material is more plasticised (softer) which corresponds to lower spindle torque. Energy input rate therefore decreases as temperature increases for a constant spindle speed (in this case 800 rev/min). The weld zone temperature therefore approaches the set-point at a lower rate of change of temperature for higher temperature set-points (as the spindle speed is limited to 800 rev/min). In addition to

this, as temperature in the weld zone increases, the rate of conduction of heat from the weld zone into the surrounding material increases according to the heat transfer equation (see Equation 5.8 ^[19]). This effect reduces the rate of change of temperature when the system approaches high weld zone temperatures.

$$\dot{Q} = k \times A \times \frac{\Delta T}{L} \quad \text{Equation 5.8}^{[19]}$$

where

- \dot{Q} is the heat energy flow rate (W or J/s).
- k is the thermal conductivity of the material (W/m.°C or J/m.°C.s).
- A is the area (m²) of the material through which the heat conducts.
- ΔT is the temperature difference (°C) over distance L .
- L is the distance (m) along the path of heat conduction over which the temperature drop ΔT is realised.

$$\alpha = \frac{k}{\rho c_p} \quad \text{Equation 5.9}^{[19]}$$

where

- α is the thermal diffusivity (m²/s) of the material.
- k is the thermal conductivity of the material (W/m.°C or J/m.°C.s).
- ρ is the density (kg/m³) of the material.
- c_p is the specific heat (J/kg.°C) of the material.

Equation 5.9 can be substituted into Equation 5.8 and then by integrating both sides of the equation with respect to time, the commonly known heat law (see Equation 5.10) can be derived. This shows that Equation 5.8 conforms to the heat law in Equation 5.10.

$$Q = m \times c_p \times \Delta T$$

Equation 5.10

where

Q is the amount of heat energy (J) required to change the material's temperature by ΔT .

m is the mass (kg) of the material.

c_p is the specific heat (J/kg.°C) of the material.

ΔT is the temperature change of the material (°C).

Considering Equation 5.8, the material's thermal conductivity (k) is approximately constant for the welding temperature range ^[19], the area (A) of the material through which heat is conducted from the weld zone is approximately constant, the length (L) between the weld zone and the surrounding material is constant, although the temperature gradient between the material in the weld zone and the surrounding material increases. This constitutes an increase in the rate of heat conducted away from the weld zone.

The longer time delay for the system to reach the high temperature set-point is thus explained by the decreasing energy input rate into the weld zone material and increasing heat energy output rate from the weld zone material as the weld zone temperature increases.

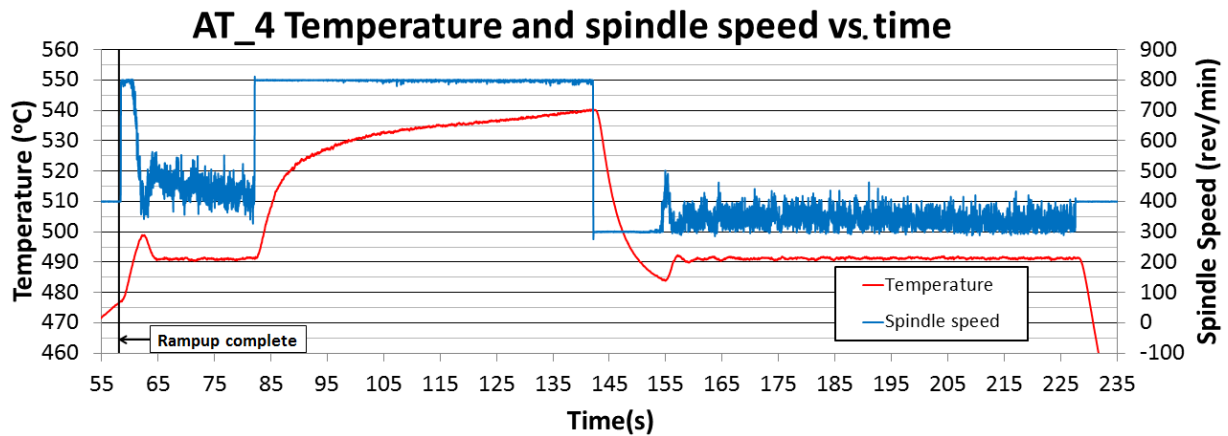


Figure 5.16. Weld AT_4

“Weld AT_4” yielded good response although the overshoot was relatively excessive (7.96°C) for the low temperature set-point. The high temperature set-point was achieved by the system at approximately the same time at which the set-point was programmed to revert to the low value. The steady state control was therefore not tested at the high temperature set-point in this weld.

The high temperature set-point was maintained for a longer duration in “Weld AT_5” (see Figure 5.17) to allow the system more time to achieve the temperature set-point. In addition to this, the wind-up limit for the integral was decreased to 100 rev/min in an effort to reduce the overshoot. This decrease in the wind-up limit worked well for decreasing the overshoot for the low temperature set-point although it caused the spindle speed to reduce from the maximum (800 rev/min) prematurely for the high temperature set-point (weld temperature was approximately 16°C below the set-point when the spindle speed began to reduce).

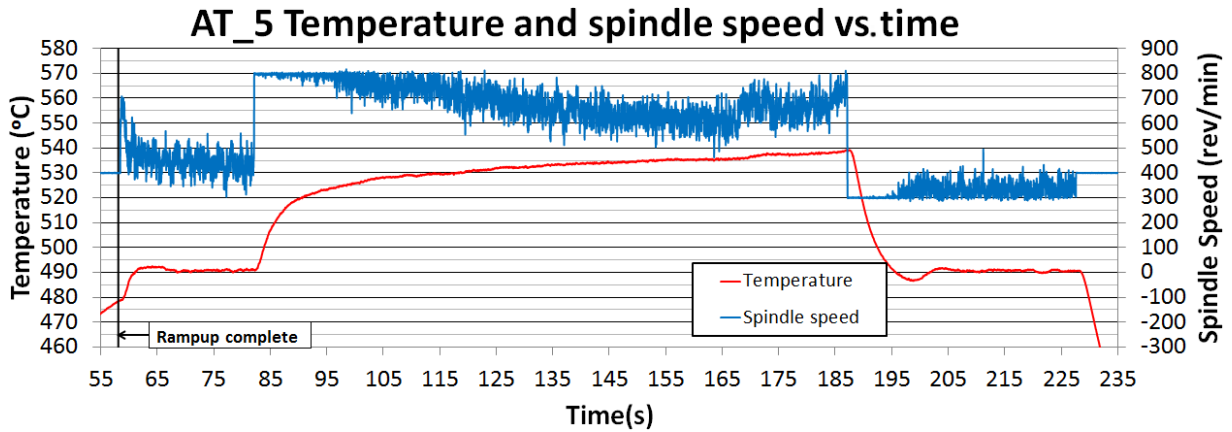


Figure 5.17. Weld AT_5

From “Weld AT_4”, it can be seen that when the system is at 491°C and the spindle is driven to the maximum speed of 800 rev/min, the weld zone temperature requires approximately 60 seconds to achieve the set-point of 540°C. No controller would be able to improve on the duration without an increased spindle speed limit.

From “Weld AT_4” it can be seen that a high set-point of 530°C would be achievable by the system in a more appropriate amount of time. From AT_4 the amount of time required for the system to achieve 530°C from 491°C would be approximately 17 seconds. This is reasonable considering that 530°C is the maximum temperature which the system is required to achieve.

An intermediate set-point was introduced for “Weld AT_6” onward. The set-points for heating and cooling are 481°C, 506°C and 530°C. “Weld AT_6” and “Weld AT_7” are essentially the same except that “Weld AT_7” has a reduced duration for maintaining the high temperature set-point in order to allow time for stabilisation after cooling to the final temperature set-point (see **Appendix E** for “Weld AT_6”). “Weld AT_7” is shown in Figure 5.18.

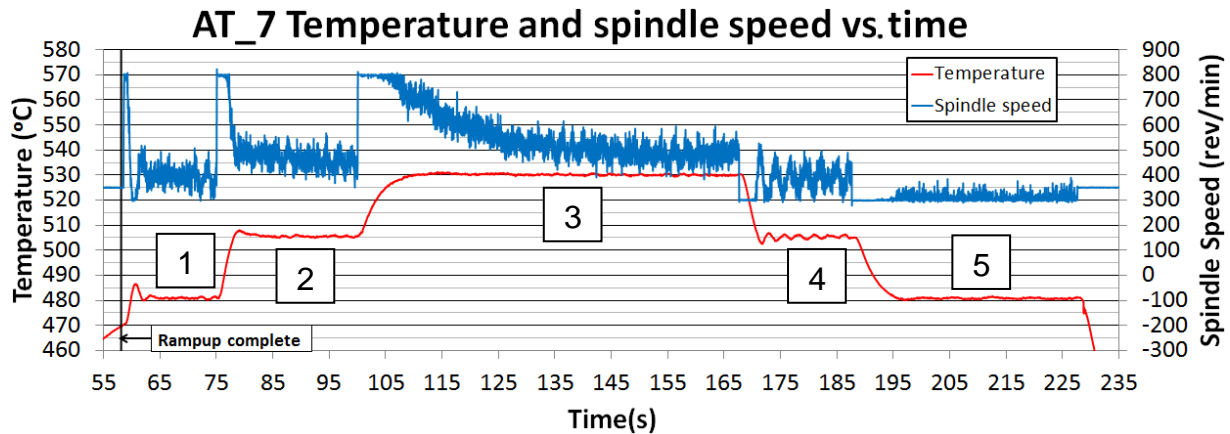


Figure 5.18. Weld AT_7

“Weld AT_7” shows that despite the fact that the system was tuned at 492°C (and assuming non-linearity of FSW temperature dynamics), the control system performance at all temperatures was acceptable and implementation of alternative control methods was not necessary.

The steady state error is defined for this system (with unitary feedback signal) as the difference between the output (measured temperature) and the set-point (operator defined) during steady state condition. The steady state error is approximately zero in all regions. This confirms that the nominal spindle speed value set by the operator was sufficiently accurate (within the integral wind-up limit of 150 rev/min) and the integral component of the controller effectively eliminated any error. There is an inherent steady state oscillation about the temperature set-point. The amplitudes of the steady state oscillation of temperature about the set-point in the five constant temperature regions (labelled in Figure 5.18) are as follows:

- Region 1 (481°C) : $\leq 1.13^{\circ}\text{C}$
- Region 2 (506°C) : $\leq 1.08^{\circ}\text{C}$
- Region 3 (530°C) : $\leq 0.89^{\circ}\text{C}$
- Region 4 (505°C) : $\leq 1.43^{\circ}\text{C}$
- Region 5 (481°C) : $\leq 0.70^{\circ}\text{C}$

Comparing region 2 and region 4, it is clear that the system does not behave linearly for heating versus cooling. The statistical data for the steady state temperature was determined using Microsoft Excel's data analysis tool. Table 5.3 shows the results. See **Appendix F** for the set of recorded data.

Region 2				
Mean (°C)	n	t-critical	Standard deviation	Uncertainty (95%)
505.5401	901	1.96	0.2802	0.0183

Region 4				
Mean (°C)	n	t-critical	Standard deviation	Uncertainty (95%)
505.4541	601	1.96	0.5540	0.0443

Table 5.3. AT_7 region 2 and region 4 statistics

The standard deviation of the temperature data in region 4 is greater than the standard deviation in region 2. The only difference in the process conditions is the position on the plate and the noticeably lower spindle speed required (in region 4) to maintain steady state condition at the set-point temperature. A plausible reason for the difference is that the temperature of the material surrounding the weld zone is higher in region 4 than in region 2 (because region 4 is nearer to the end of the weld and the previous region consisted of a higher temperature set-point) which causes a change in the dynamic characteristics of the process temperature. If the temperature of the material surrounding the weld zone is higher and the temperature of the weld zone is the same in both regions, region 4 has a smaller thermal gradient conducting heat away from the weld zone into the surrounding material. The steady state oscillation about the set-point was considered acceptable in both regions.

The researcher investigated the cause of the high frequency spindle speed oscillation observed in "Weld AT_4"; "Weld AT_5"; "Weld AT_6" and "Weld AT_7". The proportional, integral and derivative terms were logged during the "Weld AT_7". From

the highlighted consecutive derivative values (separated by 20 milliseconds) in the extract shown in Table 5.4, it is clearly seen that the derivative term is the cause of the high frequency oscillation in the spindle speed. See **Appendix G** for additional control data.

Weld AT_7 control data				
time	Error	Proportional	Integral	Derivative
145	-0.209297829	-7.974247282	-77.51202686	-744.7299345
145.02	-0.195362155	-7.443298098	-77.61429075	43.96846569
145.04	0.054693154	2.083809173	-77.64164141	22.82852918
145.06	0.084432622	3.216882896	-77.62047917	27.74369669
145.08	0.03042704	1.159270224	-77.60618563	29.46189609
145.1	0.055476033	2.11363687	-77.60854255	-651.005971
145.12	-0.005938994	-0.226275684	-77.60114914	165.1760844
145.14	-0.117756535	-4.48652399	-77.64014694	290.1891286
145.16	-0.235592413	-8.976070924	-77.71049024	536.2552022
145.18	-0.495768065	-18.88876326	-77.90437087	-390.0417655
145.2	-0.440249792	-16.77351709	-78.11738189	718.0757328
145.22	-0.235462059	-8.971104435	-78.26161222	-383.5979499
145.24	-0.136298411	-5.192969446	-78.36122699	-570.9418116
145.26	-0.050518967	-1.924772639	-78.41474566	-62.57417464
145.28	-0.027406962	-1.04420524	-78.40451387	160.3911832
145.3	-0.014260929	-0.543341395	-78.42947947	-508.3646151
145.32	-0.081256285	-3.095864444	-78.4646832	29.46391926

Table 5.4. AT_7 control data

Research on filtering the derivative term was conducted. In chapter 10, Section 10.5 of “Feedback Systems”^[9], derivative filtering is addressed. The reason for employing this filter is because the derivative term in the PID controller has high gain for high rates of change of temperature^[9]. If the temperature feedback signal contains noise, the derivative term performs as if the system is experiencing high rate of change of temperature (which is not the case). If two consecutive samples of the feedback signal happen to occur on a trough then a peak of the noise, the derivative term attempts to damp the high positive rate of change of the feedback (induced by noise and not temperature change of the system) with a high derivative term output. Conversely, if the two consecutive samples happen to fall on a peak, then a trough,

the derivative term changes sign (and magnitude) because according to the two samples, the rate of change of temperature is high in a negative direction. This explains the high magnitude alternating derivative terms highlighted in Table 5.4. The majority of the noise generated on the thermocouple signals by the electric spindle was filtered out successfully, although it was not eliminated completely. The small amount of noise remaining on the thermocouple signals is amplified by the derivative term such that it creates a considerable change to the spindle speed.

Implementing the derivative filter replaces the normal derivative term (Equation 5.11) with Equation 5.12.

$$D_1 = Kd \times dT/dt \quad \text{Equation 5.11}$$

Where D_1 is the normal derivative term.

Kd is the derivative gain.

dT/dt is the rate of change of temperature.

$$D_2 = Kd \times \frac{\frac{dT}{dt}}{1 + \frac{(\frac{dT}{dt}) \times (\frac{Kd}{Kp})}{N}} \quad \text{Equation 5.12}^{[9]}$$

Where D_2 is the filtered derivative term.

K_p is the proportional gain.

N is the filter factor (selected $2 \leq N \leq 20$).

The filter works on the principle that if $\frac{dT}{dt}$ is small, the denominator approximates unity and the derivative term generated is equivalent to the normal derivative in Equation 5.11. If $\frac{dT}{dt}$ tends toward infinitely large, the derivative term approximates Equation 5.13.

$$D = \frac{Kd}{\left(\frac{Kd}{Kp}\right)/N} = Kp \times N$$

Equation 5.13

The response of the filtered derivative versus rate of change of temperature was plotted. The approximate maximum rate of change of temperature which occurs in the system was determined from “Weld AT_7” (see Figure 5.19) to obtain a suitable range for plotting the derivative filter response.

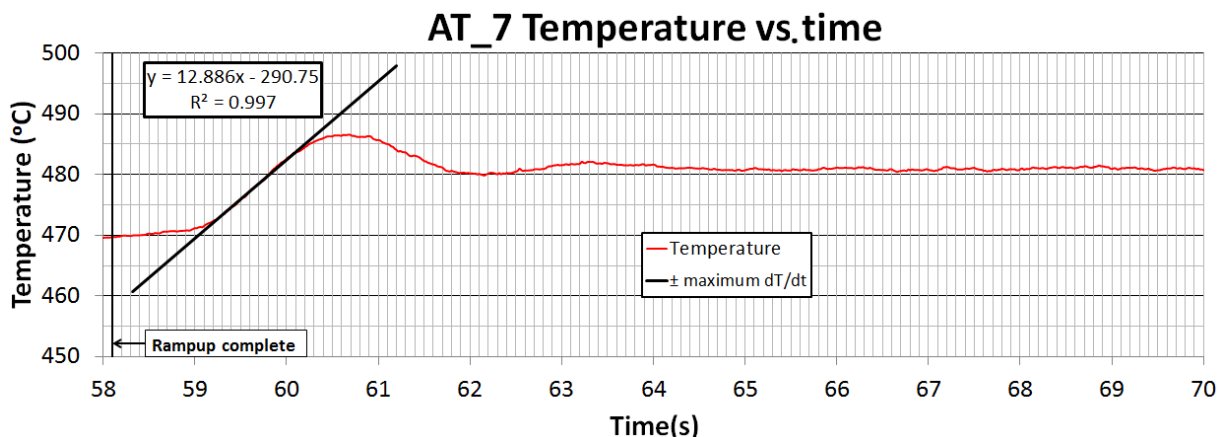


Figure 5.19. AT_7 maximum rate of temperature change

The maximum rate of change of temperature is approximately 12.9°C/s (from Figure 5.19). Rate of change of temperature considerably above this value should generate an attenuated derivative term. Using the Kp and Kd terms calculated in Section 5.3.3, the unfiltered derivative and filtered derivative responses (for $N = 2$ and $N = 20$) versus rate of change of temperature are plotted in Figure 5.20.

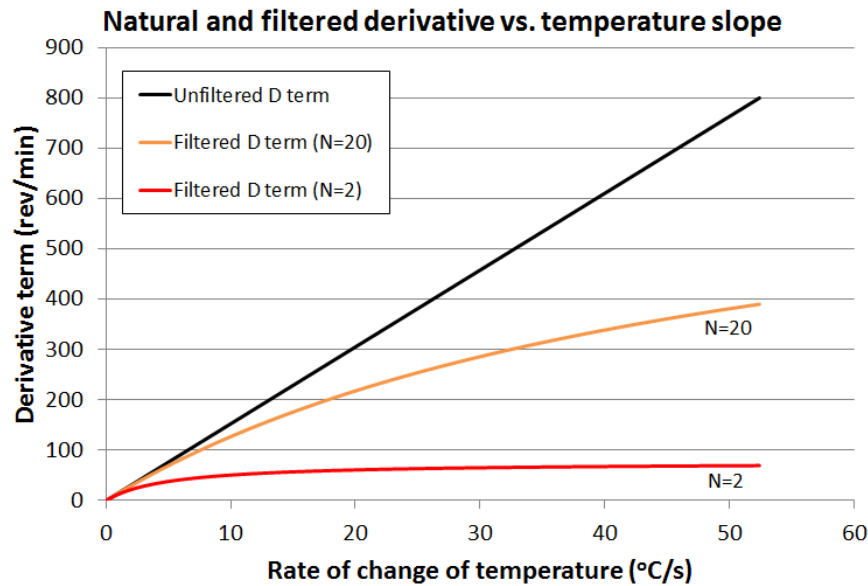


Figure 5.20. Derivative filter responses

From Figure 5.20 it can be seen that implementing the filter with $N = 2$ generates the most attenuation for high rate of change of temperature although rate of change of temperature from approximately 3°C/s to 12.9°C/s generated considerably attenuated derivative terms compared to the unfiltered derivative term. Attenuating the derivative term considerably in the operating range of the process could cause the system to respond undesirably because the derivative gain calculated from the tuning of the controller would no longer generate the required derivative term regarding magnitude necessary for damping the system. Implementing the filter with $N = 20$ generates a derivative term similar to the unfiltered derivative up to 12.9°C/s . “Weld AT_8” (shown in Figure 5.21) tested the filter with $N = 20$.

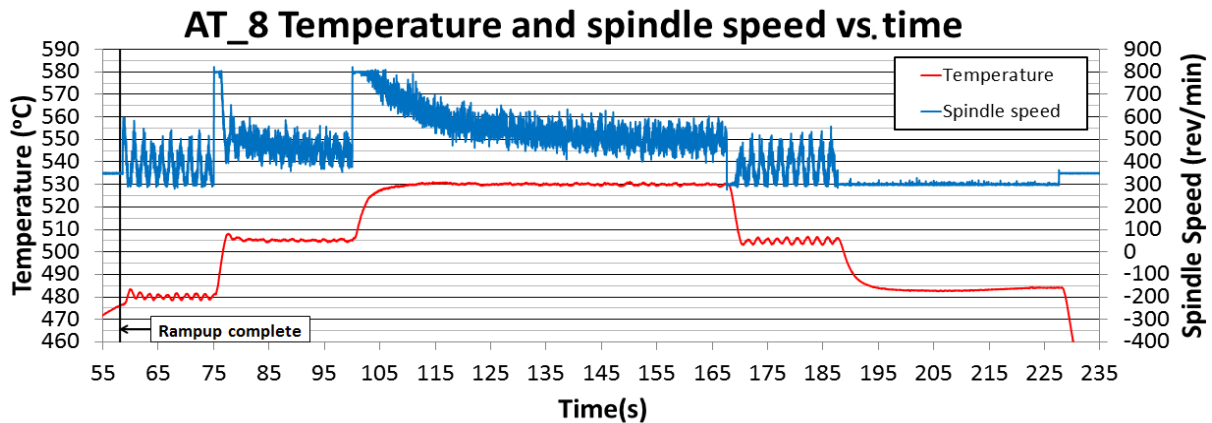


Figure 5.21. Weld AT_8

Comparison of “Weld AT_7” and “Weld AT_8” shows that the filter has not improved the high frequency oscillation of the spindle speed. Since the objective of the control system is to control the temperature to match the set-point (which has been achieved by this system), the excessive actuator (the spindle in the context of this study) oscillation could be considered unimportant. On the contrary, the excessive actuator oscillation could be important when considering factors such as energy consumption and actuator wear. Investigation of these factors was not within the scope of this study.

The researcher modified the filter in Equation 5.12 ^[9] in order to increase the attenuation of the derivative term generated from high rate of change of temperature whilst approximately maintaining unchanged damping for the operating range of the process. The modified filtered derivative is shown in Equation 5.14.

$$D_3 = Kd \times \frac{\frac{dT}{dt}}{1 + \left(\frac{dT}{dt}\right)^r \times \left(\frac{Kd}{Kp}\right) / N} \quad \text{Equation 5.14}$$

Where

D_3	is the modified filtered derivative term.
Kp	is the proportional gain.
Kd	is the derivative gain.
N	is the filter factor (N is unlimited).

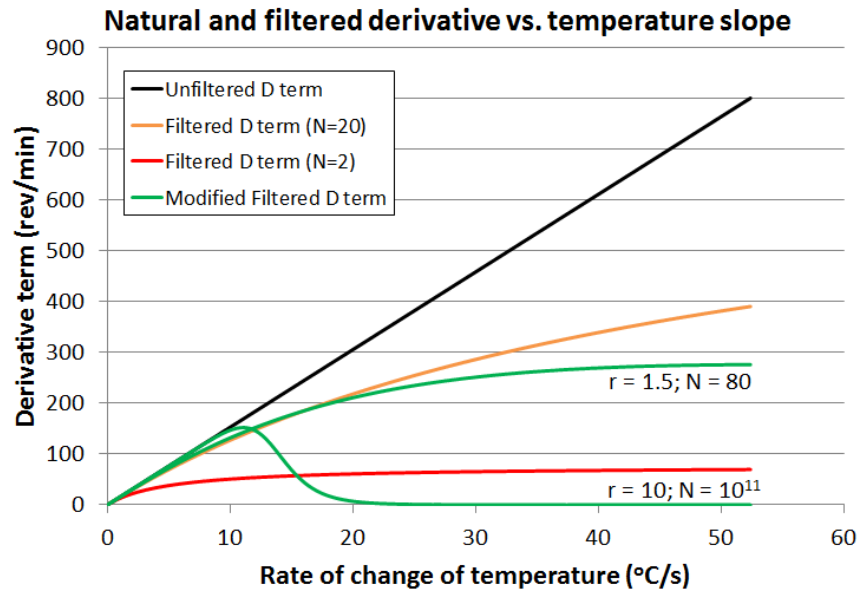
Adding the power r to the $\frac{dT}{dt}$ term in the denominator causes the denominator to increase faster than the numerator (provided $r > 1$) as the rate of change of temperature increases, causing the derivative term to decrease. D_3 approximates the normal derivative (in Equation 5.11) when $\frac{dT}{dt}$ is small which is the same value as D_2 for small $\frac{dT}{dt}$. However, if $\frac{dT}{dt}$ tends toward infinitely large, the derivative term approximates zero as shown in Equation 5.15.

$$\lim_{\frac{dT}{dt} \rightarrow \infty} D_3 = \lim_{\frac{dT}{dt} \rightarrow \infty} \left(\frac{Kd \times \frac{dT}{dt}}{1 + \left(\frac{dT}{dt} \right)^r \times \left(\frac{Kd}{Kp} \right) / N} \right) = \lim_{\frac{dT}{dt} \rightarrow \infty} \left(\frac{N \times Kp}{\left(\frac{dT}{dt} \right)^{r-1}} \right) = 0 \quad (r > 1)$$

Equation 5.15

Increasing the r term creates a sharper cut-off on the response curve although it decreases the magnitude of the derivative response curve for all rates of change of temperature. It is then required that the N term be increased so that the derivative term is not attenuated considerably in the operating range of the system (zero to 12.9°C/s in this case). Implementation of this filter should be done with caution because setting the N term too low and the r term too high for the system characteristics, the derivative term could provide insufficient damping in the operating range of the system. This could cause the system to become unstable.

The derivative responses (for two settings of r and N) versus rate of change of temperature ($\frac{dT}{dt}$) are shown in green in Figure 5.22. The filters from Figure 5.20 are retained in the figure for comparison.



The filter was tested in “Weld AT_9”; “Weld AT_11”; “Weld AT_12”; “Weld AR_1” and “Weld AR_2” (see **Appendix E**) with the following parameters:

Weld number	r	N
AT_9	1.5	80
AT_12	2	30
AT_11	2.5	300
AR_1	2.5	300
AR_2	10	10^{11}

Table 5.5. Filter parameters

The two welds showing the least spindle oscillation was “Weld AT_11” and “Weld AR_1”. The spindle speed oscillation amplitude in the 530°C region improved from approximately 100 rev/min in “Weld AT_7” (see Figure 5.18) to approximately 75 rev/min in “Weld AT_11” and approximately 60 rev/min in “Weld AR_1” (see Figure 5.23).

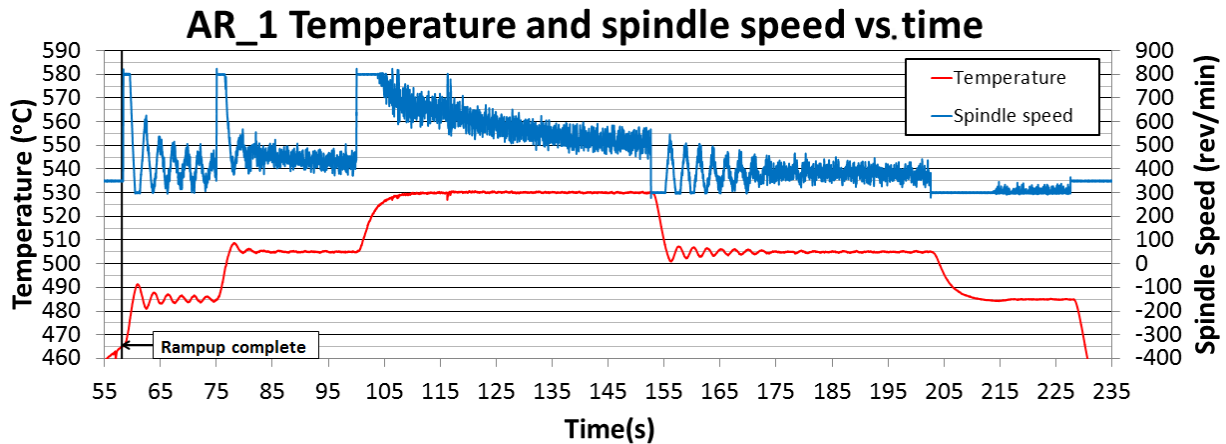


Figure 5.23. Weld AR_1

The Ziegler Nichols tuning method ^[3] contains a number of gain calculation sets for different controller options. Two of which are classic PID (implemented in the majority of the welds in this study as per the gain settings in Section 5.3.3) and PI (tested in “Weld AT_10”). A reason for which PI control would be implemented instead of PID control is that in some cases, the process does not require the derivative component because the uncompensated system naturally contains sufficient damping to limit overshoot of the set-point (provided the PI gains are not set too aggressively).

In comparison to the calculations for PID control, the gains for PI control are calculated less aggressively from the ultimate gain and oscillation period found in step 3 and step 4 of the Ziegler Nichols tuning method ^[3] (see Section 5.3.3). The main reason for this is because the controller does not add damping to the system as PID control does with the derivative term. The K_p and K_i gains therefore need to be set low enough in order to avoid excessive output oscillation and the system becoming unstable. The gains are calculated in Equation 5.16 and Equation 5.17.

$$K_p = 0.45 * K_u = 0.45 * 63.5 = 28.58 \quad \text{Equation 5.16}^{[3]}$$

$$K_i = (1.2 * K_p) / T_u = (1.2 * 28.58) / 3.2059 = 10.70 \quad \text{Equation 5.17}^{[3]}$$

The PI controller was tested in “Weld AT_10” (see Figure 5.24). From “Weld AT_10”, the spindle speed graph during steady state condition in region 3 confirms that the

derivative term is the cause of the excessive spindle speed oscillation during steady state condition in the previous welds such as “Weld AT_7”. The PI control system performed acceptably in all regions except region 4.

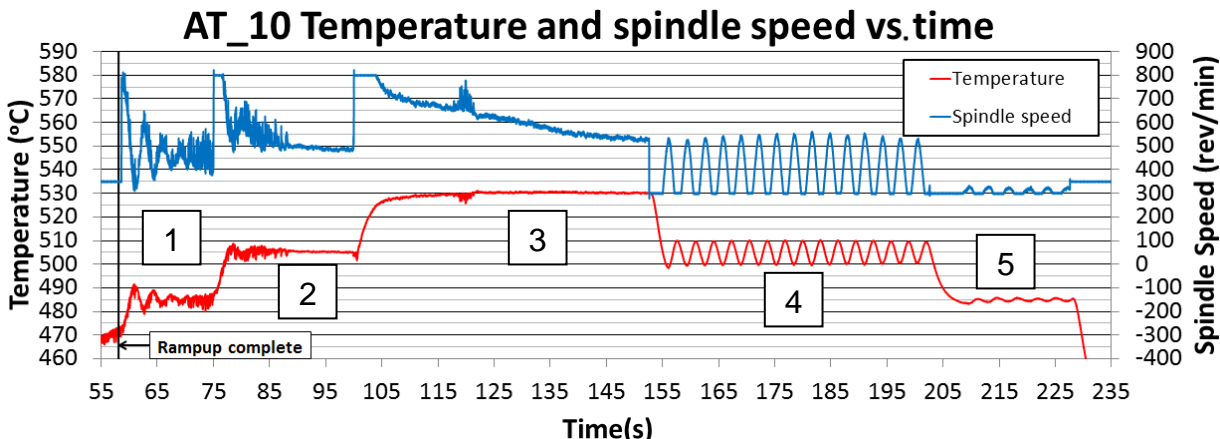


Figure 5.24. Weld AT_10

Closer inspection of “Weld AT_10” region 4 (see Figure 5.25) shows that the oscillation period matches the oscillation period of the tuning “Weld AT_3” (see Figure 5.15). The system oscillates at its natural frequency. This oscillation of temperature is an indication of an undamped system.

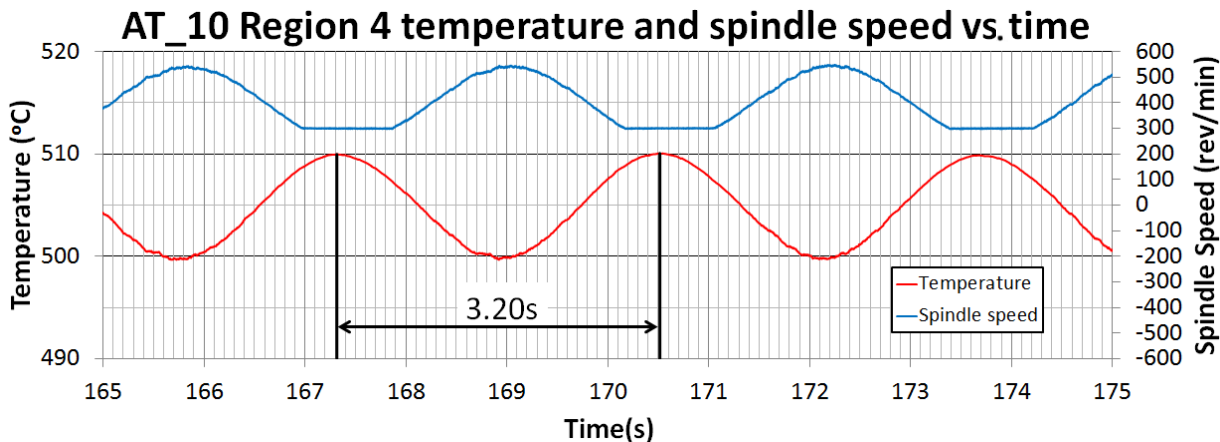


Figure 5.25. AT_10 Region 4 oscillation

5.5. Process Model (MATLAB)

5.5.1. System Transfer Function Identification

The System Identification (SID) Toolbox in Matlab (called with the “>>ident” command in the Matlab workspace) was used to generate a process model fit based on the data imported into Matlab from a file containing experimental input and output data.

In order to obtain weld data representing the dynamics of the temperature of the FSW process, exclusive of the controller, the temperature control is disengaged. This is therefore the open loop temperature response of the system given a specific spindle speed input. The experimental data was taken from “Weld 3.2” (see Figure 5.26). The open loop system was given a step command of 100 rev/min at approximately 127 seconds. Controller design considers system response to a step increase command on the input of the system. Only the step increase command data and the temperature response data is used for identification of the system model (or process transfer function). The data extract from the weld log (“Weld 3.2”) which was imported into Matlab was taken from 90 seconds to 170 seconds into the weld.

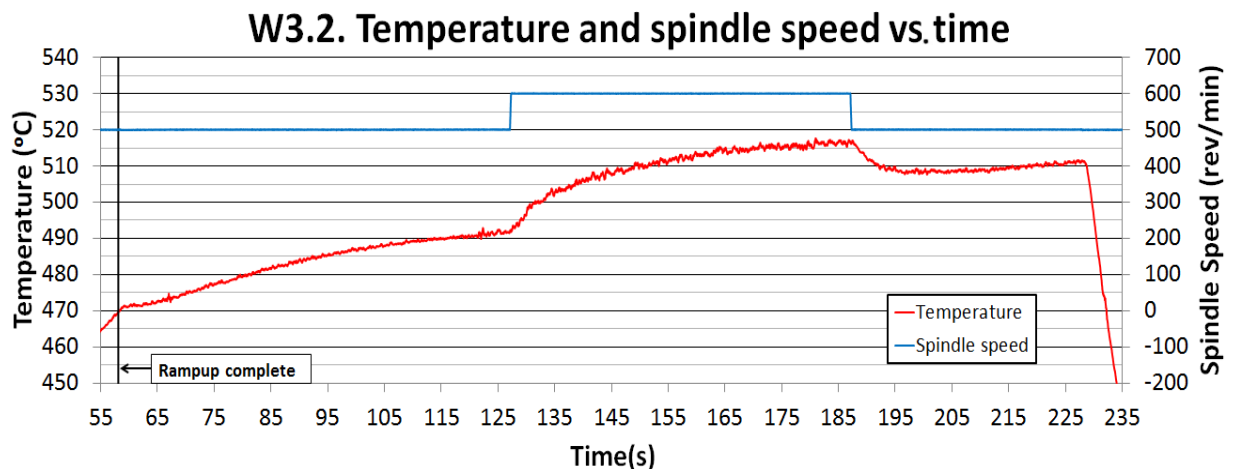


Figure 5.26. Weld 3.2

The Import data option under the “File” menu in Matlab was used to import the experimental data of weld “w3.2” from a Microsoft Excel Spreadsheet. See **Appendix H** for the temperature and spindle speed versus time graphs for weld set “w3.x”. The spreadsheet contained a spindle speed command column, a temperature output column and a time column. Vectors were created for the spindle input command (named: “rpmCommand”) and the temperature response (output named: “temperature”). The SID tool’s data import function imports the vectors for input and output data from the matlab workspace. The SID toolbox user interface and import data dialog box can be seen on **page I-1 in Appendix I**.

Second and third order linear parametric models were generated. A second order linear parametric model estimation of the system was found to be acceptable. The model fit to the experimental data was 97.27 percent. In Figure 5.27, the red graph series (smoother of the two graphs) is the model fit to the experimental data (irregular, black graph).

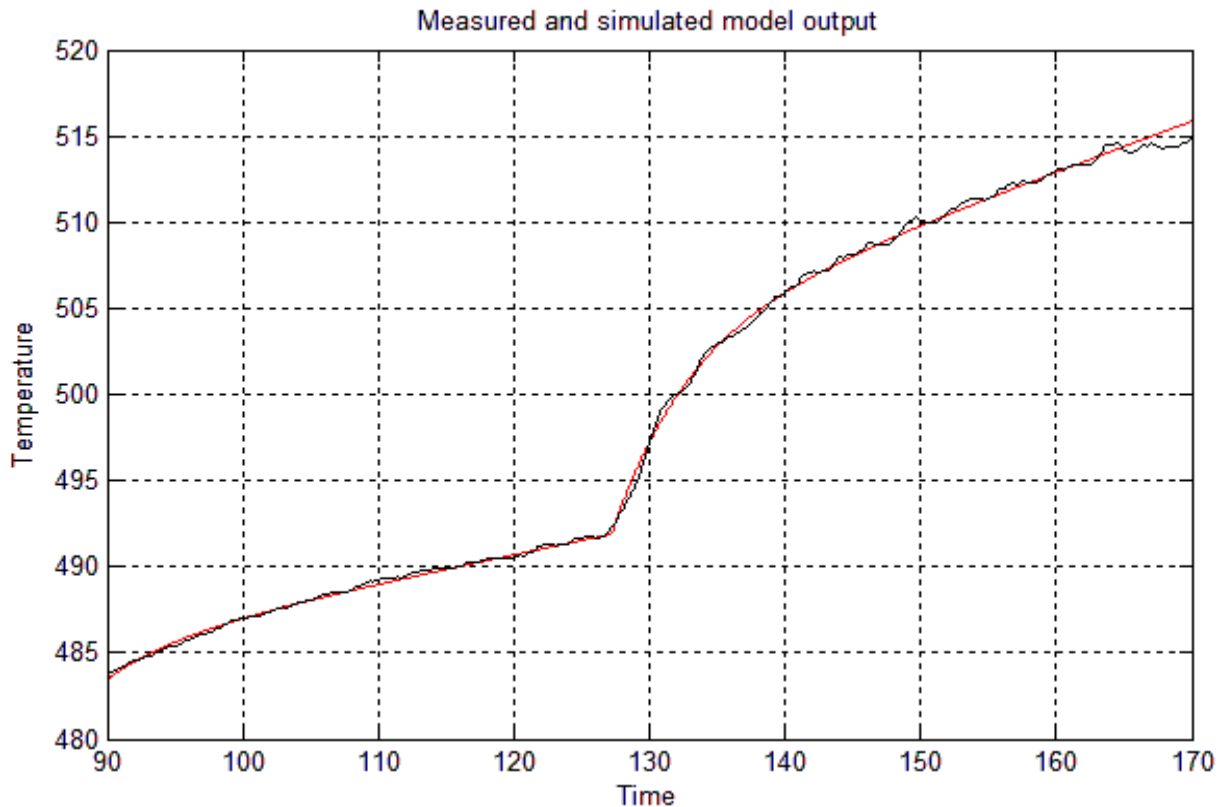


Figure 5.27. Second order model fit

The model was then dragged to the LTI viewer in the SID toolbox user interface (see **Appendix I, page I-2**) from which the transfer function of the model is exported to the Matlab workspace. The transfer function generated by the SID toolbox is a discrete transfer function (it was generated based upon discrete experimental data with 0.02 seconds sampling time). The Automatic Control Systems (ACSYS) toolbox was used to conduct the frequency design of the PID controller (see Section 5.5.2) for comparison with the PID controller found by the Ziegler Nichols tuning method ^[3] (see Section 5.3.3). The ACSYS toolbox requires a continuous transfer function in the input dialog box. The discrete transfer function model found from the SID toolbox was converted to an equivalent continuous transfer function using the “>>d2c()” Matlab command as shown in Figure 5.28.

The image shows a MATLAB 7.10.0 (R2010a) Command Window. The current folder is C:\Program Files\MATLAB\ACSYS2007. The Command Window displays the following text:

```

New to MATLAB? Watch this Video, see Demos, or read Getting Started.
>> idenc
Opening System Identification Tool ..... done.
>> oe221

Transfer function from input "u1" to output "y1":
0.0004406 z - 0.0004405
-----
z^2 - 1.996 z + 0.9963

Sampling time: 0.02
>> tf221=d2c(oe221)

Transfer function from input "u1" to output "y1":
0.02207 s + 0.0002932
-----
s^2 + 0.1872 s + 0.0002356

```

Figure 5.28. Transfer function conversion

Verification that the continuous transfer function (labelled: “FSW Process” in Figure 5.29) is a good model of the physical FSW process, the model was simulated in Matlab Simulink with closed-loop PID control implemented. The gains found from the Ziegler Nichols tuning ^[3] of the physical system were implemented in the Simulink PID controller model. The Simulink control system model was given a step command from 481°C to 506°C at 75 seconds (into the simulation). This replicates the step command at 75 seconds in “Weld AT_7”.

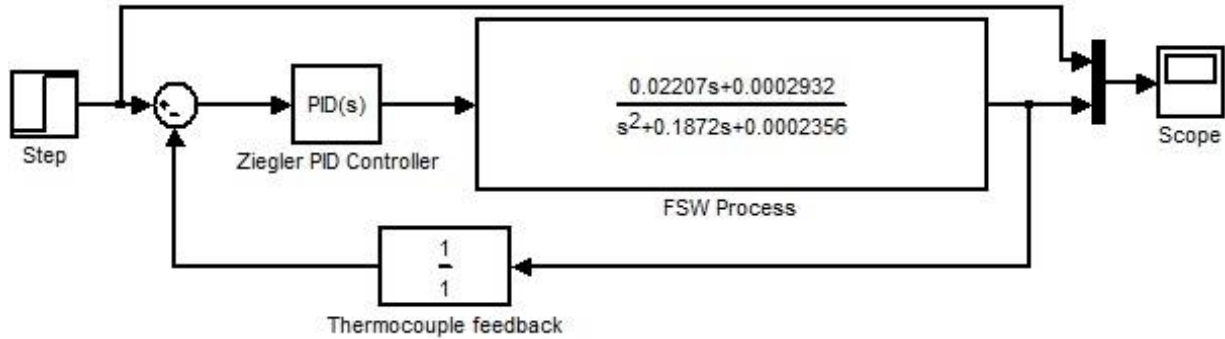


Figure 5.29. Simulink control system model

Referring to Figure 5.30 and Figure 5.31, the rise time of the control system (for a step command input) is denoted “ t_r ” and the settling time of the control system is denoted “ t_s ”. The percentage overshoot of the control system (for a step command input) is defined as the percentage of the step command magnitude by which the system response overshoots the set-point.

The temperature response of the model was compared to the physical temperature response of “Weld AT_7” and “Weld AR_1” (see **Appendix E, page E-19**) in the region of 70 seconds to 90 seconds. The simulation result is shown in Figure 5.30 and the corresponding extract from “Weld AT_7” is shown in Figure 5.31. The comparison of the results is shown in Table 5.6.

Weld/Simulation	Rise time (s)	Settling time (s)	% overshoot
Simulation	1.47	7.41	15.6
Weld AT_7	1.96	4.88	8.2
Weld AR_1	1.46	6.17	19.2

Table 5.6. Weld and simulation comparison

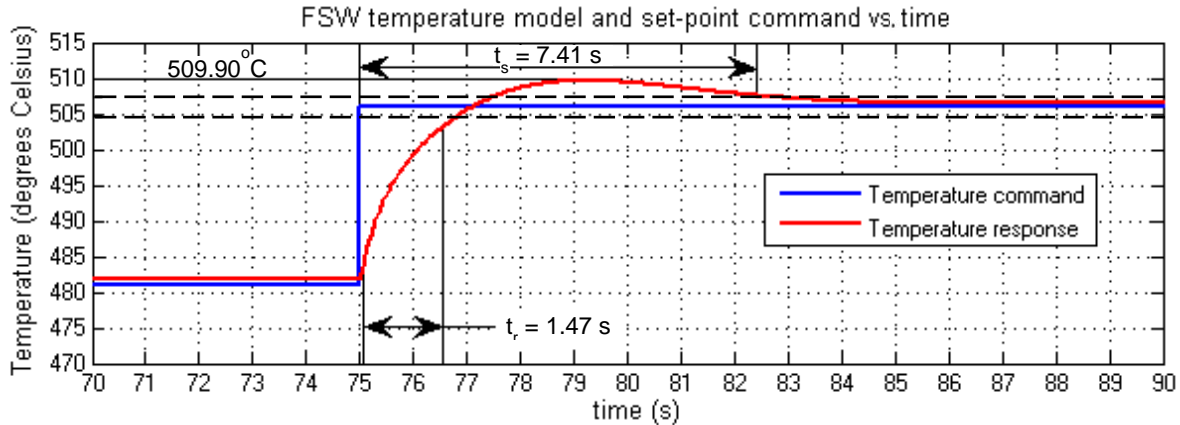


Figure 5.30. Simulink simulation of FSW control step command

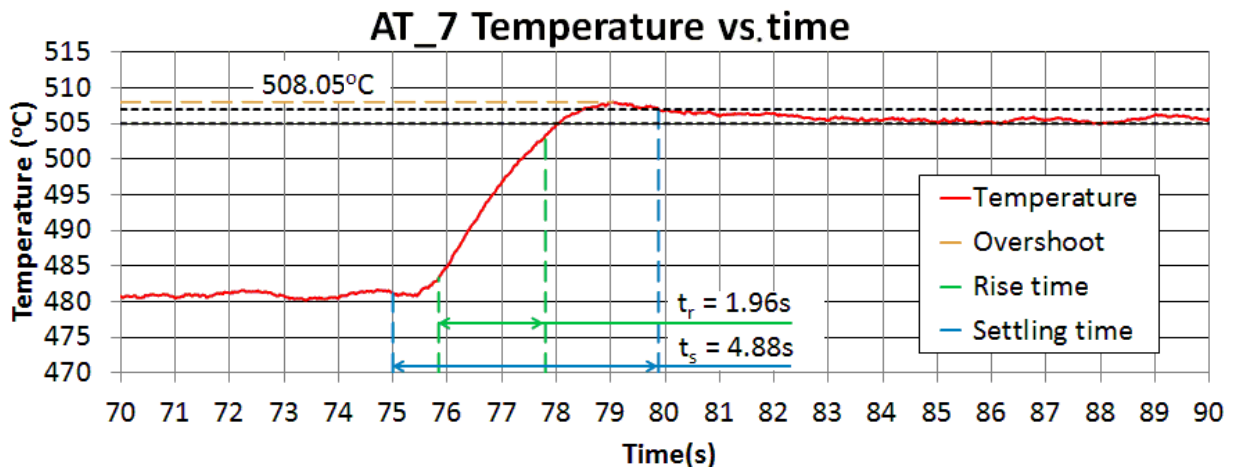


Figure 5.31. Weld AT_7 temperature response extract

The rise time of “Weld AT_7” is 0.49 seconds longer than the rise time of the simulation. The overshoot of the weld is 7.4 percent less than the overshoot of the simulation. These two observations indicate that the weld temperature control system exhibits more damping than the simulated model.

The damping ratio was calculated for each instance in Table 5.7. The model transfer function was of second order. “Automatic Control Systems”^[20] provides an equation for calculating the overshoot for a second order system from the system damping ratio ζ (see Equation 5.18). Overshoot was obtained from the experimental results, so the equation can be manipulated to calculate the damping ratios (see Table 5.7).

$$\% \text{ overshoot} = 100e^{-\pi\zeta/\sqrt{1-\zeta^2}} \quad \text{Equation 5.18}^{[20]}$$

From Equation 5.18, the damping ratio is made the subject of the formula as shown in Equation 5.19.

$$\zeta = \frac{\left[\ln\left(\frac{\% \text{ overshoot}}{100}\right)\right]^2}{\sqrt{\left[\ln\left(\frac{\% \text{ overshoot}}{100}\right)\right]^2 + \pi^2}} \quad \text{Equation 5.19}$$

Weld/Simulation	Damping ratio
Simulation	0.509
Weld AT_7	0.623
Weld AR_1	0.465

Table 5.7. Damping ratios

To put the values from Table 5.7 into perspective; from control theory, a control system is classified as negatively damped if $\zeta < 0$ ^[20], resulting in an unstable system; undamped if $\zeta = 0$ ^[20], resulting in a system with constant oscillation; underdamped if $0 < \zeta < 1$ ^[20] which results in a system which is stable and percent overshoot ranges from high to low as ζ moves from zero towards unity; critically damped if $\zeta = 1$ ^[20] in which case the system approaches the set-point as fast as possible without any overshoot and overdamped if $\zeta > 1$ ^[20], where the system exhibits no overshoot of the set-point although increasing ζ increases the rise time of the system ^[20]. Most control systems fall into the underdamped category for fastest response as well as acceptable overshoot.

The damping of the simulation model was found to be between the damping values of “Weld AT_7” and “Weld AR_1”. The model can therefore be considered a reasonable representation of the system. Considering that a damping ratio of 0.7 is considered desirable for an acceptable trade-off between overshoot and rise time ^[20] and the

range which $\zeta = 0.7$ falls into ($0 < \zeta < 1$), the damping ratios of the welds and simulation are reasonably close to each other.

5.5.2. Bode Diagram Frequency Design

Matlab's Automatic Control Systems toolbox (ACSYS) was used to design a PID controller for the FSW model via bode diagram frequency design. The model transfer function was entered into the G(s) process field in the ACSYS toolbox. **Pages J-1 and J-2 of Appendix J** show the process of entering the transfer function into ACSYS and opening the bode frequency diagram controller design tool. The open-loop bode diagram of the system (i.e. controller gain equal to unity) opens when the bode frequency controller design tool is selected. The bode diagram showing the open-loop system bandwidth (taken from the -3 dB point on the magnitude graph) is 0.00185 rad/s as shown on **page J-3 of Appendix J**. The controller was then introduced with the design tool by adding the controller gain, poles and zeros to the frequency plot as illustrated by this section. Increasing the controller gain moves the bode diagram upward in order to increase the bandwidth of the system. The design then included PI control design (adds a pole at zero (in the s domain) which is considered an integrator and a zero to the plot) and then PD control design (adds a further zero to the plot). The zero of the PI design component was placed on the bode diagram and then moved left or right in order to manipulate the shape of the bode diagram and improve the stability margin. The zero of the PD design component was moved left or right in the bode diagram in order to improve the time response (closed-loop step response which is opened simultaneously with the bode diagram) of the system. The transfer function for a PID controller in the s domain takes the form of Equation 5.20 ^[20].

$$C(s) = Kp + \frac{Ki}{s} + Kd \cdot s = \frac{Kd \cdot s^2 + Kp \cdot s + Ki}{s} \quad \text{Equation 5.20}^{[20]}$$

where

$C(s)$ is the controller transfer function.

- Kp is the proportional gain of the controller.
 Ki is the integral gain of the controller.
 Kd is the derivative gain of the controller.

In order to conduct the three controller design components (determine loop gain, PI design and PD design) separately, the controller transfer function needed to be modified in such a way that it becomes a product of the three appropriate components of the form of Equation 5.21 [20].

$$C(s) = (1 + K_{D1}s) \left(K_{P2} + \frac{K_{I2}}{s} \right) = \frac{K_{P2} \left(\frac{K_{I2}}{K_{P2}} + s \right) (1 + K_{D1}s)}{s}$$

$$= K_{I2} \frac{\left(1 + \frac{K_{P2}s}{K_{I2}} \right)}{s} (1 + K_{D1}s) \quad \text{Equation 5.21 [20]}$$

where

- K_{I2} corresponds to the controller loop gain.
 $\frac{\left(1 + \frac{K_{P2}s}{K_{I2}} \right)}{s}$ corresponds to the PI control component zero $\left(1 + \frac{K_{P2}}{K_{I2}}s \right)$ and integrator $\left(\frac{1}{s} \right)$.
 $(1 + K_{D1}s)$ corresponds to the PD control component zero.

The relationships between the terms in Equation 5.20 and Equation 5.21 are described by Equation 5.22, Equation 5.23 and Equation 5.24.

$$Kp = K_{P2} + K_{D1}K_{I2} \quad \text{Equation 5.22 [20]}$$

$$Ki = K_{I2} \quad \text{Equation 5.23 [20]}$$

$$Kd = K_{P2}K_{D1} \quad \text{Equation 5.24 [20]}$$

The closed-loop unit step response with real time update is placed next to the bode diagram as shown in Figure 5.32 and on **page J-4 in Appendix J**. As changes are made to the bode diagram, the step response automatically updates.

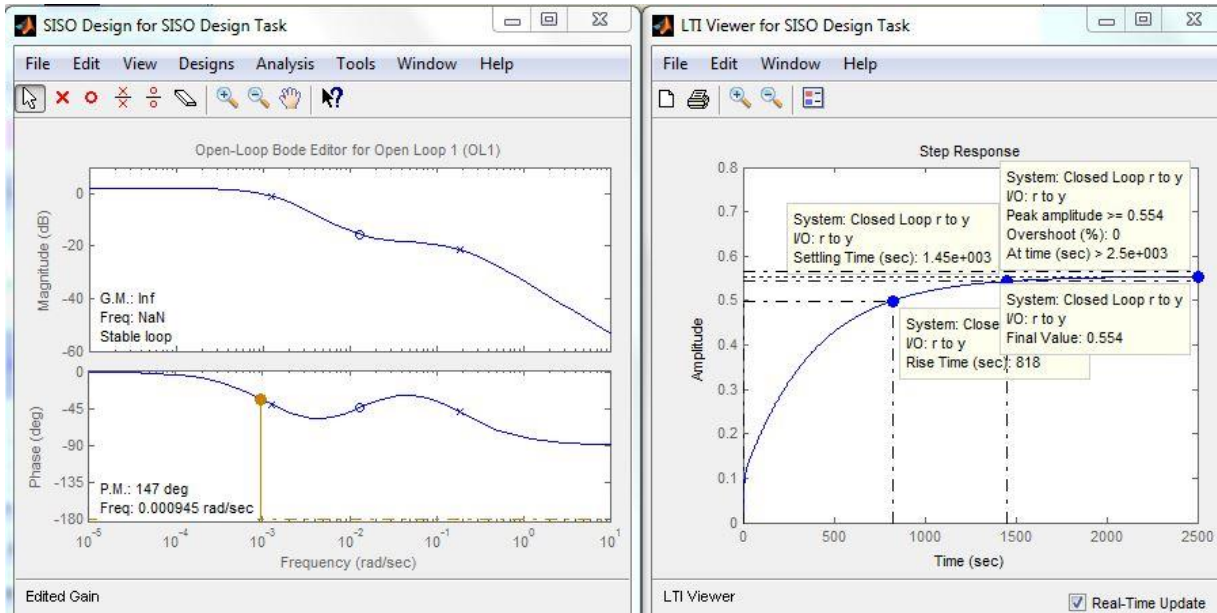


Figure 5.32. Open-loop bode and closed-loop step response

The unit step response in Figure 5.32 shows that the closed loop system without a controller (controller gain equal to unity) does not contain sufficient gain in order to drive the output to the set-point of unity (final value is 0.554). The bode diagram is moved upward in the controller design tool window using the computer mouse in order to increase the controller gain until the system step response is able to reach 95 percent of the set-point (see Figure 5.33 and **page J-5 of Appendix J**). After the integral term of the controller is added, the system will have no steady-state error (the system will reach 100 percent of the set-point).

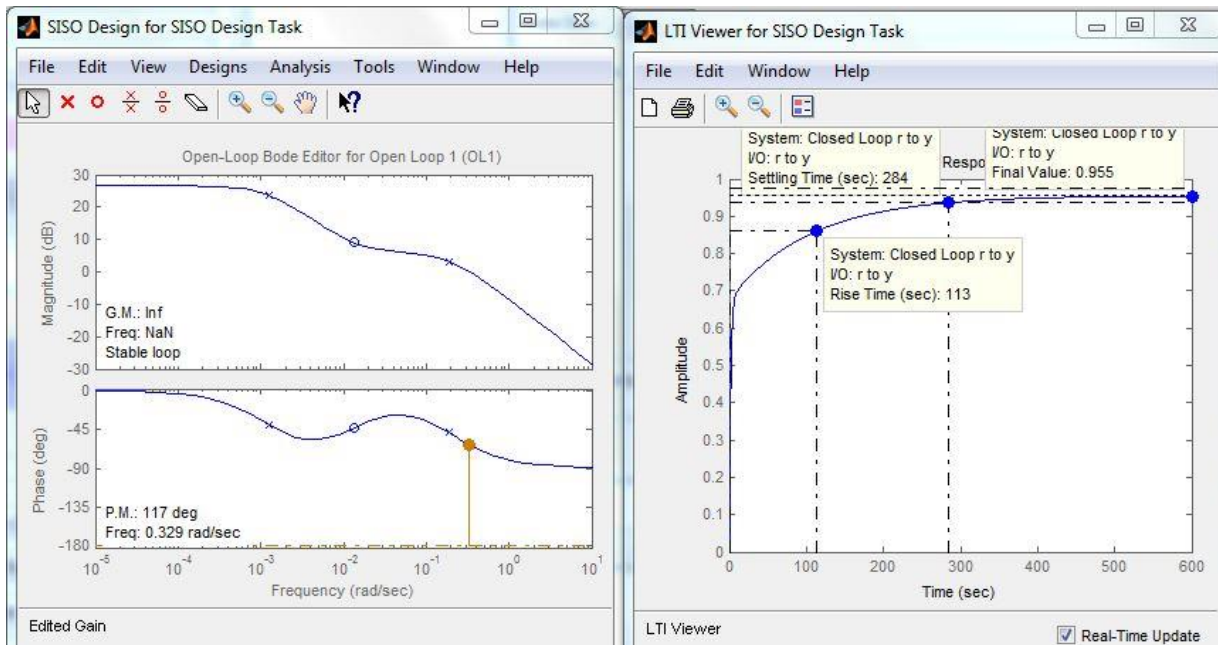


Figure 5.33. Moved bode diagram and corresponding system step response

Changing to the compensator (controller) editor (see [page J-6 of Appendix J](#)), shows that moving the bode diagram upward has increased the controller gain from unity to 17.116. After the system had sufficient gain to be within reach of the set-point, the PI design component was added to the controller.

The PI control design component consists of adding the pole at s equal to zero (in the s domain) and adding a real zero which is moved in order to achieve the required phase margin on the closed-loop bode diagram of the system. The ACSYS controller design toolbox allows you to place and move poles and zeros in the open-loop bode diagram only. In order to design for a phase margin requirement on the closed-loop bode diagram, the closed-loop bode diagram is opened simultaneously with the open-loop bode diagram with live update enabled. After adding the integrator and the zero, the zero (red circle/the circle right of 1 rad/s in [Figure 5.34 and page J-7 of Appendix J](#)) was moved on the open-loop bode diagram in order to achieve a phase margin (stability margin) on the closed-loop bode diagram of greater than 90° which is considered a good design margin in control theory.

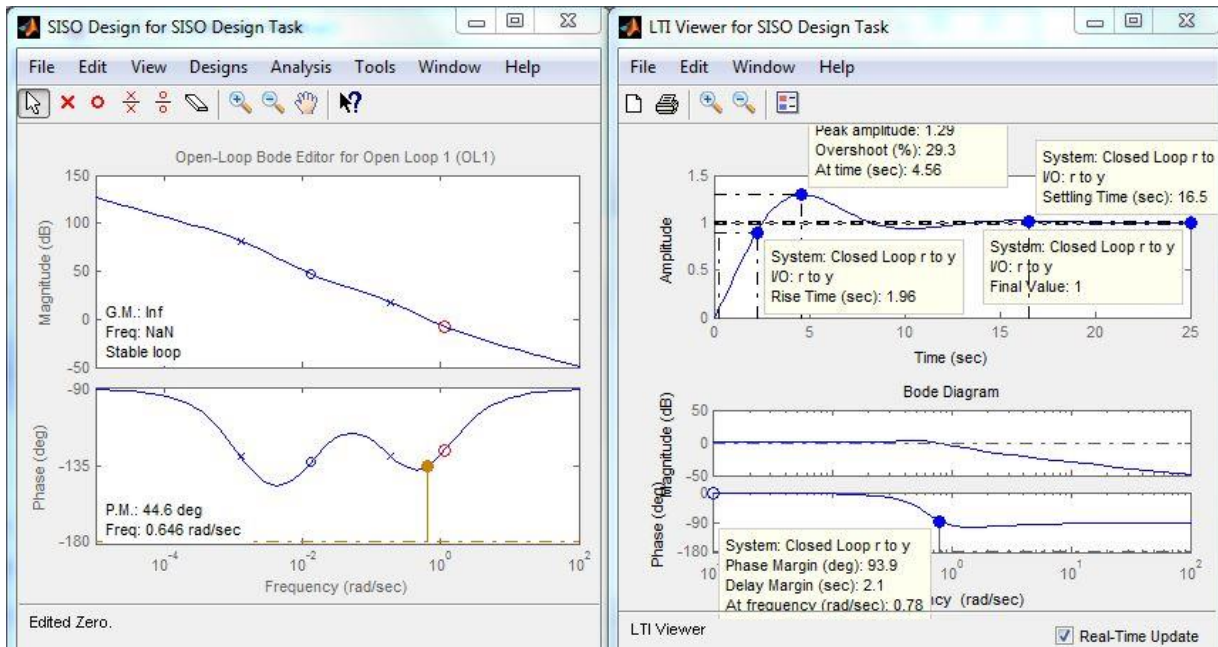


Figure 5.34. Bode diagrams and step response after PI control design

Changing to the compensator (controller) editor (see [page J-8 of Appendix J](#)), shows that after placement of the zero, its location in the s domain was $s = -1.1377$. After implementation of the PI component of the design, the PD component of the design was added.

The PD component of the controller design process increases the damping ratio of the system. Typically, the zero from the PI design and the zero from the PD design are placed close to each other on the bode diagram. The closed-loop step response (time domain) of the system was opened simultaneously with the bode diagram and live update enabled. This allows the researcher to visualise the effects which moving the zero have on the time response of the system. The zero of the PD component of the design was placed on the bode diagram near the zero placed during the PI component of the design. Moving the zero to the left improved the system overshoot although it degraded the settling time of the closed-loop step response. The purpose of this control system is to maintain the FSW temperature at the operator set-point. The beginning of the FSW process consists of the plunge and the ramp up stage during which the welding conditions are established. This region of the weld may

contain unacceptable mechanical properties and is therefore typically executed on a run-on tab which is later removed by a machining process. It was therefore decided that the temperature settling time is more important for this controller design than the temperature overshoot. It can be programmed that the overshoot and the temperature settling (at the operator set-point) will occur on the run-on tab before the weld progresses onto the weldment. At the same time overshoot should not be excessive. It was decided that less than 15 percent overshoot, which corresponds to a settling time of 9.28 seconds, was acceptable. The zero placement is shown on the bode diagram in Figure 5.35.

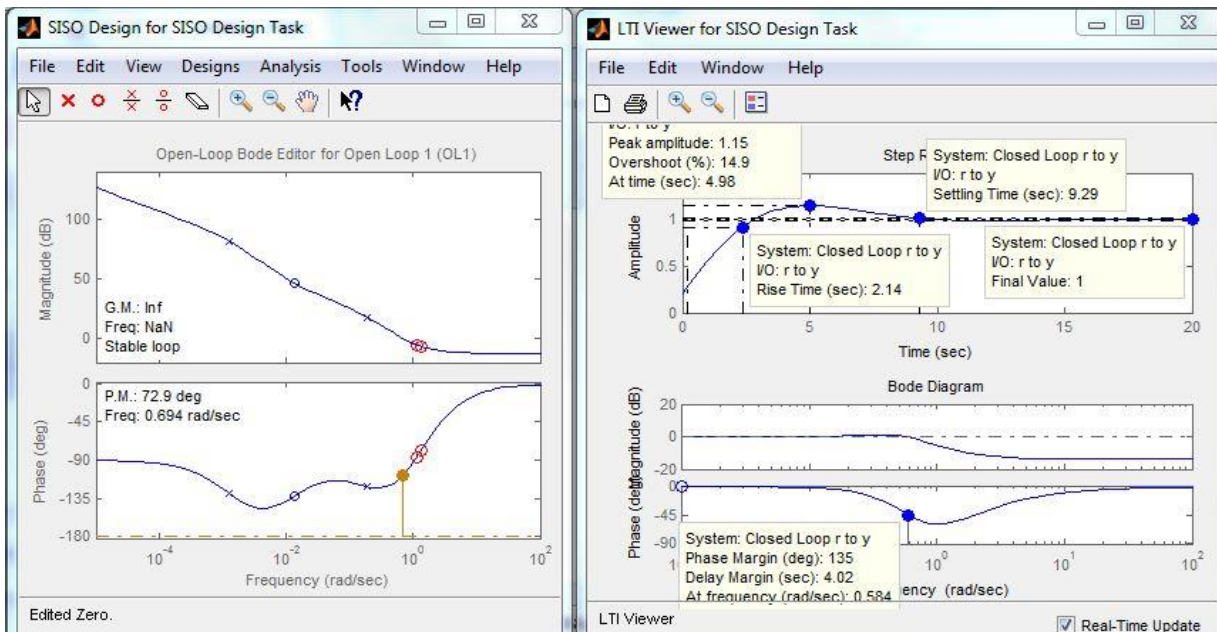


Figure 5.35. Final placement of PI and PD design zeros

The location of the PD control design zero in the s domain is $s = -1.3346$ as seen in the compensator editor in Figure 5.36. Although controller loop gain, PI and PD design are conducted separately, they are done in cascade and all three components are included in the final controller design shown in the compensator editor of Figure 5.36 after PD design was completed.

The closed-loop bode diagram of the compensated system is shown in Figure 5.36. The bandwidth of the compensated system (taken from the -3 dB point on the

magnitude graph ^[21]) is 0.797 rad/s, which is a significant improvement over the uncompensated system (bandwidth of 0.00185 rad/s). The phase margin (stability margin) is 135°. It is therefore accurate to state that the compensated system is stable.

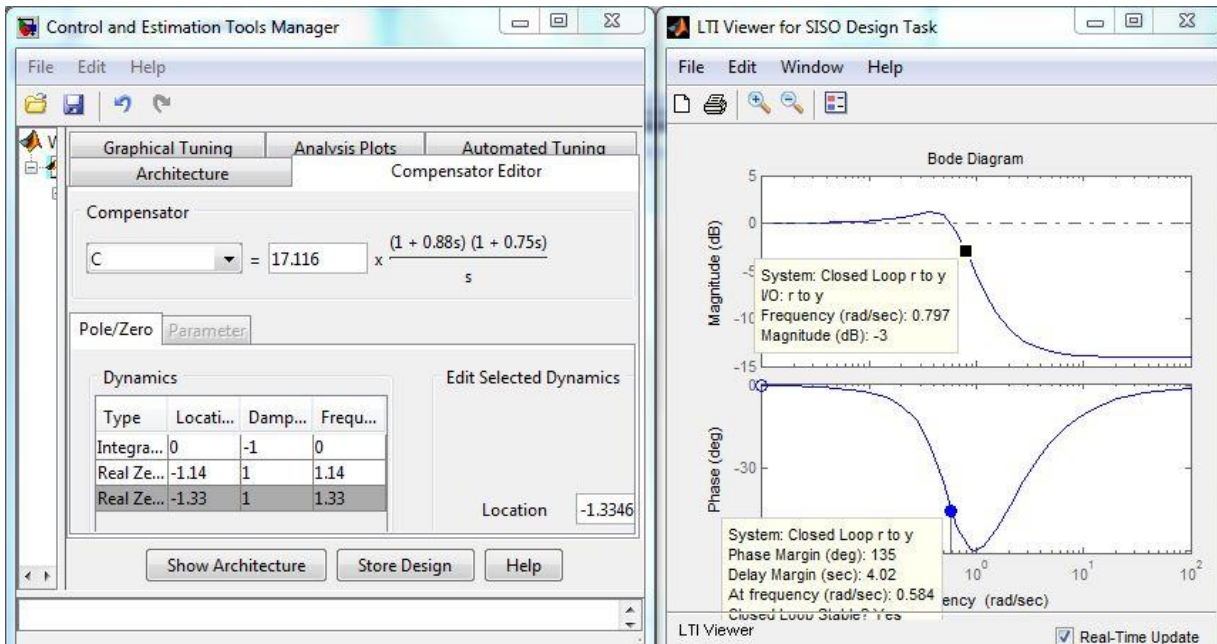


Figure 5.36. Final controller by frequency design

The coefficients of the s terms in the numerator of the compensator equation (Figure 5.36) are rounded off and are more accurately calculated as follows:

$$\text{Let the compensator equation } C(s) = 17.116 \frac{(1+As)(1+Bs)}{s}$$

$$\begin{aligned} \text{For the zero at } s = -1.1377: \quad 0 &= (1 + A(-1.1377)) \\ A &= 0.87897 \end{aligned}$$

$$\begin{aligned} \text{For the zero at } s = -1.3346: \quad 0 &= (1 + B(-1.3346)) \\ B &= 0.74929 \end{aligned}$$

The compensator equation is defined as Equation 5.25.

$$C(s) = 17.116 \frac{(1+0.87897s)(1+0.74929s)}{s} \quad \text{Equation 5.25}$$

The K_{P2} , K_{I2} and K_{D1} values are found by setting Equation 5.21 and Equation 5.25 equal to each other as shown in Equation 5.26.

$$\begin{aligned} C(s) &= K_{I2} \frac{\left(1 + \frac{K_{P2}}{K_{I2}}s\right)}{s} (1 + K_{D1}s) \\ &= 17.116 \frac{(1+0.87897s)(1+0.74929s)}{s} \end{aligned} \quad \text{Equation 5.26}$$

From inspection of Equation 5.26:

- $\frac{K_{P2}}{K_{I2}} = 0.87897$
- $K_{I2} = 17.116$
- $K_{D1} = 0.74929$.

Therefore $K_{P2} = 0.87897 \times 17.116 = 15.04445$

The terms of the controller equation are converted into K_p , K_i and K_d gains using Equation 5.22, Equation 5.23 and Equation 5.24:

$$\begin{aligned} K_p &= K_{P2} + K_{D1}K_{I2} = 15.04445 + (0.74929 \times 17.116) &&= \mathbf{27.8693} \\ K_i &= K_{I2} &&= \mathbf{17.116} \\ K_d &= K_{P2}K_{D1} = 15.04445 \times 0.74929 &&= \mathbf{11.2727} \end{aligned}$$

These K_p , K_i and K_d gains are reasonably similar, yet more conservative than the gains found from the Ziegler Nichols tuning method ^[3] (see Section 5.3.3) which were $K_p = 38.1$, $K_i = 23.769$ and $K_d = 15.268$.

The gains found from the Ziegler Nichols tuning method ^[3] were entered into ACSYS (see **page J-11 of Appendix J**) and the closed-loop bode diagram was generated

(see **page J-12 of Appendix J**). A comparison between the closed-loop bode diagrams for the Ziegler Nichols tuned ^[3] system and the bode frequency designed system (see Figure 5.36) showed that the Ziegler Nichols tuned ^[3] system had a slightly larger stability margin (141° versus 135°). The comparison also showed that the Ziegler Nichols tuned ^[3] system has a wider bandwidth (0.939 rad/s versus 0.797 rad/s).

In order to compare the performance of the Ziegler Nichols ^[3] derived PID gains and the bode frequency design derived PID gains, a Matlab Simulink simulation was conducted (see Figure 5.37, Figure 5.38 and **page J-13 to page J-16 of Appendix J**). For the comparison, the Simulink process control diagram was duplicated (FSW transfer function, feedback and PID controller), the step input was fed to the two systems and the PID gains from the two design methods were entered into the two separate PID controllers respectively. The two process outputs and the step input command were connected to a scope in order to visualise the signals.

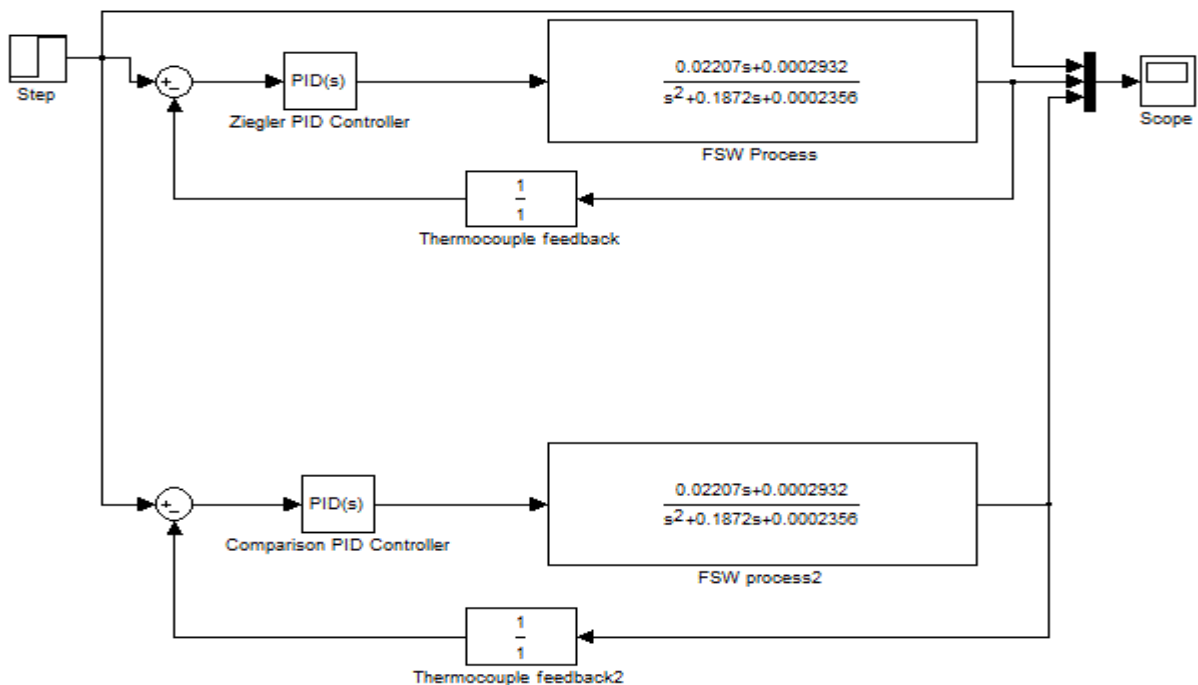


Figure 5.37. Simulink model of bode frequency design versus Ziegler Nichols design

The Simulink scope output shown in Figure 5.38 shows the step input command (blue graph) and the control system temperature outputs (Ziegler Nichols ^[3] design: red graph/graph with the least magnitude at 45 seconds; bode frequency design: green graph) versus time.

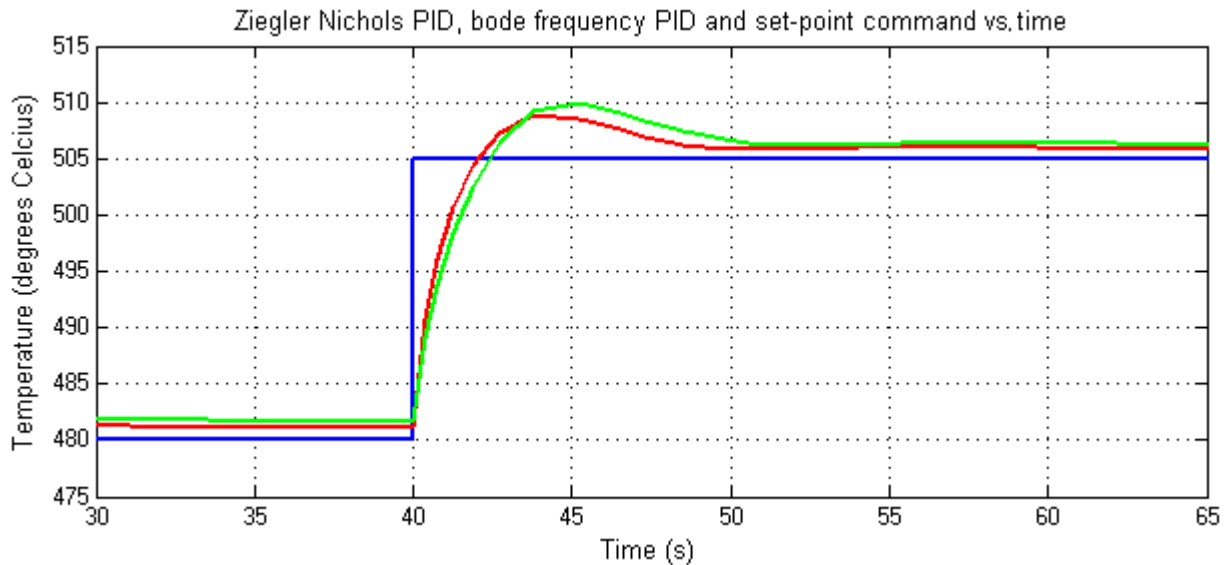


Figure 5.38. Ziegler Nichols PID design output versus bode frequency PID design

From the simulation in Figure 5.38, the Ziegler Nichols ^[3] PID design performance was marginally superior to the bode frequency PID design with a slightly faster rise time, less overshoot and a faster settling time.

Both tuning methods have their advantages and disadvantages. The disadvantages of tuning the system using the Ziegler Nichols method ^[3] could be that the tuning may contain errors from selection of the ultimate gain and measuring of the oscillation period. The disadvantages of designing a controller based on a system model (and bode diagram frequency design) is that there could be errors introduced in the generation of the system model and errors introduced in the design of the controller. The design of the controller is not completely a precise science but also a bit of an art concerning the designer because almost every system is different and will not be designed in precisely the same way.

The advantages of the Ziegler Nichols tuning method ^[3] is that it is reasonably simple to conduct without a large amount of scientific calculations and typically produces good results. The gains obtained from this method provide a good starting point which can be modified in order to improve certain aspects of the system which are specific to that system. For example, the system may oscillate more than desired by the operator and increasing the derivative gain by a small amount could improve the situation. The operator should take caution by refraining from altering the gains excessively because the three gains each have their independent effects on the dynamics of the system although it is the same system and hence the gains affect each other's optimal positions. Altering the gains excessively could lead to an unstable system. The advantage of designing a controller based on a system model (and bode diagram frequency design) is that the controller is designed based on the dynamics of that particular system which are defined by scientific equations. If an accurate model of the system is developed, an accurate controller can be designed for it which may perform better than the controller derived from the Ziegler Nichols tuning method ^[3]. In addition to this, a model can be simulated using Matlab Simulink which allows the designer to experiment with the controller without the risk of damaging the system should he/she choose a setup which creates an unstable situation.

5.5.3. Simulink PID Tuning

The PID block in Matlab Simulink has a tuning function. By double clicking on the PID function block, the PID function block parameter window opens and there is a button labelled: "Tune" which opens the tuning facility (see **Appendix K**). The Simulink tuner automatically tunes the PID controller although the amount of power available to the system is unknown and the designer therefore chooses the response time by moving the "Response time" slider. Since the spindle speed was set to the 800 rev/min limit in "Weld AT_7" which represents the maximum power input to the system (for the temperatures at which the comparison is made), the response time was selected such that the rise time was similar to the rise time seen in "Weld AT_7".

The response time was set to 2.23 seconds which corresponds to a rise time of approximately 1.8 seconds (see **page K-2 of Appendix K**). Clicking the “Apply” button sets the corresponding P, I and D gains in the controller parameter window. The performance of the controller (the green graph/graph with the greatest magnitude at 85 seconds in Figure 5.39) was similar to that of the Ziegler Nichols ^[3] PID controller design (the red graph in Figure 5.39).

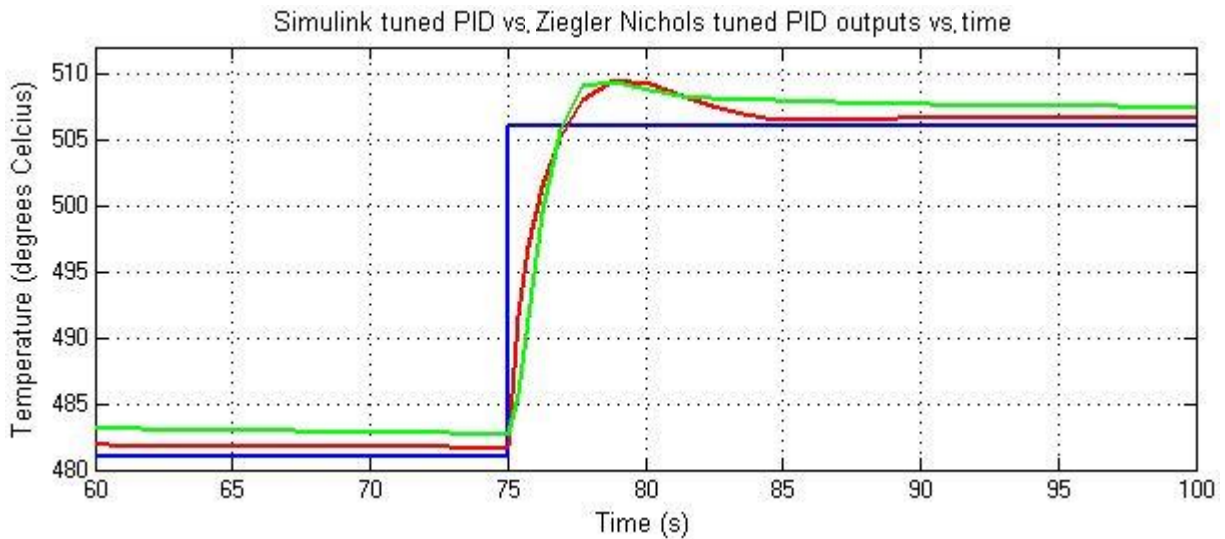


Figure 5.39. Simulink tuned PID performance versus Ziegler Nichols PID performance

A negative derivative term was generated by the Simulink PID tuner. Since the absolute values of the controller gains were similar to the gains found from the Ziegler Nichols ^[3] PID design, the simulation was executed with a positive derivative gain which has the same absolute value. The performance changed according to Figure 5.40.

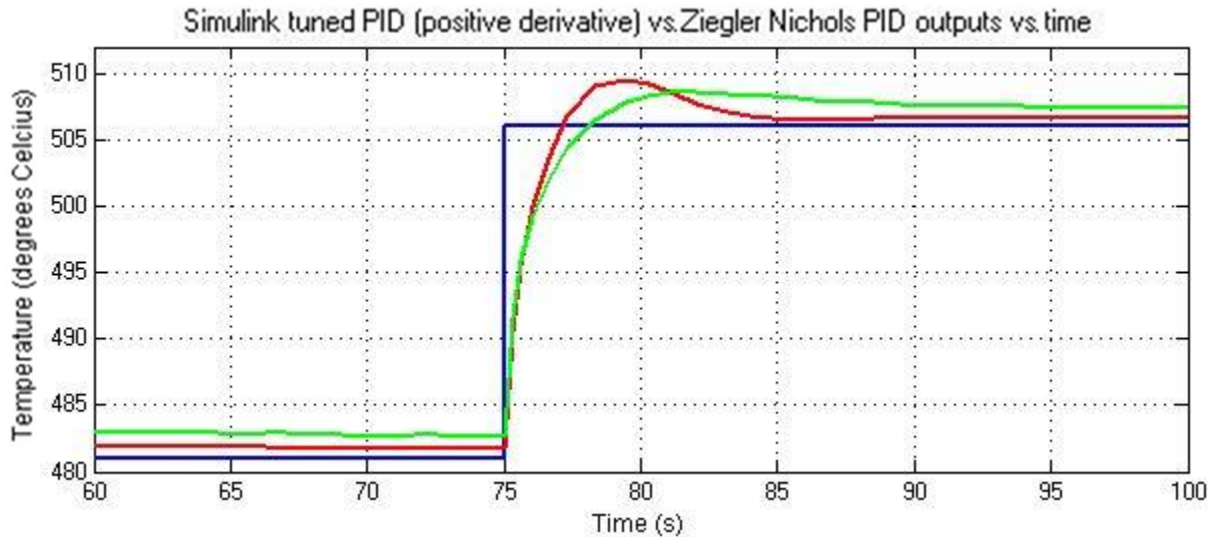


Figure 5.40. Simulink tuned PID (positive D) performance versus Ziegler Nichols PID performance

From Figure 5.39 and Figure 5.40, the performance of the PID controllers are similar although the Ziegler Nichols tuned ^[3] PID controller design consistently shows a faster settling time.

5.6. Thermal Disturbance Welds

The temperature control system utilising the PID gains found from the Ziegler Nichols tuning method ^[3] was used for the welds conducted in this section.

Welds were executed with a constant weld zone temperature of 505°C. Introducing thermal disturbances to the plate undergoing welding tests the disturbance rejection capability of the control system.

In addition to testing the disturbance rejection, weld strength consistency along the weld length was investigated. The investigation identifies any influences on weld quality which control of weld zone temperature introduces in the presence of thermal disturbances. Welds were conducted in the presence of heat sink and heat source type disturbances (detailed in Section 5.6.1 and Section 5.6.2). The area of contact

between the disturbances and the plate was approximately 3570 mm² (119 mm x 30 mm) on either side of the weld (total area of 7140 mm²). This was approximately the maximum contact area which the physical weld setup would allow between the clamps. The thermal disturbance was introduced between the two middle clamps which corresponded to the mid-point of the contact area being approximately 42 mm after the mid-point of the weld (or approximately 334 mm after the start position of the weld). Thermal paste was applied between the disturbance mechanism and the weld plate in order to eliminate any slight air gap and maximise the thermal conductivity of the junction.

The weld matrix including heat sink and heat source disturbance welds is shown in Table 5.8. The repetitions of “Weld 4.1” and “Weld 4.2” are for statistical purposes regarding the tensile results in Section 5.7.

Weld Matrix		
	Heat sink; temperature control on (505°C)	Heat source; temperature control on (505°C)
Iteration 1	4.1.1	4.3.1
Iteration 2	4.1.2	n/a
Iteration 3	4.1.3	n/a
	Heat sink; temperature control off (constant spindle speed of 492 rev/min)	Heat source; temperature control off (constant spindle speed of 492 rev/min)
Iteration 1	4.2.1	4.4.1
Iteration 2	4.2.2	n/a
Iteration 3	4.2.3	n/a

Table 5.8. Disturbance weld matrix

Measurements of room temperature; plate temperature on the weld path (at the disturbance position) before the disturbance was added; plate temperature on the weld path (at the disturbance position) after the disturbance was added; plate temperature at the start position of the weld (after the disturbance was added) and the plate temperature on the weld path immediately prior to the arrival of the welding tool at the disturbance were taken for each weld. The table containing all these measurements can be seen in Table 5.9 (heat sink disturbance welds) and Table 5.10 (heat source disturbance welds). “Weld 4.2.1.ni” corresponds to “Weld 3” in Figure 5.45 in which no disturbance was introduced and the temperature control algorithm was disengaged (for the purpose of comparison).

5.6.1. Heat Sink Disturbance

Weld	Room temperature (°C)	Plate temperature before the disturbance was added (disturbance position) (°C)	Plate temperature after the disturbance was added (disturbance position) (°C)	Plate temperature after the disturbance was added (start position) (°C)	Plate temperature prior to tool arrival at the disturbance position (°C)
4.1.1	23	21	-28	20	-30
4.1.2	23	20	-30	18	-32
4.1.3	23	20	-30	20	-31
4.2.1	22	23	-22	22	-20
4.2.2	24	21	-29	19	-31
4.2.3	23	21	-29	20	-31
4.2.1.ni	23	21	n/a	n/a	n/a

Table 5.9. Heat sink weld plate temperatures

Two dry ice containers were manufactured from AA 6082-T6 for the high thermal conductivity of aluminium. Dry ice was placed in the containers as shown in Figure

5.41. Ideally, there must be high thermal conductivity between the heat sink material (dry ice) and the weld plate. The thermal conductivity of air is low and the dry ice pellets contain air gaps between them. Methanol was used to fill these gaps to improve the thermal conductivity between the dry ice itself and the aluminium container. Methanol has a freezing point of -97.7°C ^[19] and at atmospheric pressure (below the triple point pressure (518 kPa) of carbon dioxide ^[19]), carbon dioxide transforms from its solid state (dry ice) directly to its gaseous form at -78.4°C ^[19]. The temperature of dry ice is considered to be approximately -78.5°C ^[22]. The temperature of the dry ice is therefore unable to freeze the methanol. The methanol therefore continually flows between the dry ice pellets and the container in order to improved thermal conductivity.



Figure 5.41. Dry ice and methanol heat sink

Figure 5.42 shows the positioning of a dry ice container relative to the weld.



Figure 5.42. Dry ice container placement

Since the temperature of the plate (undergoing welding) near the disturbance position varies as the weld tool approaches and then travels away from the area, the heat energy extraction rate will vary accordingly. The graph of heat extraction rate versus plate temperature (average temperature below the disturbance area) is shown in Figure 5.43. The graph was generated according to Equation 5.8 ^[19] for a range of plate temperatures from dry ice temperature to maximum weld zone temperature and the plate temperature will lie within this range. In addition to this, the graph in Figure 5.43 was generated using the following information: the thickness of the bottom of the container is ten millimeters or 0.01 m; the thermal conductivity of the container (k) is 180 W/m.°C ^[23]; the container contact area is 0.00714 m²; assuming that the methanol and dry ice mixture was able to maintain the temperature of the bottom of the container pocket at -78.4°C; assuming that the junction of the disturbance to the weld plate is of equivalent or higher thermal conductivity than the aluminium.

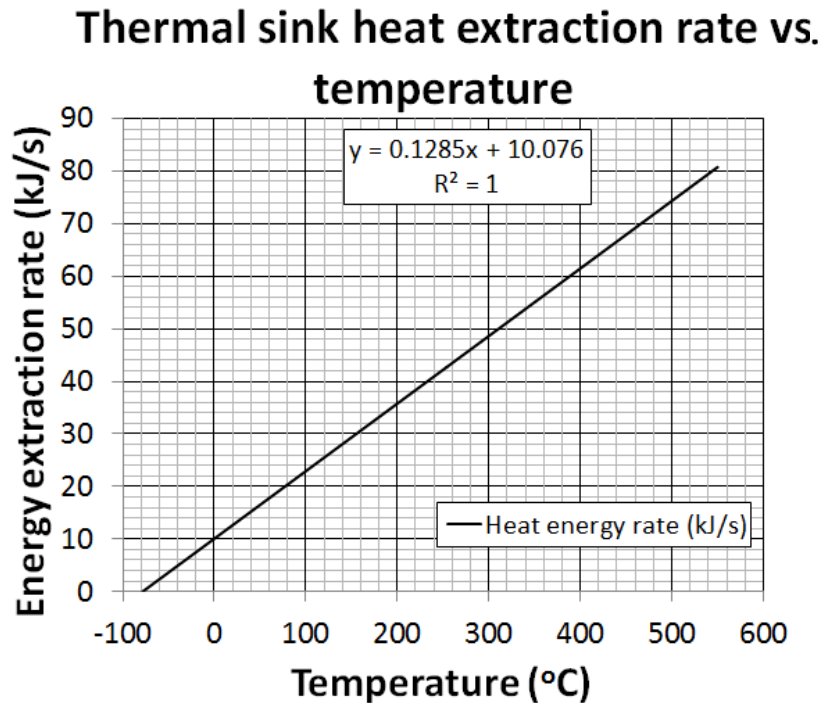


Figure 5.43. Disturbance heat extraction rate versus temperature

In the following two figures, “Weld 4.2.3”; “Weld 4.1.3” and weld “4.2.1.ni” are labelled: “Weld 1”; “Weld 2” and “Weld 3” respectively for clarity in this discussion.

“Weld 1” and “Weld 2” in Figure 5.44 compare weld zone temperature with respect to time. “Weld 1” was conducted with constant spindle speed (temperature control disengaged) set to approximately 492 rev/min. “Weld 2” was conducted with the temperature control engaged (spindle speed varies in order to maintain weld zone temperature) and the temperature set-point was set to 505°C. Both welds had the dry ice disturbance present between the middle clamps. It is clear from the graph of “Weld 2” in Figure 5.44 that the temperature control algorithm exhibits good disturbance rejection characteristics because the constant temperature region deviates from the set-point of 505°C by no more than 1.1°C including the cooled region (disturbance position) indicated on the graph.

Temperature vs.time

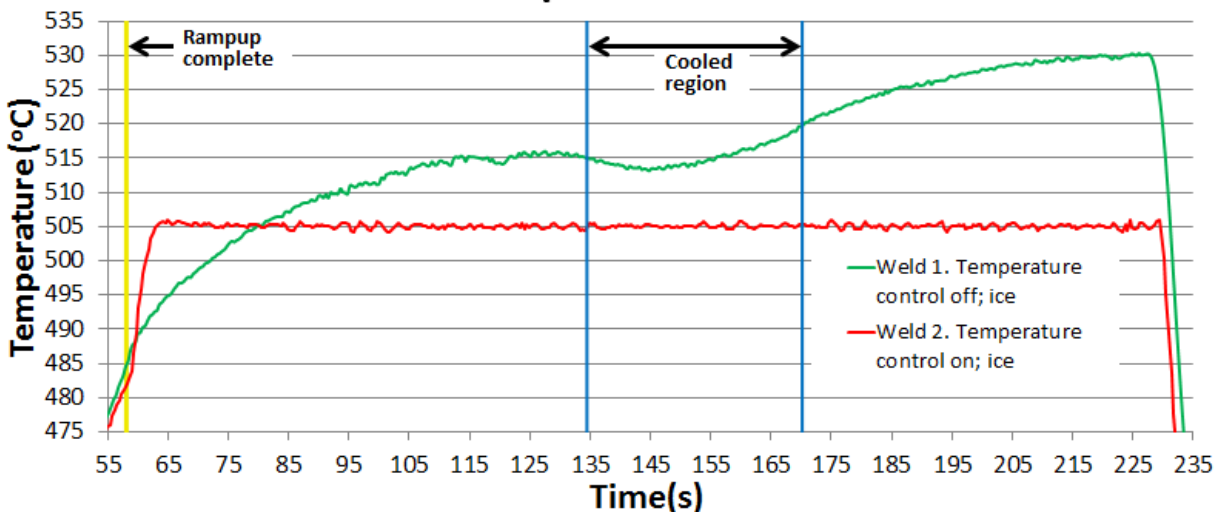


Figure 5.44. Temperature control engaged/disengaged heat sink welds

“Weld 3” (in Figure 5.45) was conducted with no dry ice disturbance and no temperature control (constant spindle speed of 492 rev/min), for comparison with “Weld 1” and “Weld 2”. Comparing the graphs of “Weld 1” and “Weld 3”, the effect of the dry ice disturbance is clear. The temperature difference between the two temperature graphs varies and the maximum temperature difference in the cooled region is approximately 5.6°C.

Temperature vs.time

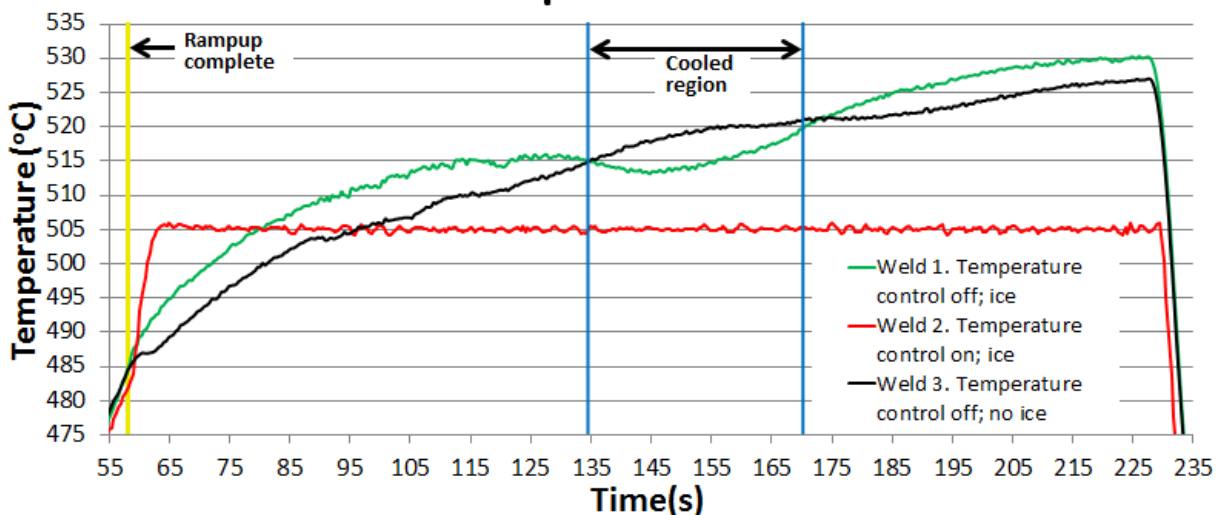


Figure 5.45. Weld 3 added for comparison with weld 1 and weld 2

The spindle speeds of the three welds are shown in Figure 5.46. The spindle speed of “Weld 1” and “Weld 3” was constant at approximately 492 rev/min. The temperature control algorithm varied the spindle speed of “Weld 2” in order to maintain the weld zone temperature at the set-point of 505°C. It is clear from the spindle speed graph of “Weld 2” that the controller increased the spindle speed as the weld tool approached and traversed into the cooled region in order to compensate for the dry ice disturbance.

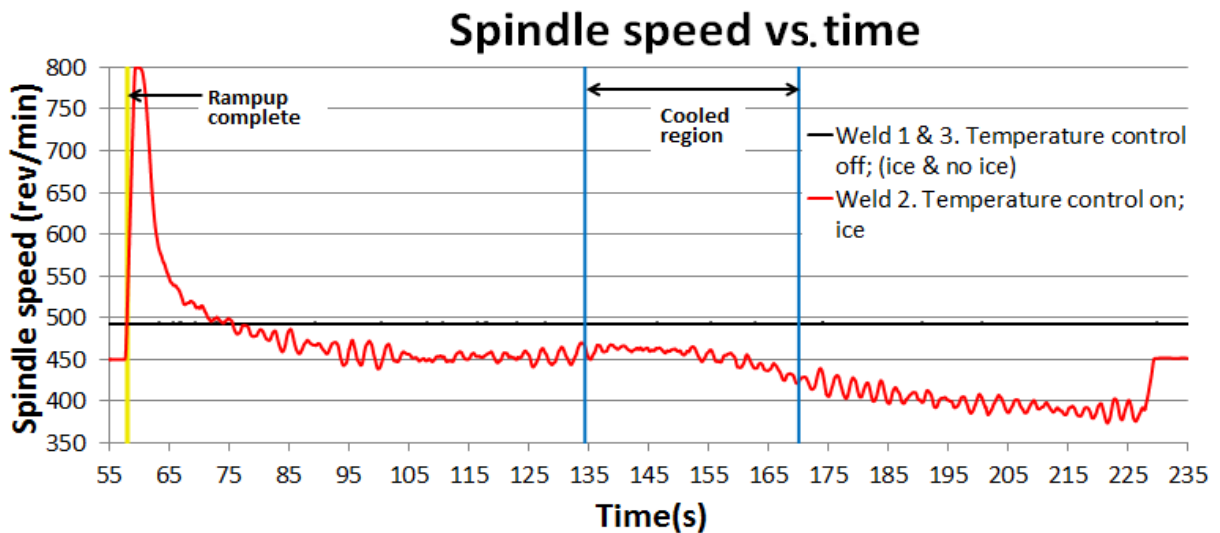


Figure 5.46. Spindle speed of weld 1, weld 2 and weld 3

5.6.2. Heat Source Disturbance

Weld	Room temperature (°C)	Plate temperature before the disturbance was added (disturbance position) (°C)	Plate temperature after the disturbance was added (disturbance position) (°C)	Plate temperature after the disturbance was added (start position) (°C)	Plate temperature prior to tool arrival at the disturbance position (°C)	Plate temperature post weld completion at the disturbance position (°C)
4.3.1	21	20	121	25	110	105
4.4.1	21	24	126	28	121	106

Table 5.10. Heat source weld plate temperatures

A heat energy source disturbance was introduced to the weld plate. This disturbance causes the temperature controller to decrease the spindle speed (hence decreasing frictional heat energy input) to compensate for the disturbance.

The heat energy source was introduced by heating two steel blocks to approximately 400°C in a furnace and placing them on either side of the weld path with thermal paste between them and the weld plate. The blocks covered approximately the same area as the heat sink disturbance containers. The bottom face of the blocks were surface ground in order to maximise the contact area with the weld plate and eliminate any rust which would contaminate the thermal junction. The block positioning is shown in Figure 5.47.



Figure 5.47. Heated block disturbance close view

The heat source disturbance welds were tensile tested although the welds were not repeated for statistical purposes. The heat source disturbance welds were conducted primarily to verify that the temperature control system successfully compensates for this type of disturbance. The statistical analysis was deemed unnecessary following the statistical analysis (see Section 5.7) conducted for the welds completed and

discussed in Section 5.6.1. The positioning of the blocks relative to the weld setup is shown in Figure 5.48.



Figure 5.48. Heated steel block disturbance position relative to the weld setup

In the following two figures, “Weld 4.2.1.ni”; “Weld 4.4.1” and “Weld 4.3.1” are labelled: “Weld 3”; “Weld 4” and “Weld 5” respectively for clarity in this discussion.

The temperature versus time relationship of “Weld 4” in Figure 5.49 shows that with the temperature control disengaged and the heat source disturbance introduced, the temperature of the weld increases in the vicinity of the disturbance.

From the temperature versus time relationship of “Weld 5” in Figure 5.49, it is clear that the control system was successful in maintaining the weld zone temperature set-point of 505°C despite the presence of the disturbance.

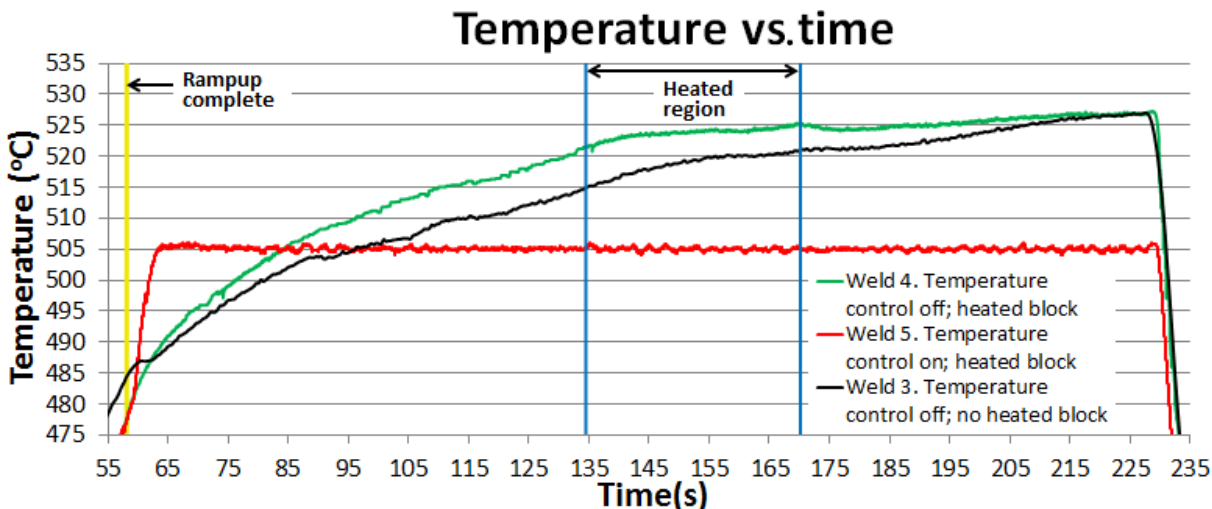


Figure 5.49. Temperature control engaged/disengaged heat source welds

The spindle speeds of the three welds are shown in Figure 5.50. The spindle speed of “Weld 3” and “Weld 4” was constant at approximately 492 rev/min. The temperature control algorithm varied the spindle speed of “Weld 5” in order to maintain the weld zone temperature at the set-point of 505°C. It is clear from the spindle speed graph of “Weld 5” that the controller decreased the spindle speed when the weld tool approached and entered the heated region in order to compensate for the heated block disturbance.

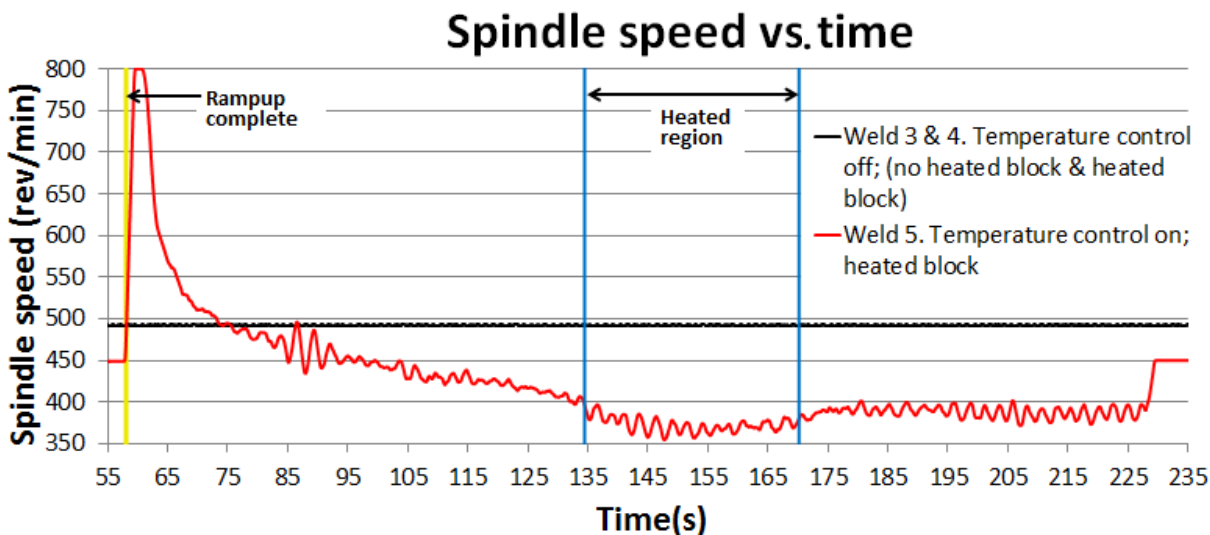


Figure 5.50. Spindle speed of weld 3, weld 4 and weld 5

5.7. Tensile Testing and Analysis

Weld strength consistency was investigated by means of tensile testing. This testing was done on the welds discussed in Section 5.6. The width of the plates on which welding was conducted was no less than 100 mm. The tensile samples were taken transversely through the welds. The tensile samples were machined to the ASTM E 8M standard for a tensile subsize specimen. Two examples of the as welded and machined tensile specimens are shown in Figure 5.51.



Figure 5.51. Tensile samples

Four positions along the weld length were tensile tested. The distance of these positions from the start point of the weld include 50 mm (near the start of the weld); 334.11 mm (mid-point of the disturbance area); 388.61 mm (end of the disturbance area) and 546 mm (near the end of the weld). The four tensile sample cut-out positions are labelled in Figure 5.52.

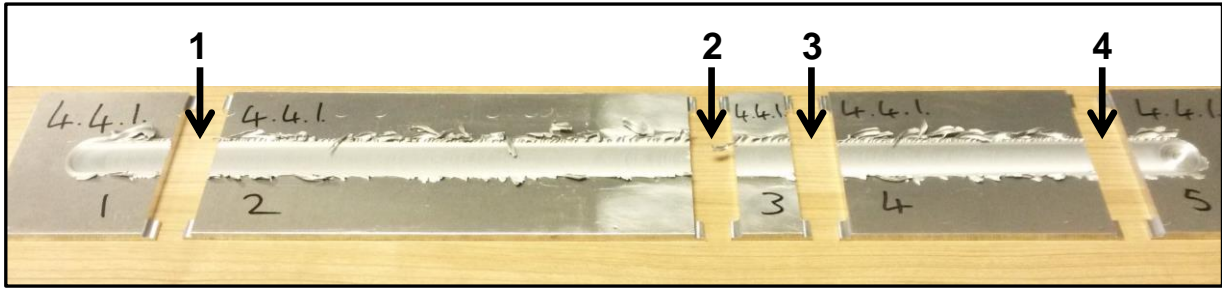


Figure 5.52. Tensile sample positions

All welds failed in the heat affected zone due to over aging of AA 6082-T6 (material strength is reduced by over aging) in this region. The welds do not fail in the parent material (over aging is approximately negligible); the weld nugget or the thermo-mechanically affected zone (TMAZ). Failure does not occur in the weld nugget or TMAZ because dynamic recrystallisation is experienced in these areas and smaller grain sizes are generated in these regions^[8]. The parent material, TMAZ and weld nugget are therefore stronger than the heat affected zone (next to the weld) provided that voids do not exist in the weld nugget or TMAZ.

5.7.1. Comparison of Weld Strength at each Tensile Sample Position

The tensile test results and the statistical data for the heat sink disturbance welds are shown in Table 5.11 (Weld set 4.1: temperature controlled welds with set-point set to 505°C) and Table 5.12 (Weld set 4.2: constant spindle speed welds with spindle speed set to 492 rev/min).

Weld repetition number	Yield strength (MPa)				Ultimate tensile strength (MPa)			
	sample position 1	sample position 2	sample position 3	sample position 4	sample position 1	sample position 2	sample position 3	sample position 4
4.1.1	147.54	152.48	147.27	141.69	235.00	236.42	231.27	227.80
4.1.2	146.27	144.21	144.61	142.53	231.28	230.93	229.57	226.60
4.1.3	146.27	143.51	145.73	139.08	229.81	230.21	229.98	228.72
mean	146.69	146.73	145.87	141.10	232.03	232.52	230.27	227.71
standard deviation	0.735	4.986	1.335	1.800	2.675	3.397	0.887	1.063
n	3	3	3	3	3	3	3	3
t critical	4.303	4.303	4.303	4.303	4.303	4.303	4.303	4.303
uncertainty (95%)	1.825	12.387	3.315	4.471	6.646	8.438	2.204	2.641

Table 5.11. Tensile results of temperature controlled, heat sink disturbance welds (4.1)

Weld repetition number	Yield strength (MPa)				Ultimate tensile strength (MPa)			
	sample position 1	sample position 2	sample position 3	sample position 4	sample position 1	sample position 2	sample position 3	sample position 4
4.2.1	144.65	150.97	147.07	146.17	231.83	234.11	234.27	228.71
4.2.2	141.21	149.31	150.36	148.12	228.55	233.80	235.30	232.22
4.2.3	141.80	150.54	150.57	149.08	230.01	234.81	235.28	231.58
mean	142.55	150.27	149.33	147.79	230.13	234.24	234.95	230.84
standard deviation	1.840	0.860	1.958	1.483	1.643	0.517	0.589	1.869
n	3	3	3	3	3	3	3	3
t critical	4.303	4.303	4.303	4.303	4.303	4.303	4.303	4.303
uncertainty (95%)	4.572	2.138	4.864	3.683	4.082	1.285	1.463	4.644

Table 5.12. Tensile results of constant spindle speed, heat sink disturbance welds (4.2)

Three parent samples were tensile tested in order to calculate the parent strength with statistical uncertainty. The ultimate tensile strength (UTS) of AA6082-T6 parent plate was 328.86 ± 1.18 MPa (95 percent confidence). The weakest mean UTS from the weld tensile data was 227.71 ± 2.64 MPa (95 percent confidence) which is approximately 69.24 percent of the parent UTS. The strongest mean UTS from the weld tensile data is 234.95 ± 1.46 MPa (95 percent confidence) which is approximately 71.44 percent of the parent UTS. The minimum and maximum tensile strengths are both greater than 66 percent of the strength of the parent plate which is considered a good weld for heat treatable aluminium alloys^[7].

The data presented in Table 5.11 and Table 5.12 was used to generate graphs comparing the weld strength consistency of a weld conducted with constant weld zone temperature (and therefore varying spindle speed) versus a typical FSW weld which is conducted with constant spindle speed (and therefore varying weld zone temperature). Both welds have the heat sink disturbance introduced. The comparison of weld strength at the four tensile sample positions between weld sets 4.1 and 4.2 is shown in Figure 5.53 (yield strength comparison) and Figure 5.54 (ultimate strength comparison).

Yield strength vs.tensile sample position

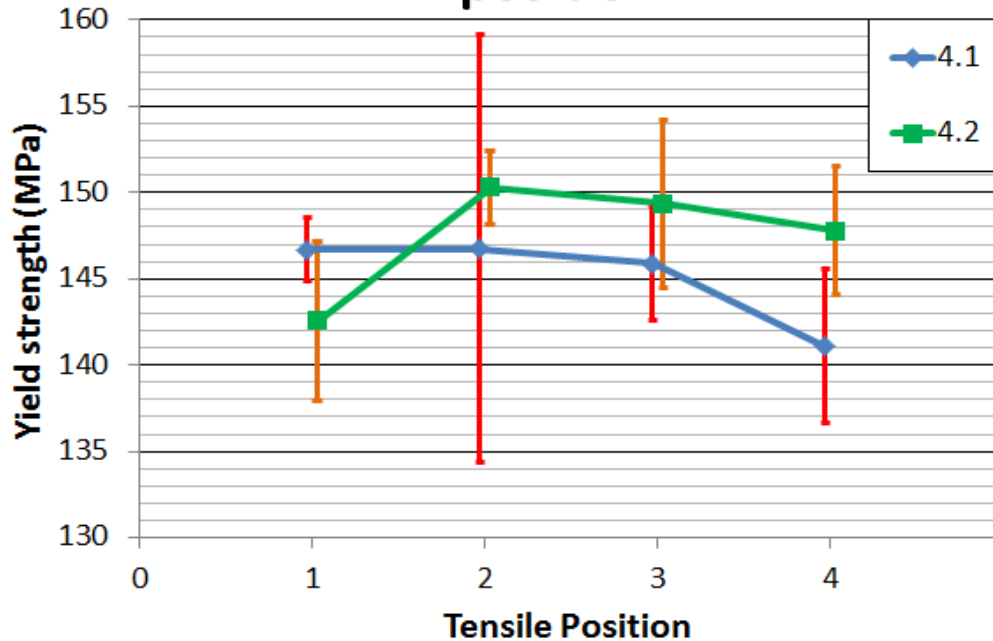


Figure 5.53. Tensile yield strength comparison between weld sets 4.1 and 4.2

The error bars of the yield strengths for position 2 and position 3 overlap substantially. This suggests that the difference between weld set 4.1 and weld set 4.2 at these positions can be attributed to experimental error. The yield strengths at position 1 and position 4 also have overlapping error bars although the amount by which they overlap is less than for position 2 or position 3. Statistical t-tests were conducted using Microsoft Excel's data analysis tool. Each t-test compared the weld yield strength of the two weld sets (4.1 and 4.2) at each of the four tensile sample positions. The t-tests determine whether or not the difference in weld strength can be attributed to experimental error or not, with 95 percent confidence. The results of the t-tests are shown in Table 5.13.

t-test results	Yield strength position 1	Yield strength position 2	Yield strength position 3	Yield strength position 4
p value	0.022443	0.292119	0.064690	0.007659

Table 5.13. Yield strength t-test results

The results from the t-tests suggest that the difference between weld set 4.1 and weld set 4.2 at position 1 cannot be attributed to experimental error ($p=0.022<0.05$ or 2.2 percent probability that the difference can be attributed to experimental error). The test result for position 2 suggests that the difference between weld set 4.1 and weld set 4.2 can be attributed to experimental error with relatively large probability ($p=0.292>0.05$). The t-test result for position 3 suggests that the difference between weld set 4.1 and weld set 4.2 can be attributed to experimental error ($p=0.065>0.05$) although the p value is marginally larger than 0.05 which means that it could be argued that the difference may or may not be attributed to experimental error. The t-test for position 4 suggests strongly that the strength difference between weld set 4.1 and weld set 4.2 cannot be attributed to experimental error ($p=0.008<0.05$).

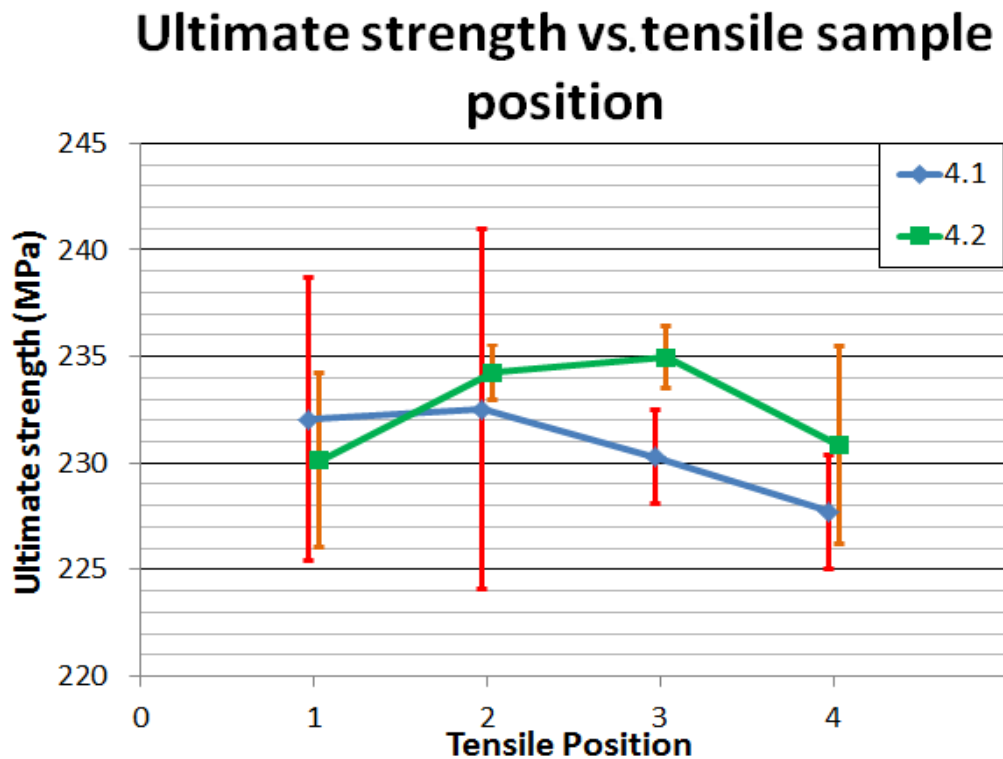


Figure 5.54. Ultimate tensile strength comparison between weld sets 4.1 and 4.2

T-tests were conducted for the ultimate tensile strengths at each tensile sample position. The results are shown in Table 5.14.

t-test results	Ultimate strength position 1	Ultimate strength position 2	Ultimate strength position 3	Ultimate strength position 4
p value	0.35369	0.434816	0.001603	0.065289

Table 5.14. Ultimate strength t-test results

The t-tests conducted for the ultimate strength results suggest strongly that the ultimate strength difference between weld set 4.1 and weld set 4.2 at position 1 and position 2 are attributed to experimental error ($p=0.354>0.05$ and $p=0.435>0.05$). The t-test for position 3 suggests strongly that the ultimate strength difference between weld set 4.1 and weld set 4.2 cannot be attributed to experimental error. The t-test for position 4 suggests that the strength difference between weld set 4.1 and weld set 4.2 can be attributed to experimental error although it is not a strong suggestion because the p value is marginally larger than 0.05 ($p=0.065>0.05$). The t-tests generated using the Microsoft Excel data analysis tool are shown in **Appendix L**.

In conclusion of the presented statistical t-tests and referring to Table 5.13 and Table 5.14, the yield strength at position 1 can be considered different for weld set 4.1 and weld set 4.2, although the ultimate strength can be considered the same. Regarding position 2, both the yield strength and the ultimate strength can be considered the same between weld set 4.1 and weld set 4.2. Regarding position 3, the yield strength can be argued to be different and the ultimate strength can be considered different between weld set 4.1 and weld set 4.2. Regarding position 4, the yield strength can be considered different and the ultimate strength can be argued to be different between weld set 4.1 and weld set 4.2.

5.7.2. Investigation of Weld Strength Consistency

For the purpose of this study, the standard deviation of the weld strength along the weld length is considered an indication of weld strength consistency. The difference in weld strength consistency between weld set 4.1 and weld set 4.2 is calculated from the data taken from Table 5.11 and Table 5.12 and shown in Table 5.15 and Table 5.16.

		Yield strength (Mpa)				
Weld number	Weld repetition	sample position 1	sample position 2	sample position 3	sample position 4	standard deviation
4.1	4.1.1	147.54	152.48	147.27	141.69	4.407
	4.1.2	146.27	144.21	144.61	142.53	1.535
	4.1.3	146.27	143.51	145.73	139.08	3.271
4.2	4.2.1	144.65	150.97	147.07	146.17	2.697
	4.2.2	141.21	149.31	150.36	148.12	4.130
	4.2.3	141.80	150.54	150.57	149.08	4.186

Table 5.15. Yield tensile strength standard deviations

A statistical t-test was conducted to investigate the weld yield strength consistency (represented by the standard deviation) difference between weld set 4.1 and weld set 4.2. The two sets of data on which the test was conducted are highlighted green and blue in Table 5.15. The mean standard deviation for weld set 4.1 is 3.071 MPa and the mean standard deviation for weld set 4.2 is 3.671 MPa. The standard deviation of weld set 4.1 is smaller than the standard deviation of weld set 4.2 which proposes that the strength is more consistent in weld set 4.1 although the p value of the t-test was 0.569. This strongly suggests that this difference between the standard deviations of strength in weld set 4.1 and the standard deviations of strength in weld set 4.2 can be attributed to experimental error. The t-test generated by the Microsoft Excel data analysis tool can be seen in **Appendix L, page L-3**.

Ultimate tensile strength (MPa)						
Weld number	Weld repetition	sample position 1	sample position 2	sample position 3	sample position 4	standard deviation
4.1	4.1.1	235.00	236.42	231.27	227.80	3.880
	4.1.2	231.28	230.93	229.57	226.60	2.129
	4.1.3	229.81	230.21	229.98	228.72	0.661
4.2	4.2.1	231.83	234.11	234.27	228.71	2.598
	4.2.2	228.55	233.80	235.30	232.22	2.899
	4.2.3	230.01	234.81	235.28	231.58	2.543

Table 5.16. Ultimate tensile strength standard deviations

A statistical t-test was conducted to investigate the weld ultimate strength consistency (represented by the standard deviation) difference between weld set 4.1 and weld set 4.2. The two sets of data on which the test was conducted are highlighted green and blue in Table 5.16. The mean standard deviation for weld set 4.1 is 2.223 MPa and the mean standard deviation for weld set 4.2 is 2.680 MPa. The standard deviation of weld set 4.1 is smaller than the standard deviation of weld set 4.2 which proposes that the strength is more consistent in weld set 4.1 although the p value of the t-test was 0.651. This strongly suggests that this difference between the standard deviations of strength in weld set 4.1 and the standard deviations of strength in weld set 4.2 can be attributed to experimental error. The t-test generated by the Microsoft Excel data analysis tool can be seen in **Appendix L, page L-3**.

5.8. Summary

Initially, the process window was established on the MTS FSW platform. This process discovered the correct tool tilt angle, the correct forge force and the safe maximum and minimum limits for spindle speed such that the tool does not seize/fracture nor over plunge. This process window is unique to the particular weld setup in this study.

In the preliminary stage of the study, the weld zone temperature response to spindle speed changes was investigated and the process found to be non-linear. This stage of the study provided the researcher with a better understanding of the process temperature response to changes in spindle speed and a set of data from which to generate a mathematical model of the process.

The PID temperature control algorithm layout, design and implementation were explained in detail. The tuning theory (Ziegler Nichols tuning method ^[3]) by which the algorithm was tuned and the method carried out by the researcher was explained in detail. After implementation of the control algorithm, the procedure for testing the response of the control system by implementing step command changes in the temperature set-point was explained. The results from the tuning welds and performance testing welds were discussed. Various derivative filter designs were developed and tested in order to deduce the oscillation of the spindle speed during temperature control.

A mathematical model (transfer function) was developed using Matlab's system identification tool. The result was a second order transfer function. The PID gains found from the Ziegler Nichols tuning method ^[3] were used in the PID controller connected to the process model in Matlab Simulink. The simulation response was found to be relatively similar to the response of the actual system.

Two Matlab controller design tools were utilised to generate PID controllers based on the process model (transfer function) generated. The performance of each of these controllers was simulated in comparison to simulation of the Ziegler Nichols ^[3] PID controller design mentioned in the previous paragraph. The two controller design tools utilised include Matlab's Automatic Control Systems toolbox (ACSYS) and Matlab Simulink PID tuner. The ACSYS toolbox was used to perform bode diagram frequency design of a PID controller. The purpose of the development of these controllers was for comparison with the controller designed using the Ziegler Nichols tuning method ^[3].

Utilising the PID controller found from the Ziegler Nichols tuning method ^[3], the disturbance rejection capability of the control system was tested. Heat sink and heat source type disturbances were introduced and the control system successfully compensated for them by maintaining constant weld zone temperature to within 1.1°C of the set-point temperature (505°C).

In order to investigate weld strength consistency of a constant temperature weld versus a typical FSW conducted with constant spindle speed (in the presence of a heat sink disturbance), tensile tests were conducted. The welds from which the tensile samples were machined, consisted of a constant temperature weld with repetitions (weld set 4.1; temperature: 505°C) and a constant spindle speed weld with repetitions (weld set 4.2; spindle speed: 492 rev/min). Four tensile samples were machined from each weld. Each weld set consisted of three repetitions in order to produce a sufficient number of tensile samples for statistical purposes. Differences in weld strength between weld set 4.1 and weld set 4.2 at various positions which could not be attributed to experimental error were found statistically. Some differences in weld strength between weld set 4.1 and weld set 4.2 at various positions which could be attributed to experimental error were also found statistically.

An investigation of weld strength standard deviation along the weld length as a representation of weld strength consistency was carried out.

Chapter 6

Conclusions and Future Research

As proven by this study, weld zone temperature of FSW can be controlled using PID control provided that the performance reported in this document is acceptable to the specific production process for which it is used. Typically there is no reason to change weld temperature during a weld and the production process setup usually contains a run-on tab or a limited region at the beginning of the weld where reduced weld quality can be tolerated. All FSW welds need to ramp up weld zone temperature from room temperature to the required weld temperature in the beginning stage. Once up to temperature, a well-tuned PID controller is able to maintain the weld zone temperature with deviation from the set-point of less than 1.1°C as proven by this study. If any undesirable overshoot were to occur whilst the system achieves welding temperature, it could be programmed to take place in the ramp up region on the run-on tab.

The results show that FSW temperature response to spindle speed changes can be relatively accurately modelled using Matlab's system identification tool. The results also show that the Matlab ACSYS controller design tool as well as Matlab Simulink can be used to design PID controllers which closely match the controller design obtained from the practical Ziegler Nichols tuning method^[3].

This study identified that in some control cases; the derivative term of the PID controller may cause undesirable oscillation of the system actuator due to the derivative term's high gain for high frequency signals (generally caused by noise on the sensor feedback signal). The study showed that filter design and implementation on the feedback signal and/or implementation of a filter type derivative equation

(executed during calculation of the derivative term) can reduce the oscillation of the system actuator.

The PID controller implemented in this study (designed using the Ziegler Nichols tuning method ^[3]) improved the system bandwidth from 0.00185 rad/s (of the uncompensated system) to 0.939 rad/s (of the PID compensated system). The PID control system exhibits good thermal disturbance rejection as evidenced by the heat energy sink and heat energy source disturbance welds conducted in this study (see Section 5.6). The control system was able to maintain the weld temperature to within 1.1°C of the set-point despite the presence of the disturbances.

Tensile testing showed no significant improvement of weld quality by maintaining constant weld temperature. It is important to note that this statement pertains to welds conducted with weld zone temperature in the range of temperature reported in this study. Minimum UTS to maximum UTS recorded in this study ranged from 227.71±2.641 MPa (95 percent confidence), which is approximately 69.24 percent of the parent UTS, to 234.95±1.463 MPa (95 percent confidence) which is approximately 71.44 percent of the parent UTS. This range is 7.24±4.104 MPa (95 percent confidence) which is small relative to the weld strength (less than 5%) which could be considered insignificant.

Weld zone temperature which is too low will cause defects to develop in the weld which would reduce weld strength considerably. A weld of this nature was not executed in this study. The temperature control system ensures that the weld is conducted with sufficient weld zone temperature in order to avoid defect production (provided the temperature set-point is correct for the specific weld setup). In the process window of FSW weld zone temperature, above a certain critical temperature, according to results found in literature titled: “Effects of Tool-Workpiece Interference Temperature on Weld Quality and Quality Improvements Through Temperature Control in Friction Stir Welding” ^[8], weld quality is approximately constant although

weld zone temperature below a critical value resulted in the production of defects and therefore reduced weld quality.

6.1. Future Research

Future research could include executing low temperature welds (minimum spindle speed) which introduce a heat energy sink which creates a larger temperature gradient between itself and the weld plate (such as liquid nitrogen placed in the containers instead of dry ice and methanol) which would cause a lower weld temperature at the disturbance. This could possibly reduce the weld zone temperature (with the temperature control disengaged) to a value below the critical temperature where voids begin to form in the weld (hence dramatically reducing weld quality). This would further test the control algorithm although it would introduce risks such as tool seizure and/or fracture. From common knowledge and literature titled: "Effects of Tool-Workpiece Interference Temperature on Weld Quality and Quality Improvements Through Temperature Control in Friction Stir Welding" [8], it is known that below a certain temperature, voids will begin to form, dramatically reducing weld quality. From this study it was found that the critical temperature below which weld quality is dramatically reduced lies below the temperature obtained when conducting a weld at the lower safe limit of spindle speed determined for the particular weld setup in this study. A wide range of weld temperature therefore exists in which the resultant weld strength is approximately constant.

Alternative control algorithms could be developed such as fuzzy logic and genetic algorithms. The performance of these control methods could be compared to the results obtained in this study. The thermal disturbances could be modelled in order to be able to introduce them into the control system simulation. The disturbance rejection of the simulated model can then be compared to the disturbance rejection of the actual control system.

Bibliography

1. Blignault C, Hattingh DG, van Niekerk TI. A Friction Stir Weld Tool-force and Response Surface Model Characterizing Tool Performance and Weld Joint Integrity. Phd Thesis. Port Elizabeth: Nelson Mandela Metropolitan University, Mechanical Engineering; 2006.
2. Buffa G, Fratini L, Micari F. On the Choice of Tool Material in Friction Stir Welding of Titanium Alloys. Proceedings of NAMRI/SME. 2012; 40.
3. Ziegler JG, Nichols NB. Optimum Settings for Automatic Controllers. Transactions of the ASME. 1942; 64: p. 759-768.
4. Threadgill PL, Leonard AJ, Shercliff HR, Withers PJ. Friction stir welding of aluminium alloys. International Materials Reviews. 2009; 54(2): p. 49-93.
5. Fehrenbacher A, Cole EG, Zinn MR, Ferrier NJ, Duffie NA, Pfefferkorn FE. Towards Process Control of Friction Stir Welding for Different Aluminum Alloys, in Friction Stir Welding and Processing VI (eds R. Mishra, M. W. Mahoney, Y. Sato, Y. Hovanski and R. Verma) Hoboken, New Jersey, USA: John Wiley & Sons, Inc.; 2011.
6. Ross K, Sorensen C. Investigation of Methods to Control Friction Stir Weld Power with Spindle Speed Changes, in Friction Stir Welding and Processing VI (eds R. Mishra, M. W. Mahoney, Y. Sato, Y. Hovanski and R. Verma) Hoboken, New Jersey, USA: John Wiley & Sons, Inc.; 2011.
7. Chao YJ, Qi X, Tang W. Heat Transfer in Friction Stir Welding-Experimental and Numerical Studies. Journal of Manufacturing Science and Engineering. 2003; 125: p. 138-145.
8. Fehrenbacher A, Duffie NA, Ferri NJ, Pfefferkorn FE, Zinn MR. Effects of Tool-Workpiece Interference Temperature on Weld Quality and Quality Improvements Through Temperature Control in Friction Stir Welding. Research. Madison, USA: University of Wisconsin, Mechanical Engineering; 2012.
9. Astrom KJ, Murray RM. Feedback Systems An Introduction for Scientists and Engineers. 2nd ed. New Jersey: Princeton University Press; 2012.
10. Melendez M, Tang+ W, Schmidt C, McClure JC, Nunes* AC, Murr LE. Tool Forces Developed During Friction Stir Welding. University of Texas at El Paso;

+University of South Carolina, Columbia, S.C; *Huntsville, Alabama, Metallurgical and Materials Engineering Department; +Mechanical Engineering Department; *NASA Marshall Space Flight Center.

11. Kumbhar NT, Bhanumurthy K. Friction Stir Welding of Al 6061 Alloy. Asian Journal of Experimental Sciences. 2008; 22(2): p. 63-74.
12. Yokoyama T, Nakai K, Suedai E, Katoh K. Tensile Properties and Constitutive Modeling of Friction Stir Welded AA6061-T6 Butt Joints. Journal of Solid Mechanics and Materials Engineering. 2011 July; 5(12): p. 780-792.
13. Lakshman Rao M, Suresh Babu P, Rammohan T, Seenaiah Y. Study of Tool Geometry in Friction Stir Welding Applications. AKGEC International Journal of Technology. ; 3(2): p. 15-18.
14. Hao LU, Peilin LI, Zhongfeng XU, Meng XU. The Influence of Thread Form on Refilling Friction Stir Welding of 2219 Aluminum Alloy Sheets. Transactions of JWRI. 2011;(Special Issue on WSE2011): p. 41-42.
15. Venkateswarlu D, Mandal NR, Mahapatra MM, Harsh SP. Tool Design Effects for FSW of AA7039. Welding Journal. 2013 February; 92: p. 41-47.
16. Mohanty HK, Mahapatra MM, Kumar P, Biswas P, Mandal NR. Effect of Tool Shoulder and Pin Probe Profiles on Friction Stirred Aluminum Welds – a Comparative Study. Journal of Marine Science and Application. 2012; 11: p. 200-207.
17. Omega. [Online].; 2014 [cited 2014 September 25. Available from: <http://www.omega.com/temperature/Z/pdf/z216-217.pdf>.
18. Terasrenki. [Online]. [cited 2014 September 23. Available from: http://cdna.terasrenki.com/ds/6082_Aluminum_Datasheet_1.pdf.
19. Cengel YA, Turner RH, Cimbala JM. Fundamentals of Thermal-Fluid Sciences. 3rd ed. Singapore: McGraw-Hill; 2008.
20. Golnaraghi F, Kuo BC. Automatic Control Systems. 9th ed.: John Wiley & sons, inc; 2009.
21. Phillips CL, Nagle HT. Digital Control System Analysis and Design. 3rd ed. New Jersey: Pearson Education International Inc.; 1998.

22. dryiceinfo.com. [Online].; 2014 [cited 2014 11 23. Available from: <http://www.dryiceinfo.com/>.
23. aalco. [Online].; 2013 [cited 2014 11 23. Available from: http://www.aalco.co.uk/datasheets/Aluminium-Alloy-6082-T6T651-Sheet_335.ashx.

Additional References

(References consulted prior to initiation of the experimental study)

24. Mishra R, Mahoney MW, Sato Y, Hovanski Y, Verma R. Friction Stir Welding and Processing VI. 1st ed. Hoboken, New Jersey: John Wiley & Sons,inc; 2011.
25. Sattari S, Bisadi H, Sajed M. Mechanical Properties and Temperature Distributions of Thin Friction Stir Welded Sheets of AA5083. International Journal of Mechanics and Applications. 2012; 2(1): p. 1-6.
26. Blignault C, Hattingh DG, Kruger GH, van Niekerk TI, James MN. Friction stir weld process evaluation by multi-axial transducer. Measurement. 2008; 41(1): p. 32-43.
27. van Niekerk TI, Hattingh DG, Clark I, Majara KE. A Fuzzy Logic Control System for a Friction Stir Welding Process. Masters Dissertation. Port Elizabeth: Nelson Mandela Metropolitan University, Electrical Engineering; 2006.
28. Hua T. Monitoring and Intelligent Control for Complex Curvature Friction Stir Welding. PhD Thesis. Port Elizabeth: Nelson Mandela Metropolitan University; 2006.
29. Hattingh DG, van Niekerk TI, Blignault C. Analysis of The FSW Force Footprint and its Relationship with Process Parameters to Optimise Weld Performance and Tool Design. Welding in the World. 2004 February; 48(1).
30. Hattingh DG, van Niekerk TI, Blignault C. Design, Development and Analysis of the Friction Stir Welding Process. Masters Dissertation. Port Elizabeth: Port Elizabeth Technikon, Mechanical Engineering; 2002.
31. van Niekerk TI, Hattingh DG, Adlam F, Kruger G. Intelligent Monitoring and Control System for a Friction Stir Welding Process. Masters Dissertation. Port Elizabeth: Port Elizabeth Technikon; 2003.

32. Els-Botes A, Hattingh DG, MJALI KV. Analysing the Effect of Friction Stir Processing on MIG-Laser Hybrid Welded AA 6082-T6 Joints. Masters Dissertation. Nelson Mandela Metropolitan University, Mechanical Engineering; 2007.

Appendix A- Thermocouple data and calibration

J-type thermocouple table obtained from:

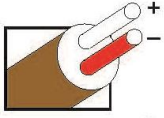
Omega. [Online].; 2014 [cited 2014 September 25]. Available from:

<http://www.omega.com/temperature/Z/pdf/z216-217.pdf>.

Revised Thermocouple Reference Tables


TYPE J

Reference Tables
N.I.S.T.
Monograph 175
Revised to ITS-90



Thermocouple Grade

Iron vs. Copper-Nickel



Extension Grade

MAXIMUM TEMPERATURE RANGE

Thermocouple Grade
32 to 1382°F
0 to 750°C

Extension Grade
32 to 392°F
0 to 200°C

LIMITS OF ERROR
(whichever is greater)
Standard: 2.2°C or 0.75%
Special: 1.1°C or 0.4%

COMMENTS, BARE WIRE ENVIRONMENT:
Reducing, Vacuum, Inert; Limited Use in Oxidizing at High Temperatures;
Not Recommended for Low Temperatures

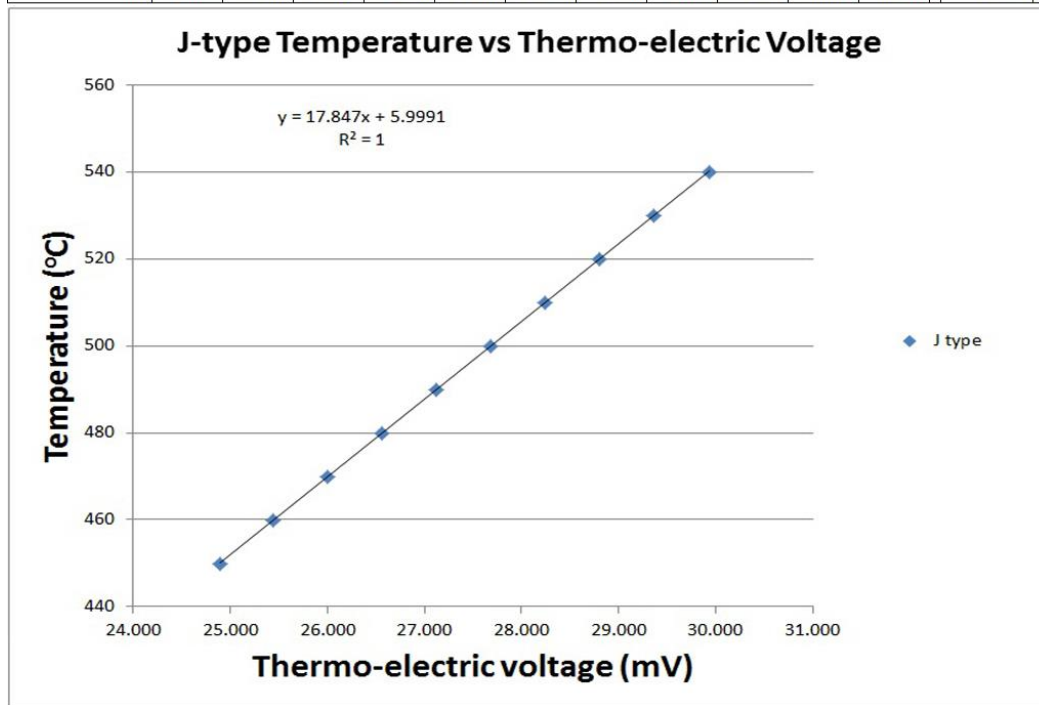
TEMPERATURE IN DEGREES °C
REFERENCE JUNCTION AT 0°C

Thermoelectric Voltage in Millivolts																																																																																																																																																																																																																																																																																																																																																																																																																																																																																																																																																																																																																																																																																																																																																																																																																																																																																																																																																																																																																																																																																																																																													
°C	-10	-8	-6	-4	-2	-1	0	1	2	3	4	5	6	7	8	9	10	°C	°C	°C																																																																																																																																																																																																																																																																																																																																																																																																																																																																																																																																																																																																																																																																																																																																																																																																																																																																																																																																																																																																																																																																																																																									
-200	-8.095	-8.076	-8.057	-8.037	-8.017	-7.996	-7.976	-7.955	-7.934	-7.912	-7.890	-7.868	-7.846	-7.824	-7.801	-7.778	-7.755	-7.731	-7.707	-7.683	-7.659	-7.635	-7.611	-7.587	-7.563	-7.539	-7.515	-7.491	-7.467	-7.443	-7.419	-7.395	-7.371	-7.347	-7.323	-7.299	-7.275	-7.251	-7.227	-7.203	-7.179	-7.155	-7.131	-7.107	-7.083	-7.059	-7.035	-7.011	-6.987	-6.963	-6.939	-6.915	-6.891	-6.867	-6.843	-6.819	-6.795	-6.771	-6.747	-6.723	-6.699	-6.675	-6.651	-6.627	-6.603	-6.579	-6.555	-6.531	-6.507	-6.483	-6.459	-6.435	-6.411	-6.387	-6.363	-6.339	-6.315	-6.291	-6.267	-6.243	-6.219	-6.195	-6.171	-6.147	-6.123	-6.099	-6.075	-6.051	-6.027	-6.003	-5.979	-5.955	-5.931	-5.907	-5.883	-5.859	-5.835	-5.811	-5.787	-5.763	-5.739	-5.715	-5.691	-5.667	-5.643	-5.619	-5.595	-5.571	-5.547	-5.523	-5.499	-5.475	-5.451	-5.427	-5.403	-5.379	-5.355	-5.331	-5.307	-5.283	-5.259	-5.235	-5.211	-5.187	-5.163	-5.139	-5.115	-5.091	-5.067	-5.043	-5.019	-5.000	-4.976	-4.952	-4.928	-4.904	-4.880	-4.856	-4.832	-4.808	-4.784	-4.760	-4.736	-4.712	-4.688	-4.664	-4.640	-4.616	-4.592	-4.568	-4.544	-4.520	-4.496	-4.472	-4.448	-4.424	-4.400	-4.376	-4.352	-4.328	-4.304	-4.280	-4.256	-4.232	-4.208	-4.184	-4.160	-4.136	-4.112	-4.088	-4.064	-4.040	-4.016	-3.992	-3.968	-3.944	-3.920	-3.896	-3.872	-3.848	-3.824	-3.800	-3.776	-3.752	-3.728	-3.704	-3.680	-3.656	-3.632	-3.608	-3.584	-3.560	-3.536	-3.512	-3.488	-3.464	-3.440	-3.416	-3.392	-3.368	-3.344	-3.320	-3.296	-3.272	-3.248	-3.224	-3.200	-3.176	-3.152	-3.128	-3.104	-3.080	-3.056	-3.032	-3.008	-2.984	-2.960	-2.936	-2.912	-2.888	-2.864	-2.840	-2.816	-2.792	-2.768	-2.744	-2.720	-2.696	-2.672	-2.648	-2.624	-2.600	-2.576	-2.552	-2.528	-2.504	-2.480	-2.456	-2.432	-2.408	-2.384	-2.360	-2.336	-2.312	-2.288	-2.264	-2.240	-2.216	-2.192	-2.168	-2.144	-2.120	-2.096	-2.072	-2.048	-2.024	-2.000	-1.976	-1.952	-1.928	-1.904	-1.880	-1.856	-1.832	-1.808	-1.784	-1.760	-1.736	-1.712	-1.688	-1.664	-1.640	-1.616	-1.592	-1.568	-1.544	-1.520	-1.496	-1.472	-1.448	-1.424	-1.400	-1.376	-1.352	-1.328	-1.304	-1.280	-1.256	-1.232	-1.208	-1.184	-1.160	-1.136	-1.112	-1.088	-1.064	-1.040	-1.016	-0.992	-0.968	-0.944	-0.920	-0.896	-0.872	-0.848	-0.824	-0.800	-0.776	-0.752	-0.728	-0.704	-0.680	-0.656	-0.632	-0.608	-0.584	-0.560	-0.536	-0.512	-0.488	-0.464	-0.440	-0.416	-0.392	-0.368	-0.344	-0.320	-0.296	-0.272	-0.248	-0.224	-0.200	-0.176	-0.152	-0.128	-0.104	-0.080	-0.056	-0.032	-0.008	0.016	0.040	0.064	0.088	0.112	0.136	0.160	0.184	0.208	0.232	0.256	0.280	0.304	0.328	0.352	0.376	0.400	0.424	0.448	0.472	0.496	0.520	0.544	0.568	0.592	0.616	0.640	0.664	0.688	0.712	0.736	0.760	0.784	0.808	0.832	0.856	0.880	0.904	0.928	0.952	0.976	1.000	1.024	1.048	1.072	1.096	1.120	1.144	1.168	1.192	1.216	1.240	1.264	1.288	1.312	1.336	1.360	1.384	1.408	1.432	1.456	1.480	1.504	1.528	1.552	1.576	1.600	1.624	1.648	1.672	1.696	1.720	1.744	1.768	1.792	1.816	1.840	1.864	1.888	1.912	1.936	1.960	1.984	2.008	2.032	2.056	2.080	2.104	2.128	2.152	2.176	2.200	2.224	2.248	2.272	2.296	2.320	2.344	2.368	2.392	2.416	2.440	2.464	2.488	2.512	2.536	2.560	2.584	2.608	2.632	2.656	2.680	2.704	2.728	2.752	2.776	2.800	2.824	2.848	2.872	2.896	2.920	2.944	2.968	2.992	3.016	3.040	3.064	3.088	3.112	3.136	3.160	3.184	3.208	3.232	3.256	3.280	3.304	3.328	3.352	3.376	3.400	3.424	3.448	3.472	3.496	3.520	3.544	3.568	3.592	3.616	3.640	3.664	3.688	3.712	3.736	3.760	3.784	3.808	3.832	3.856	3.880	3.904	3.928	3.952	3.976	4.000	4.024	4.048	4.072	4.096	4.120	4.144	4.168	4.192	4.216	4.240	4.264	4.288	4.312	4.336	4.360	4.384	4.408	4.432	4.456	4.480	4.504	4.528	4.552	4.576	4.600	4.624	4.648	4.672	4.696	4.720	4.744	4.768	4.792	4.816	4.840	4.864	4.888	4.912	4.936	4.960	4.984	5.008	5.032	5.056	5.080	5.104	5.128	5.152	5.176	5.200	5.224	5.248	5.272	5.296	5.320	5.344	5.368	5.392	5.416	5.440	5.464	5.488	5.512	5.536	5.560	5.584	5.608	5.632	5.656	5.680	5.704	5.728	5.752	5.776	5.800	5.824	5.848	5.872	5.896	5.920	5.944	5.968	5.992	6.016	6.040	6.064	6.088	6.112	6.136	6.160	6.184	6.208	6.232	6.256	6.280	6.304	6.328	6.352	6.376	6.400	6.424	6.448	6.472	6.496	6.520	6.544	6.568	6.592	6.616	6.640	6.664	6.688	6.712	6.736	6.760	6.784	6.808	6.832	6.856	6.880	6.904	6.928	6.952	6.976	7.000	7.024	7.048	7.072	7.096	7.120	7.144	7.168	7.192	7.216	7.240	7.264	7.288	7.312	7.336	7.360	7.384	7.408	7.432	7.456	7.480	7.504	7.528	7.552	7.576	7.600	7.624	7.648	7.672	7.696	7.720	7.744	7.768	7.792	7.816	7.840	7.864	7.888	7.912	7.936	7.960	7.984	8.008	8.032	8.056	8.080	8.104	8.128	8.152	8.176	8.200	8.224	8.248	8.272	8.296	8.320	8.344	8.368	8.392	8.416	8.440	8.464	8.488	8.512	8.536	8.560	8.584	8.608	8.632	8.656	8.680	8.704	8.728	8.752	8.776	8.800	8.824	8.848	8.872	8.896	8.920	8.944	8.968	8.992	9.016	9.040	9.064	9.088	9.112	9.136	9.160	9.184	9.208	9.232	9.256	9.280	9.304	9.328	9.352	9.376	9.400	9.424	9.448	9.472	9.496	9.520	9.544	9.568	9.592	9.616	9.640	9.664	9.688	9.712	9.736	9.760	9.784	9.808	9.832	9.856	9.880	9.904	9.928	9.952	9.976	10.000	10.024	10.048	10.072	10.096	10.120	10.144	10.168	10.192	10.216	10.240	10.264	10.288	10.312	10.336	10.360	10.384	10.408	10.432	10.456	10.480	10.504	10.528	10.552	10.576	10.600	10.624	10.648	10.672	10.696	10.720	10.744	10.768	10.792	10.816	10.840	10.864	10.888	10.912	10.936	10.960	10.984	11.008	11.032	11.056	11.080	11.104	11.128	11.152	11.176	11.200	11.224	11.248	11.272	11.296	11.320	11.344	11.368	11.392	11.416	11.440	11.464	11.488	11.512	11.536	11.560	11.584	11.608	11.632	11.656	11.680	11.704	11.728	11.752	11.776	11.800	11.824	11.848	11.872	11.896	11.920	11.944	11.968	11.992	12.016	12.040	12.064	12.088	12.112	12.136	12.160	12.184	12.208	12.232	12.256	12.280	12.304	12.328	12.352	12.376	12.400	12.424	12.448	12.472	12.496	12.520	12.544	12.568	12.592	12.616	12.640	12.664	12.688	12.712	12.736	12.760	12.784	12.808	12.832	12.856	12.880	12.904	12.928	12.952	12.976	13.000	13.024	13.048	13.072	13.096	13.120	13.144	13.168	13.192	13.216	13.240	13.264	13.288	13.312	13.336	13.360	13.384	13.408	13.432	13.456	13.480	13.504	13.528	13.552	13.576	13.600	13.624	13.648	13.672	13.696	13.720	13.744	13.768	13.792	13.816	13.840	13.864	13.888	13.912	13.936	13.960	13.984	14.008	14.032	14.056	14.080	14.104	14.128	14.152	14.176	14.200	14.224	14.248	14.272	14.296	14.320	14.344	14.368	14.392	14.416	14.440	14.464	14.488	14.512	14.536	14.560	14.584	14.608	14.632	14.656	14.680	14.704	14.728	14.752	14.776	14.800	14.824	14.848	14.872	14.896	14.920	14.944	14.968	14.992	15.016	15.040	15.064	15.088	15.112	15.136	15.160	15.184	15.208	15.232	15.256	15.280	15.304	15.328	15.352	15.376	15.400	15.424	15.448	15.472	15.496	15.520	15.544	15.568	15.592	15.616	15.640	15.664	15.688	15.712	15.736	15.760	15.784	15.808	15.832	15.856	15.880	15.904	15.928	15.952	15.976	16.000	16.024	16.048	16.072	16.096	16.120	16.144	16.168	16.192	16.216	16.240	16.264	16.288	16.312	16.336	16.360	16.384	16.408	16.432	16.456	16.480	16.504	16.528	16.552	16.576	16.600	16.624	16.648	16.672	16.696	16.720	16.744	16.768	16.792	16.816	16.840	16.864	16.888	16.912	16.936	16.960	16.984	17.008	17.032	17.056	17.080	17.104	17.128	17.152	17.176	17.200	17.224	17.248	17.272	17.296	17.320	17.344	17.368	17.392	17.416	17.440	17.464	17.488	17.512	17.536	17.560	17.584	17.608	17.632	17.656	17.680	17.704	17.728	17.752	17.776	17.800	17.824	17.848	17.872	17.896	17.920	17.944	17.968	17.992	18.016	18.040	18.064	18.088	18.112	18.136	18.160	18.184	18.208	18.232	18.256</

Appendix A- Thermocouple data and calibration

Relevant extract from the J-type thermocouple table:

J-type thermocouple table													
sample no. T °C	1	2	3	4	5	6	7	8	9	10	11	average (mV)	standard deviation (mV)
450	24.61	24.665	24.721	24.776	24.832	24.887	24.943	24.998	25.053	25.109	25.164	24.887	0.184
460	25.164	25.22	25.275	25.331	25.386	25.442	25.497	25.553	25.608	25.664	25.72	25.442	0.184
470	25.72	25.775	25.831	25.886	25.942	25.998	26.053	26.109	26.165	26.22	26.276	25.998	0.184
480	26.276	26.332	26.387	26.443	26.499	26.555	26.61	26.666	26.722	26.778	26.834	26.555	0.185
490	26.834	26.889	26.945	27.001	27.057	27.113	27.169	27.225	27.281	27.337	27.393	27.113	0.186
500	27.393	27.449	27.505	27.561	27.617	27.673	27.729	27.785	27.841	27.897	27.953	27.673	0.186
510	27.953	28.01	28.066	28.122	28.178	28.234	28.291	28.347	28.403	28.46	28.516	28.235	0.187
520	28.516	28.572	28.629	28.685	28.741	28.798	28.854	28.911	28.967	29.024	29.08	28.798	0.187
530	29.08	29.137	29.194	29.25	29.307	29.363	29.42	29.477	29.534	29.59	29.647	29.364	0.188
540	29.647	29.704	29.761	29.818	29.874	29.931	29.988	30.045	30.102	30.159	30.216	29.931	0.189



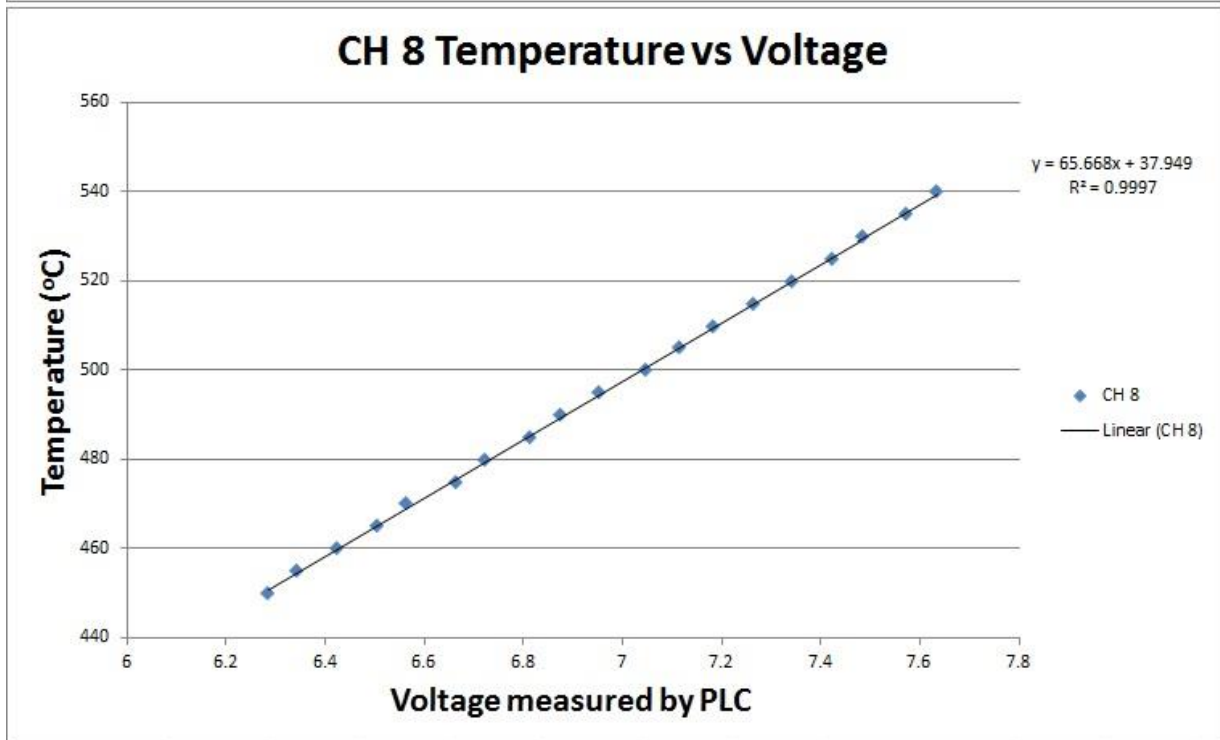
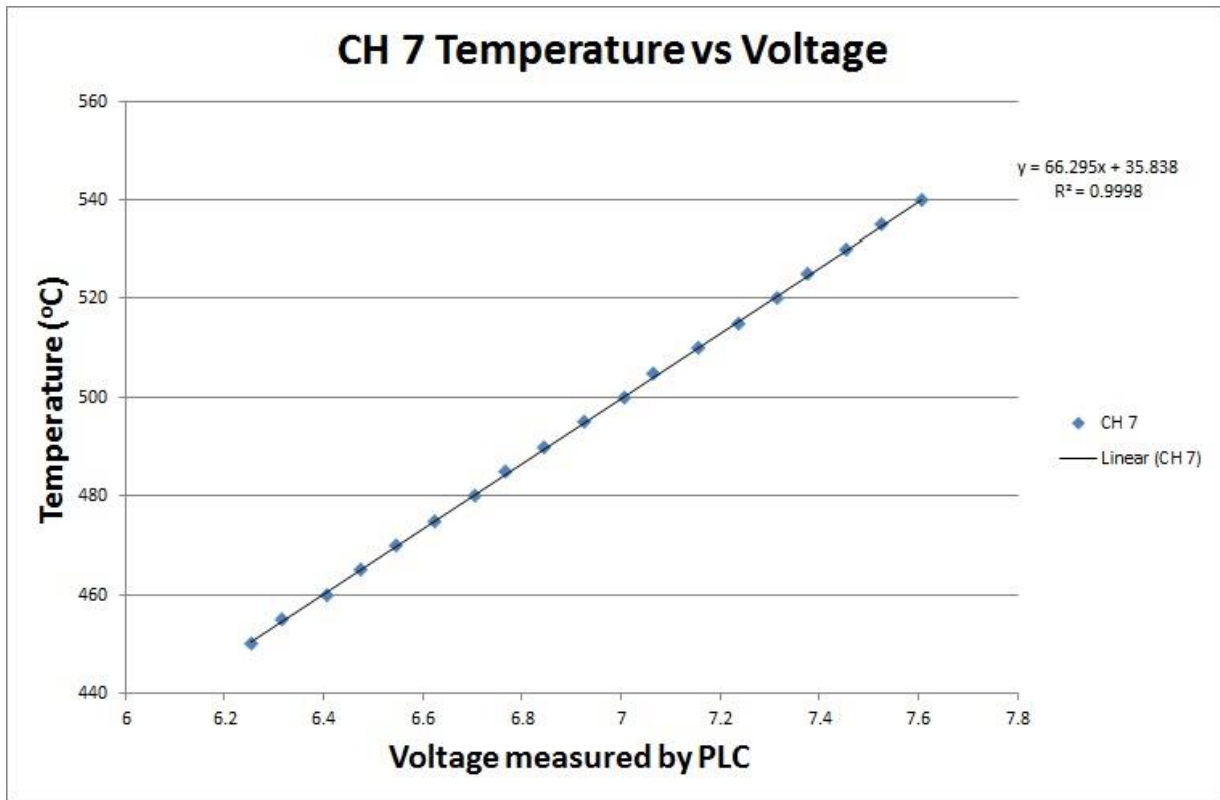
Appendix A- Thermocouple data and calibration

Thermocouple calibration data obtained experimentally where Temperature was measured with a digital thermometer and the voltage output from the telemetry system was measured by the PLC via its analog input cards:

Temp (°C) (thermometer)	CH 7 (voltage)	CH 8 (voltage)
450	6.25	6.28
450	6.26	6.29
455	6.31	6.34
455	6.32	6.35
460	6.41	6.42
460	6.4	6.43
465	6.47	6.5
465	6.48	6.51
470	6.54	6.56
470	6.55	6.57
475	6.63	6.66
475	6.62	6.67
480	6.7	6.72
480	6.71	6.73
485	6.76	6.81
485	6.77	6.82
490	6.85	6.87
490	6.84	6.88
495	6.92	6.96
495	6.93	6.95
500	7	7.04
500	7.01	7.06
505	7.07	7.11
505	7.06	7.12
510	7.15	7.19
510	7.16	7.18
515	7.23	7.27
515	7.24	7.26
520	7.31	7.35
520	7.32	7.34
525	7.38	7.43
525	7.37	7.42
530	7.45	7.48
530	7.46	7.49
535	7.52	7.57
535	7.53	7.58
540	7.61	7.64
540	7.6	7.63

Temp (°C)	CH 7 voltage average	CH 8 voltage average
450	6.255	6.285
455	6.315	6.345
460	6.405	6.425
465	6.475	6.505
470	6.545	6.565
475	6.625	6.665
480	6.705	6.725
485	6.765	6.815
490	6.845	6.875
495	6.925	6.955
500	7.005	7.05
505	7.065	7.115
510	7.155	7.185
515	7.235	7.265
520	7.315	7.345
525	7.375	7.425
530	7.455	7.485
535	7.525	7.575
540	7.605	7.635

Appendix A- Thermocouple data and calibration



Appendix A- Thermocouple data and calibration

	A	B	C	D	E	F	G	H	I	J	K	L	M	N	O	P	Q	R	S	T	U	V	W	X	Y	Z	AA	AB	AC
54																													
55																													
56	Temp. (°C) (thermometer)	450		455		460		465		470		475		480		485		490		495		500		505		510			
57	thermocouple voltage mV	24.887		25.164		25.442		25.720		25.998		26.276		26.555		26.834		27.113		27.393		27.673		27.954		28.235		28.516	
58	CH 7 calibration reading (voltage)	6.25	6.26	6.31	6.32	6.41	6.40	6.47	6.48	6.54	6.55	6.63	6.62	6.70	6.71	6.76	6.77	6.85	6.84	6.92	6.93	7.00	7.01	7.07	7.06	7.15	7.16	7.23	7.24
59	apparent gain	251.134		250.751		251.947		251.557		251.560		252.319		252.309		251.920		252.645		252.619		252.954		252.918		253.236		253.540	
60																													
61	std dev	0.00707		0.00707		0.00707		0.00707		0.00707		0.00707		0.00707		0.00707		0.00707		0.00707		0.00707		0.00707		0.00707		0.00707	
62	t critical	12.710		12.710		12.710		12.710		12.710		12.710		12.710		12.710		12.710		12.710		12.710		12.710		12.710		12.710	
63	n	2.000		2.000		2.000		2.000		2.000		2.000		2.000		2.000		2.000		2.000		2.000		2.000		2.000		2.000	
64	uncertainty (95%)	0.0635		0.0636		0.0635		0.0636		0.0635		0.0635		0.0635		0.0635		0.0635		0.0635		0.0635		0.0636		0.0635		0.0635	
65	mean	6.255		6.315		6.405		6.475		6.545		6.625		6.705		6.765		6.845		6.925		7.005		7.065		7.155		7.235	
66																													
67	max thermocouple voltage (mV)	29.931																											
68	CH 7 (voltage max)	7.610																											
69	thermocouple error (%)	0.0075																											
70	maximum thermocouple voltage error (mV)	0.2245																											
71	CH7 gain	252.6651																											
72	maximum thermocouple voltage error after telemetry gain (V)	0.0567																											
73	CH7 maximum uncertainty (V) (confidence: 95%)	0.0636																											
74	Combined error (V) (confidence: 95%)	0.085																											
75	Combined error (%) (confidence: 95%)	1.119																											
76																													
77	Temp. (°C) (thermometer)	450		455		460		465		470		475		480		485		490		495		500		505		510			
78	thermocouple voltage mV	24.887		25.164		25.442		25.720		25.998		26.276		26.555		26.834		27.113		27.393		27.673		27.954		28.235		28.516	
79	CH 8 calibration reading (voltage)	6.28	6.29	6.34	6.35	6.43	6.43	6.50	6.51	6.56	6.57	6.66	6.67	6.72	6.73	6.81	6.82	6.87	6.88	6.96	6.95	7.04	7.06	7.11	7.12	7.19	7.18	7.27	7.26
80	apparent gain	252.340		251.943		252.340		252.724		252.330		253.461		253.062		253.783		253.383		254.079		254.400		254.348		254.653		254.943	
81																													
82	std dev	0.00707		0.00707		0.00707		0.00707		0.00707		0.00707		0.00707		0.00707		0.00707		0.00707		0.01414		0.00707		0.00707		0.00707	
83	t critical	12.710		12.710		12.710		12.710		12.710		12.710		12.710		12.710		12.710		12.710		12.710		12.710		12.710		12.710	
84	n	2.000		2.000		2.000		2.000		2.000		2.000		2.000		2.000		2.000		2.000		2.000		2.000		2.000		2.000	
85	uncertainty (95%)	0.064		0.064		0.064		0.064		0.064		0.064		0.064		0.064		0.064		0.064		0.127		0.064		0.064		0.064	
86	mean	6.285		6.345		6.425		6.505		6.565		6.665		6.725		6.815		6.875		6.955		7.050		7.115		7.185		7.265	
87																													
88	max thermocouple voltage (mV)	29.931																											
89	CH 8 (voltage max)	7.640																											
90	thermocouple error (%)	0.0075																											
91	maximum thermocouple voltage error (mV)	0.2245																											
92	CH8 gain	253.8860																											
93	maximum thermocouple voltage error after telemetry gain (V)	0.0570																											
94	CH8 maximum uncertainty (V) (confidence: 95%)	0.1271																											
95	Combined error (V) (confidence: 95%)	0.139																											
96	Combined error (%) (confidence: 95%)	1.823																											

Appendix A- Thermocouple data and calibration

#	AC	AD	AE	AF	AG	AH	AI	AJ	AK	AL	AM
54											
55											
56		520		525		530		535		540	
57		28.798		29.081		29.364		29.647		29.931	
58	7.24	7.31	7.32	7.38	7.37	7.43	7.46	7.52	7.53	7.61	7.60
59		253.838		253.776		253.716		253.647		254.248	
60											
61		0.00707		0.00707		0.00707		0.00707		0.00707	
62		12.710		12.710		12.710		12.710		12.710	
63		2.000		2.000		2.000		2.000		2.000	
64		0.0636		0.0635		0.0635		0.0636		0.0636	
65		7.315		7.375		7.455		7.525		7.605	
66											
67											
68											
69											
70											
71											
72											
73											
74											
75											
76											
77		520		525		530		535		540	
78		28.798		29.081		29.364		29.647		29.931	
79	7.25	7.35	7.34	7.43	7.42	7.48	7.49	7.57	7.58	7.64	7.63
80		255.227		255.486		254.738		255.334		255.251	
81											
82		0.00707		0.00707		0.00707		0.00707		0.00707	
83		12.710		12.710		12.710		12.710		12.710	
84		2.000		2.000		2.000		2.000		2.000	
85		0.064		0.064		0.064		0.064		0.064	
86		7.345		7.425		7.485		7.575		7.635	
87											
88											
89											
90											
91											
92											
93											
94											
95											
96											

Appendix A- Thermocouple data and calibration

	A	B	C	D	E	F	G	H	I	J	K	L	M
54	statistical error												
55													
56		Temp (°C) (thermometer)	450	455	460	465				470	475		
57		thermocouple voltage mv	24.8870909090909	25.1644545454545	25.4418181818182	25.7197272727273				25.9972727272727	26.2762272727273		
58		CH 7 calibration reading (voltage)	6.25	6.31	6.32	6.47				6.48	6.54		
59		apparent gain	=B59/(B57/1000)	=D58/(D57/1000)	=F58/(F57/1000)	=H58/(H57/1000)				=J58/(J57/1000)	=L58/(L57/1000)		
60		std dev	=STDEV(B58:C58)	=STDEV(D58:E58)	=STDEV(F58:G58)	=STDEV(H58:I58)				=STDEV(J58:K58)	=STDEV(L58:M58)		
61		t critical	12.71	12.71	12.71	12.71				12.71	12.71		
62		n	2	2	2	2				2	2		
63		uncertainty (95%)	=B63*B61/SQRT(B63)	=D63*D61/SQRT(D63)	=F63*F61/SQRT(F63)	=H63*H61/SQRT(H63)				=J63*J61/SQRT(J63)	=L63*L61/SQRT(L63)		
64		mean	=AVERAGE(B58:C58)	=AVERAGE(D58:E58)	=AVERAGE(F58:G58)	=AVERAGE(H58:I58)				=AVERAGE(J58:K58)	=AVERAGE(L58:M58)		
65		max thermocouple voltage (mV)	=MAX(B7:57)										
66		CH 7 (voltage max)	=MAX(B58:58)										
67		thermocouple error (%)	0.0075										
68		maximum thermocouple voltage error (mV)	=B69*B67										
69		CH7 gain	=AVERAGE(B59:AM59)										
70		maximum thermocouple voltage error after telemetry gain (V)	=B70*B71/1000										
71		CH7 maximum uncertainty (V) (confidence: 95%)	=MAX(B64:AM64)										
72		Combined error (V) (confidence: 95%)	=SQRT(B72*B73*2)										
73		Combined error (%) (confidence: 95%)	=B74/B69*100										
74													
75													
76													
77		Temp (°C) (thermometer)	450	455	460	465				470	475		
78		thermocouple voltage mv	24.8870909090909	25.1644545454545	25.4418181818182	25.7197272727273				25.9972727272727	26.2762272727273		
79	CH 8 calibration reading (voltage)	6.28	6.34	6.35	6.42				6.51	6.56			
80	apparent gain	=B79/(B78/1000)	=D79/(D78/1000)	=F79/(F78/1000)	=H79/(H78/1000)				=J79/(J78/1000)	=L79/(L78/1000)			
81	std dev	=STDEV(B79:C79)	=STDEV(D79:E79)	=STDEV(F79:G79)	=STDEV(H79:I79)				=STDEV(J79:K79)	=STDEV(L79:M79)			
82	t critical	12.71	12.71	12.71	12.71				12.71	12.71			
83	n	2	2	2	2				2	2			
84	uncertainty (95%)	=B85*B82/SQRT(B84)	=D85*D82/SQRT(D84)	=F85*F82/SQRT(F84)	=H85*H82/SQRT(H84)				=J85*J82/SQRT(J84)	=L85*L82/SQRT(L84)			
85	mean	=AVERAGE(B79:C79)	=AVERAGE(D79:E79)	=AVERAGE(F79:G79)	=AVERAGE(H79:I79)				=AVERAGE(J79:K79)	=AVERAGE(L79:M79)			
86	max thermocouple voltage (mV)	=MAX(B78:78)											
87	CH 8 (voltage max)	=MAX(B79:79)											
88	thermocouple error (%)	0.0075											
89	maximum thermocouple voltage error (mV)	=B90*B88											
90	CH8 gain	=AVERAGE(B80:AM80)											
91	maximum thermocouple voltage error after telemetry gain (V)	=B91*B92/1000											
92	CH8 maximum uncertainty (V) (confidence: 95%)	=MAX(B85:AM85)											
93	Combined error (V) (confidence: 95%)	=SQRT(B93*B94*2)											
94	Combined error (%) (confidence: 95%)	=B95/B89*100											
95													
96													

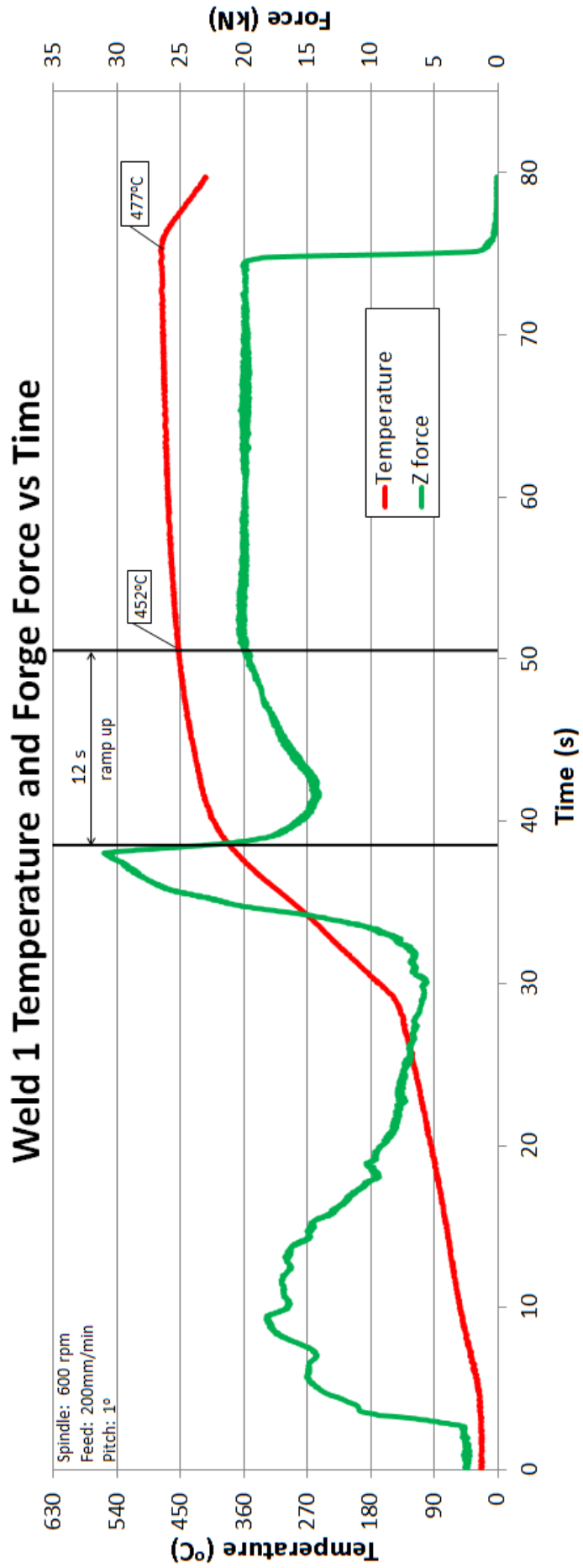
Appendix A- Thermocouple data and calibration

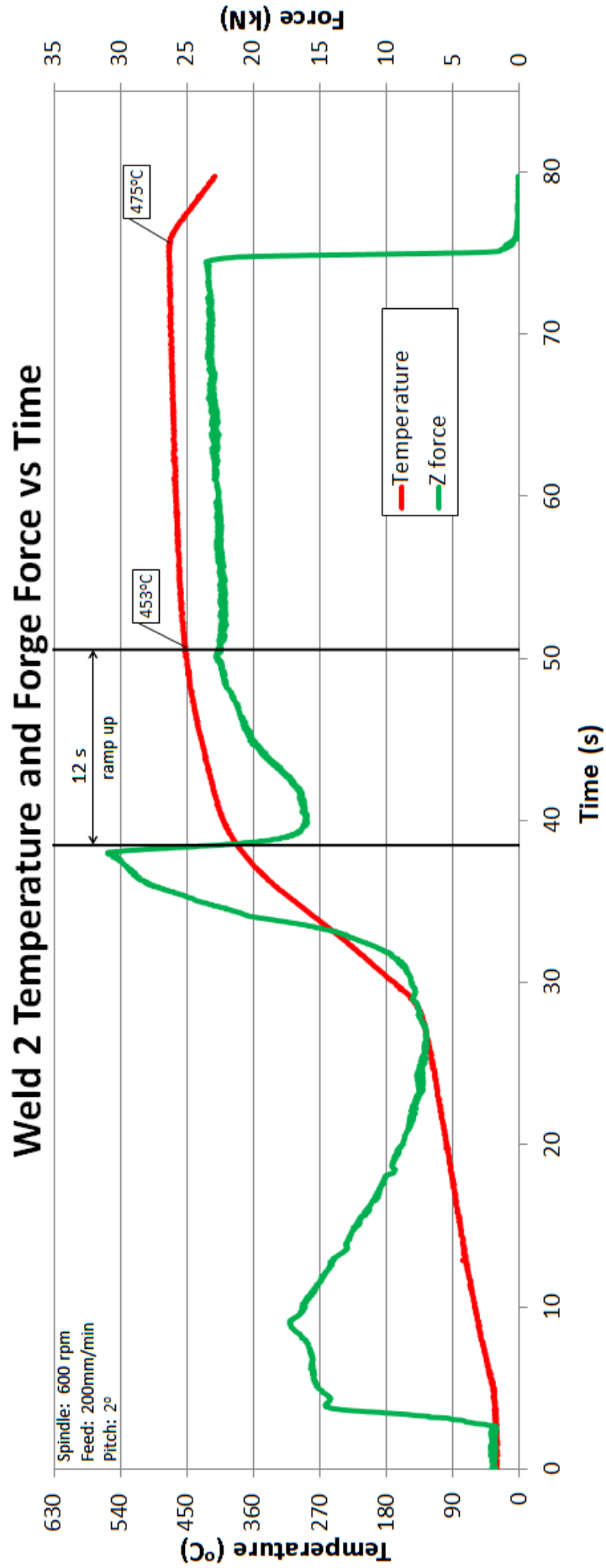
M	N	O	P	Q	R	S	T	U	V	W	X	Y	Z	AA	AB	AC	AD	AE	AF	AG
54																				
55																				
56	480		485		490	495		500		505		510		515		520		525		
57	26.5547272727273		26.8339090909091		27.1130090909091	27.3930454545455		27.673		27.9537727272727		28.2345454545455		28.5162272727273		28.7979090909091		29.0807272727273		
58	6.62	6.7	6.76	6.85	6.84	6.92		6.93		7.01	7.07	7.06	7.15	7.16	7.23	7.24	7.31	7.32	7.38	7.37
59	=N59/(N57/1000)		=P58/(P57/1000)		=R58/(R57/1000)	=S58/(S57/1000)		=V58/(V57/1000)		=W58/(W57/1000)		=Z58/(Z57/1000)		=AB58/(AB57/1000)		=AD58/(AD57/1000)		=AF58/(AF57/1000)		
60	STDEV(N58:O58)		STDEV(P58:Q58)		STDEV(R58:S58)	STDEV(T58:U58)		STDEV(V58:W58)		STDEV(X58:Y58)		STDEV(Z58:AA58)		STDEV(AB58:AC58)		STDEV(AD58:AE58)		STDEV(AE58:AG58)		
61	12.71	12.71	12.71	12.71	12.71	12.71	12.71	12.71	12.71	12.71	12.71	12.71	12.71	12.71	12.71	12.71	12.71	12.71	12.71	
62	2	2	2	2	2	2	2	2	2	2	2	2	2	2	2	2	2	2	2	
63																				
64	=N62*N61/SQRT(N63)		=P62*P61/SQRT(P63)		=R62*R61/SQRT(R63)	=S62*S61/SQRT(S63)		=V62*V61/SQRT(V63)		=W62*W61/SQRT(W63)		=Z62*Z61/SQRT(Z63)		=AB62*AB61/SQRT(AB63)		=AD62*AD61/SQRT(AD63)		=AF62*AF61/SQRT(AF63)		
65	AVERAGE(N58:O58)		AVERAGE(P58:Q58)		AVERAGE(R58:S58)	AVERAGE(T58:U58)		AVERAGE(V58:W58)		AVERAGE(X58:Y58)		AVERAGE(Z58:AA58)		AVERAGE(AB58:AC58)		AVERAGE(AD58:AE58)		AVERAGE(AE58:AG58)		
66																				
67																				
68																				
69																				
70																				
71																				
72																				
73																				
74																				
75																				
76																				
77	480		485		490	495		500		505		510		515		520		525		
78	26.5547272727273		26.8339090909091		27.1130090909091	27.3930454545455		27.673		27.9537727272727		28.2345454545455		28.5162272727273		28.7979090909091		29.0807272727273		
79	6.67	6.7	6.73	6.81	6.82	6.87	6.88	6.96	6.95	7.04	7.06	7.11	7.12	7.19	7.18	7.27	7.26	7.35	7.34	7.43
80	=N79/(N78/1000)		=P79/(P78/1000)		=R79/(R78/1000)	=S79/(S78/1000)		=V79/(V78/1000)		=W79/(W78/1000)		=Z79/(Z78/1000)		=AB79/(AB78/1000)		=AD79/(AD78/1000)		=AF79/(AF78/1000)		
81	STDEV(N79:O79)		STDEV(P79:Q79)		STDEV(R79:S79)	STDEV(T79:U79)		STDEV(V79:W79)		STDEV(X79:Y79)		STDEV(Z79:AA79)		STDEV(AB79:AC79)		STDEV(AD79:AE79)		STDEV(AE79:AG79)		
82	12.71	12.71	12.71	12.71	12.71	12.71	12.71	12.71	12.71	12.71	12.71	12.71	12.71	12.71	12.71	12.71	12.71	12.71	12.71	
83	2	2	2	2	2	2	2	2	2	2	2	2	2	2	2	2	2	2	2	
84																				
85	=N83*N82/SQRT(N84)		=P83*P82/SQRT(P84)		=R83*R82/SQRT(R84)	=S83*S82/SQRT(S84)		=V83*V82/SQRT(V84)		=W83*W82/SQRT(W84)		=Z83*Z82/SQRT(Z84)		=AB83*AB82/SQRT(AB84)		=AD83*AD82/SQRT(AD84)		=AF83*AF82/SQRT(AF84)		
86	AVERAGE(N79:O79)		AVERAGE(P79:Q79)		AVERAGE(R79:S79)	AVERAGE(T79:U79)		AVERAGE(V79:W79)		AVERAGE(X79:Y79)		AVERAGE(Z79:AA79)		AVERAGE(AB79:AC79)		AVERAGE(AD79:AE79)		AVERAGE(AE79:AG79)		
87																				
88																				
89																				
90																				
91																				
92																				
93																				
94																				
95																				
96																				

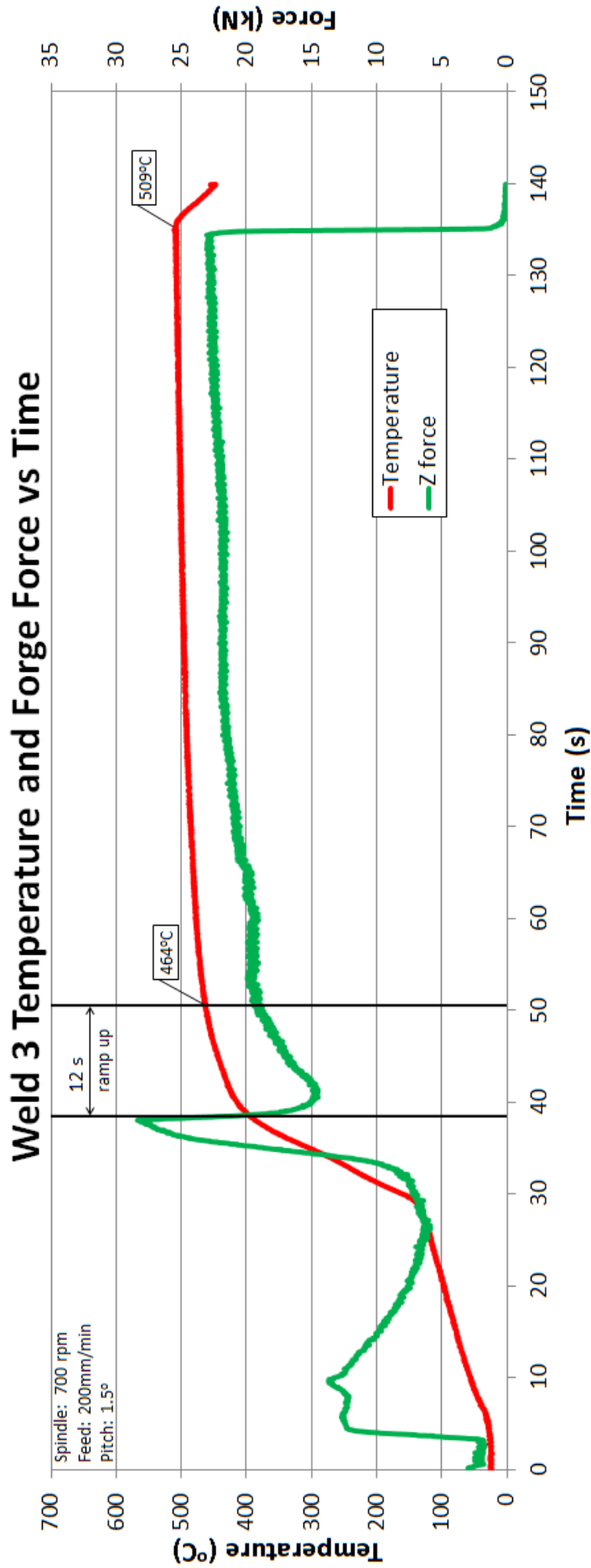
Appendix A- Thermocouple data and calibration

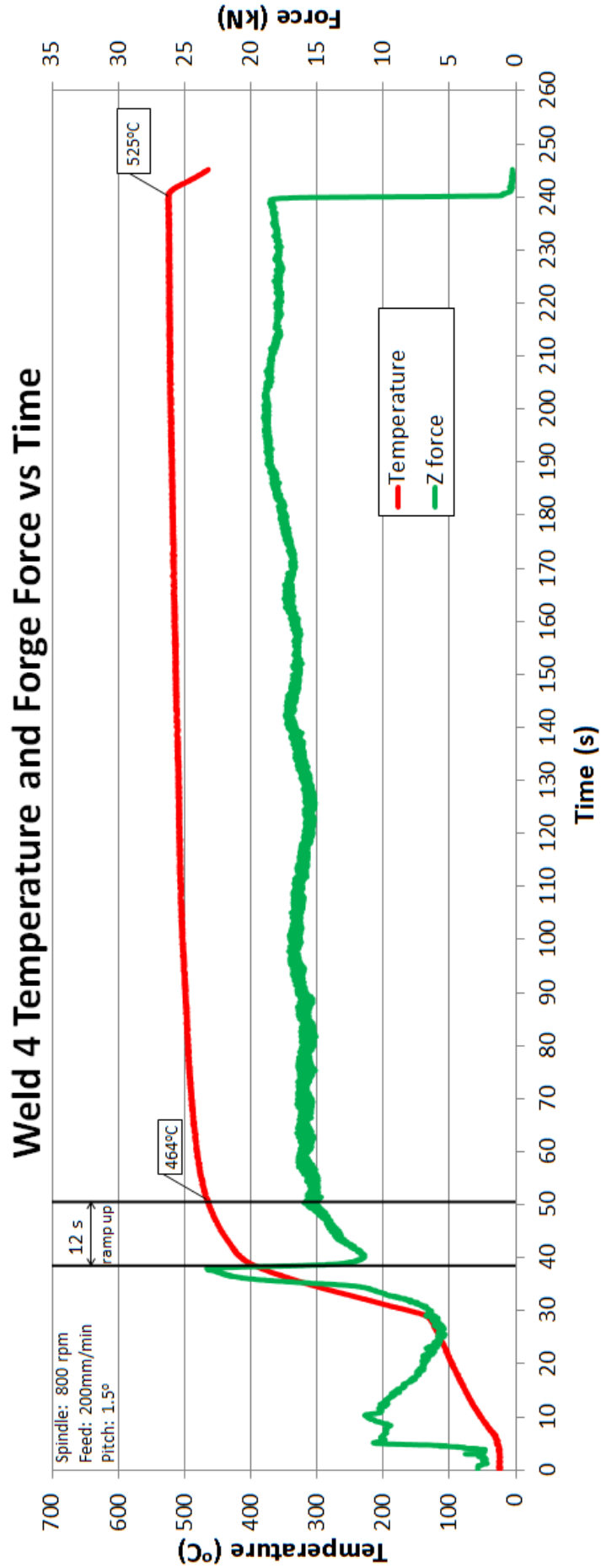
AG	AH	AI	AJ	AK	AL	AM
54						
55						
56	530		535		540	
57	29.3635454545455		29.6474545454545		29.9313636363636	
58	7.37	7.48	7.59	7.69	7.79	7.8
59	=AH58/(AH57/1000)		=AI59/(AI57/1000)		=AL59/(AL57/1000)	
60						
61	=STDEV(AH58:A158)		=STDEV(AI58:AK58)		=STDEV(AL58:AM59)	
62	12.71		12.71		12.71	
63	2		2		2	
64	=AH62*AH61/SQRT(AH63)		=AI62*AI61/SQRT(AI63)		=AL62*AL61/SQRT(AL63)	
65	=AVERAGE(AH58:A158)		=AVERAGE(AI58:AK58)		=AVERAGE(AL58:AM59)	
66						
67						
68						
69						
70						
71						
72						
73						
74						
75						
76						
77	530		535		540	
78	29.3635454545455		29.6474545454545		29.9313636363636	
79	7.42	7.48	7.49	7.57	7.58	7.64
80	=AH79/(AH78/1000)		=AI79/(AI78/1000)		=AL79/(AL78/1000)	
81						
82	=STDEV(AH79:A179)		=STDEV(AI79:AK79)		=STDEV(AL79:AM79)	
83	12.71		12.71		12.71	
84	2		2		2	
85	=AH83*AH82/SQRT(AH84)		=AI83*AI82/SQRT(AI84)		=AL83*AL82/SQRT(AL84)	
86	=AVERAGE(AH79:A179)		=AVERAGE(AI79:AK79)		=AVERAGE(AL79:AM79)	
87						
88						
89						
90						
91						
92						
93						
94						
95						
96						

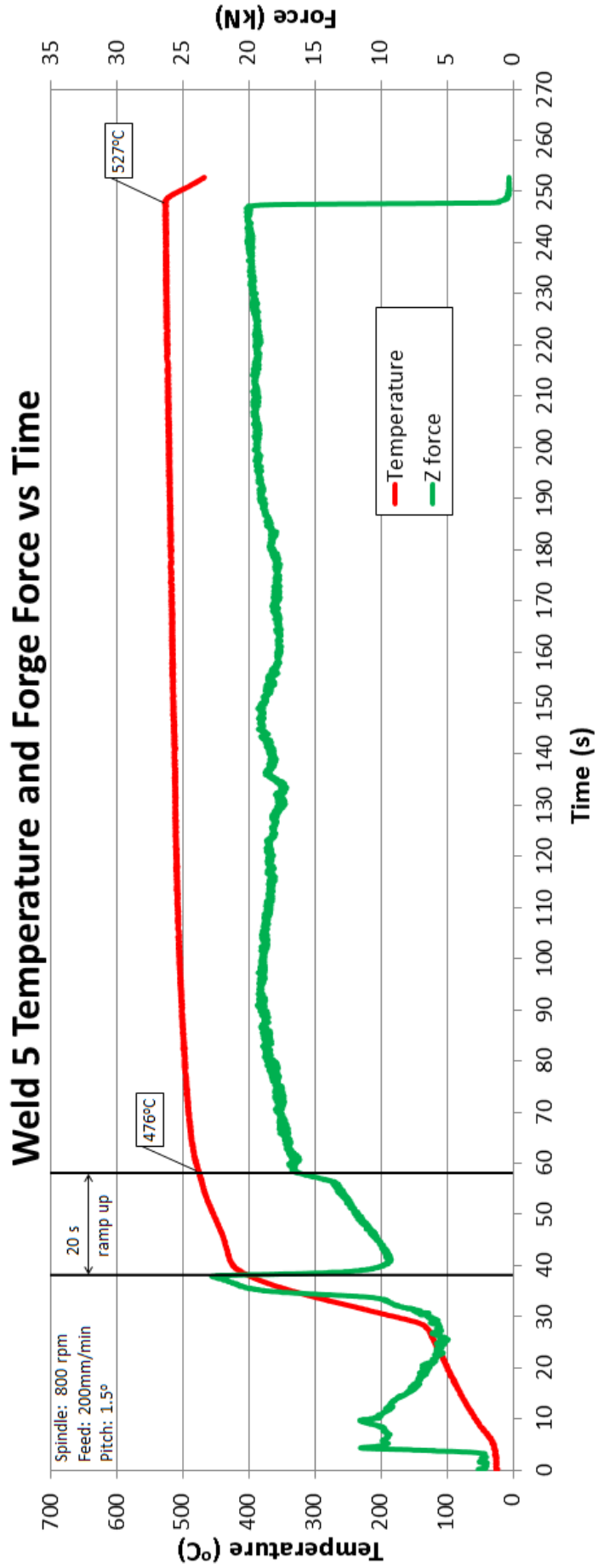
Appendix B- Establishment welds; position control



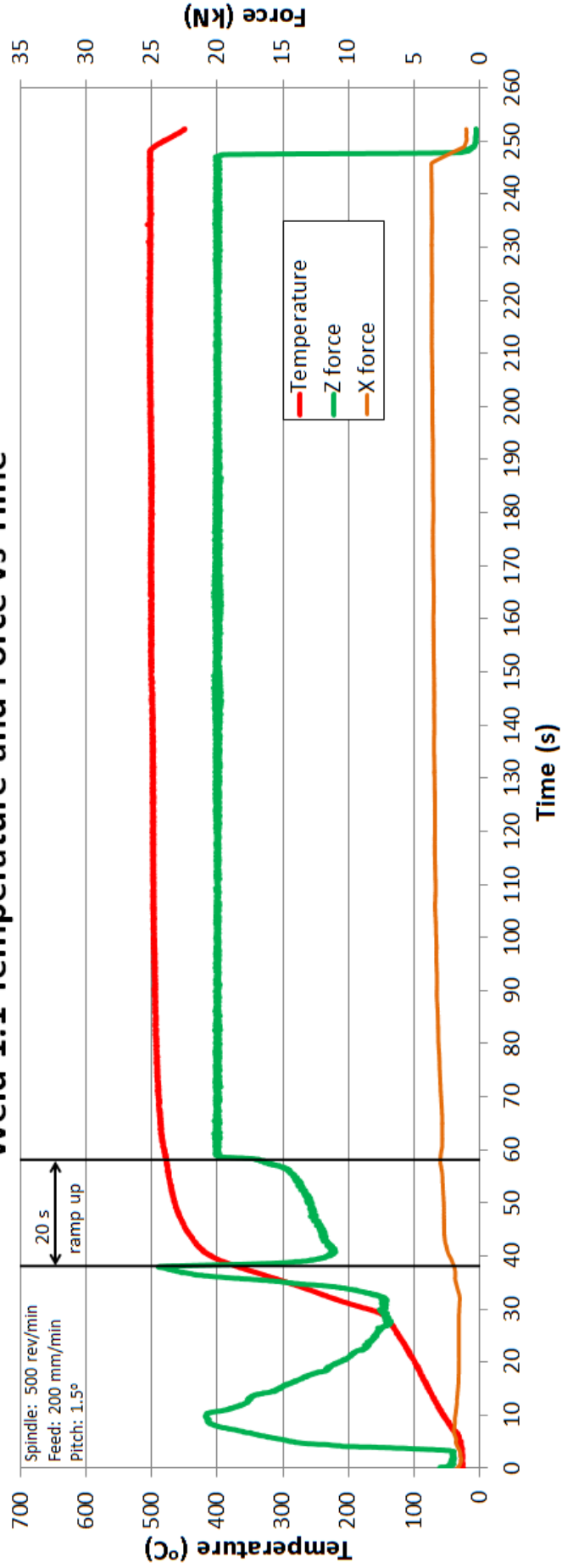


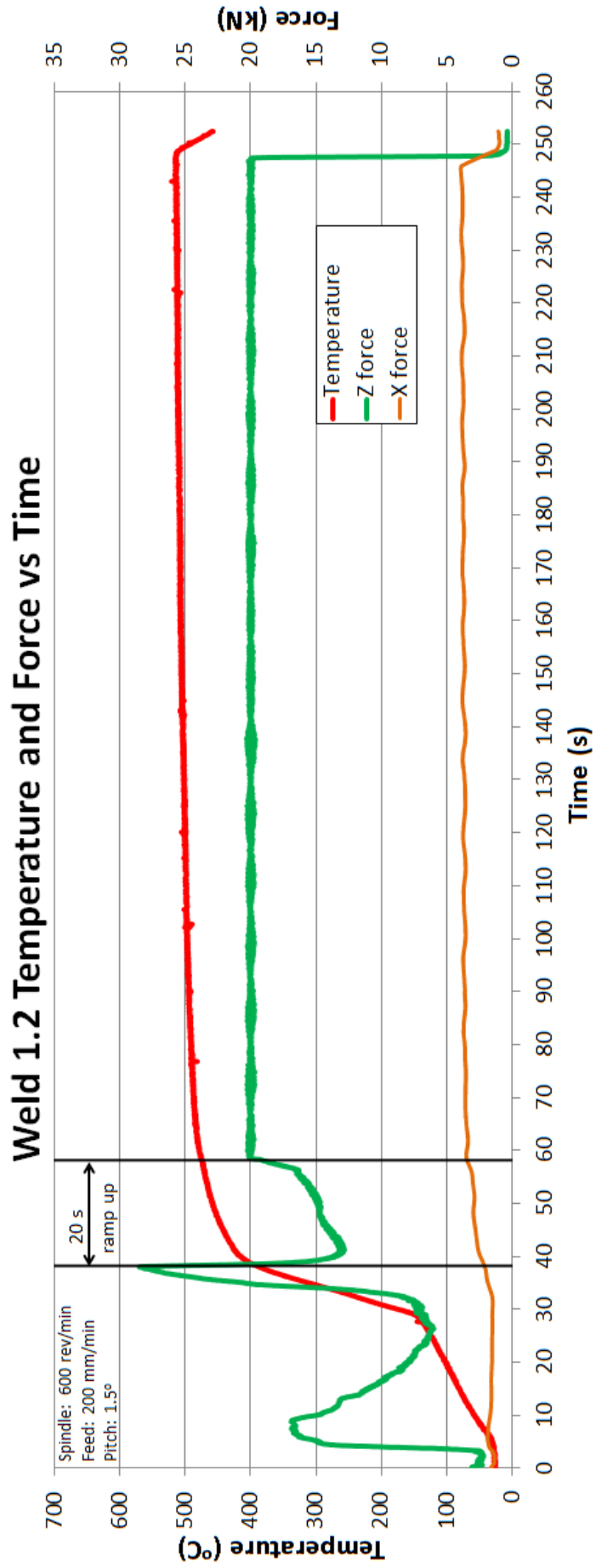




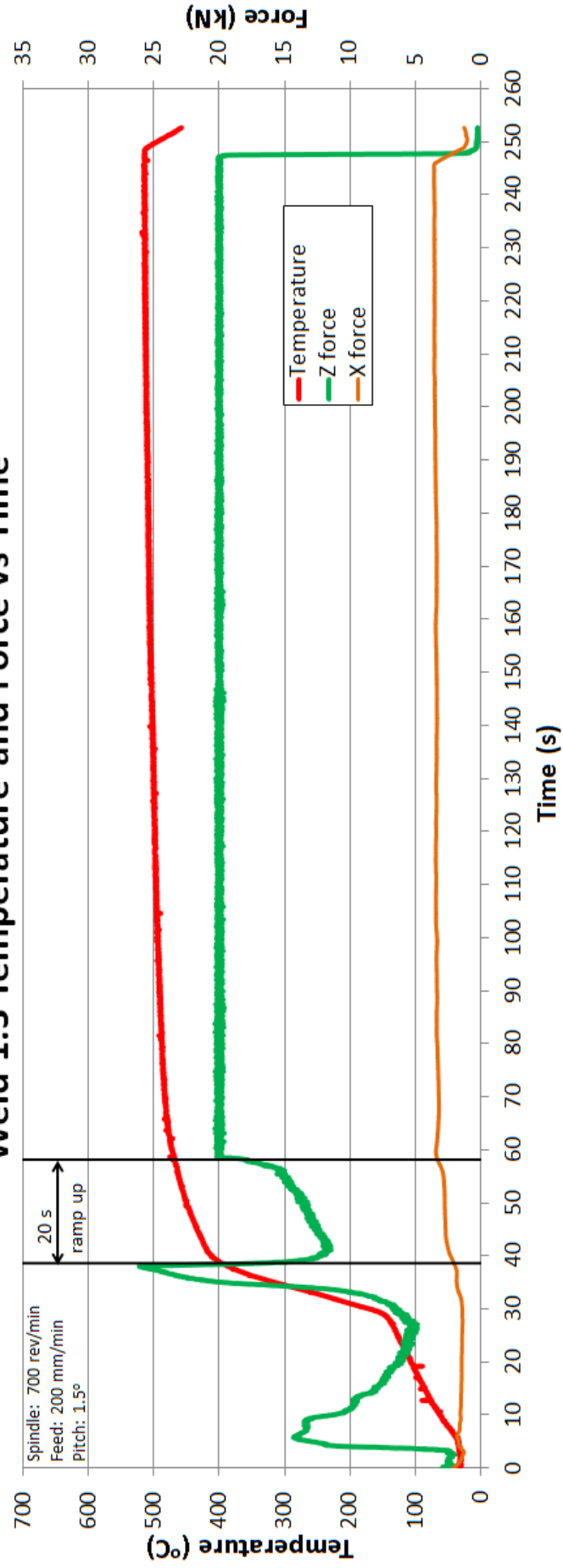


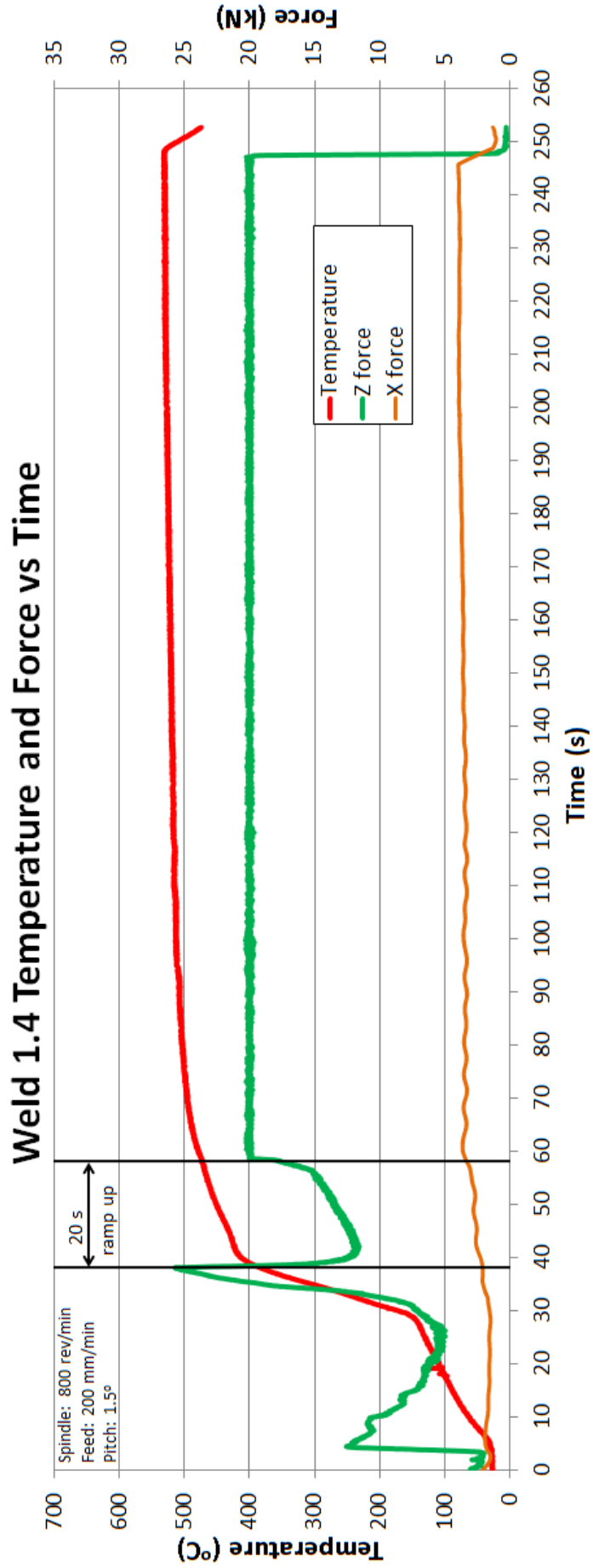
Weld 1.1 Temperature and Force vs Time

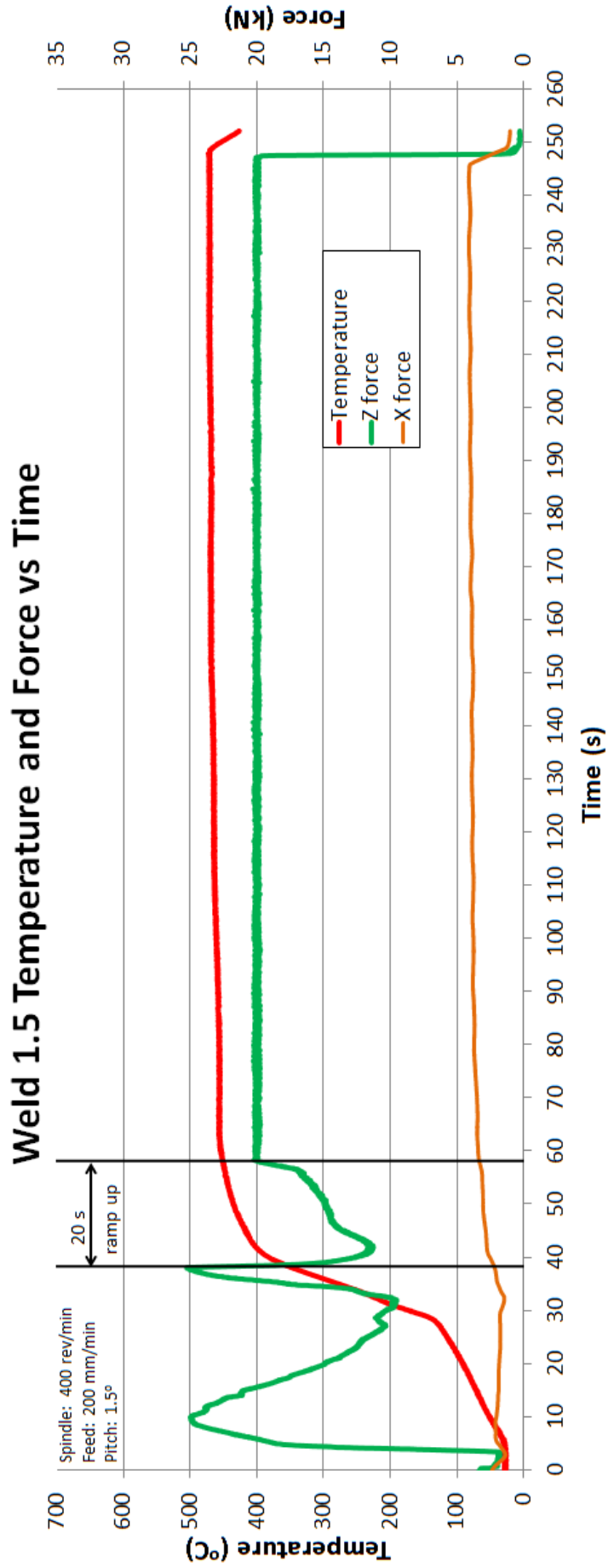




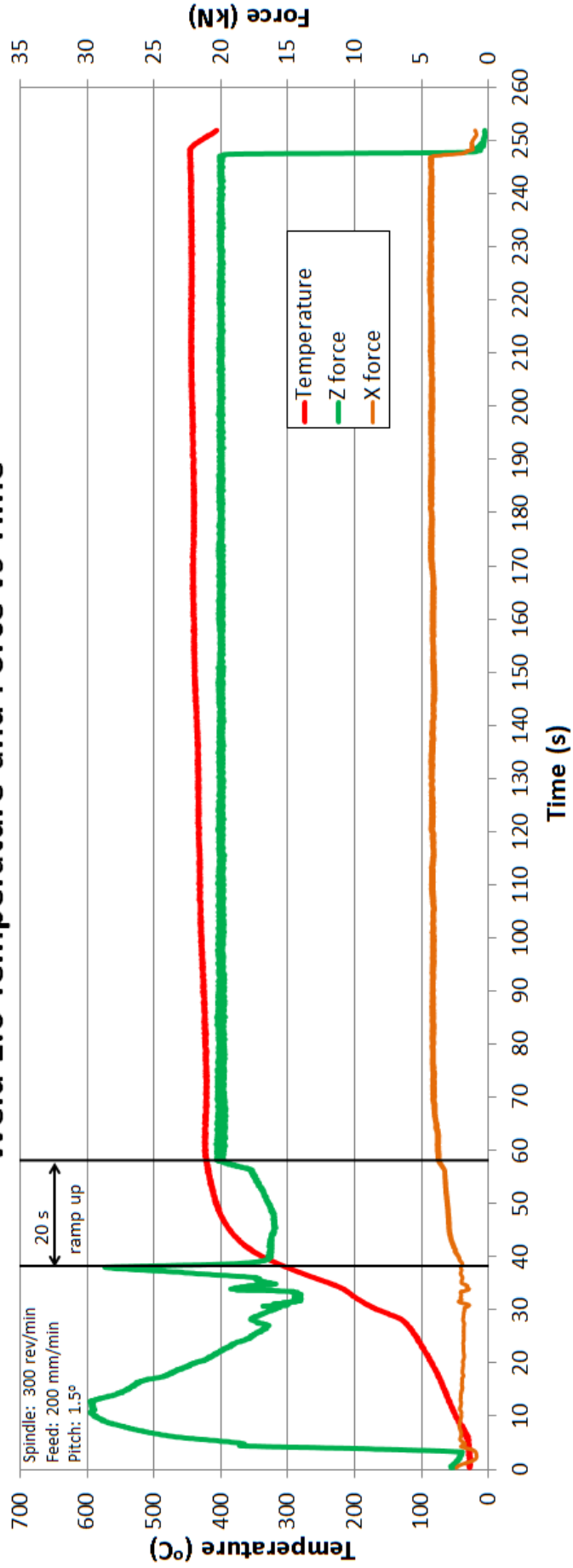
Weld 1.3 Temperature and Force vs Time



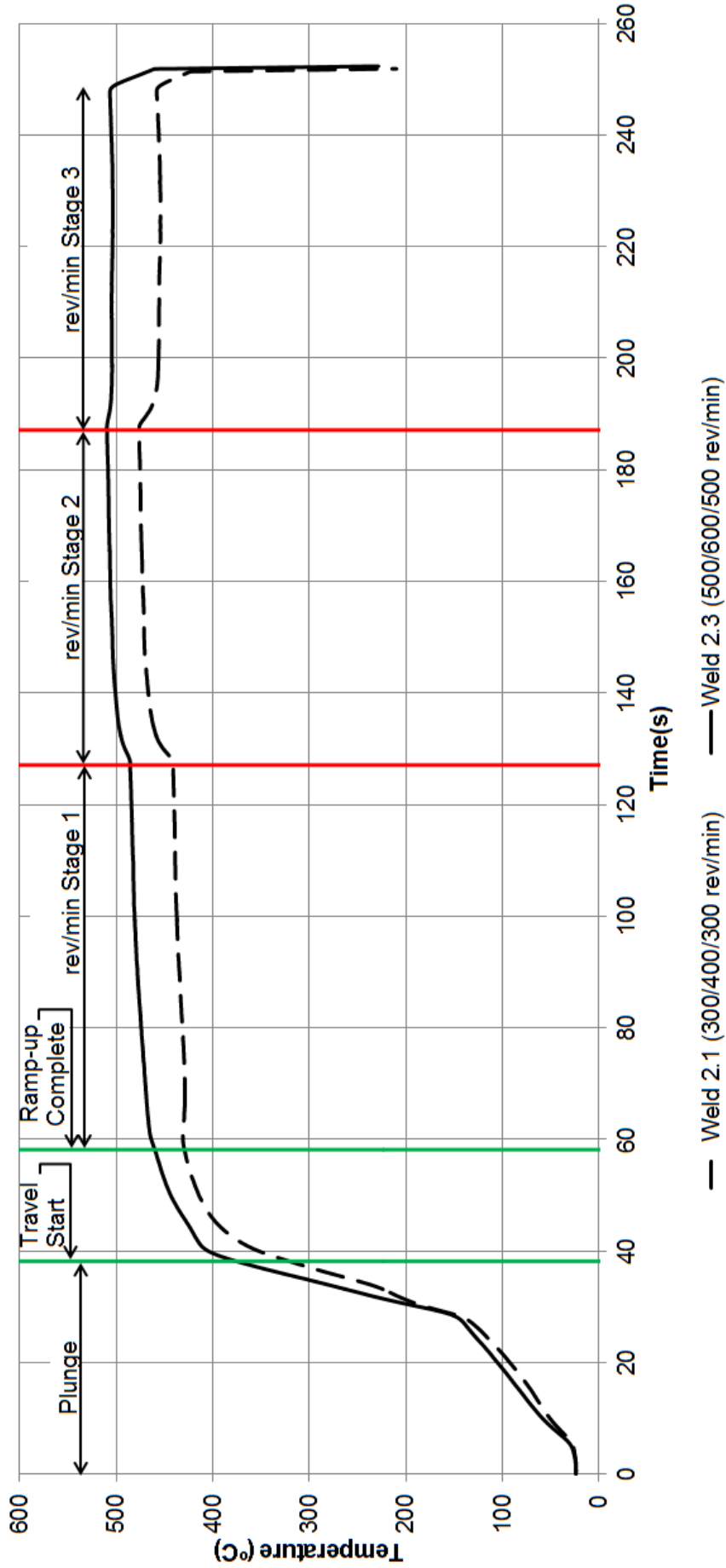




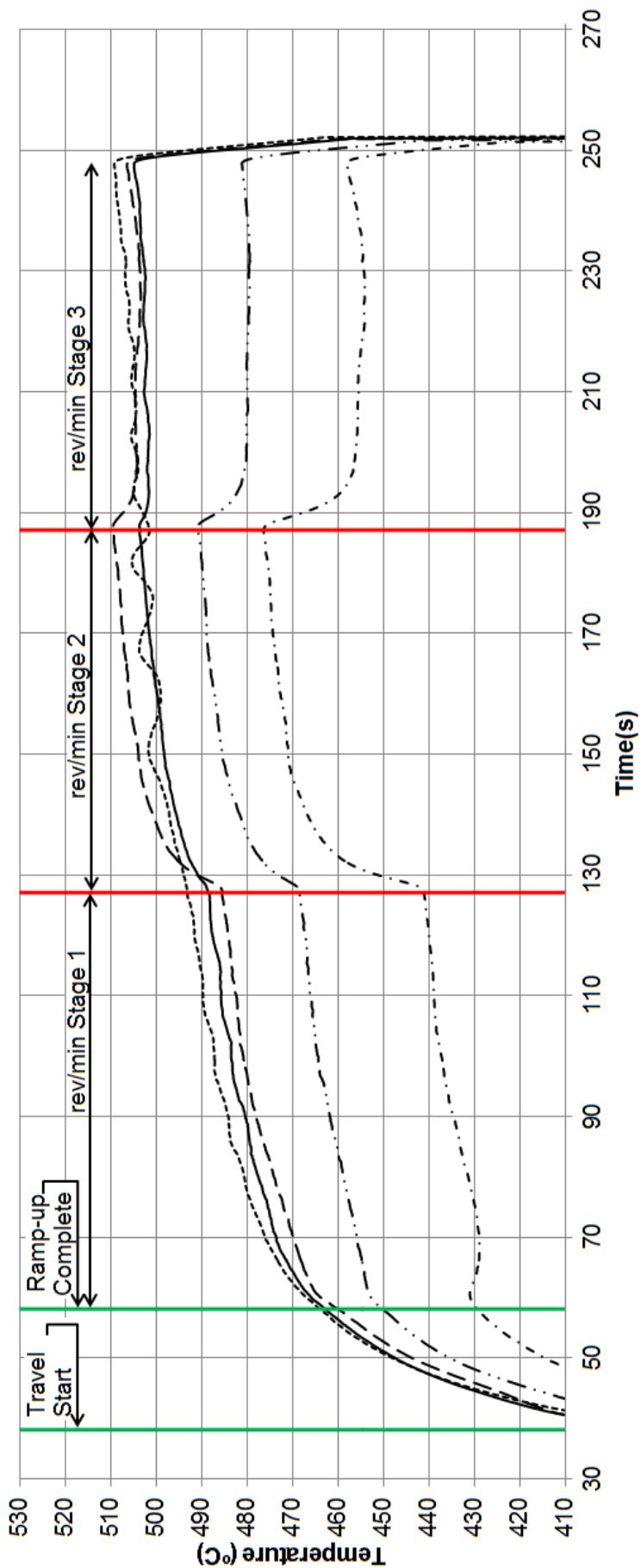
Weld 1.6 Temperature and Force vs Time



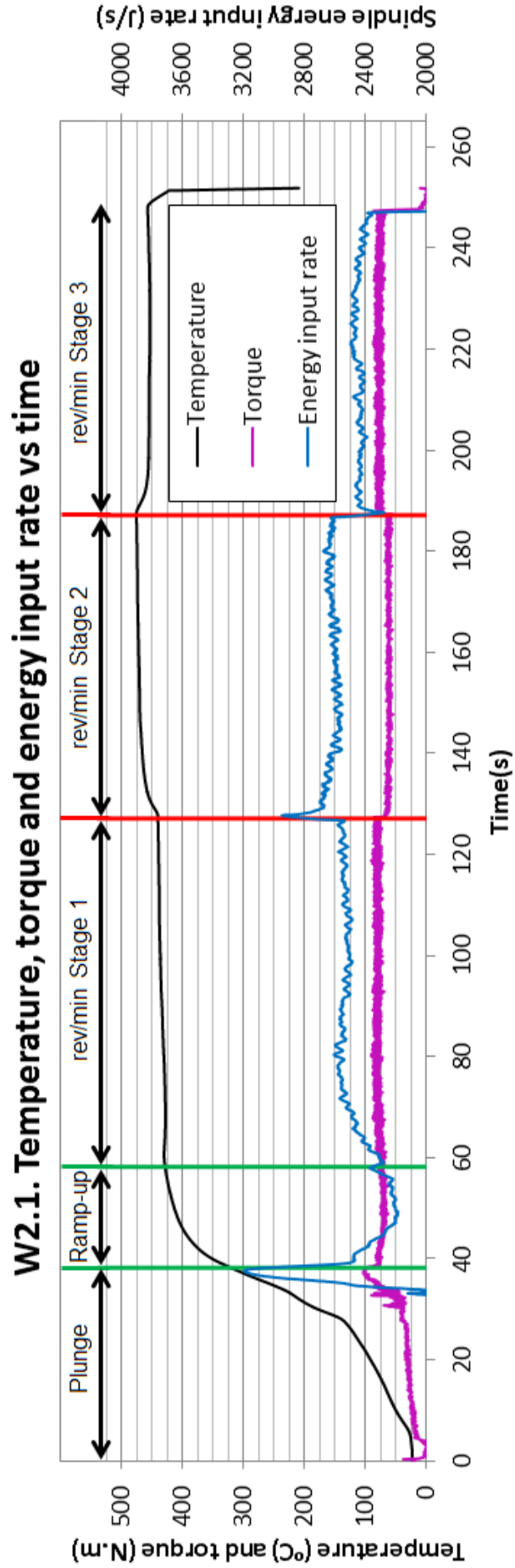
FSW AA 6082-T6 Weld Temperature vs Time



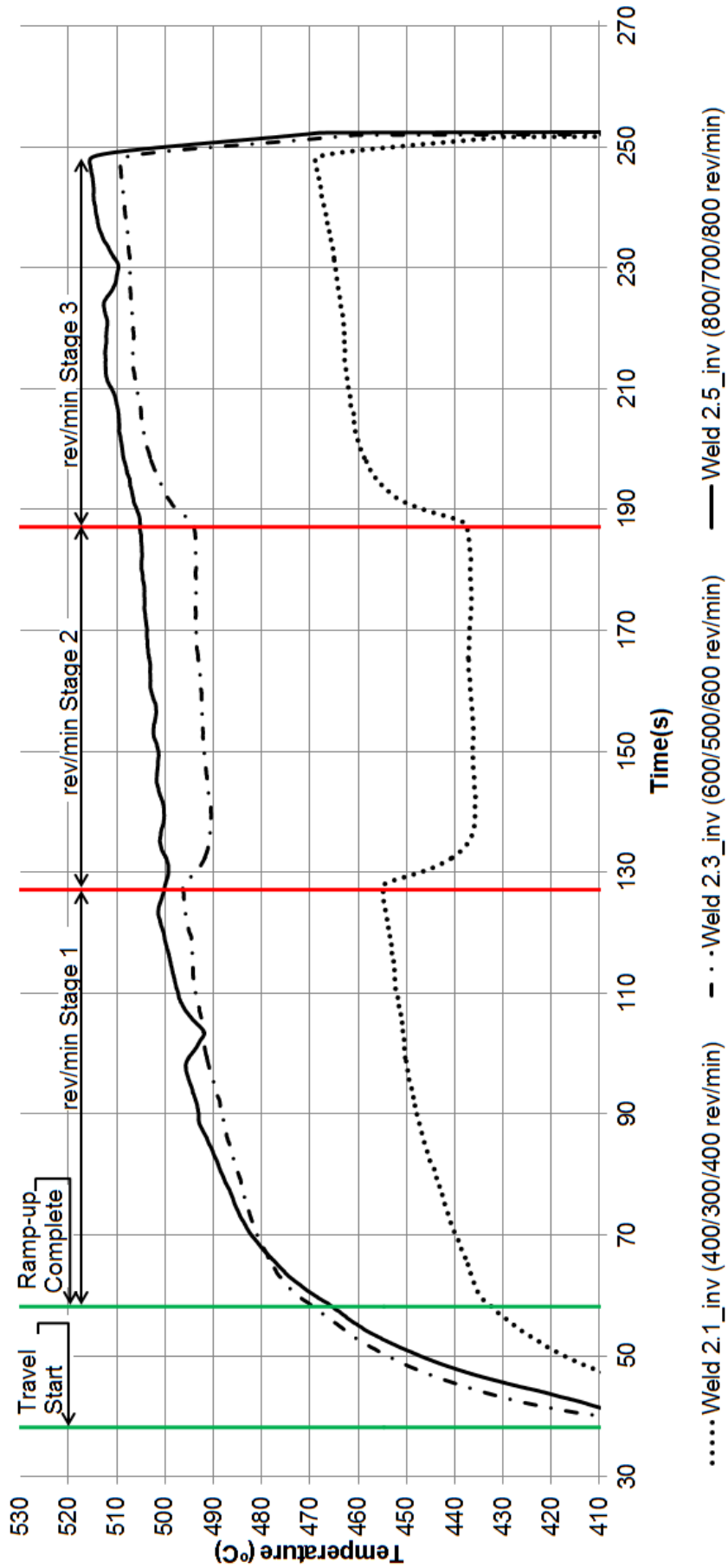
FSW AA 6082-T6 Temperature vs Time: Increased rev/min in Stage 2



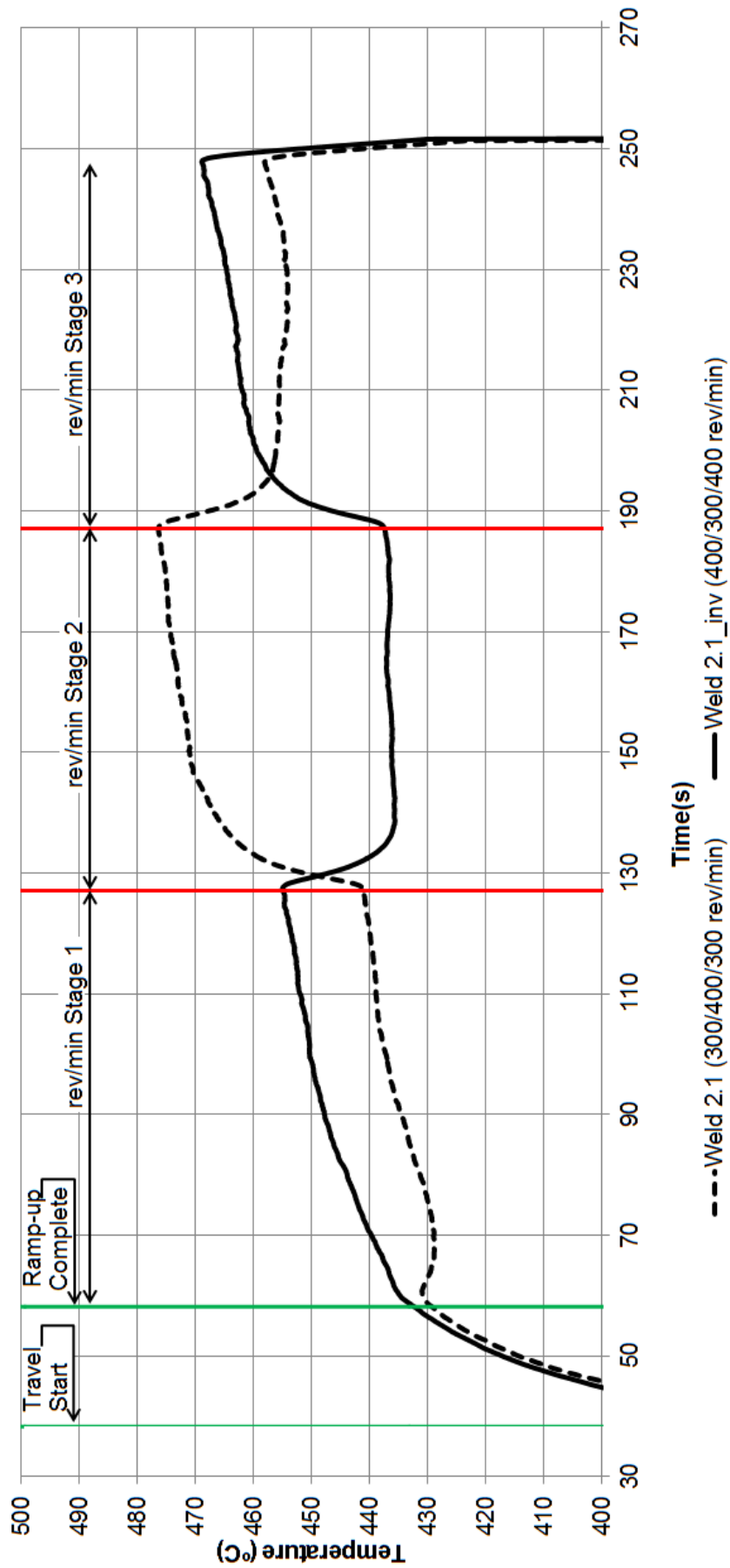
- - - Weld 2.1 (300/400/300 rev/min) — ··· Weld 2.2 (400/500/400 rev/min) — — Weld 2.3 (500/600/500 rev/min)
 — Weld 2.4 (600/700/600 rev/min) - - - - - Weld 2.5 (700/800/700 rev/min)



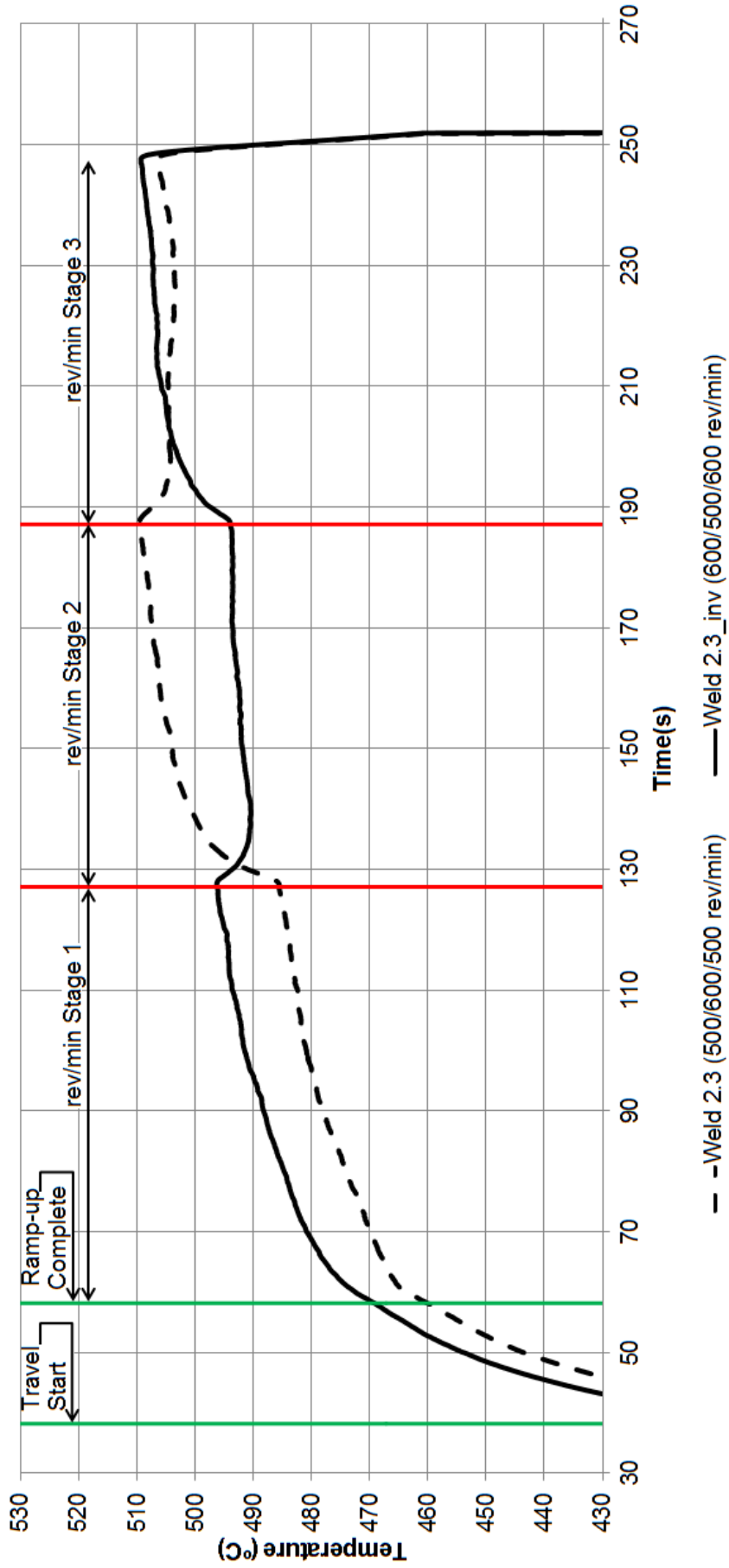
FSW AA 6082-T6 Temperature vs Time: Decreased rev/min in Stage 2



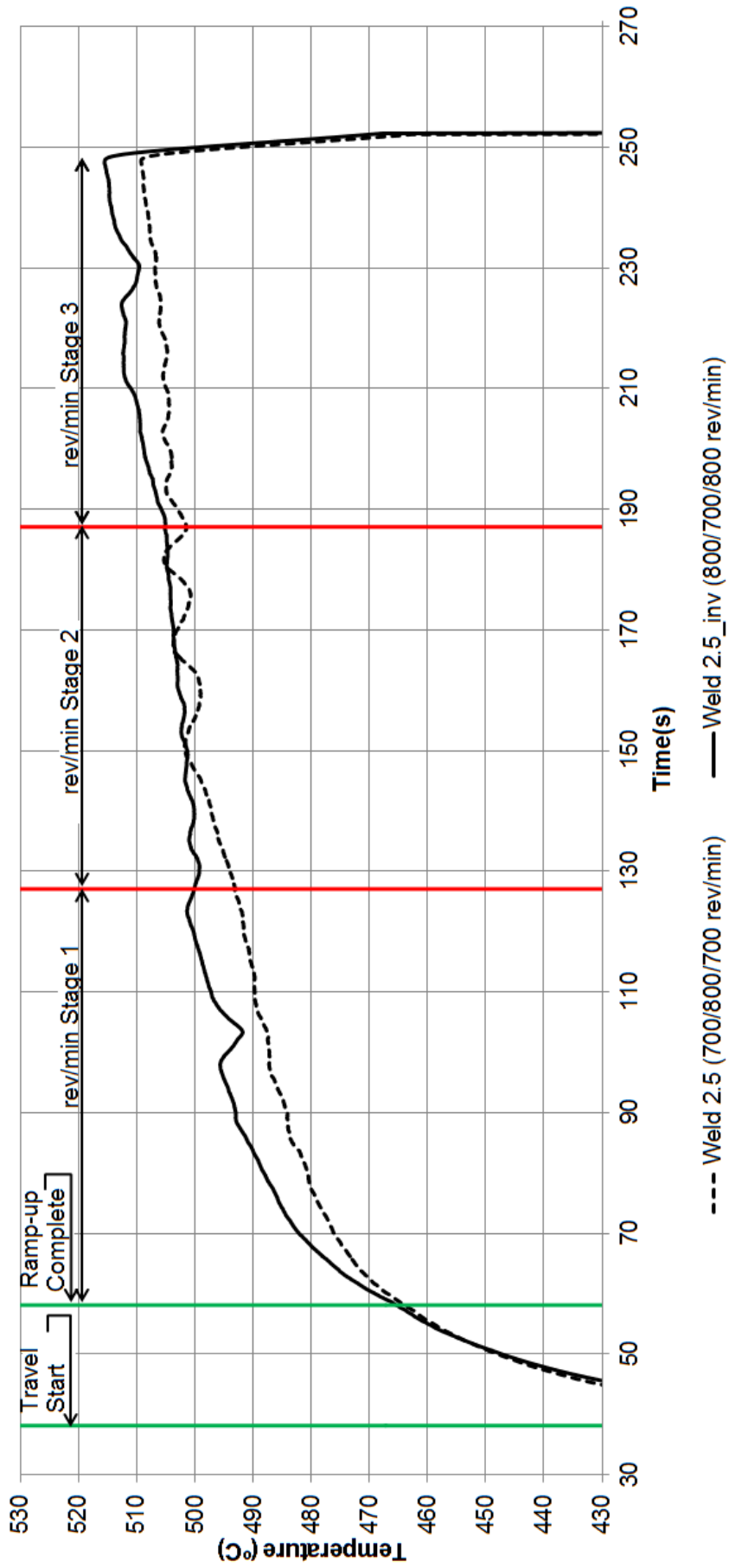
FSW AA 6082-T6 Temperature vs Time: 300 and 400 rev/min Inverted Weld Stages



FSW AA 6082-T6 Temperature vs Time: 500 and 600 rev/min Inverted Weld Stages



FSW AA 6082-T6 Temperature vs Time: 700 and 800 rev/min Inverted Weld Stages



Appendix E- PLC code and Algorithm tuning welds

```
eSDCM_TemperatureControl:
  pstSMC^.stOutputs.bDriveEnable      := TRUE;
  pstSMC^.stOutputs.bDriveNotHalt    := TRUE;
  pstSMC^.stOutputs.bDriveOn         := TRUE;
  pstSMC^.stOutputs.eControlMode     := eSDCM_VelocityControl;

IF (pstSMC^.stInputs.fRpmNom >=0) THEN
  pstSMC^.stInternal.fSpindleDirection := 1.0;
ELSE
  pstSMC^.stInternal.fSpindleDirection := -1.0;
END_IF

(*Calculate moving average of temperature*)
FOR iLoop:= 0 TO 99 DO
  IF (iLoop<99) THEN
    pstSMC^.stInternal.arrTemperature_history[iLoop] := pstSMC^.stInternal.arrTemperature_history[iLoop + 1];
  ELSE
    pstSMC^.stInternal.arrTemperature_history[iLoop] := ((pstSMC^.stInputs.pfTempFeedback^ +
    pstSMC^.stInputs.pfTempFeedback2^)/2);
  END_IF
END_FOR

pstSMC^.stInternal.fSmoothTemp := 0;

FOR nLoop:= 0 TO 99 DO
  pstSMC^.stInternal.fSmoothTemp := pstSMC^.stInternal.fSmoothTemp +
  pstSMC^.stInternal.arrTemperature_history[nLoop];
END_FOR

pstSMC^.stInternal.fSmoothTemp := pstSMC^.stInternal.fSmoothTemp / 100;

(*Calculate Error*)
IF (pstSMC^.stInputs.pfTempFeedback <> 0) THEN
  pstSMC^.stInternal.fTempError := pstSMC^.stInputs.fSwTempSetpoint - pstSMC^.stInternal.fSmoothTemp;
ELSE
```

```

    pstSMC^.stInternal.fTempError := 0;
END_IF
(*original: (*Calculate Error*)
IF (pstSMC^.stInputs.pfTempFeedback <> 0) THEN
    pstSMC^.stInternal.fTempError := pstSMC^.stInputs.fswTempSetpoint - ((pstSMC^.stInputs.pfTempFeedback +
    pstSMC^.stInputs.pfTempFeedback2)/2);
ELSE
    pstSMC^.stInternal.fTempError := 0;
END_IF
*)
(*Calculate Proportional term*)
pstSMC^.stInternal.fProportional := pstSMC^.stConfig.fTempP * pstSMC^.stInternal.fTempError;
(* Calculate integral *)
IF ((pstSMC^.stInputs.pbEnableIntegrator <> 0) AND (pstSMC^.stInputs.pbEnableIntegrator = TRUE)) THEN
    pstSMC^.stInternal.fIntegral := pstSMC^.stInternal.fIntegral + (pstSMC^.stInternal.fTempError *
    stPlatform.stPLC.fPLCCycleTime * pstSMC^.stConfig.fTempI);
ELSE
    pstSMC^.stInternal.fIntegral := 0;
END_IF
(* Apply wind-up limit (integral rpm contribution limit (positive amount)) *)
IF (pstSMC^.stInternal.fIntegral >= pstSMC^.stConfig.fTempWindupLimit) THEN
    pstSMC^.stInternal.fIntegral := pstSMC^.stConfig.fTempWindupLimit;
ELSIF (pstSMC^.stInternal.fIntegral <= (-1.0) * pstSMC^.stConfig.fTempWindupLimit) THEN
    pstSMC^.stInternal.fIntegral := (-1.0) * pstSMC^.stConfig.fTempWindupLimit;
END_IF
(* Calculate derivative *)
pstSMC^.stInternal.fdTdt := ((pstSMC^.stInternal.fSmoothTemp - pstSMC^.stInternal.fTempPrev) /
    stPlatform.stPLC.fPLCCycleTime);
pstSMC^.stInternal.fdTdt_abs := ABS(pstSMC^.stInternal.fdTdt);
(*Filter 2*)
pstSMC^.stInternal.fDerivative := pstSMC^.stConfig.fTempD * pstSMC^.stInternal.fdTdt_abs /

```


Appendix E- PLC code and Algorithm tuning welds

```

(1+(((pstSMC^.stInternal.fdTdt_abs * pstSMC^.stInternal.fdTdt_abs *
  SQRT(pstSMC^.stInternal.fdTdt_abs)) * (pstSMC^.stConfig.fTempD / pstSMC^.stConfig.fTempP) /
  300));

(**Filter 3*)
pstSMC^.stInternal.fDerivative := pstSMC^.stConfig.fTempD * pstSMC^.stInternal.fdTdt_abs / (1+((pstSMC^.stInternal.fdTdt_abs *
  pstSMC^.stInternal.fdTdt_abs) * (pstSMC^.stConfig.fTempD / pstSMC^.stConfig.fTempP) / 30));
*)

(**Filter 4*)
(*pstSMC^.stInternal.fDtpower10 = pstSMC^.stInternal.fdTdt_abs;
FOR iLoop:= 0 TO 8 DO
  pstSMC^.stInternal.fDtpower10 = pstSMC^.stInternal.fDtpower10 * pstSMC^.stInternal.fdTdt_abs;
END_FOR
pstSMC^.stInternal.fDerivative := pstSMC^.stConfig.fTempD * pstSMC^.stInternal.fDtpower10 / (1+((pstSMC^.stInternal.fDtpower10 *
  (pstSMC^.stConfig.fTempD / pstSMC^.stConfig.fTempP) / 100000000000));
*)

IF(pstSMC^.stInternal.fDtdt >= 0) THEN
  pstSMC^.stInternal.fDerivative := pstSMC^.stInternal.fDerivative;
ELSE
  pstSMC^.stInternal.fDerivative := (-1) * pstSMC^.stInternal.fDerivative;
END_IF

pstSMC^.stInternal.fTempPrev := pstSMC^.stInternal.fSmoothTemp;

(* PID output to Spindle speed with the correct direction *)
pstSMC^.stOutputs.fSpeed := pstSMC^.stInputs.fRpmNom + ((pstSMC^.stInternal.fProportional + pstSMC^.stInternal.fIntegral -
  pstSMC^.stInternal.fDerivative) * pstSMC^.stInternal.fSpindleDirection); (*set direction of spindle
  (same as weld direction)*)

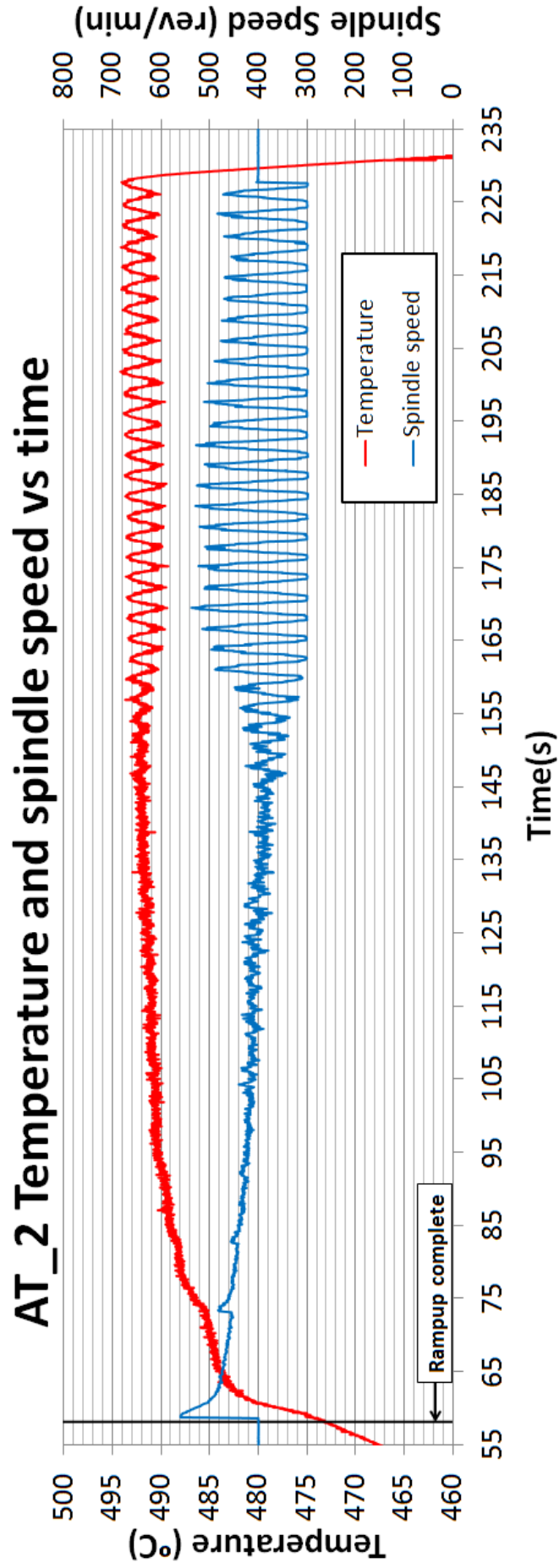
(**for PI control only*)
(*pstSMC^.stOutputs.fSpeed := pstSMC^.stInputs.fRpmNom + ((pstSMC^.stInternal.fProportional + pstSMC^.stInternal.fIntegral) *
  pstSMC^.stInternal.fSpindleDirection);*)

```

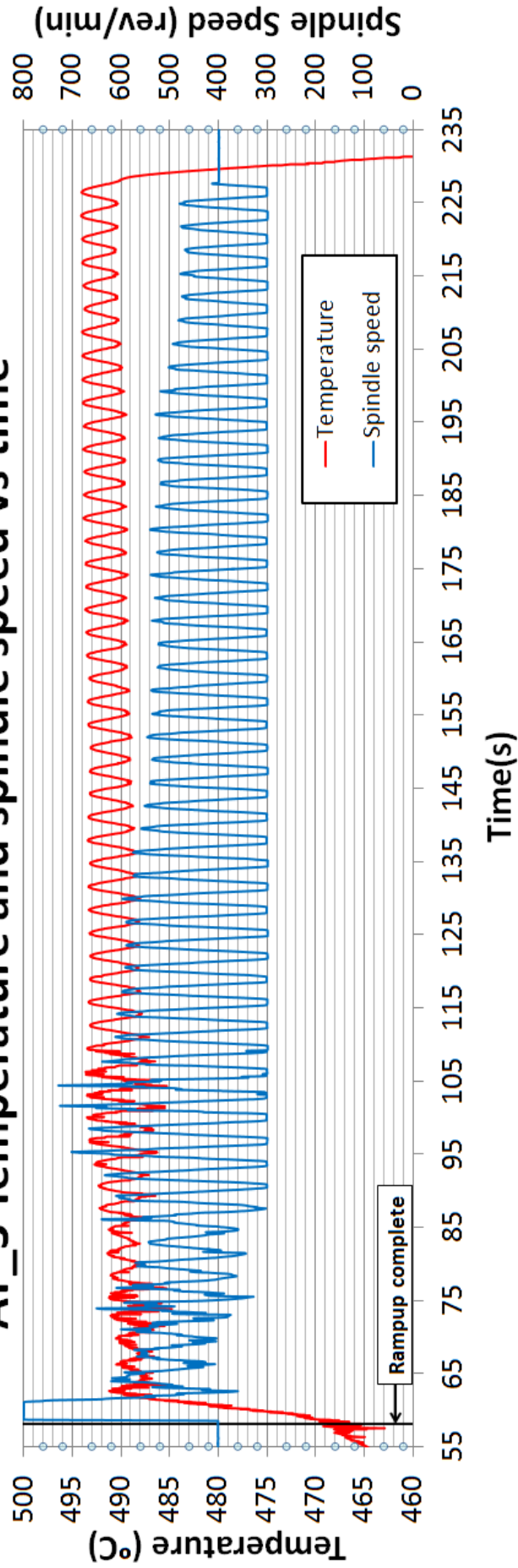
Appendix E- PLC code and Algorithm tuning welds

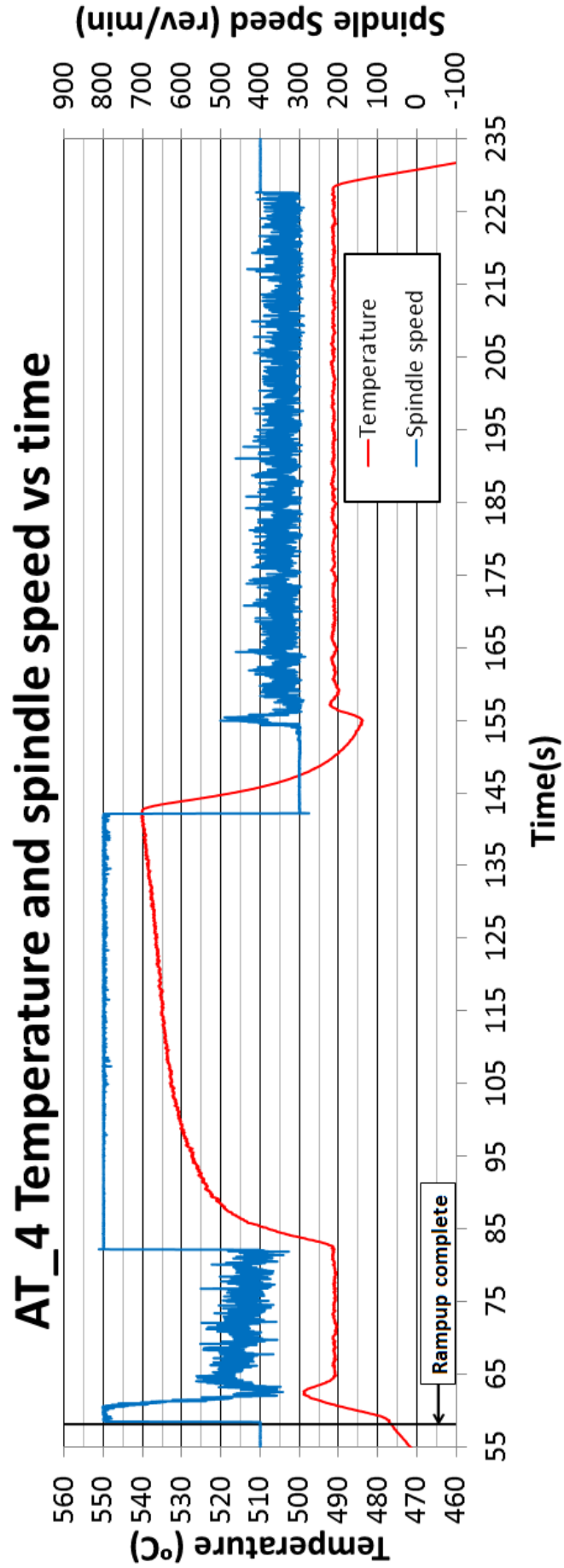
```
IF (pstSMC^.stInternal.fSpindleDirection > 0) THEN
  IF (pstSMC^.stOutputs.fSpeed < pstSMC^.stInputs.fRpmMin) THEN
    pstSMC^.stOutputs.fSpeed := pstSMC^.stInputs.fRpmMin;
  ELSIF (pstSMC^.stOutputs.fSpeed > pstSMC^.stInputs.fRpmMax) THEN
    pstSMC^.stOutputs.fSpeed := pstSMC^.stInputs.fRpmMax;
  END_IF
ELSE
  IF (pstSMC^.stOutputs.fSpeed > pstSMC^.stInputs.fRpmMin) THEN
    pstSMC^.stOutputs.fSpeed := pstSMC^.stInputs.fRpmMin;
  ELSIF (pstSMC^.stOutputs.fSpeed < pstSMC^.stInputs.fRpmMax) THEN
    pstSMC^.stOutputs.fSpeed := pstSMC^.stInputs.fRpmMax;
  END_IF
END_IF

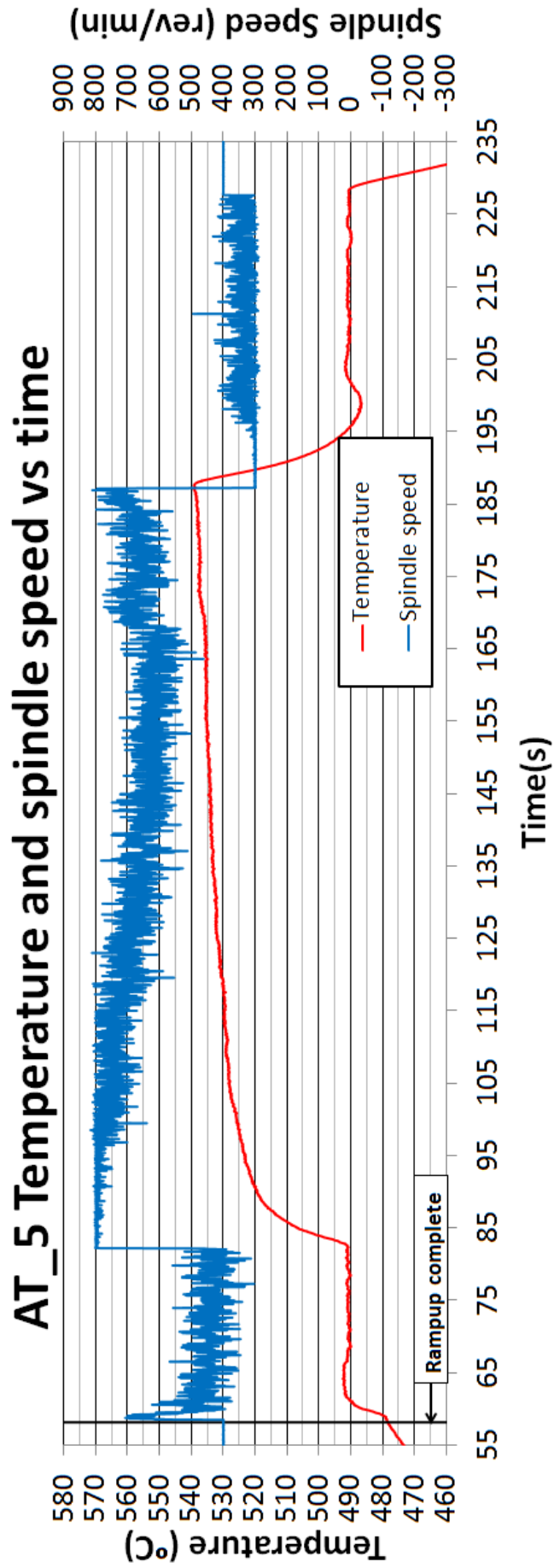
pstSMC^.stOutputs.fPosition := 0.0;
pstSMC^.stOutputs.fTorque := 0.0;
pstSMC^.stInternal.fCoolerTimer := stPlatform.stPLC.fPLCCycleTime;
```

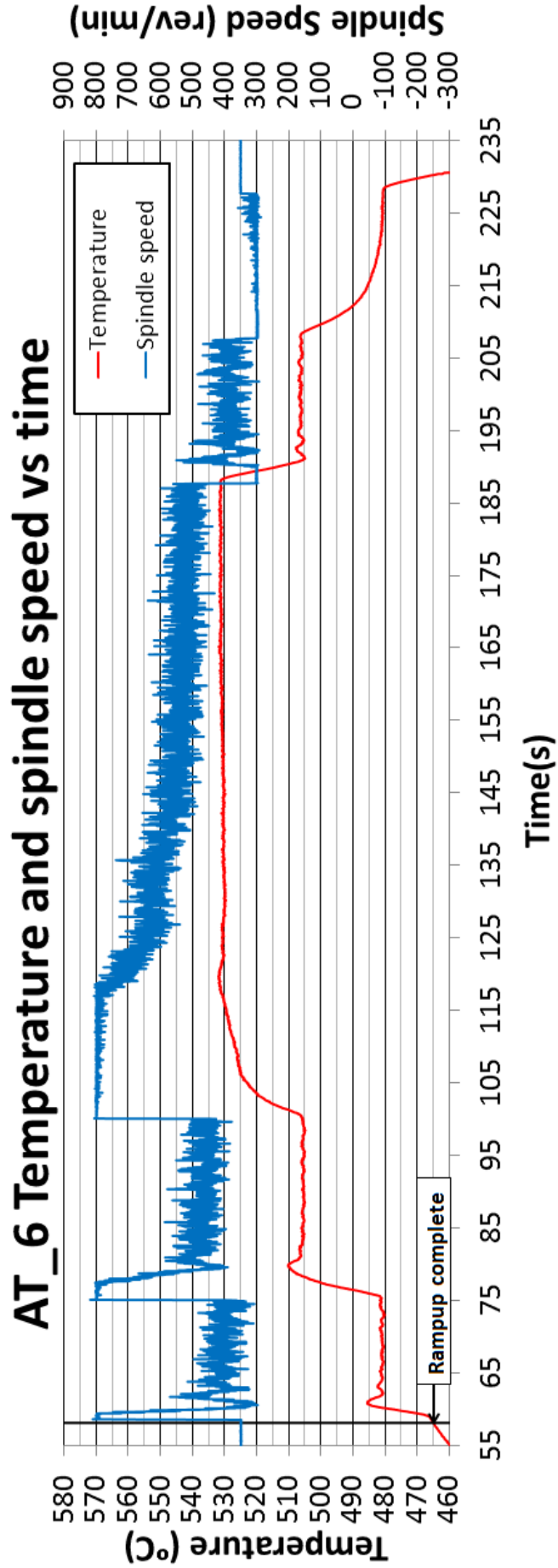



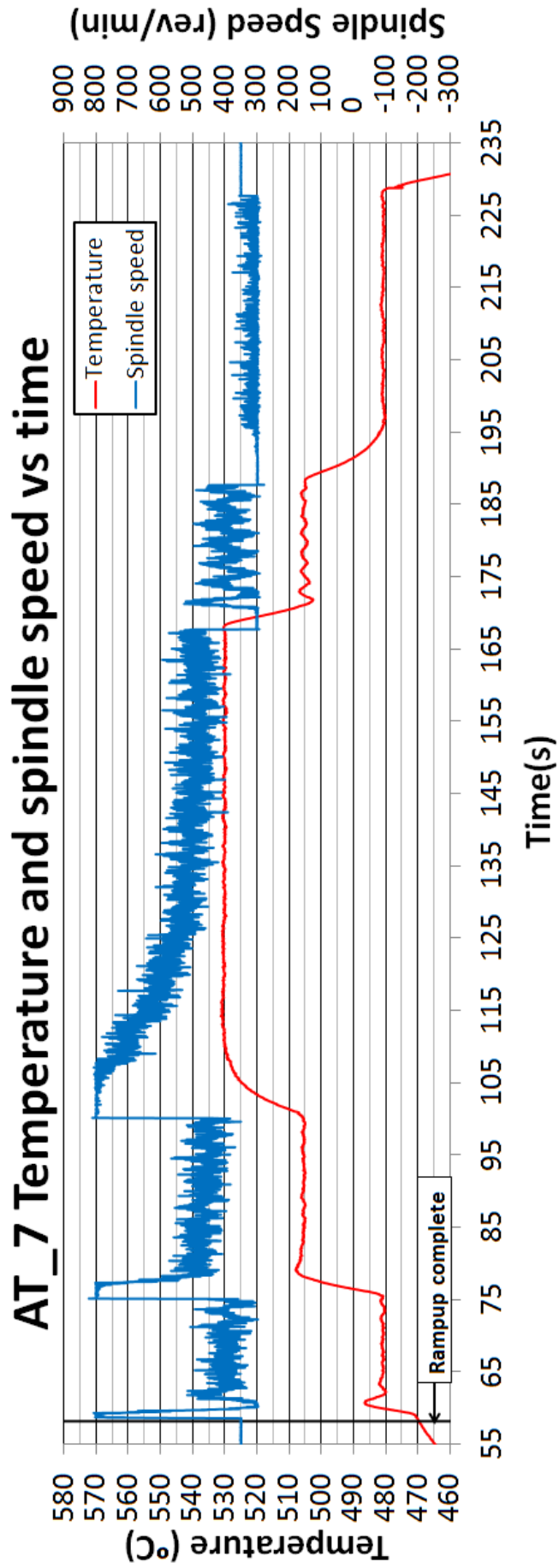
AT_3 Temperature and spindle speed vs time

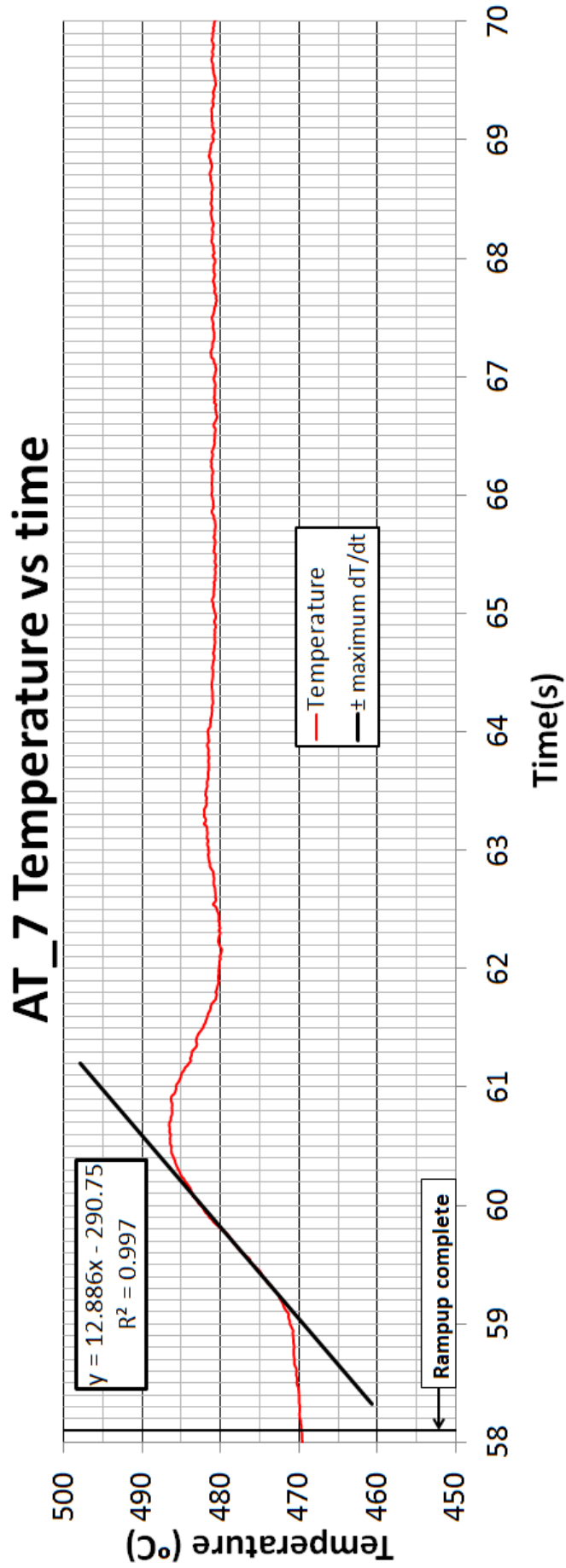


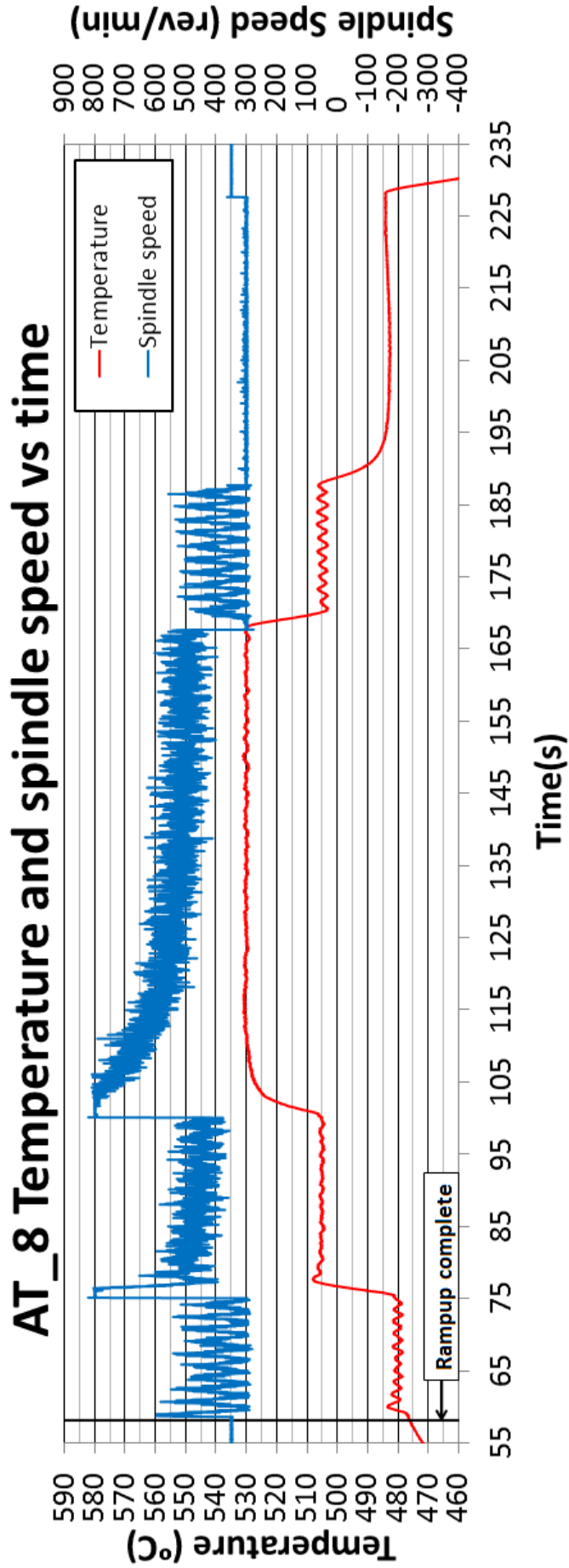


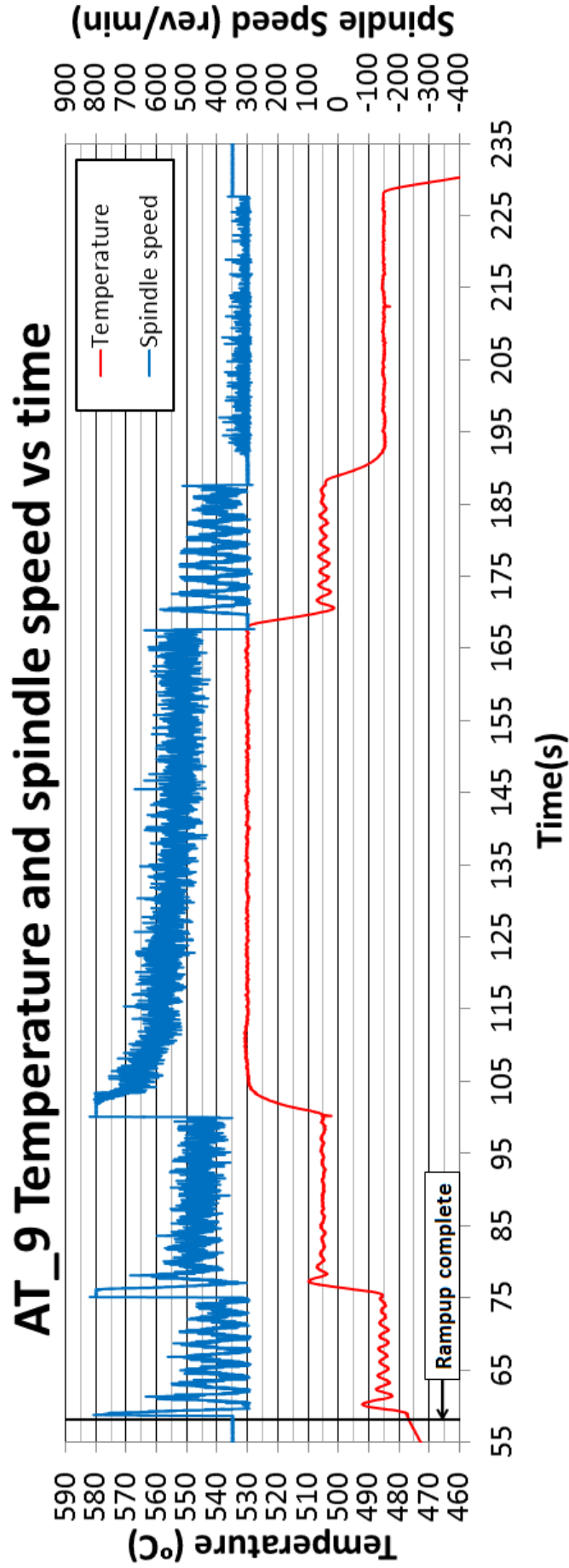


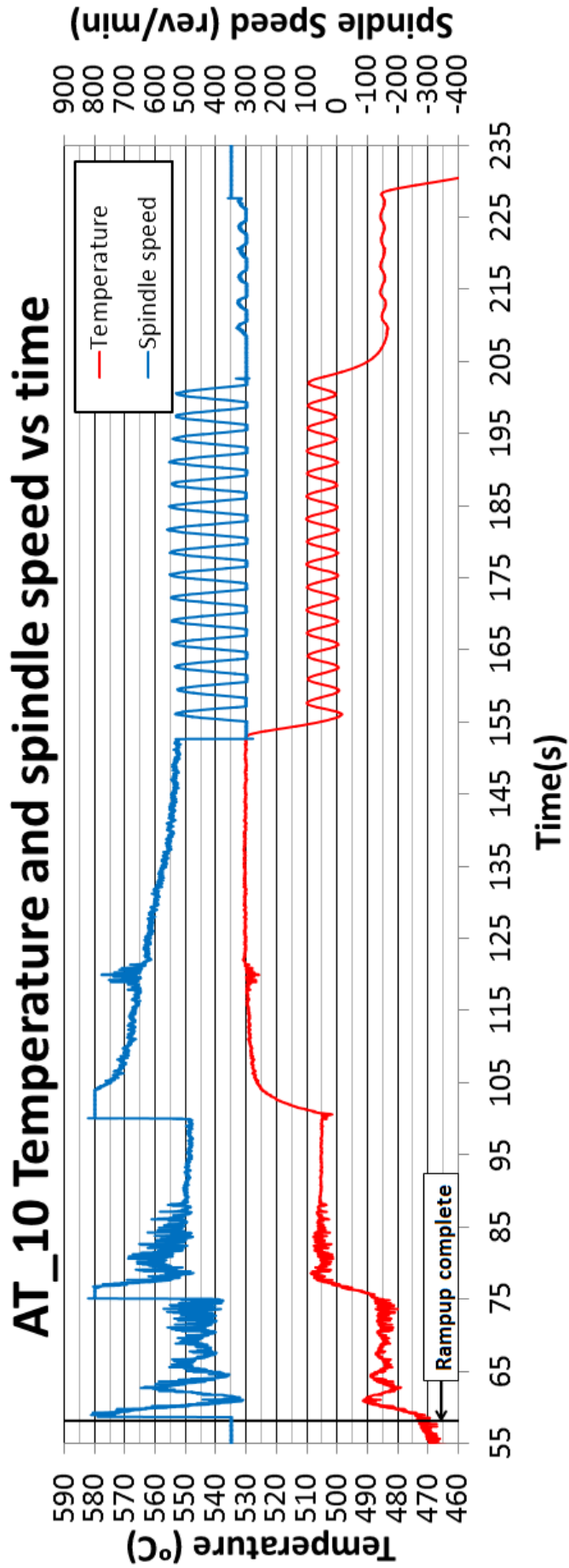


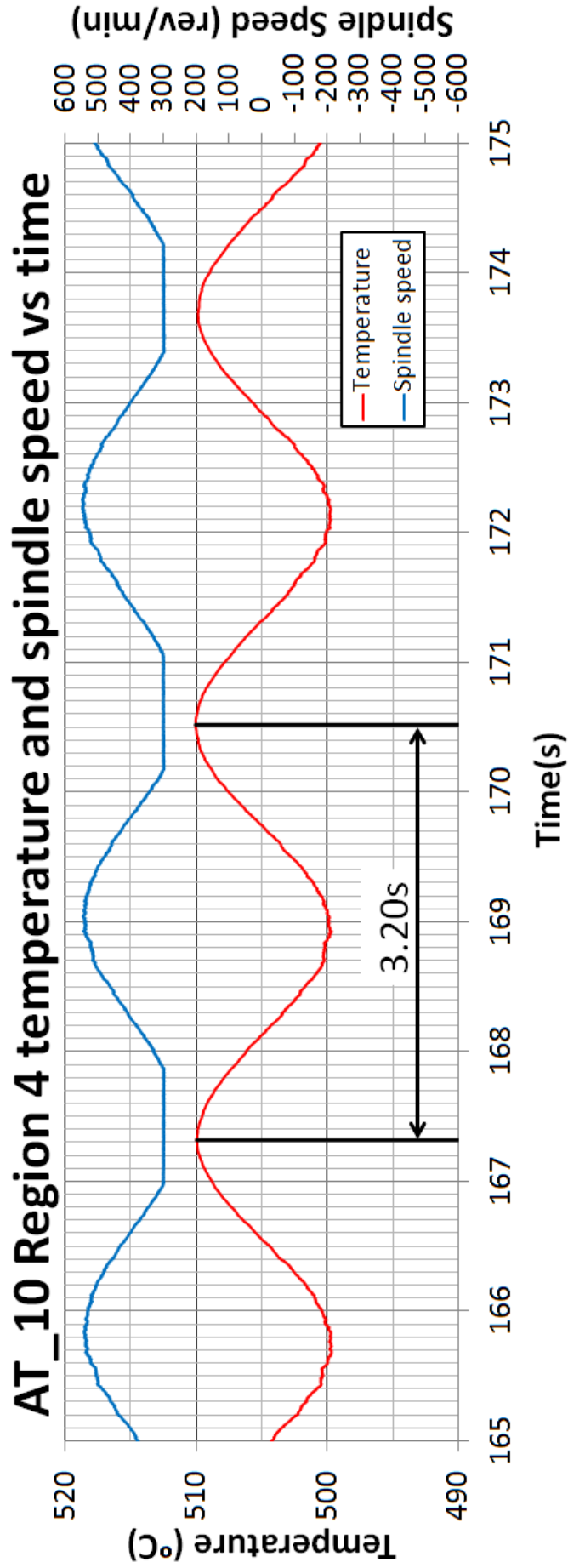


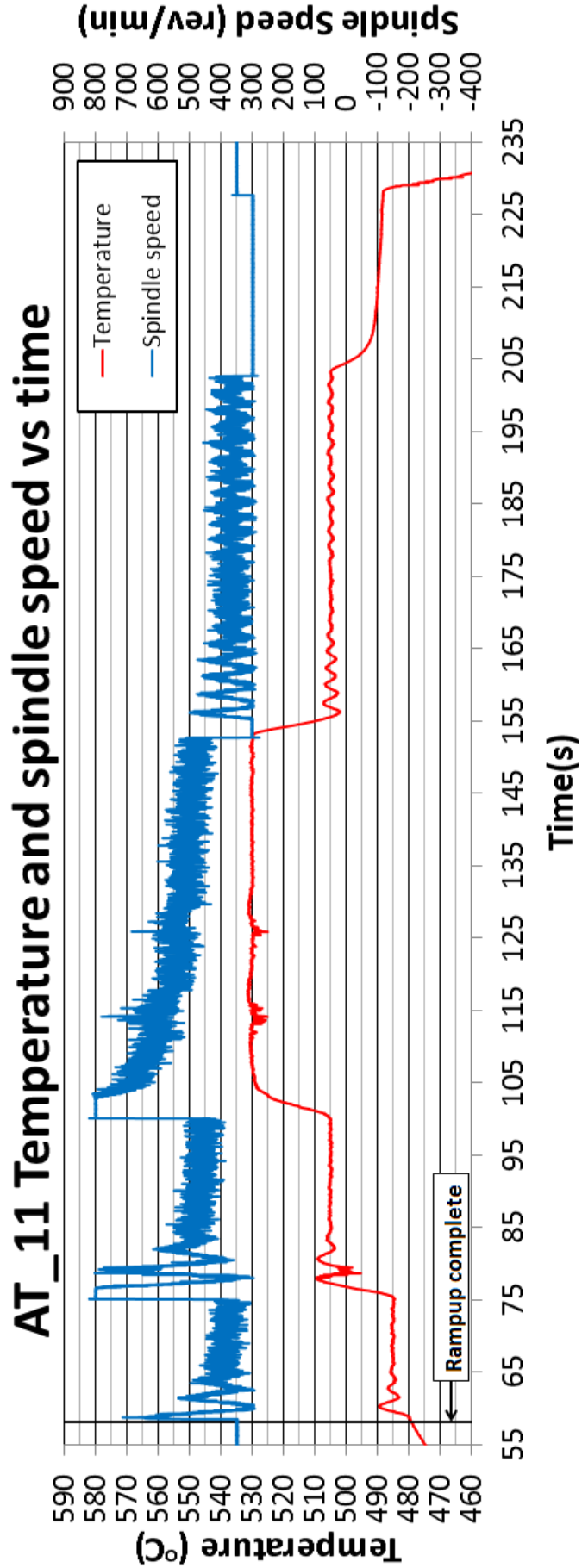


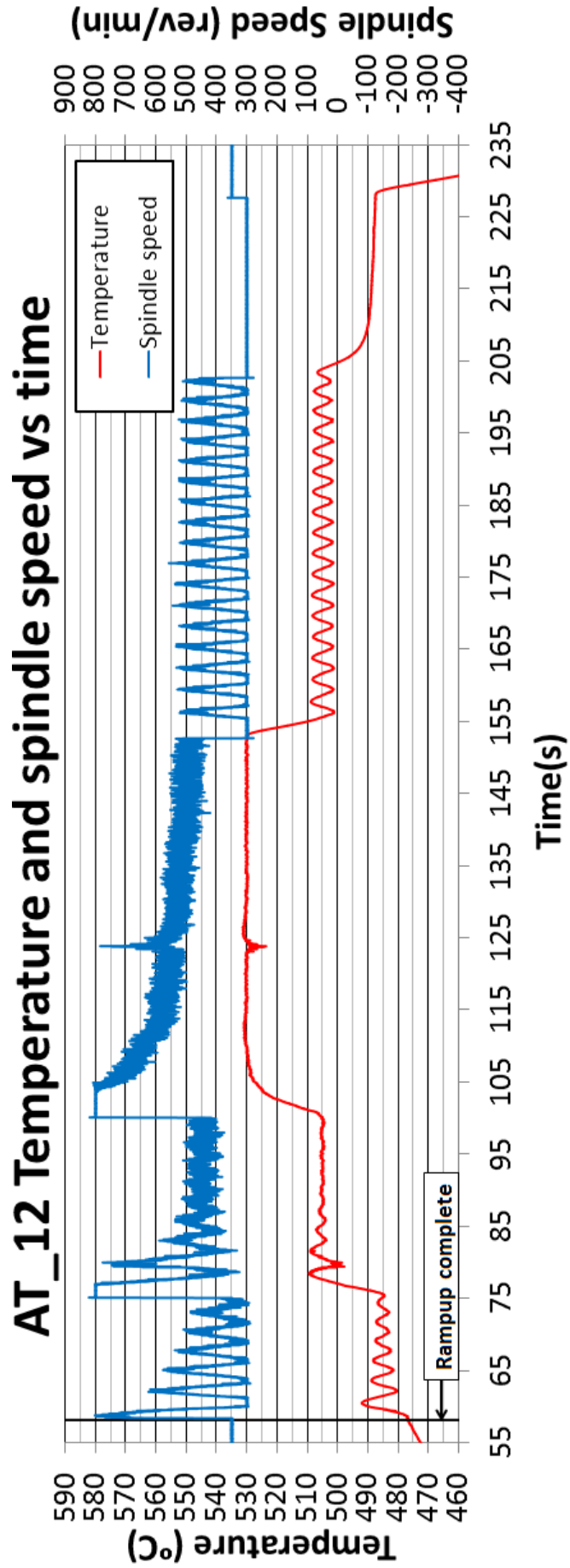


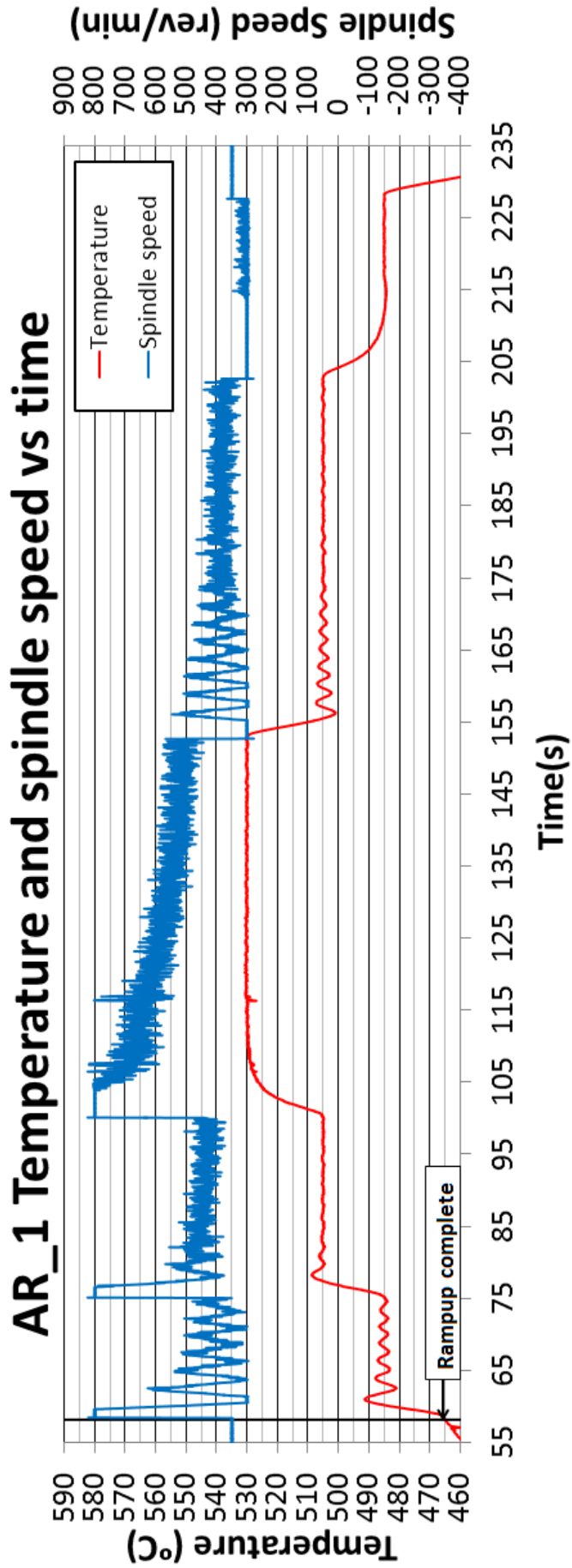


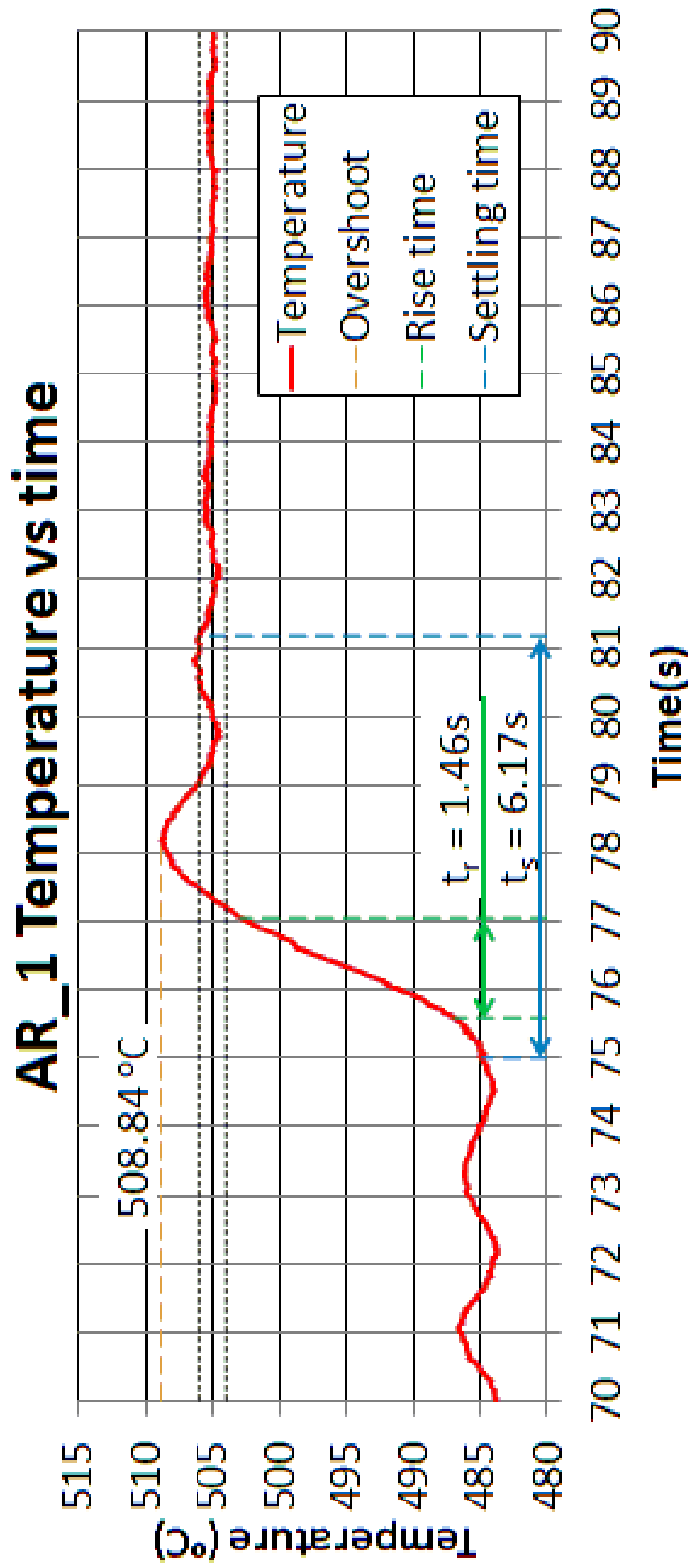


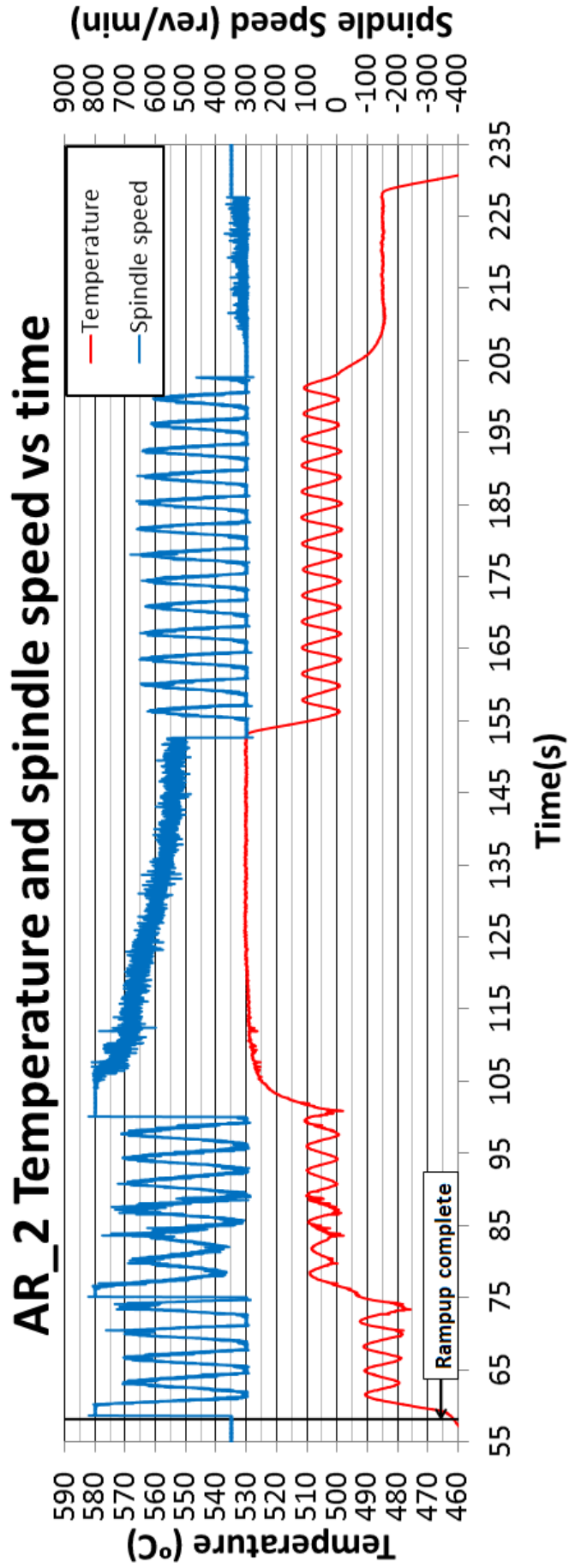












Appendix F- Weld AT 7 data

AT_7 steady state regions			
Region 2 time (s)	Region 2 temperature (°C)	Region 4 time (s)	Region 4 temperature (°C)
82	506.4276	175	505.2010
82.02	506.4370	175.02	505.3032
82.04	506.2319	175.04	505.2334
82.06	506.2922	175.06	505.2229
82.08	506.1275	175.08	505.1837
82.1	506.2932	175.1	505.2465
82.12	506.2361	175.12	505.3329
82.14	506.1663	175.14	505.4301
82.16	506.2219	175.16	505.5032
82.18	506.2329	175.18	505.4712
82.2	506.2314	175.2	505.5257
82.22	506.1856	175.22	505.5754
82.24	506.1929	175.24	505.6701
82.26	506.0652	175.26	505.7098
82.28	506.0945	175.28	505.6221
82.3	506.1558	175.3	505.6781
82.32	506.1102	175.32	505.8021
82.34	506.1986	175.34	505.5572
82.36	506.0921	175.36	505.6992
82.38	506.0209	175.38	505.6872
82.4	506.0856	175.4	505.9018
82.42	506.1528	175.42	505.9619
82.44	506.0825	175.44	505.9640
82.46	505.9920	175.46	505.9605
82.48	505.9980	175.48	505.9849
82.5	505.9562	175.5	506.0990
82.52	505.9063	175.52	505.9943
82.54	505.8178	175.54	506.1356
82.56	505.7907	175.56	506.1799
82.58	505.8235	175.58	506.3083
82.6	505.8792	175.6	506.3756
82.62	505.8384	175.62	506.2402
82.64	505.8940	175.64	506.2416
82.66	505.8164	175.66	506.3371
82.68	505.7475	175.68	506.3434

Region 2				
Mean (°C)	n	t-critical	Standard deviation	Uncertainty (95%)
505.5401	901	1.96	0.2802	0.0183

Region 4				
Mean (°C)	n	t-critical	Standard deviation	Uncertainty (95%)
505.4541	601	1.96	0.5540	0.0443

*Note: data sampling period is 20 ms although the PLC program (including the temperature control algorithm code) is executed every millisecond

Appendix F- Weld AT 7 data

82.7	505.7297	175.7	506.3901
82.72	505.6256	175.72	506.4330
82.74	505.6166	175.74	506.3421
82.76	505.5431	175.76	506.3217
82.78	505.6464	175.78	506.3784
82.8	505.6783	175.8	506.3527
82.82	505.6746	175.82	506.3452
82.84	505.7170	175.84	506.2554
82.86	505.6886	175.86	506.1596
82.88	505.6908	175.88	506.1369
82.9	505.6114	175.9	506.1438
82.92	505.7011	175.92	506.1251
82.94	505.6056	175.94	506.0302
82.96	505.4452	175.96	505.9876
82.98	505.5348	175.98	505.9377
83	505.4462	176	506.0070
83.02	505.4932	176.02	505.9258
83.04	505.7212	176.04	505.8791
83.06	505.7446	176.06	505.7398
83.08	505.7681	176.08	505.7926
83.1	505.8811	176.1	505.7663
83.12	505.9248	176.12	505.7461
83.14	505.9785	176.14	505.7283
83.16	505.8027	176.16	505.7343
83.18	505.7637	176.18	505.6902
83.2	505.7410	176.2	505.6608
83.22	505.7962	176.22	505.4998
83.24	505.9669	176.24	505.4174
83.26	505.8956	176.26	505.4109
83.28	505.7298	176.28	505.2624
83.3	505.7822	176.3	505.1792
83.32	505.7715	176.32	505.1039
83.34	505.7451	176.34	505.2878
83.36	505.7539	176.36	505.2702
83.38	505.7426	176.38	505.1331
83.4	505.7223	176.4	505.0037
83.42	505.6635	176.42	505.0802
83.44	505.7246	176.44	505.2138
83.46	505.5428	176.46	505.0453
83.48	505.6355	176.48	505.0808
83.5	505.5715	176.5	505.0436
83.52	505.4879	176.52	505.0183
83.54	505.4161	176.54	505.0830

Appendix F- Weld AT 7 data

83.56	505.5096	176.56	504.9205
83.58	505.6250	176.58	504.7950
83.6	505.7408	176.6	504.8107
83.62	505.8048	176.62	504.7838
83.64	505.5313	176.64	504.5655
83.66	505.5111	176.66	504.4793
83.68	505.4583	176.68	504.6601
83.7	505.3917	176.7	504.5045
83.72	505.4489	176.72	504.4554
83.74	505.5110	176.74	504.5236
83.76	505.4505	176.76	504.5073
83.78	505.5990	176.78	504.4674
83.8	505.6369	176.8	504.3194
83.82	505.5546	176.82	504.3448
83.84	505.5591	176.84	504.2129
83.86	505.6025	176.86	504.3568
83.88	505.6332	176.88	504.3878
83.9	505.6326	176.9	504.5345
83.92	505.4234	176.92	504.5003
83.94	505.4068	176.94	504.5393
83.96	505.4913	176.96	504.6085
83.98	505.4525	176.98	504.6186
84	505.4826	177	504.5515
84.02	505.5999	177.02	504.5165
84.04	505.6276	177.04	504.5314
84.06	505.6732	177.06	504.5821
84.08	505.6076	177.08	504.6411
84.1	505.7481	177.1	504.6500
84.12	505.7277	177.12	504.7165
84.14	505.6862	177.14	504.8363
84.16	505.7603	177.16	504.7386
84.18	505.8647	177.18	504.7712
84.2	505.6187	177.2	504.8450
84.22	505.6237	177.22	504.9184
84.24	505.6106	177.24	504.9986
84.26	505.6906	177.26	504.9115
84.28	505.7352	177.28	504.9915
84.3	505.5414	177.3	505.0813
84.32	505.4872	177.32	505.0927
84.34	505.6447	177.34	505.2184
84.36	505.7279	177.36	505.3386
84.38	505.7341	177.38	505.3190
84.4	505.5120	177.4	505.3685

Appendix F- Weld AT 7 data

84.42	505.4873	177.42	505.3860
84.44	505.4062	177.44	505.5661
84.46	505.3336	177.46	505.7314
84.48	505.3892	177.48	505.6707
84.5	505.3725	177.5	505.6415
84.52	505.4863	177.52	505.6710
84.54	505.5792	177.54	505.6924
84.56	505.5513	177.56	505.5984
84.58	505.5021	177.58	505.5440
84.6	505.5515	177.6	505.5813
84.62	505.5540	177.62	505.8460
84.64	505.6017	177.64	505.7160
84.66	505.7224	177.66	505.8457
84.68	505.5842	177.68	505.6345
84.7	505.4326	177.7	505.6623
84.72	505.5138	177.72	505.7248
84.74	505.6174	177.74	505.7588
84.76	505.6466	177.76	505.8478
84.78	505.5830	177.78	505.8771
84.8	505.4145	177.8	505.7635
84.82	505.4811	177.82	505.9049
84.84	505.3760	177.84	506.0367
84.86	505.1632	177.86	505.9844
84.88	505.2467	177.88	506.1098
84.9	505.3425	177.9	506.0981
84.92	505.2590	177.92	506.0569
84.94	505.2438	177.94	506.1091
84.96	505.3235	177.96	506.0048
84.98	505.1670	177.98	505.8425
85	505.1825	178	505.9323
85.02	505.1721	178.02	506.0723
85.04	505.2962	178.04	506.1675
85.06	505.3237	178.06	506.0806
85.08	505.4547	178.08	506.1269
85.1	505.4726	178.1	506.0809
85.12	505.7141	178.12	506.0907
85.14	505.5529	178.14	506.1928
85.16	505.4796	178.16	506.1397
85.18	505.3677	178.18	506.1082
85.2	505.3866	178.2	506.0852
85.22	505.2083	178.22	506.0261
85.24	505.2353	178.24	505.9257
85.26	505.3211	178.26	505.9336

Appendix F- Weld AT 7 data

85.28	505.4141	178.28	505.9516
85.3	505.3633	178.3	506.2919
85.32	505.4287	178.32	506.2376
85.34	505.5702	178.34	506.2557
85.36	505.7534	178.36	506.2427
85.38	505.5661	178.38	506.3063
85.4	505.4255	178.4	506.1519
85.42	505.4752	178.42	506.0983
85.44	505.4387	178.44	506.1402
85.46	505.4390	178.46	506.1040
85.48	505.5765	178.48	505.8192
85.5	505.3091	178.5	506.0310
85.52	505.1033	178.52	506.0646
85.54	505.1355	178.54	506.0387
85.56	505.1864	178.56	505.9824
85.58	505.1334	178.58	505.9618
85.6	505.3142	178.6	505.8924
85.62	505.2514	178.62	505.9431
85.64	505.2977	178.64	505.9174
85.66	505.2601	178.66	505.8585
85.68	505.3296	178.68	505.8610
85.7	505.3454	178.7	505.8046
85.72	505.2129	178.72	505.6899
85.74	505.0318	178.74	505.8088
85.76	505.0149	178.76	505.7209
85.78	505.1422	178.78	505.5909
85.8	504.9819	178.8	505.6676
85.82	505.1378	178.82	505.5691
85.84	505.1934	178.84	505.4219
85.86	505.2023	178.86	505.3214
85.88	505.2223	178.88	505.2367
85.9	505.2175	178.9	505.1169
85.92	505.3226	178.92	505.0646
85.94	505.2904	178.94	505.0396
85.96	505.1988	178.96	504.9403
85.98	505.2524	178.98	504.9270
86	505.2573	179	504.9853
86.02	505.1837	179.02	504.9593
86.04	505.1180	179.04	505.0309
86.06	505.1179	179.06	505.1288
86.08	505.0388	179.08	505.1075
86.1	505.1786	179.1	505.0607
86.12	505.0711	179.12	505.1402

Appendix F- Weld AT 7 data

86.14	505.0888	179.14	505.0644
86.16	504.9519	179.16	505.0269
86.18	505.0373	179.18	505.0756
86.2	505.1116	179.2	505.0030
86.22	505.2252	179.22	504.7715
86.24	505.3534	179.24	504.7085
86.26	505.2538	179.26	504.4897
86.28	505.1315	179.28	504.5373
86.3	505.1434	179.3	504.6154
86.32	505.2915	179.32	504.6095
86.34	505.4223	179.34	504.6905
86.36	505.4460	179.36	504.6415
86.38	505.4731	179.38	504.5122
86.4	505.5273	179.4	504.4366
86.42	505.5952	179.42	504.3981
86.44	505.6208	179.44	504.3362
86.46	505.6521	179.46	504.3815
86.48	505.6702	179.48	504.3371
86.5	505.6903	179.5	504.4404
86.52	505.7518	179.52	504.5753
86.54	505.7203	179.54	504.5708
86.56	505.8988	179.56	504.6102
86.58	505.8260	179.58	504.5189
86.6	505.7026	179.6	504.4794
86.62	505.6694	179.62	504.4331
86.64	505.6948	179.64	504.6190
86.66	505.6958	179.66	504.6067
86.68	505.7463	179.68	504.6373
86.7	505.8070	179.7	504.4872
86.72	505.8520	179.72	504.4036
86.74	505.8384	179.74	504.3321
86.76	505.9706	179.76	504.2932
86.78	505.8468	179.78	504.3221
86.8	505.7535	179.8	504.2755
86.82	505.7289	179.82	504.2269
86.84	505.7184	179.84	504.3410
86.86	505.5687	179.86	504.4478
86.88	505.6860	179.88	504.3708
86.9	505.6040	179.9	504.3650
86.92	505.5486	179.92	504.4801
86.94	505.6060	179.94	504.4699
86.96	505.4428	179.96	504.4543
86.98	505.4767	179.98	504.5984

Appendix F- Weld AT 7 data

87	505.5858	180	504.6487
87.02	505.5255	180.02	504.5886
87.04	505.5614	180.04	504.7249
87.06	505.5087	180.06	504.8053
87.08	505.6061	180.08	504.9738
87.1	505.5793	180.1	505.0309
87.12	505.6976	180.12	504.9899
87.14	505.6098	180.14	505.0868
87.16	505.7692	180.16	505.0346
87.18	505.7677	180.18	504.8929
87.2	505.8080	180.2	504.8945
87.22	505.8572	180.22	505.0582
87.24	505.7922	180.24	505.0069
87.26	505.7893	180.26	505.1369
87.28	505.7385	180.28	505.1472
87.3	505.6260	180.3	505.2388
87.32	505.5303	180.32	505.1489
87.34	505.6183	180.34	505.1082
87.36	505.6634	180.36	505.0947
87.38	505.6104	180.38	505.1766
87.4	505.6315	180.4	505.1595
87.42	505.5954	180.42	505.3561
87.44	505.6839	180.44	505.4894
87.46	505.5544	180.46	505.4524
87.48	505.5105	180.48	505.4139
87.5	505.3965	180.5	505.4646
87.52	505.4811	180.52	505.5780
87.54	505.5175	180.54	505.5748
87.56	505.3433	180.56	505.7221
87.58	505.2698	180.58	505.6430
87.6	505.2847	180.6	505.5116
87.62	505.2704	180.62	505.6217
87.64	505.3397	180.64	505.6632
87.66	505.3231	180.66	505.7310
87.68	505.4064	180.68	505.9004
87.7	505.3552	180.7	505.7956
87.72	505.2661	180.72	505.9903
87.74	505.3271	180.74	505.9559
87.76	505.3801	180.76	506.0650
87.78	505.2947	180.78	505.9798
87.8	505.2103	180.8	506.0988
87.82	505.2013	180.82	506.2224
87.84	505.1194	180.84	506.2711

Appendix F- Weld AT 7 data

87.86	505.0223	180.86	506.3467
87.88	505.0342	180.88	506.4268
87.9	505.0739	180.9	506.2978
87.92	505.1113	180.92	506.1431
87.94	505.0441	180.94	506.2307
87.96	504.9707	180.96	506.1201
87.98	504.9455	180.98	506.1914
88	505.0406	181	506.1172
88.02	505.0913	181.02	505.9760
88.04	505.1206	181.04	505.9420
88.06	505.1648	181.06	506.1215
88.08	505.0924	181.08	506.3252
88.1	505.0708	181.1	506.1981
88.12	505.1643	181.12	506.1607
88.14	505.1018	181.14	506.1852
88.16	505.1901	181.16	506.0975
88.18	505.1427	181.18	506.0205
88.2	505.1581	181.2	505.9384
88.22	505.0813	181.22	505.9960
88.24	505.1297	181.24	506.0129
88.26	505.2291	181.26	506.1286
88.28	505.1781	181.28	506.0148
88.3	505.2096	181.3	505.8329
88.32	505.2141	181.32	505.8162
88.34	505.2188	181.34	505.8445
88.36	505.2985	181.36	505.7768
88.38	505.3315	181.38	505.9215
88.4	505.2536	181.4	505.9162
88.42	505.2438	181.42	506.0260
88.44	505.3189	181.44	505.9307
88.46	505.4141	181.46	505.7676
88.48	505.3971	181.48	505.7912
88.5	505.6275	181.5	505.7975
88.52	505.4977	181.52	505.8465
88.54	505.5096	181.54	505.7921
88.56	505.5646	181.56	505.6962
88.58	505.6749	181.58	505.4908
88.6	505.6828	181.6	505.4508
88.62	505.6911	181.62	505.4387
88.64	505.6612	181.64	505.3122
88.66	505.5979	181.66	505.4329
88.68	505.6754	181.68	505.4171
88.7	505.5211	181.7	505.3835

Appendix F- Weld AT 7 data

88.72	505.5980	181.72	505.2943
88.74	505.7850	181.74	505.1895
88.76	505.6522	181.76	505.0835
88.78	505.7059	181.78	505.0769
88.8	505.7332	181.8	504.9840
88.82	505.6928	181.82	504.9376
88.84	505.7554	181.84	504.9571
88.86	505.8923	181.86	505.0805
88.88	505.8759	181.88	505.1917
88.9	505.9229	181.9	504.9875
88.92	505.9248	181.92	505.0719
88.94	506.0492	181.94	504.9772
88.96	506.0705	181.96	504.8713
88.98	506.1597	181.98	504.7947
89	506.2739	182	504.7829
89.02	506.3318	182.02	504.7925
89.04	506.1872	182.04	504.7074
89.06	506.1189	182.06	504.7391
89.08	506.2268	182.08	504.8920
89.1	506.2044	182.1	504.9000
89.12	506.2512	182.12	504.8102
89.14	506.1561	182.14	504.8141
89.16	506.1202	182.16	504.6619
89.18	506.1756	182.18	504.6401
89.2	506.1511	182.2	504.8155
89.22	505.9796	182.22	504.7932
89.24	505.9428	182.24	504.7479
89.26	506.0132	182.26	504.6093
89.28	505.9270	182.28	504.5416
89.3	506.0224	182.3	504.5307
89.32	506.0367	182.32	504.4821
89.34	506.1279	182.34	504.5736
89.36	506.0834	182.36	504.5961
89.38	506.1668	182.38	504.7280
89.4	506.2000	182.4	504.7264
89.42	506.1655	182.42	504.5804
89.44	505.9869	182.44	504.6060
89.46	506.0507	182.46	504.6817
89.48	506.0195	182.48	504.7624
89.5	506.0529	182.5	504.8449
89.52	506.1307	182.52	504.7881
89.54	506.0071	182.54	504.8854
89.56	506.0607	182.56	504.9473

Appendix F- Weld AT 7 data

89.58	505.9491	182.58	504.7956
89.6	506.0100	182.6	504.9253
89.62	505.9929	182.62	505.0227
89.64	505.8919	182.64	505.2636
89.66	505.7343	182.66	505.3455
89.68	505.7171	182.68	505.2803
89.7	505.7355	182.7	505.2871
89.72	505.8016	182.72	505.1307
89.74	505.9028	182.74	505.1207
89.76	505.8791	182.76	505.0429
89.78	505.7736	182.78	504.9710
89.8	505.7095	182.8	504.9844
89.82	505.6738	182.82	504.9913
89.84	505.6682	182.84	504.9763
89.86	505.6197	182.86	505.0663
89.88	505.6242	182.88	504.9706
89.9	505.5413	182.9	505.0246
89.92	505.5571	182.92	504.9440
89.94	505.4406	182.94	505.2510
89.96	505.4802	182.96	505.4070
89.98	505.7146	182.98	505.4034
90	505.6850	183	505.4679
90.02	505.5592	183.02	505.4262
90.04	505.5687	183.04	505.5839
90.06	505.4911	183.06	505.6005
90.08	505.4118	183.08	505.7155
90.1	505.4732	183.1	505.6108
90.12	505.5189	183.12	505.6096
90.14	505.6170	183.14	505.7344
90.16	505.8246	183.16	505.7436
90.18	505.8716	183.18	505.8831
90.2	505.7961	183.2	505.9765
90.22	505.7201	183.22	506.0271
90.24	505.6919	183.24	506.0272
90.26	505.8151	183.26	506.0985
90.28	505.8216	183.28	506.1161
90.3	505.7906	183.3	506.1458
90.32	505.7941	183.32	506.2164
90.34	505.6603	183.34	506.1943
90.36	505.5865	183.36	506.2448
90.38	505.4176	183.38	506.0839
90.4	505.5175	183.4	506.0062
90.42	505.5917	183.42	505.9362

Appendix F- Weld AT 7 data

90.44	505.5486	183.44	505.8508
90.46	505.4080	183.46	505.8514
90.48	505.3962	183.48	505.8196
90.5	505.3657	183.5	505.8731
90.52	505.4949	183.52	505.7876
90.54	505.4973	183.54	505.7015
90.56	505.3828	183.56	505.7641
90.58	505.6078	183.58	505.7033
90.6	505.4799	183.6	505.7161
90.62	505.3811	183.62	505.8249
90.64	505.3202	183.64	505.7963
90.66	505.3373	183.66	505.8447
90.68	505.2800	183.68	505.8228
90.7	505.4103	183.7	505.8528
90.72	505.3725	183.72	505.7855
90.74	505.3229	183.74	505.7563
90.76	505.3584	183.76	505.7106
90.78	505.4834	183.78	505.6208
90.8	505.4687	183.8	505.7148
90.82	505.4218	183.82	505.7042
90.84	505.3374	183.84	505.7771
90.86	505.4378	183.86	505.7084
90.88	505.4711	183.88	505.7048
90.9	505.5439	183.9	505.8013
90.92	505.6342	183.92	505.8196
90.94	505.4965	183.94	505.7637
90.96	505.4440	183.96	505.7677
90.98	505.5621	183.98	505.7828
91	505.7184	184	505.6948
91.02	505.6723	184.02	505.7237
91.04	505.6290	184.04	505.6311
91.06	505.5749	184.06	505.6680
91.08	505.6687	184.08	505.6029
91.1	505.6928	184.1	505.5971
91.12	505.6249	184.12	505.5901
91.14	505.6952	184.14	505.5502
91.16	505.6054	184.16	505.6139
91.18	505.6431	184.18	505.6237
91.2	505.6031	184.2	505.6151
91.22	505.6379	184.22	505.6942
91.24	505.5584	184.24	505.7404
91.26	505.4337	184.26	505.8236
91.28	505.5558	184.28	505.7165

Appendix F- Weld AT 7 data

91.3	505.6035	184.3	505.7857
91.32	505.6542	184.32	505.7530
91.34	505.4916	184.34	505.6167
91.36	505.4241	184.36	505.6219
91.38	505.3377	184.38	505.4807
91.4	505.2919	184.4	505.4843
91.42	505.3229	184.42	505.6173
91.44	505.3485	184.44	505.6312
91.46	505.4958	184.46	505.8109
91.48	505.3276	184.48	505.7310
91.5	505.3572	184.5	505.6393
91.52	505.4020	184.52	505.5864
91.54	505.2298	184.54	505.5407
91.56	505.3239	184.56	505.5401
91.58	505.3453	184.58	505.3859
91.6	505.5034	184.6	505.3241
91.62	505.4898	184.62	505.2589
91.64	505.4916	184.64	505.3285
91.66	505.3936	184.66	505.2900
91.68	505.3418	184.68	505.2762
91.7	505.3567	184.7	505.3402
91.72	505.2026	184.72	505.3580
91.74	505.1424	184.74	505.3478
91.76	505.0705	184.76	505.3671
91.78	505.2602	184.78	505.2766
91.8	505.1685	184.8	505.2940
91.82	505.1771	184.82	505.2357
91.84	505.1271	184.84	505.3491
91.86	505.0512	184.86	505.2524
91.88	505.1502	184.88	505.2303
91.9	505.2694	184.9	505.2172
91.92	505.2887	184.92	505.1949
91.94	505.3043	184.94	505.1549
91.96	505.4704	184.96	505.0862
91.98	505.3651	184.98	505.0732
92	505.3380	185	505.0332
92.02	505.3299	185.02	505.1308
92.04	505.4250	185.04	505.1800
92.06	505.2883	185.06	505.2572
92.08	505.2382	185.08	505.1465
92.1	505.4275	185.1	505.2501
92.12	505.4147	185.12	505.1442
92.14	505.4456	185.14	505.2300

Appendix F- Weld AT 7 data

92.16	505.4486	185.16	505.0798
92.18	505.4809	185.18	505.0994
92.2	505.3937	185.2	505.0297
92.22	505.4590	185.22	504.9878
92.24	505.2326	185.24	505.0215
92.26	505.1851	185.26	505.0020
92.28	505.1951	185.28	504.9228
92.3	505.2810	185.3	504.9626
92.32	505.2964	185.32	505.0032
92.34	505.2918	185.34	504.9177
92.36	505.0994	185.36	504.8932
92.38	505.0587	185.38	505.0071
92.4	504.9983	185.4	504.9594
92.42	504.9230	185.42	504.8533
92.44	504.9290	185.44	504.9170
92.46	504.9588	185.46	504.8330
92.48	505.0161	185.48	504.9642
92.5	505.0378	185.5	505.0565
92.52	505.0422	185.52	505.2729
92.54	505.0380	185.54	505.3632
92.56	505.2340	185.56	505.3619
92.58	505.1501	185.58	505.4438
92.6	505.0900	185.6	505.5956
92.62	505.0103	185.62	505.6570
92.64	505.0625	185.64	505.6489
92.66	505.1682	185.66	505.5863
92.68	505.0777	185.68	505.5884
92.7	505.1767	185.7	505.5889
92.72	505.2153	185.72	505.7372
92.74	505.4119	185.74	505.7138
92.76	505.4513	185.76	505.7629
92.78	505.5465	185.78	505.6325
92.8	505.6269	185.8	505.6690
92.82	505.6045	185.82	505.6712
92.84	505.5005	185.84	505.7942
92.86	505.3918	185.86	505.7257
92.88	505.5202	185.88	505.7541
92.9	505.4105	185.9	505.7634
92.92	505.3731	185.92	505.8832
92.94	505.3299	185.94	505.9021
92.96	505.2627	185.96	506.0140
92.98	505.2408	185.98	505.8557
93	505.1428	186	505.9977

Appendix F- Weld AT 7 data

93.02	505.2208	186.02	506.0382
93.04	505.2506	186.04	506.0021
93.06	505.2971	186.06	506.1257
93.08	505.2631	186.08	506.0152
93.1	505.3054	186.1	505.9965
93.12	505.3298	186.12	506.0857
93.14	505.4218	186.14	505.9959
93.16	505.4615	186.16	505.9792
93.18	505.3410	186.18	506.1324
93.2	505.4123	186.2	506.1275
93.22	505.3038	186.22	506.1467
93.24	505.3427	186.24	506.1772
93.26	505.3452	186.26	506.1117
93.28	505.4066	186.28	506.0236
93.3	505.4835	186.3	505.9887
93.32	505.3946	186.32	506.0178
93.34	505.4683	186.34	506.0622
93.36	505.3732	186.36	506.1246
93.38	505.4586	186.38	506.0050
93.4	505.4028	186.4	506.0595
93.42	505.4664	186.42	506.1007
93.44	505.3883	186.44	506.2129
93.46	505.4185	186.46	506.3976
93.48	505.4085	186.48	506.4007
93.5	505.5248	186.5	506.2902
93.52	505.3895	186.52	506.3214
93.54	505.4574	186.54	506.3374
93.56	505.4909	186.56	506.2842
93.58	505.4543	186.58	506.2536
93.6	505.4147	186.6	506.2094
93.62	505.3122	186.62	506.1171
93.64	505.3985	186.64	506.1819
93.66	505.3816	186.66	506.0574
93.68	505.5048	186.68	505.9872
93.7	505.3741	186.7	505.9523
93.72	505.4428	186.72	505.9099
93.74	505.4073	186.74	505.8006
93.76	505.4246	186.76	505.7220
93.78	505.3212	186.78	505.8902
93.8	505.4347	186.8	505.8718
93.82	505.4787	186.82	505.8193
93.84	505.5470	186.84	505.8122
93.86	505.5360	186.86	505.6673

Appendix F- Weld AT 7 data

93.88	505.6079	186.88	505.6029
93.9	505.6461	186.9	505.4502
93.92	505.6886	186.92	505.2472
93.94	505.5591	186.94	505.2702
93.96	505.5640	186.96	505.2604
93.98	505.6271	186.98	505.2674
94	505.7747	187	505.2065
94.02	505.7501		
94.04	505.7922		
94.06	505.5673		
94.08	505.4481		
94.1	505.4997		
94.12	505.5263		
94.14	505.4551		
94.16	505.5072		
94.18	505.4987		
94.2	505.5638		
94.22	505.7365		
94.24	505.7943		
94.26	505.8325		
94.28	505.8117		
94.3	505.6870		
94.32	505.6475		
94.34	505.6770		
94.36	505.6806		
94.38	505.7874		
94.4	505.7487		
94.42	505.7963		
94.44	505.8793		
94.46	505.5406		
94.48	505.4491		
94.5	505.5645		
94.52	505.5415		
94.54	505.5399		
94.56	505.4174		
94.58	505.4707		
94.6	505.3713		
94.62	505.3593		
94.64	505.2590		
94.66	505.2069		
94.68	505.2288		
94.7	505.2919		
94.72	505.3606		

Appendix F- Weld AT 7 data

94.74	505.3092		
94.76	505.3518		
94.78	505.3149		
94.8	505.4678		
94.82	505.3215		
94.84	505.3293		
94.86	505.3801		
94.88	505.4231		
94.9	505.4058		
94.92	505.2990		
94.94	505.3160		
94.96	505.3363		
94.98	505.5026		
95	505.6866		
95.02	505.6115		
95.04	505.6729		
95.06	505.6085		
95.08	505.6449		
95.1	505.7444		
95.12	505.7353		
95.14	505.7953		
95.16	505.8391		
95.18	505.7079		
95.2	505.7359		
95.22	505.6537		
95.24	505.5549		
95.26	505.6448		
95.28	505.5686		
95.3	505.6243		
95.32	505.5834		
95.34	505.6135		
95.36	505.7294		
95.38	505.8729		
95.4	505.9182		
95.42	505.9684		
95.44	505.8690		
95.46	505.9075		
95.48	505.8850		
95.5	505.8249		
95.52	505.7977		
95.54	505.8768		
95.56	505.9775		
95.58	505.9610		

Appendix F- Weld AT 7 data

95.6	505.9433		
95.62	505.8779		
95.64	505.8322		
95.66	505.8441		
95.68	505.8565		
95.7	505.8326		
95.72	505.9270		
95.74	505.9429		
95.76	505.8389		
95.78	505.8689		
95.8	505.8891		
95.82	505.9669		
95.84	506.0810		
95.86	506.0425		
95.88	505.9041		
95.9	506.0606		
95.92	505.8086		
95.94	505.7612		
95.96	505.9294		
95.98	505.8874		
96	505.9131		
96.02	506.1279		
96.04	506.0956		
96.06	506.1496		
96.08	505.9029		
96.1	505.9749		
96.12	505.7424		
96.14	505.6687		
96.16	505.7211		
96.18	505.7288		
96.2	505.8027		
96.22	505.7212		
96.24	505.7067		
96.26	505.6991		
96.28	505.8095		
96.3	505.8046		
96.32	505.6553		
96.34	505.6418		
96.36	505.5508		
96.38	505.4693		
96.4	505.5052		
96.42	505.6086		
96.44	505.7008		

Appendix F- Weld AT 7 data

96.46	505.5576		
96.48	505.4653		
96.5	505.4570		
96.52	505.3074		
96.54	505.2735		
96.56	505.4132		
96.58	505.4954		
96.6	505.3764		
96.62	505.2529		
96.64	505.2283		
96.66	505.2732		
96.68	505.2974		
96.7	505.3279		
96.72	505.2870		
96.74	505.3822		
96.76	505.3153		
96.78	505.2062		
96.8	505.3282		
96.82	505.3421		
96.84	505.5006		
96.86	505.5348		
96.88	505.5097		
96.9	505.4139		
96.92	505.3502		
96.94	505.4518		
96.96	505.3868		
96.98	505.4186		
97	505.4600		
97.02	505.3397		
97.04	505.3848		
97.06	505.3385		
97.08	505.1214		
97.1	505.2530		
97.12	505.2837		
97.14	505.3744		
97.16	505.5292		
97.18	505.3485		
97.2	505.4758		
97.22	505.5506		
97.24	505.4605		
97.26	505.4871		
97.28	505.4501		
97.3	505.3735		

Appendix F- Weld AT 7 data

97.32	505.2957		
97.34	505.3364		
97.36	505.3780		
97.38	505.3685		
97.4	505.2536		
97.42	505.2940		
97.44	505.3361		
97.46	505.3104		
97.48	505.3562		
97.5	505.4622		
97.52	505.6121		
97.54	505.6444		
97.56	505.7096		
97.58	505.6288		
97.6	505.6129		
97.62	505.5576		
97.64	505.5417		
97.66	505.5595		
97.68	505.6712		
97.7	505.7490		
97.72	505.6965		
97.74	505.7109		
97.76	505.6958		
97.78	505.7354		
97.8	505.4799		
97.82	505.5351		
97.84	505.6600		
97.86	505.8134		
97.88	505.7407		
97.9	505.7413		
97.92	505.7613		
97.94	505.9338		
97.96	505.9722		
97.98	505.7316		
98	505.6489		
98.02	505.7025		
98.04	505.8939		
98.06	505.8877		
98.08	506.0452		
98.1	506.1126		
98.12	506.0312		
98.14	505.9034		
98.16	505.7572		

Appendix F- Weld AT 7 data

98.18	505.6248		
98.2	505.5996		
98.22	505.6629		
98.24	505.7117		
98.26	505.8248		
98.28	505.7434		
98.3	505.6654		
98.32	505.7541		
98.34	505.6766		
98.36	505.6369		
98.38	505.5003		
98.4	505.5082		
98.42	505.5169		
98.44	505.6287		
98.46	505.6761		
98.48	505.5433		
98.5	505.5803		
98.52	505.4863		
98.54	505.4149		
98.56	505.3743		
98.58	505.4714		
98.6	505.3341		
98.62	505.2233		
98.64	505.3037		
98.66	505.2504		
98.68	505.2543		
98.7	505.3194		
98.72	505.3438		
98.74	505.3958		
98.76	505.2748		
98.78	505.3253		
98.8	505.2641		
98.82	505.2944		
98.84	505.3968		
98.86	505.4497		
98.88	505.4772		
98.9	505.4916		
98.92	505.5445		
98.94	505.5036		
98.96	505.3252		
98.98	505.3435		
99	505.3796		
99.02	505.3101		

Appendix F- Weld AT 7 data

99.04	505.2321		
99.06	505.1502		
99.08	505.1210		
99.1	505.1436		
99.12	505.1076		
99.14	505.0218		
99.16	505.0581		
99.18	505.1300		
99.2	505.1906		
99.22	505.1187		
99.24	505.1020		
99.26	505.1151		
99.28	505.1121		
99.3	505.0807		
99.32	505.0225		
99.34	505.0146		
99.36	505.1153		
99.38	505.1621		
99.4	505.2080		
99.42	505.1290		
99.44	505.1589		
99.46	505.0644		
99.48	505.1941		
99.5	505.1895		
99.52	505.2504		
99.54	505.4371		
99.56	505.4458		
99.58	505.4788		
99.6	505.5506		
99.62	505.5827		
99.64	505.5307		
99.66	505.6910		
99.68	505.6889		
99.7	505.7156		
99.72	505.6129		
99.74	505.6065		
99.76	505.6928		
99.78	505.6923		
99.8	505.6805		
99.82	505.4715		
99.84	505.5928		
99.86	505.4147		
99.88	505.4184		

Appendix F- Weld AT 7 data

99.9	505.4160		
99.92	505.4294		
99.94	505.4281		
99.96	505.4460		
99.98	505.5851		
100	505.5222		

Appendix G- Weld AT 7 control data

Weld AT_7 control data				
time	Error	Proportional	Integral	Derivative
145	-0.209297829	-7.974247282	-77.51202686	-744.7299345
145.02	-0.195362155	-7.443298098	-77.61429075	43.96846569
145.04	0.054693154	2.083809173	-77.64164141	22.82852918
145.06	0.084432622	3.216882896	-77.62047917	27.74369669
145.08	0.03042704	1.159270224	-77.60618563	29.46189609
145.1	0.055476033	2.11363687	-77.60854255	-651.005971
145.12	-0.005938994	-0.226275684	-77.60114914	165.1760844
145.14	-0.117756535	-4.48652399	-77.64014694	290.1891286
145.16	-0.235592413	-8.976070924	-77.71049024	536.2552022
145.18	-0.495768065	-18.88876326	-77.90437087	-390.0417655
145.2	-0.440249792	-16.77351709	-78.11738189	718.0757328
145.22	-0.235462059	-8.971104435	-78.26161222	-383.5979499
145.24	-0.136298411	-5.192969446	-78.36122699	-570.9418116
145.26	-0.050518967	-1.924772639	-78.41474566	-62.57417464
145.28	-0.027406962	-1.04420524	-78.40451387	160.3911832
145.3	-0.014260929	-0.543341395	-78.42947947	-508.3646151
145.32	-0.081256285	-3.095864444	-78.4646832	29.46391926
145.34	-0.10159715	-3.870851417	-78.53325747	-317.0417726
145.36	-0.215097308	-8.195207447	-78.61696692	574.7840468
145.38	-0.229833482	-8.756655651	-78.72330866	-196.0744483
145.4	-0.385109003	-14.67265302	-78.87298006	57.36724361
145.42	-0.32137258	-12.24429529	-79.03499978	448.1142828
145.44	-0.33283831	-12.68113961	-79.18943429	-152.5486202
145.46	-0.229425807	-8.741123257	-79.3365239	-116.7859997
145.48	-0.309942189	-11.80879741	-79.47107941	9.259494926
145.5	-0.179979717	-6.8572272	-79.60350093	-277.333119
145.52	-0.205311887	-7.822382876	-79.68855924	277.4157128
145.54	-0.181954959	-6.93248394	-79.78330322	-13.02595106
145.56	-0.278495229	-10.61066823	-79.89012999	-32.88907374
145.58	-0.308459928	-11.75232327	-80.02561289	-44.96454301
145.6	-0.243525324	-9.278314849	-80.14664813	-291.8143417
145.62	-0.180513394	-6.877560306	-80.25391156	-700.6799952
145.64	-0.132409688	-5.044809117	-80.32779747	623.0813203
145.66	-0.011832391	-0.4508141	-80.3860564	-252.9306891
145.68	-0.026624136	-1.014379568	-80.40611959	-163.0332609
145.7	0.041588478	1.584521009	-80.38447481	-151.2300936
145.72	0.042645179	1.624781314	-80.37271855	-338.0954863
145.74	0.044462575	1.694024122	-80.35983204	-172.3468942
145.76	0.056411091	2.149262581	-80.34109604	-397.9681861
145.78	0.079758661	3.038804979	-80.31049	-46.51107528

Appendix G- Weld AT 7 control data

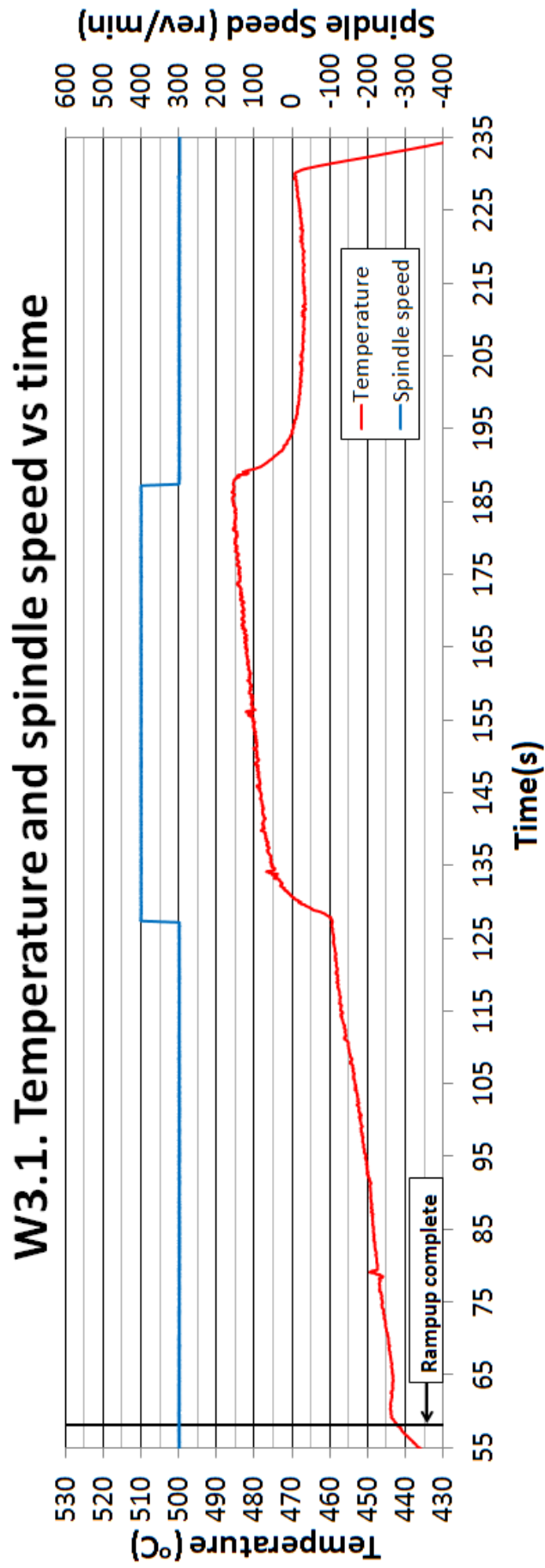
145.8	0.125282985	4.773281715	-80.25760203	-251.1008652
145.82	0.087490181	3.333375906	-80.19360801	709.0521933
145.84	0.211638557	8.063429037	-80.11790728	102.7578924
145.86	0.278415159	10.60761755	-80.01330618	-84.65330304
145.88	0.157752293	6.010362358	-79.89642755	51.96576369
145.9	0.077651097	2.958506805	-79.85990782	50.0215473
145.92	0.146532306	5.58288086	-79.83204896	-694.6924523
145.94	0.16781523	6.393760267	-79.76859868	-577.9243481
145.96	0.090027925	3.430063947	-79.70929461	-688.3669374
145.98	0.053395075	2.034352345	-79.70083822	-164.4405882
146	0.085096043	3.242159252	-79.67285395	930.4936173
146.02	-0.083921137	-3.197395337	-79.66851174	851.4191484
146.04	-0.081126904	-3.090935051	-79.70610822	-72.43874341
146.06	0.033533401	1.277622591	-79.71540053	6.362761026
146.08	-0.106790471	-4.068716943	-79.73453012	-53.96888621
146.1	-0.122919277	-4.683224447	-79.77140217	780.2984872
146.12	-0.175363583	-6.681352528	-79.81626753	953.3307014
146.14	-0.18465081	-7.035195861	-79.88749036	932.254277
146.16	-0.041380661	-1.576603186	-79.95510123	-13.85497117
146.18	-0.123006792	-4.686558783	-79.97169492	-73.96912145
146.2	-0.317744797	-12.10607678	-80.06160224	971.5294168
146.22	-0.197648366	-7.530402735	-80.18029854	-98.77041059
146.24	-0.289800533	-11.04140029	-80.28625674	153.4714166
146.26	-0.279814907	-10.66094796	-80.41889257	-37.80840832
146.28	-0.145989363	-5.562194745	-80.51465361	-160.471528
146.3	-0.024452636	-0.931645434	-80.57151988	-288.8447719
146.32	-0.006014549	-0.229154322	-80.59579719	-340.1730711
146.34	-0.196603791	-7.49060442	-80.64484918	-18.41519738
146.36	-0.222208759	-8.466153728	-80.72975227	716.6195388
146.38	-0.052388841	-1.996014833	-80.80094624	-93.86518018
146.4	-0.005210137	-0.198506207	-80.81303344	-67.02707286
146.42	-0.001956056	-0.074525735	-80.822266	-456.6882256
146.44	-0.068306063	-2.602460998	-80.85533799	193.9778442
146.46	0.000112291	0.004278279	-80.9052371	2.510288682
146.48	-0.038073425	-1.450597478	-80.89190983	223.532149
146.5	-6.64194E-05	-0.00253058	-80.88436167	-34.84854512
146.52	-0.028849442	-1.09916375	-80.89291681	45.46738497
146.54	-0.006659331	-0.253720523	-80.92212944	-538.2369686
146.56	0.107727452	4.104415921	-80.90327896	15.50531859
146.58	0.027591095	1.051220712	-80.88322466	105.7098623
146.6	-0.010444388	-0.397931183	-80.87341452	343.7370856
146.62	-0.031466789	-1.198884676	-80.87540918	-77.57198094
146.64	0.048405482	1.844248866	-80.86903334	-266.2065381

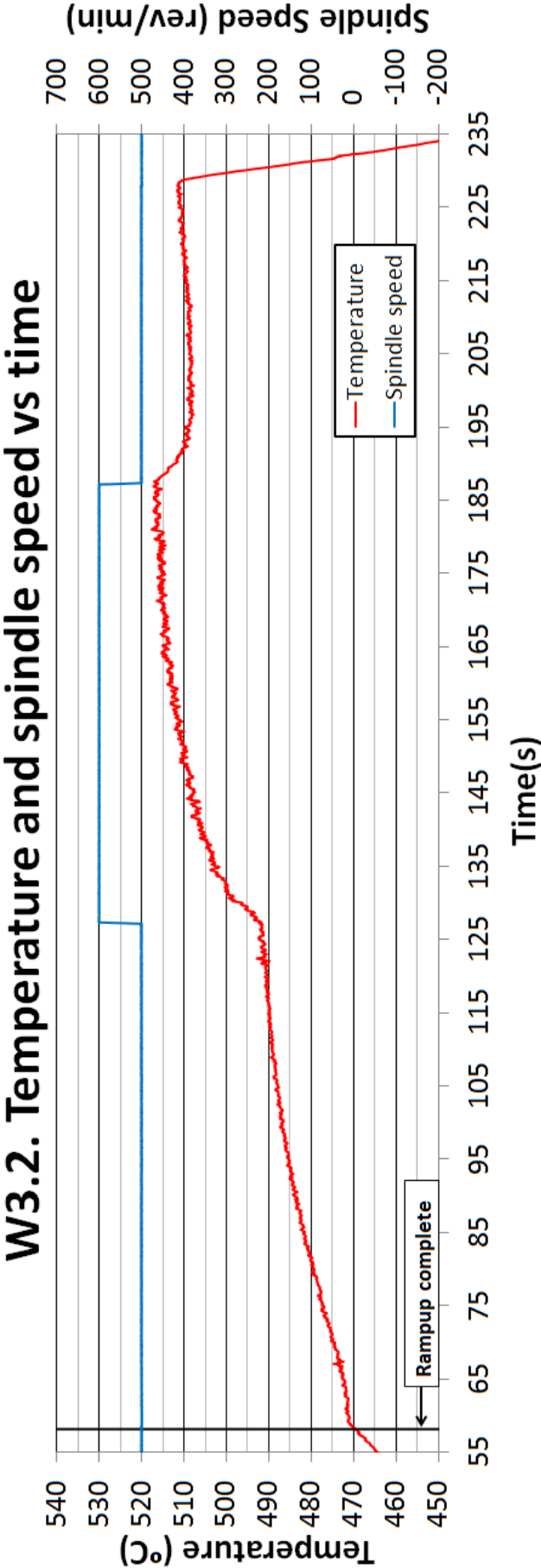
Appendix G- Weld AT 7 control data

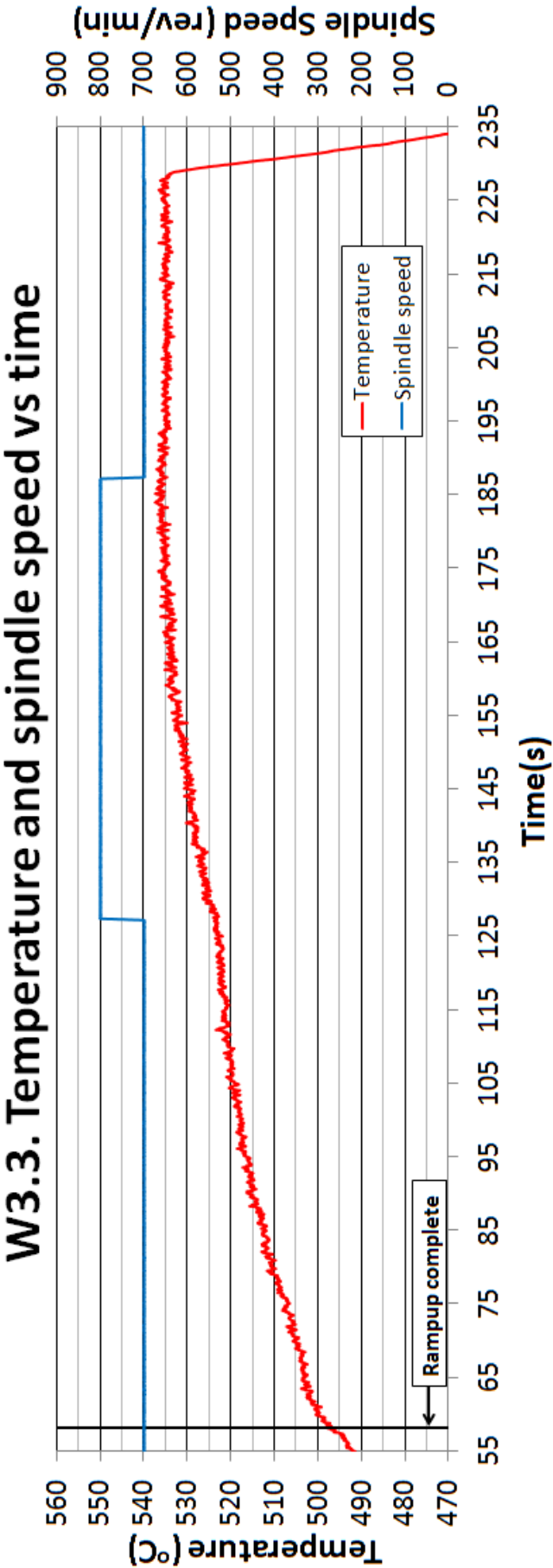
146.66	-0.048279059	-1.839432161	-80.87623164	-62.33895573
146.68	-0.102875276	-3.919548008	-80.90362215	-62.36934023
146.7	-0.008133495	-0.309886162	-80.91203772	27.86690911
146.72	-0.074856123	-2.852018273	-80.95080347	31.31466998
146.74	-0.221733746	-8.448055713	-81.02484093	-82.65500364
146.76	0.042928512	1.635576321	-81.03740587	-19.15315961
146.78	-0.020436054	-0.778613664	-81.01958442	445.3526726
146.8	-0.149175992	-5.683605308	-81.06329562	-20.13018478
146.82	-0.095712985	-3.646664735	-81.10428522	-5.381264236
146.84	-0.245871768	-9.367714364	-81.19493721	1013.541252
146.86	-0.286156089	-10.90254698	-81.32560512	153.445003
146.88	-0.373066247	-14.21382402	-81.48259195	-22.15432962
146.9	-0.547382421	-20.85527023	-81.67384934	461.9675745
146.92	-0.592436888	-22.57184543	-81.9380889	11.12170539
146.94	-0.535569076	-20.40518181	-82.2102473	-38.61685792
146.96	-0.51590496	-19.65597899	-82.45204903	70.79728222
146.98	-0.421820658	-16.07136707	-82.65822549	-256.346258
147	-0.415711178	-15.83859587	-82.86618455	-296.9715257
147.02	-0.405905014	-15.46498102	-83.08284238	103.3340606
147.04	-0.558975569	-21.29696917	-83.29902789	47.04920697
147.06	-0.492180238	-18.75206706	-83.52957117	-3.973665453
147.08	-0.257440028	-9.80846507	-83.71410754	-397.5099123
147.1	-0.343606433	-13.0914051	-83.85507958	-92.5559533
147.12	-0.342388523	-13.04500274	-84.01989193	-311.7865398
147.14	-0.25429273	-9.688553024	-84.16379229	-53.96979774
147.16	-0.094425517	-3.597612208	-84.23273815	-247.7834127
147.18	-0.143844324	-5.48046875	-84.30565147	-456.4522174
147.2	-0.195325523	-7.441902441	-84.36908796	-65.09010316
147.22	-0.238135823	-9.072974859	-84.48042736	-366.9052835
147.24	-0.373787199	-14.24129228	-84.65729523	-329.6913554
147.26	-0.352326227	-13.42362926	-84.84832689	-26.9281884
147.28	-0.178042489	-6.78341882	-84.97188193	-481.3459295
147.3	-0.227525974	-8.66873962	-85.05048358	-78.50395909
147.32	-0.256322585	-9.765890477	-85.17484389	-340.918057
147.34	-0.290665911	-11.0743712	-85.28907232	-5.660234989
147.36	-0.38715614	-14.75064894	-85.46951015	-56.16407177
147.38	-0.313890861	-11.95924181	-85.64251482	-24.02897315
147.4	-0.401752994	-15.30678907	-85.82670753	84.92968029
147.42	-0.327072912	-12.46147794	-85.99939109	-94.98502987
147.44	-0.390559955	-14.88033429	-86.15601056	380.5123736
147.46	-0.467593276	-17.81530381	-86.37201213	-68.37059107
147.48	-0.526456089	-20.057977	-86.61422312	122.2487982
147.5	-0.337127736	-12.84456675	-86.82428473	-287.3555406

Appendix G- Weld AT 7 control data

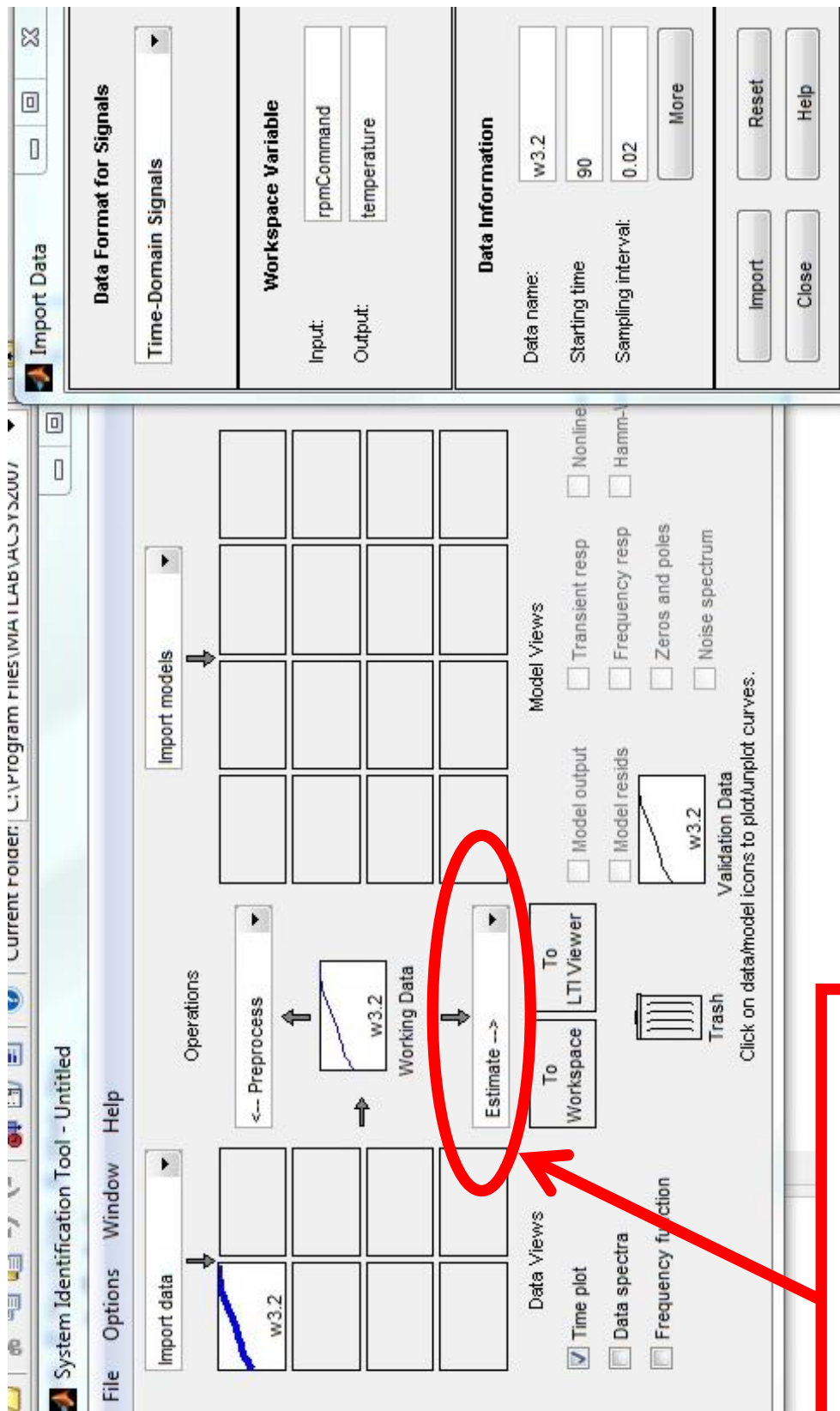
147.52	-0.308076782	-11.73772539	-86.96576719	273.8055596
147.54	-0.075147218	-2.863108995	-87.04699724	175.2672164
147.56	-0.089182534	-3.397854564	-87.08392843	66.08131344
147.58	-0.046879259	-1.78609977	-87.12421003	133.7372245
147.6	0.023570511	0.898036463	-87.12316096	55.2143542
147.62	0.076023586	2.896498618	-87.11650996	-189.9243968
147.64	-0.001326548	-0.05054147	-87.08062331	56.81694946
147.66	0.131627259	5.01499858	-87.06482313	-90.32969855
147.68	0.106074255	4.041429112	-86.99775141	60.59130539
147.7	-0.041510045	-1.581532712	-87.00149975	-377.709243
147.72	-0.052077727	-1.984161401	-87.0446439	-393.0882965
147.74	0.069671396	2.654480189	-87.03898093	-236.2319811
147.76	0.18761249	7.14803585	-86.98128328	-44.46918117
147.78	0.14932102	5.689130857	-86.89883759	1.462570454
147.8	-0.013334089	-0.508028808	-86.88659078	-385.1280575
147.82	0.064885938	2.472154251	-86.88192416	47.92932817
147.84	-0.041118347	-1.566609007	-86.90053156	-8.130873702
147.86	-0.110524578	-4.210986416	-86.94490685	-119.8742138
147.88	-0.054346086	-2.070585863	-86.96113686	103.650414
147.9	-0.004962396	-0.189067272	-86.95505057	353.7512809
147.92	-0.104351824	-3.975804485	-86.97754254	-21.59111553
147.94	0.115624944	4.405310381	-86.98570578	-225.7089597
147.96	0.188229772	7.171554295	-86.90577025	8.111875297
147.98	0.08660872	3.29979223	-86.83491628	-19.69596134
148	0.264836948	10.09028772	-86.76333474	132.9169578







Appendix I- Matlab System Modelling



Controller Design Tool © 2002-2008 Farid Golnaraghi

Time Response Frequency Response Controller Design Tool Calculator Unit Conversion Help

Block Diagram

Closed Loop Transfer Function:

$$\frac{Y}{R} = \frac{0.5}{1}$$

TF Zeros are: TF Poles are:

Transfer Functions

Click on blocks to change transfer functions

$F = 1$

$G(s) = \frac{1}{1}$

$C(s) = \frac{1}{1}$

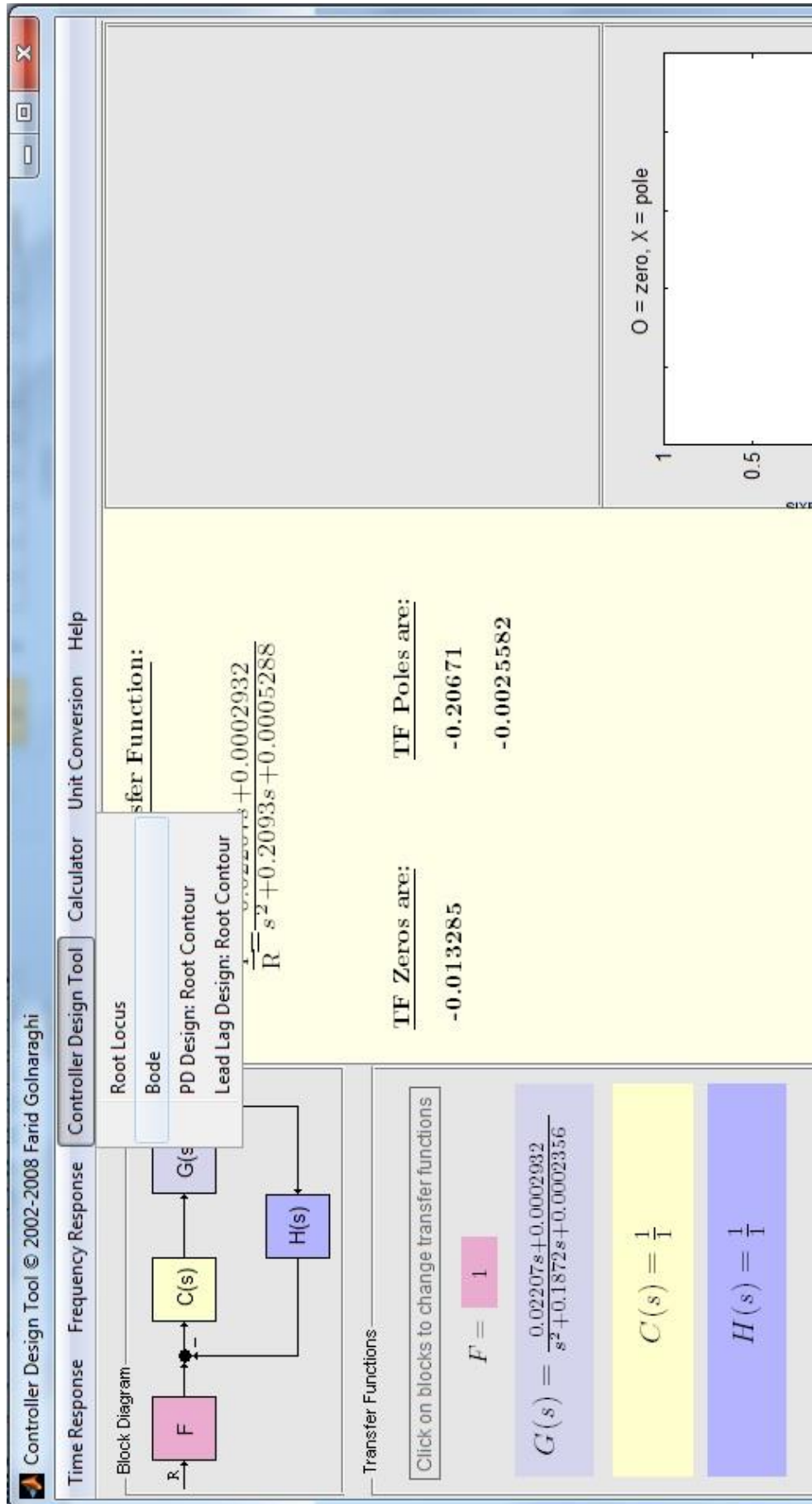
$H(s) = \frac{1}{1}$

G(s) = /

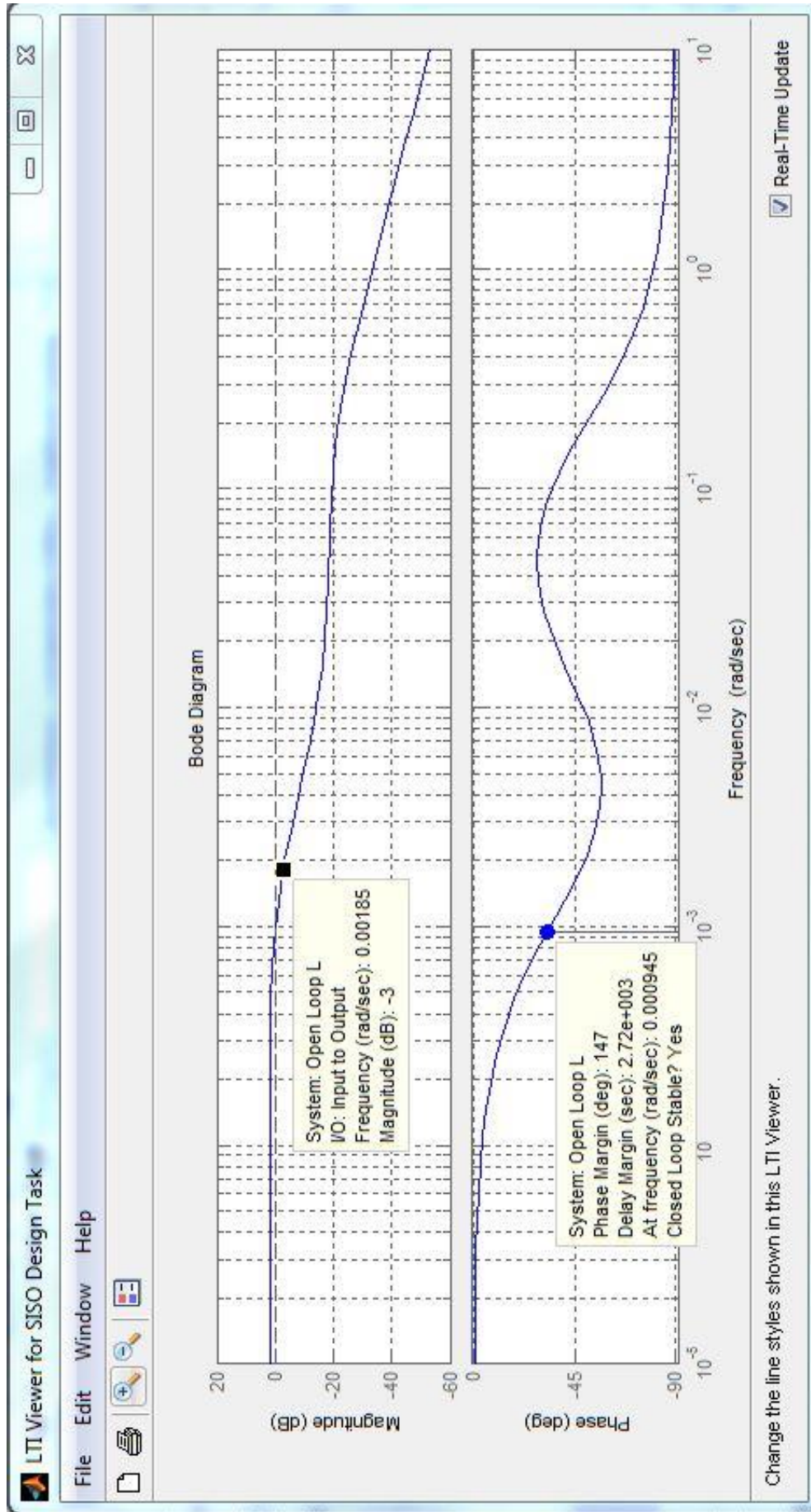
Enter coefficients of the polynomials
eg. for $s^3 + 3s - 7$
enter 1 0 3 -7

O = zero, X = pole

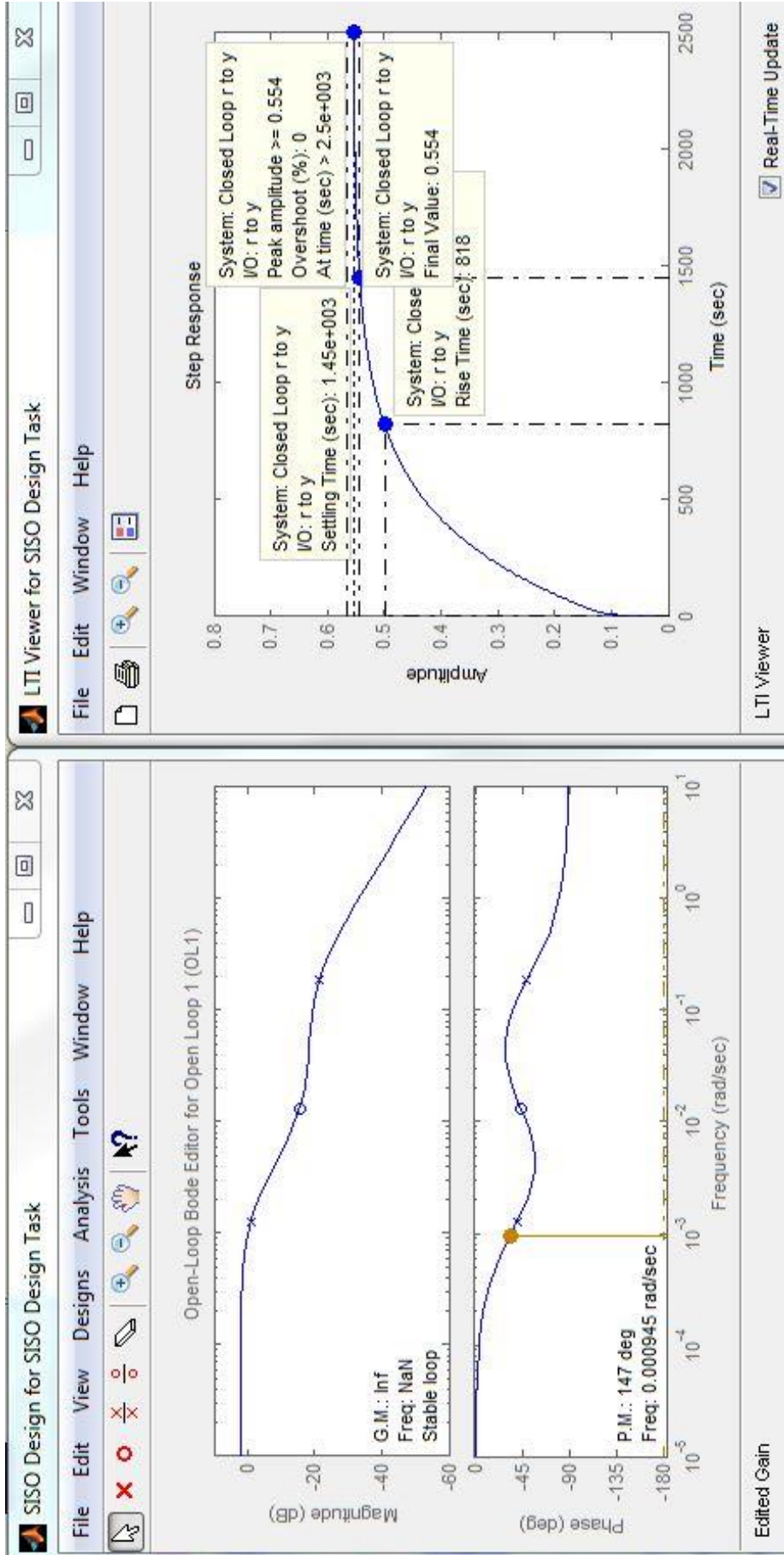
Appendix J- Matlab ACSYS PID bode design



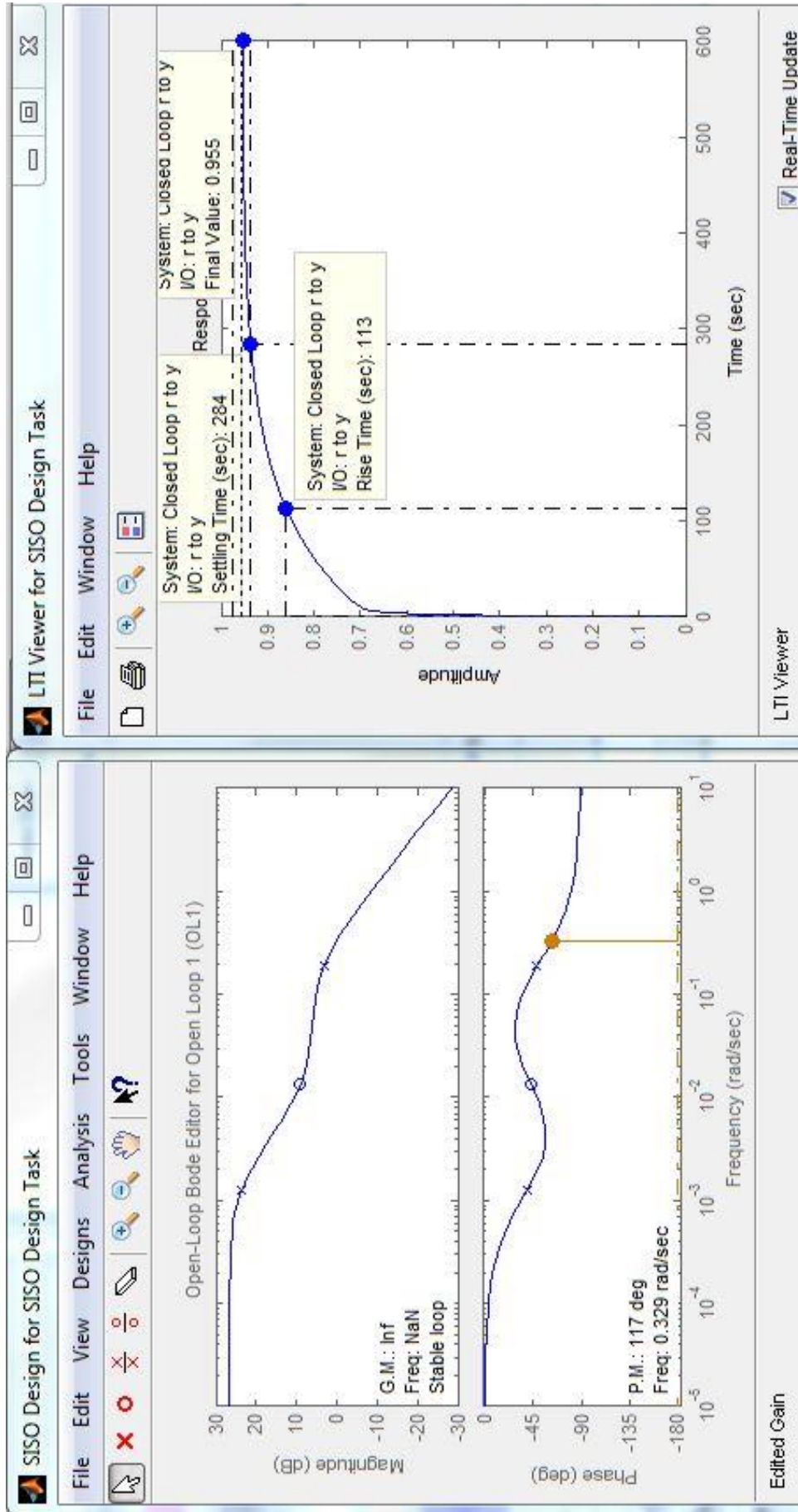
Appendix J- Matlab ACSYS PID bode design



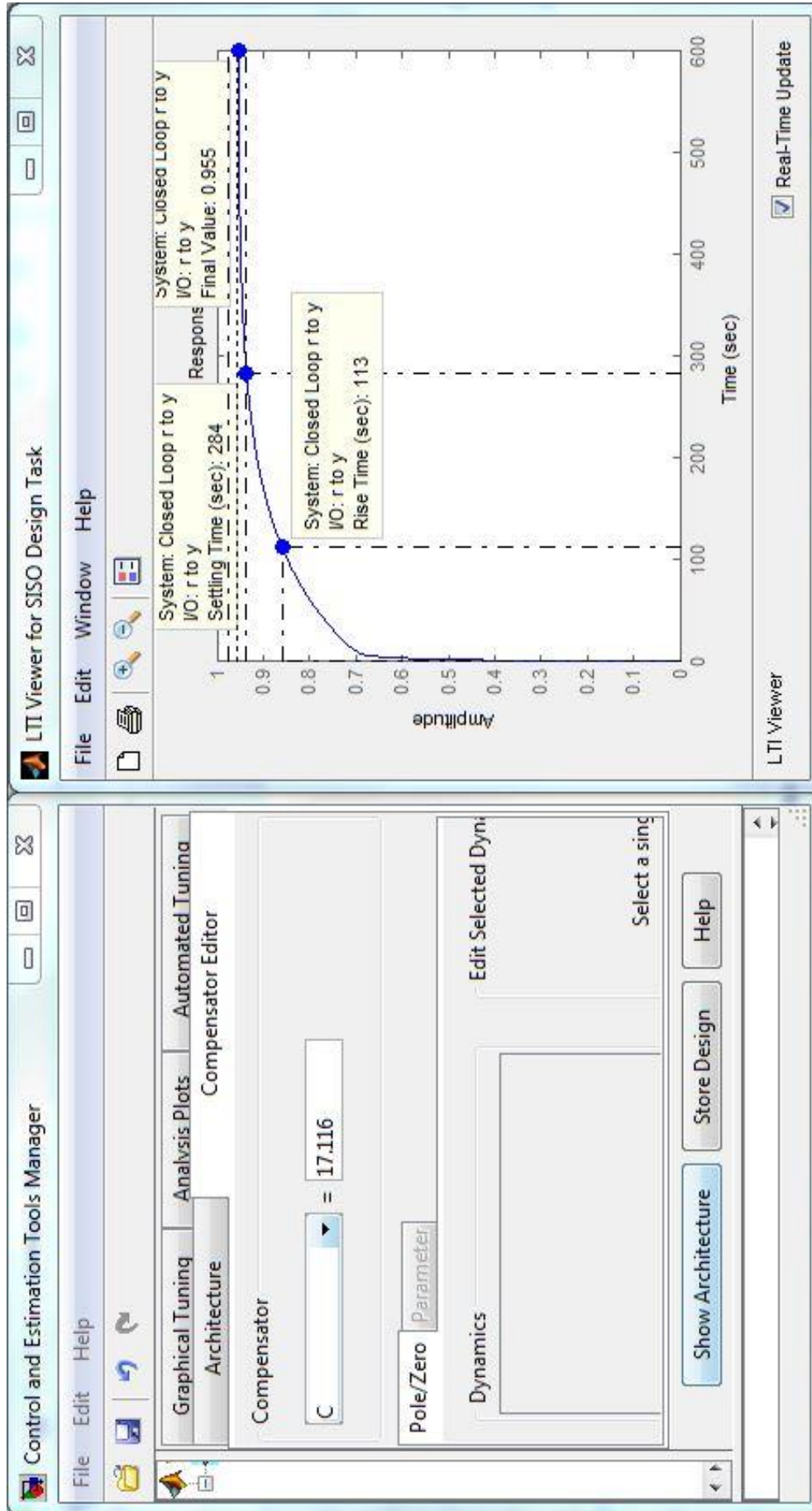
Appendix J- Matlab ACSYS PID bode design



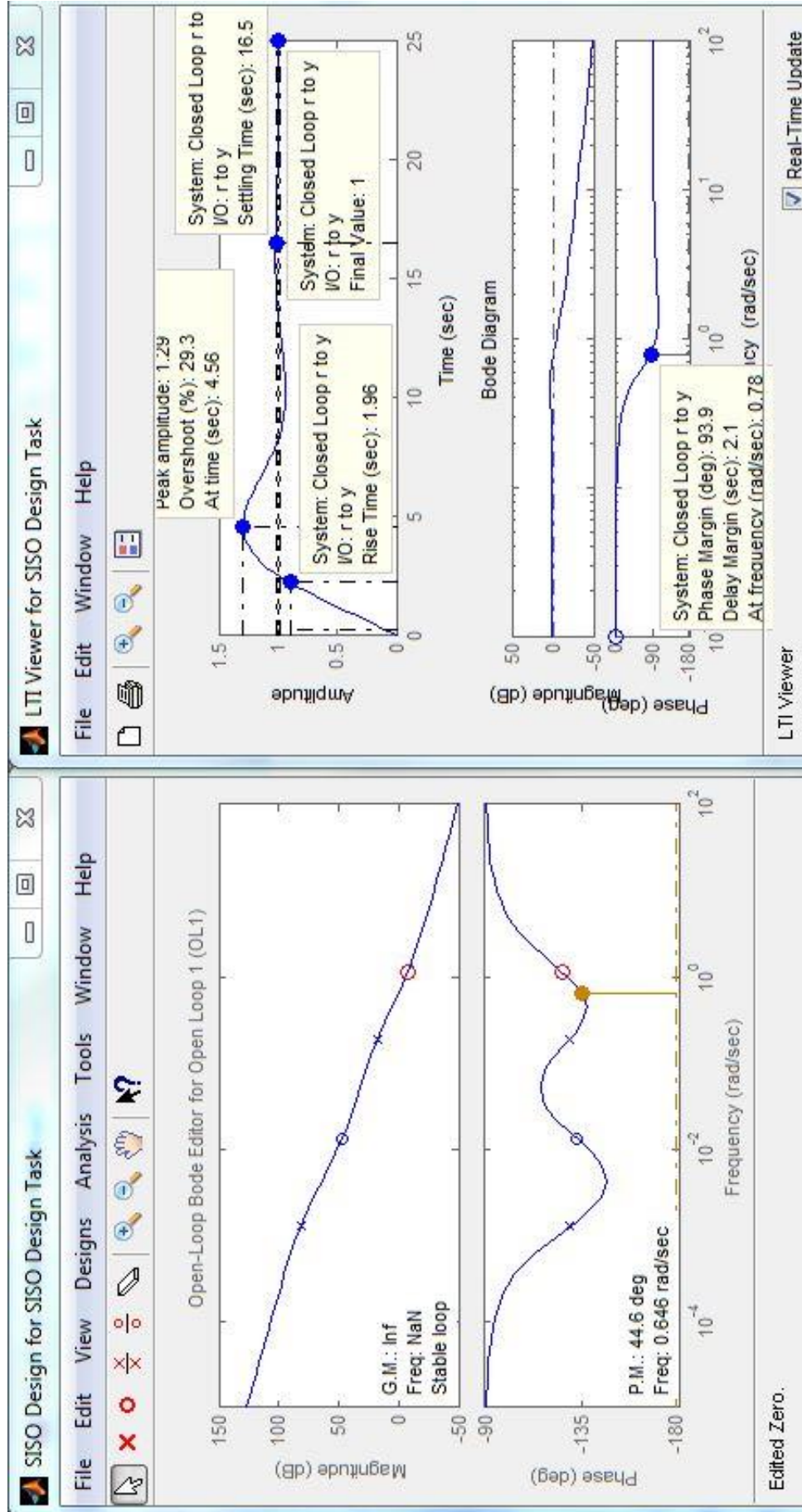
Appendix J- Matlab ACSYS PID bode design



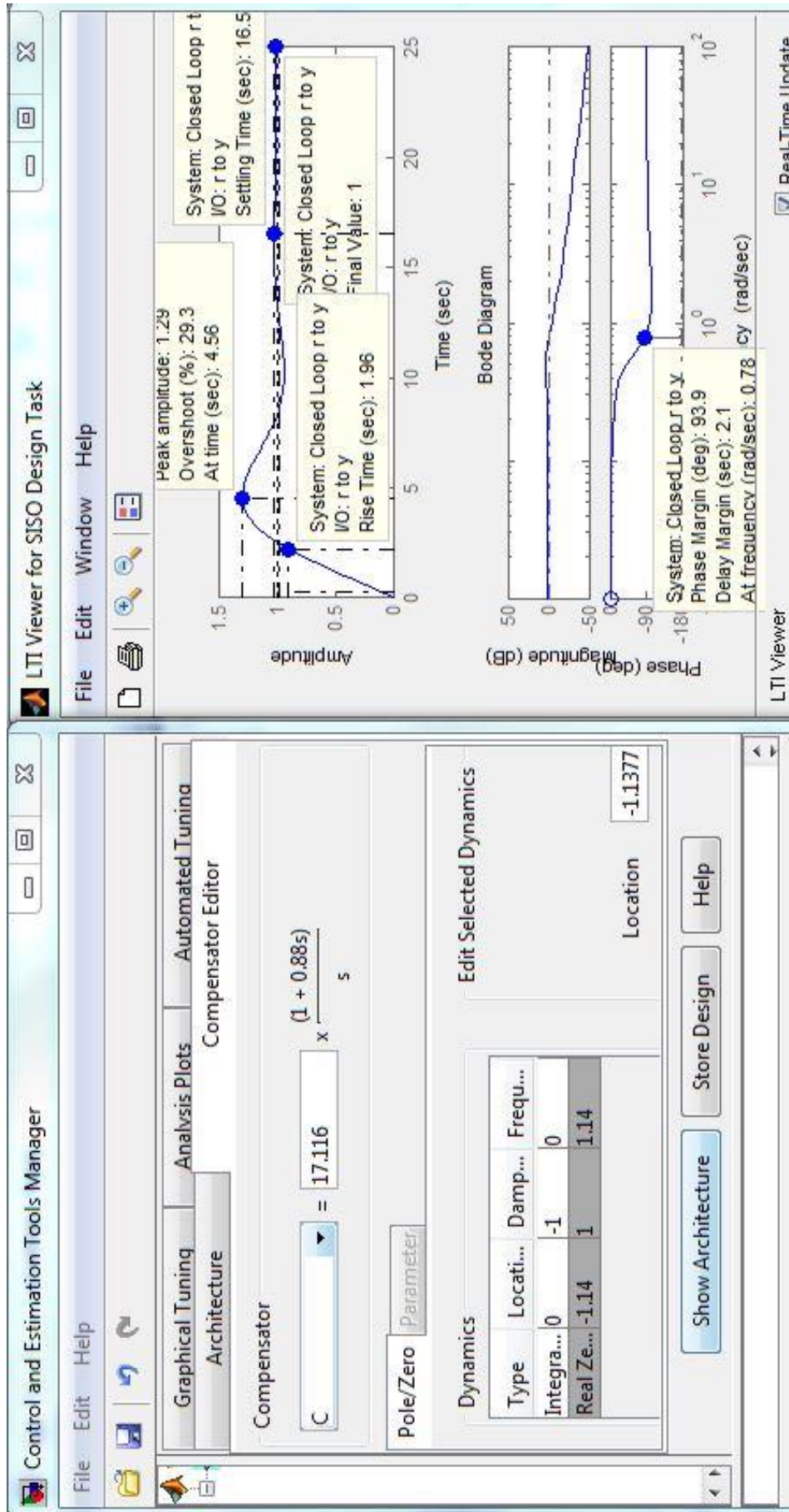
Appendix J- Matlab ACSYS PID bode design



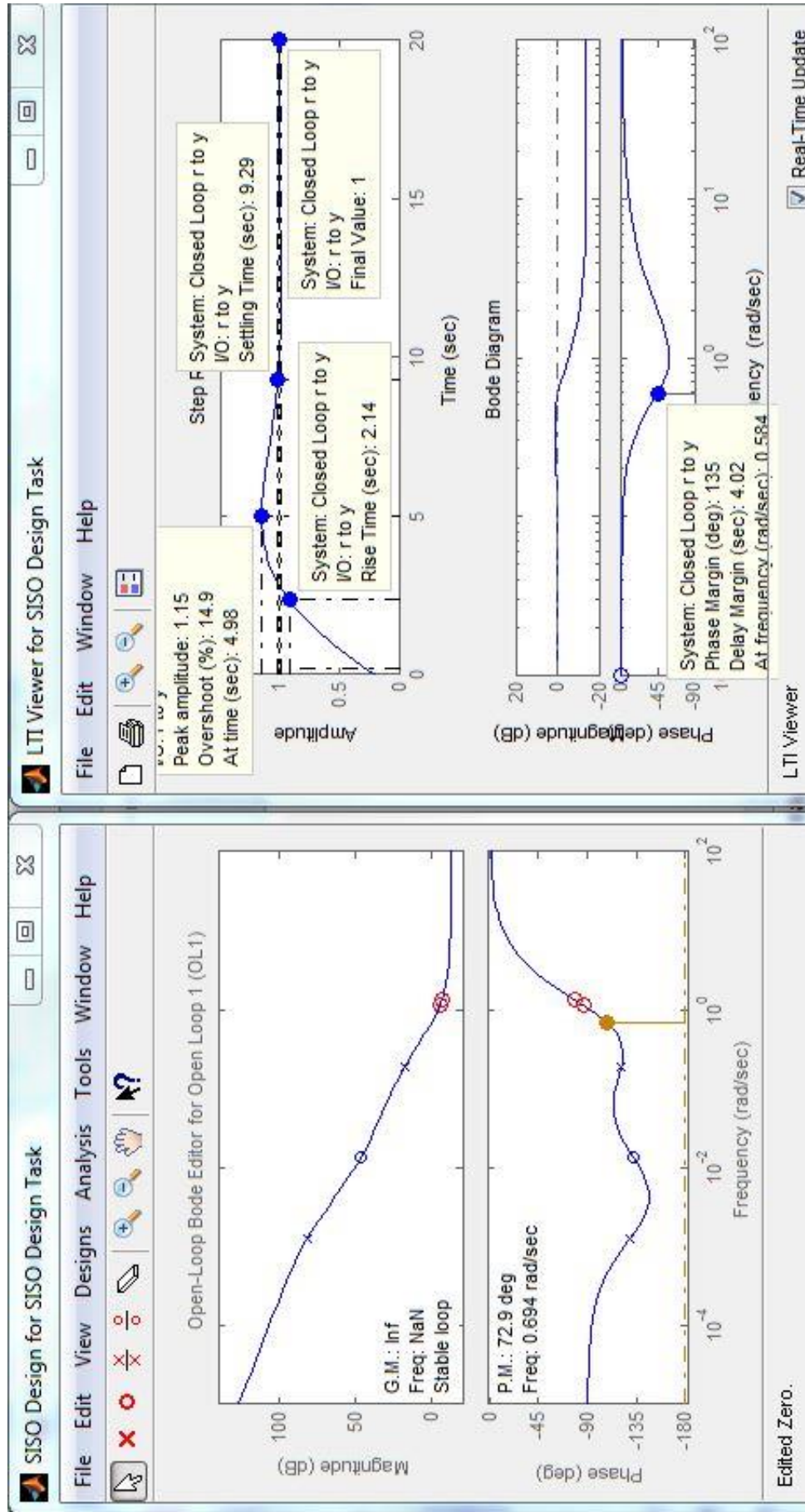
Appendix J- Matlab ACSYS PID bode design



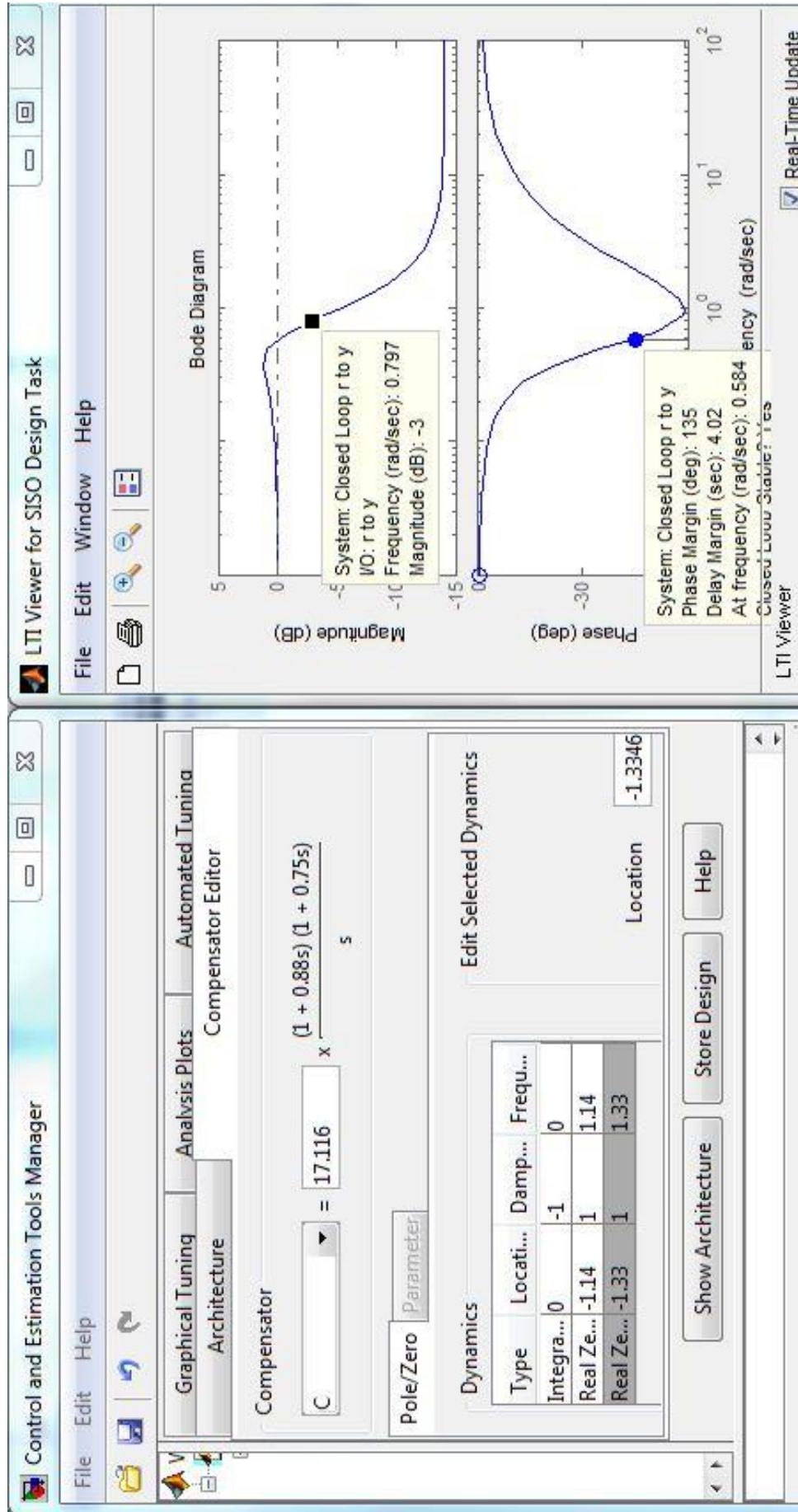
Appendix J- Matlab ACSYS PID bode design



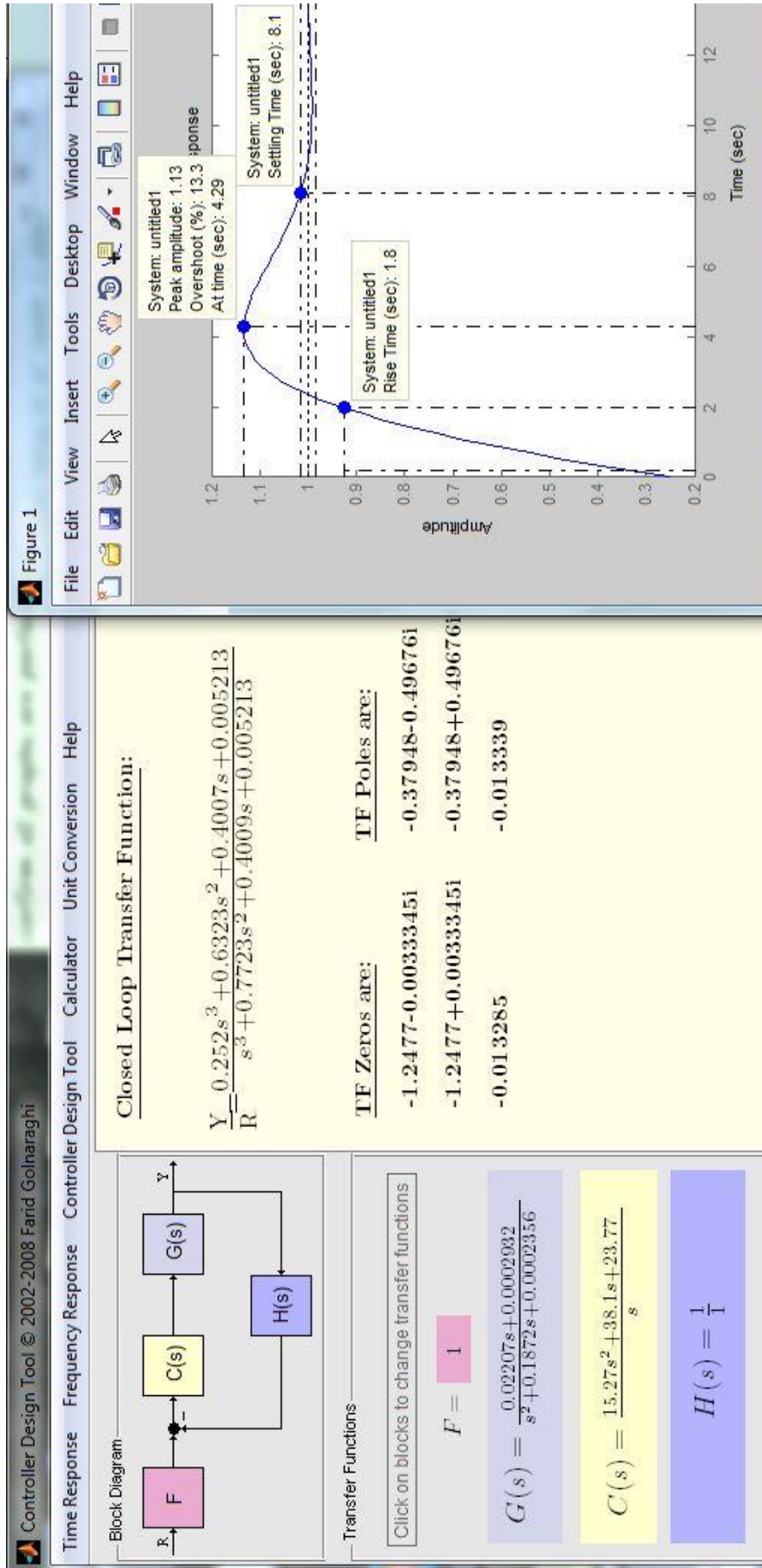
Appendix J- Matlab ACSYS PID bode design



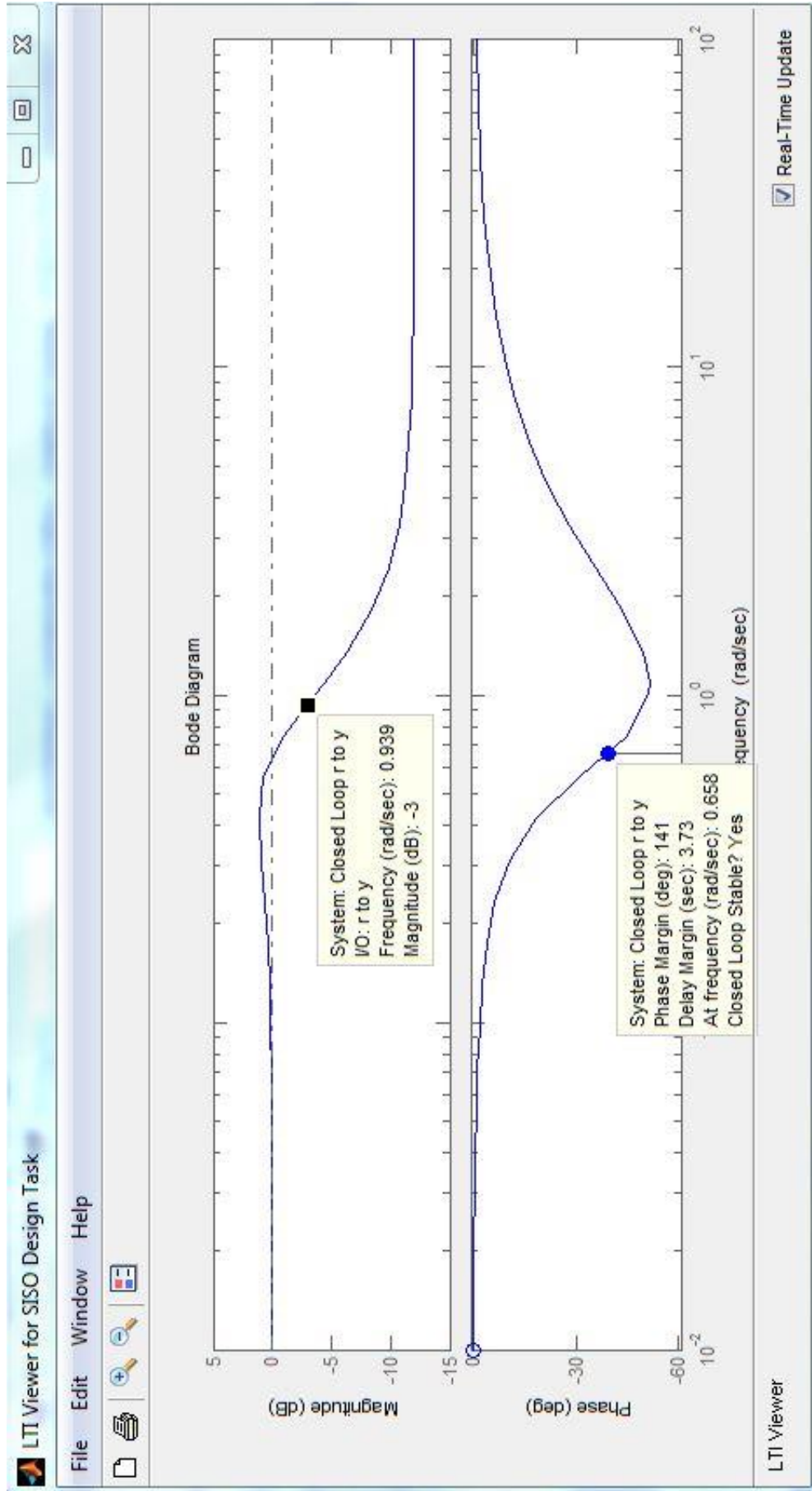
Appendix J- Matlab ACSYS PID bode design



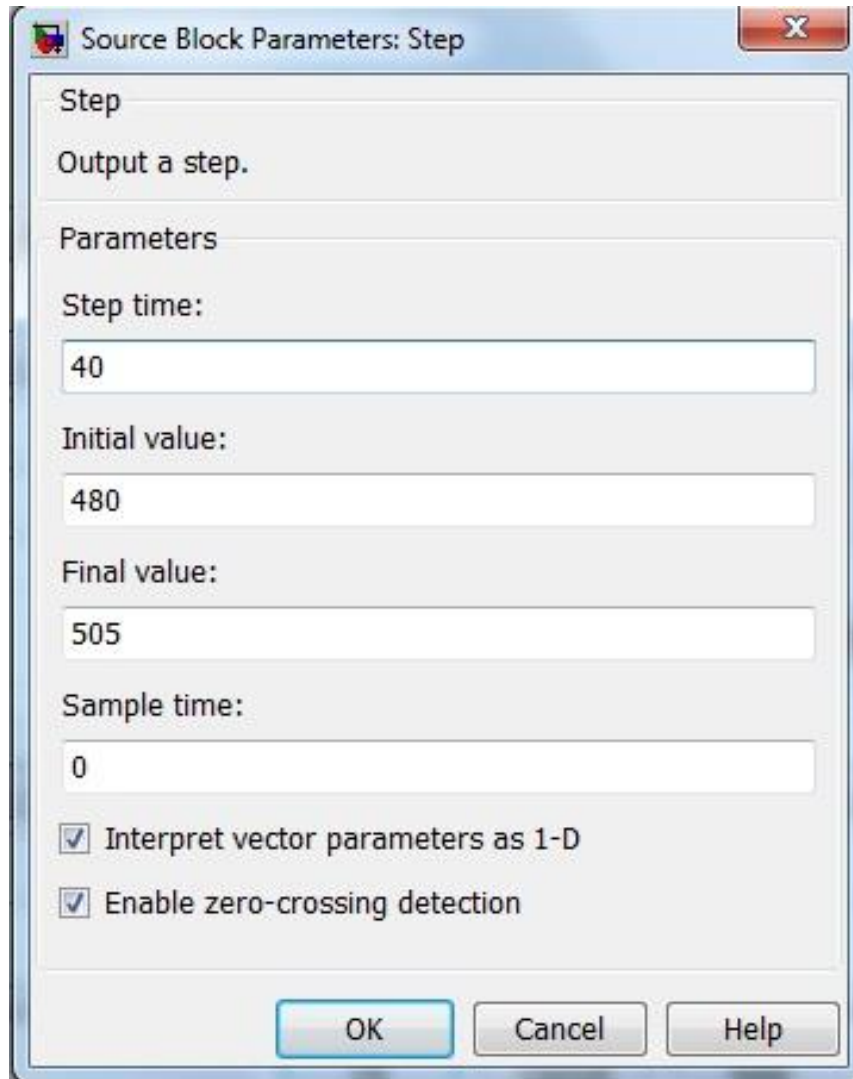
Appendix J- Matlab ACSYS PID bode design



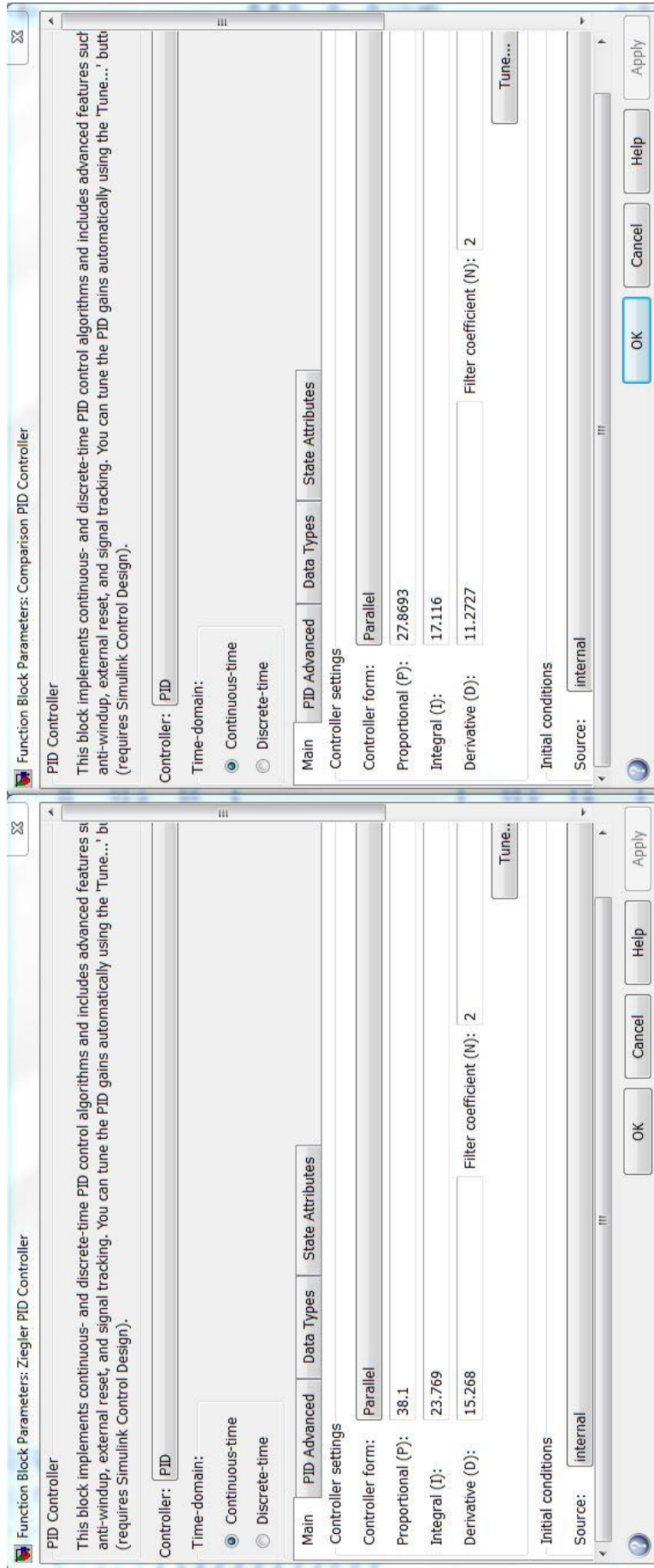
Appendix J- Matlab ACSYS PID bode design



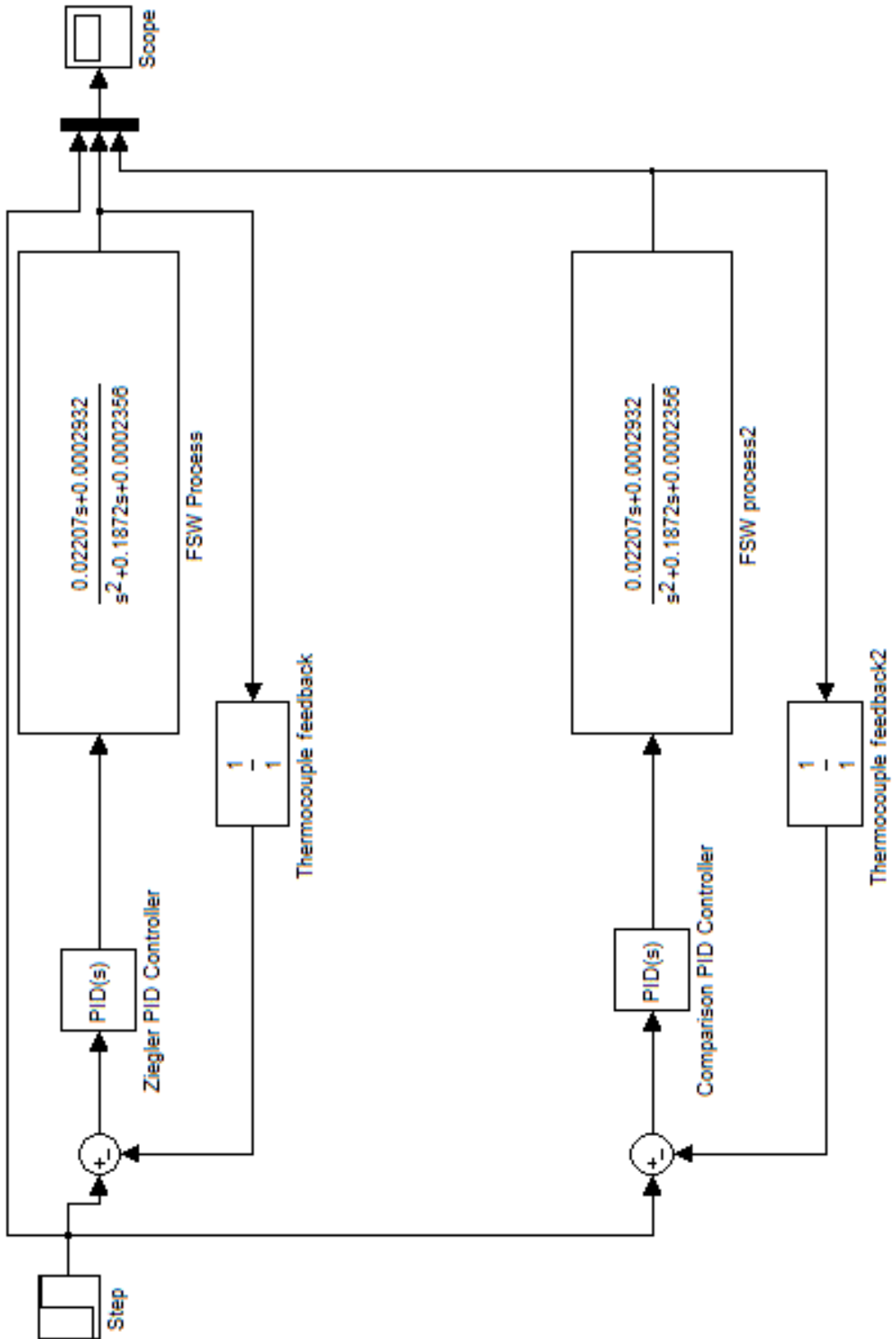
Appendix J- Matlab ACSYS PID bode design

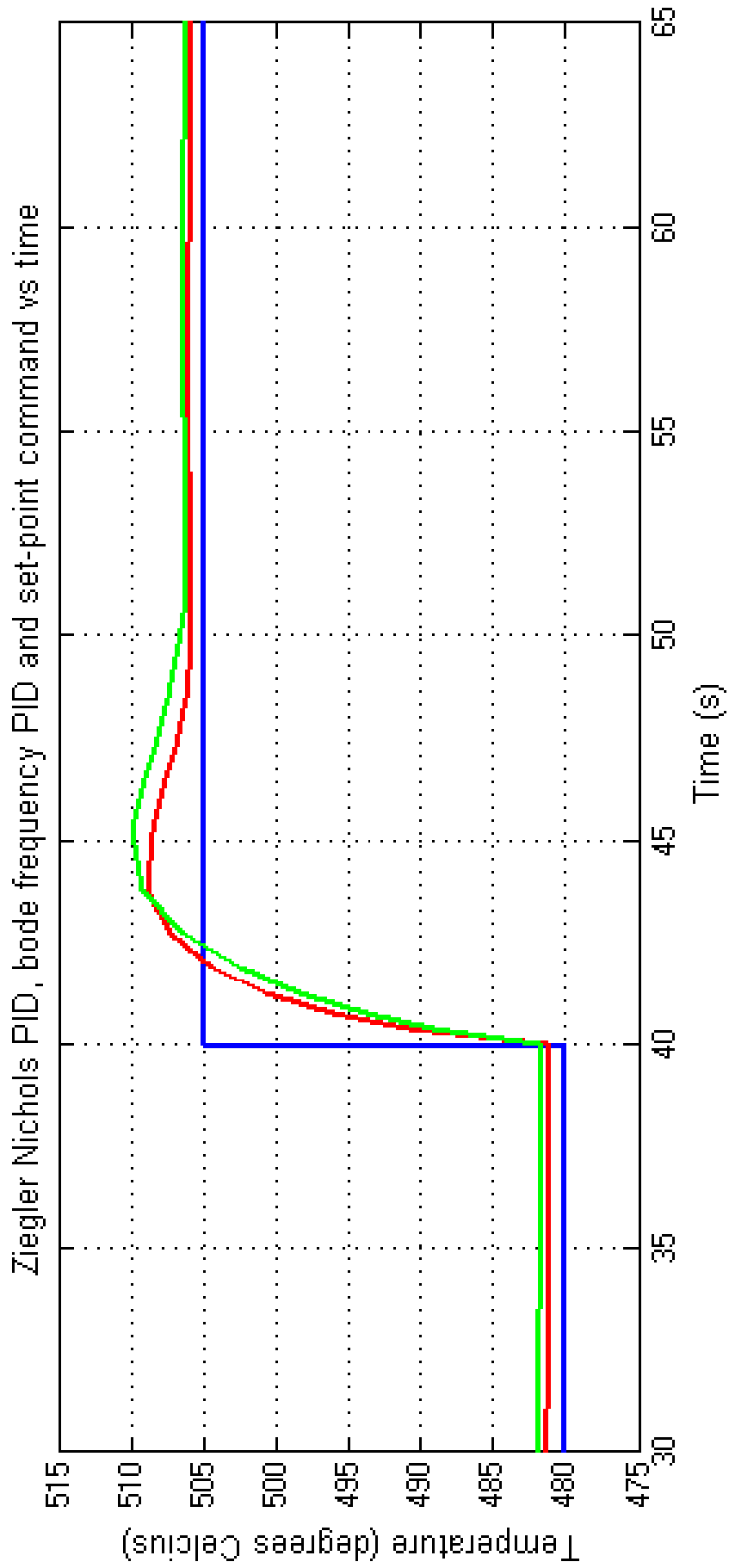


Appendix J- Matlab ACSYS PID bode design

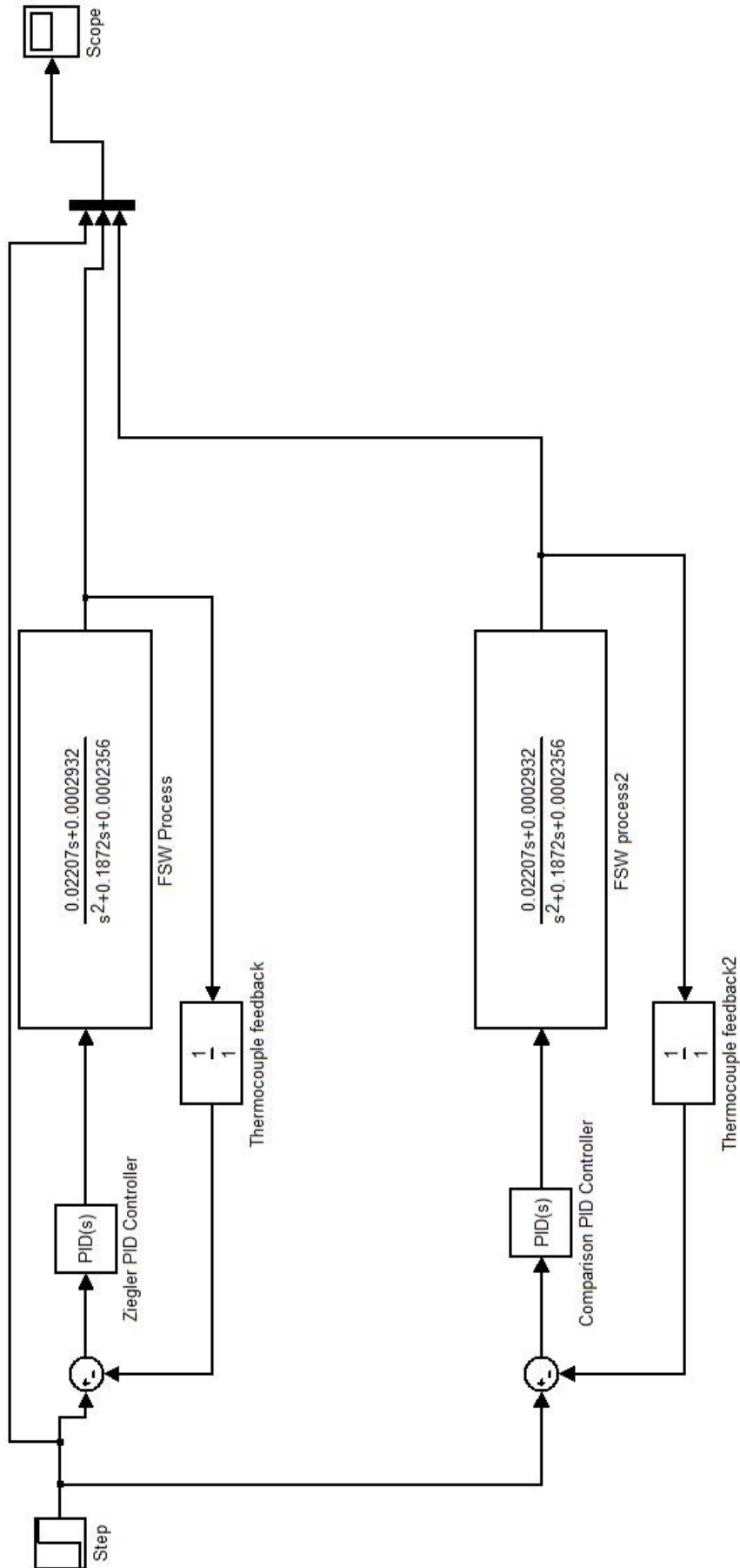


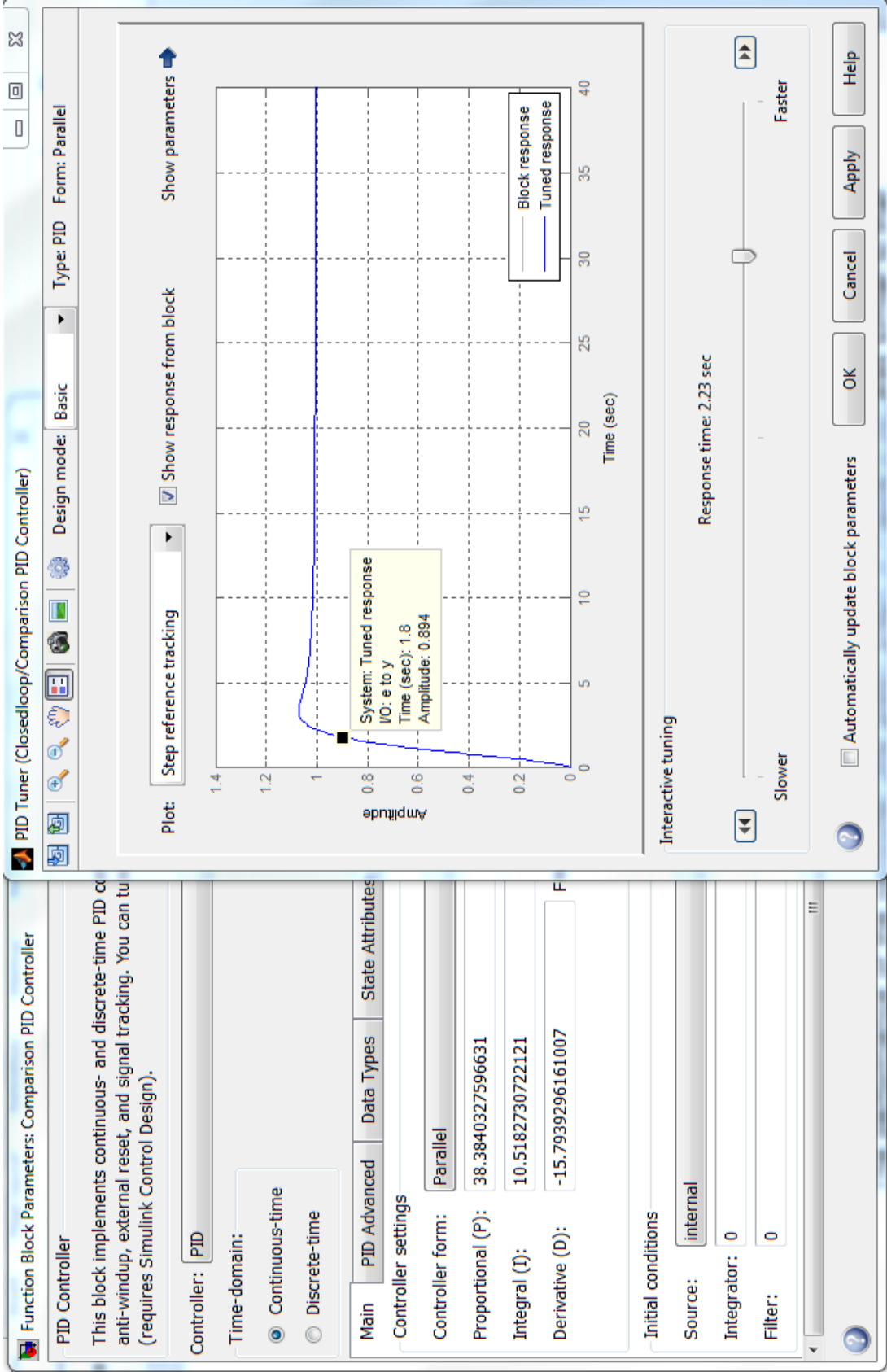
Appendix J- Matlab ACSYS PID bode design



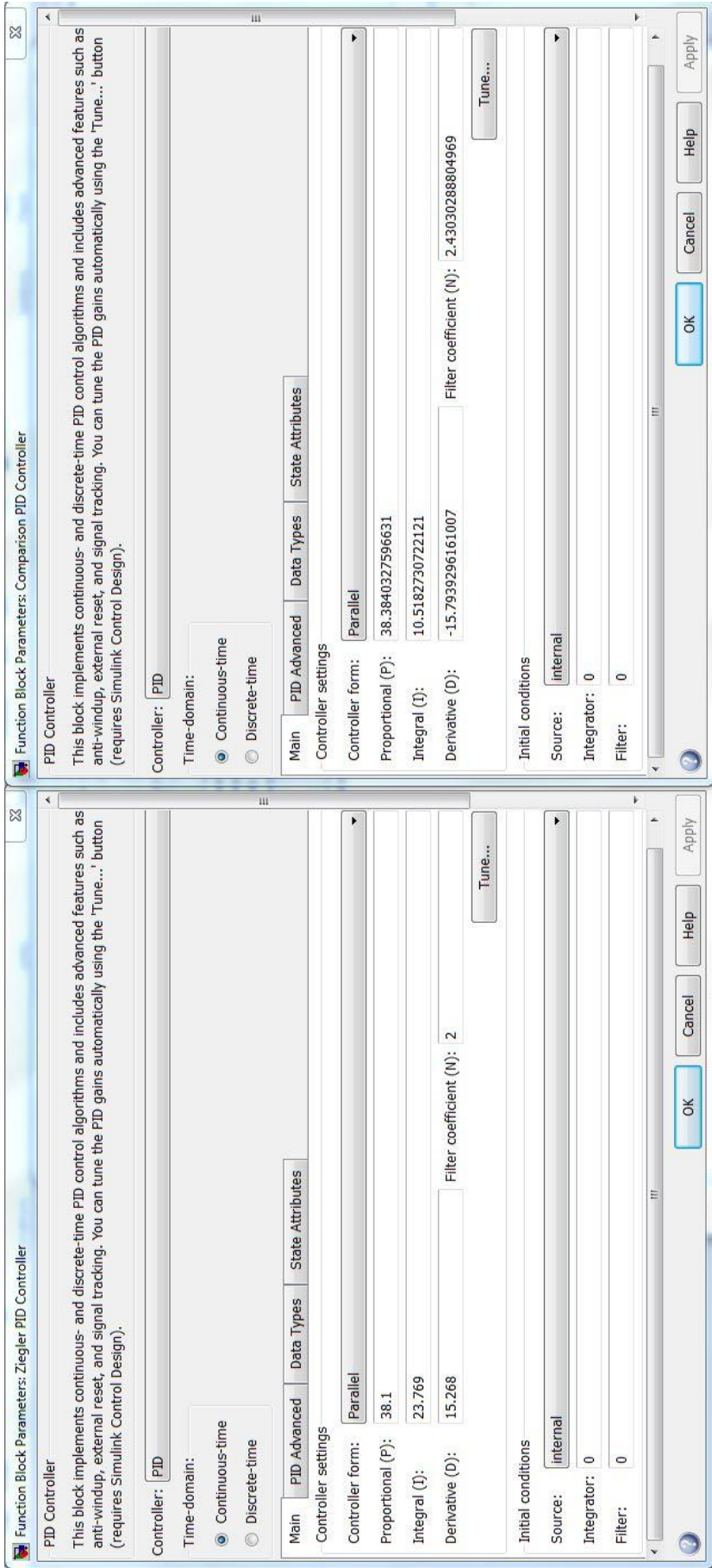


Appendix K- Matlab Simulink PID tune

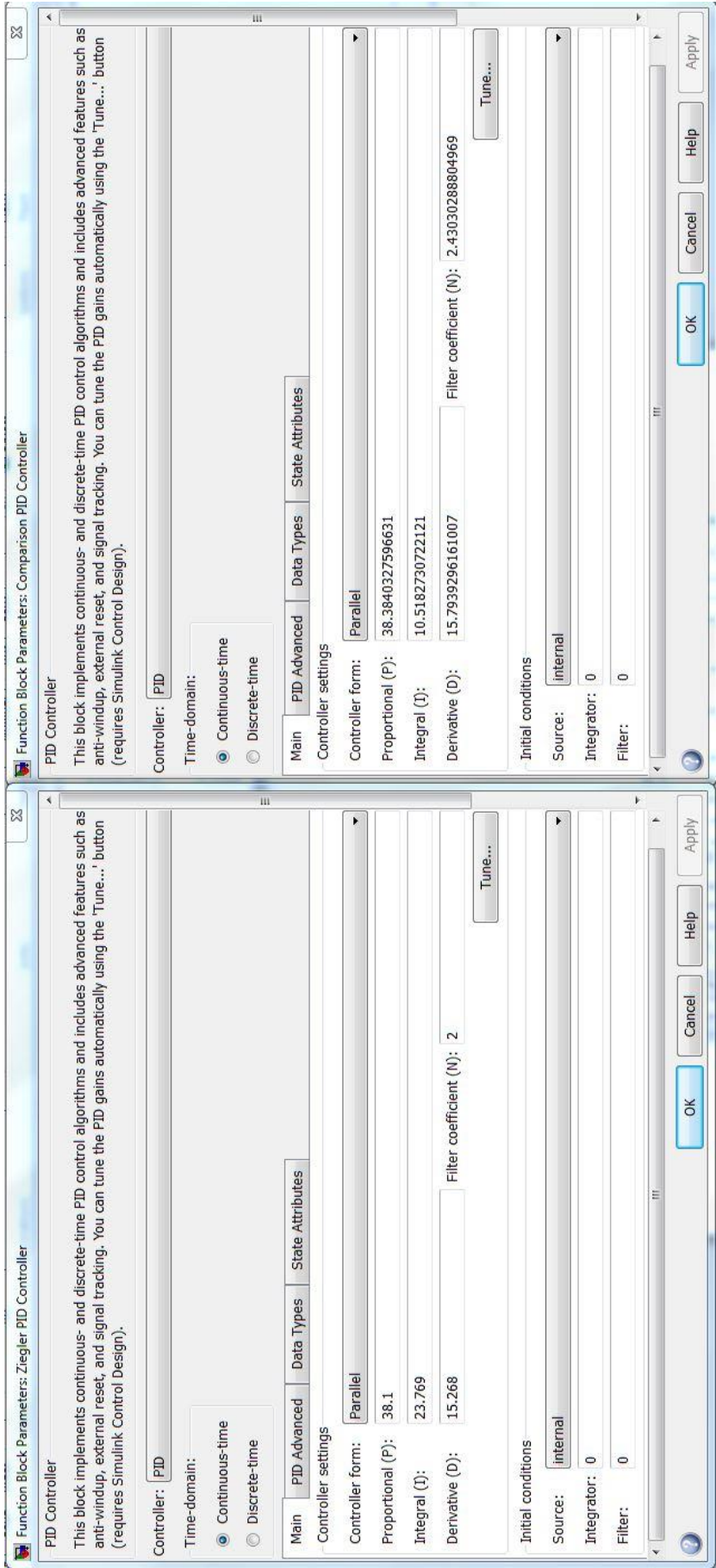


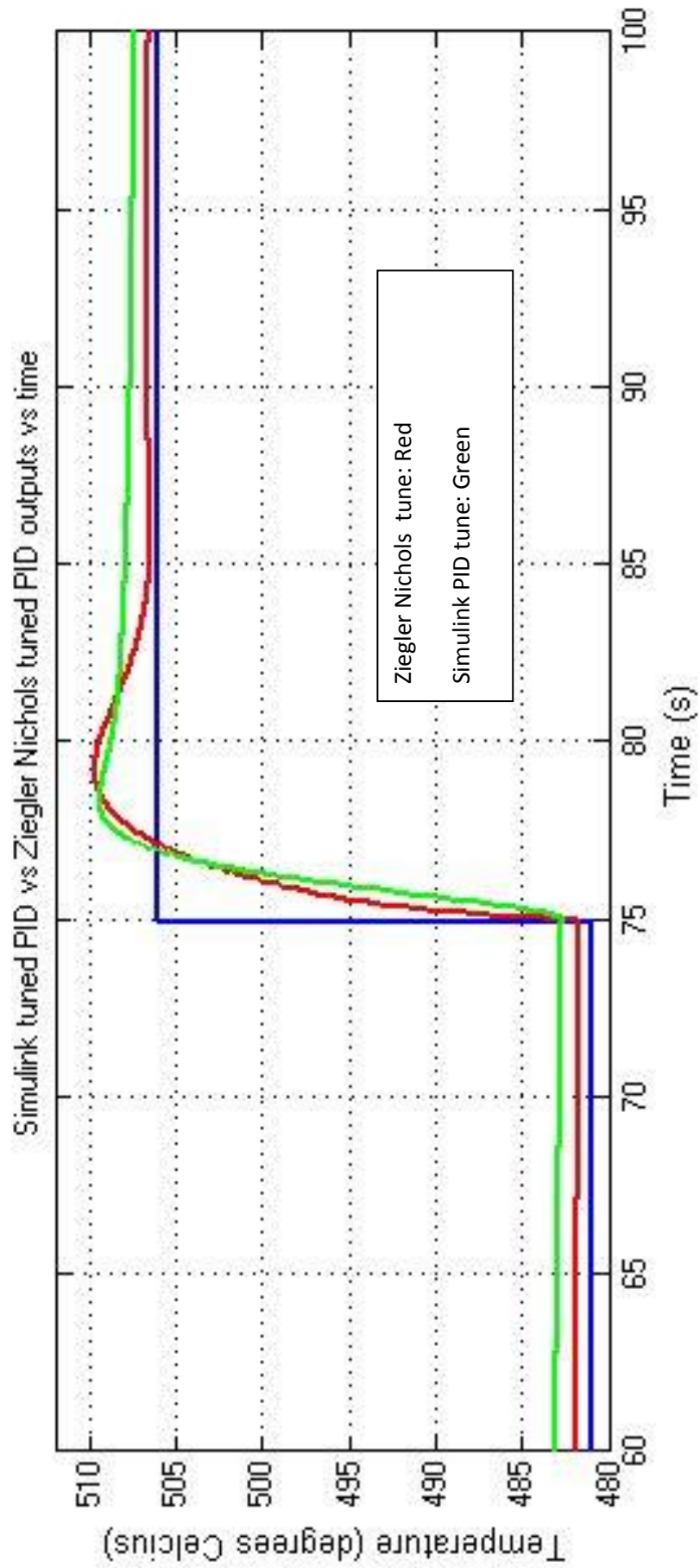


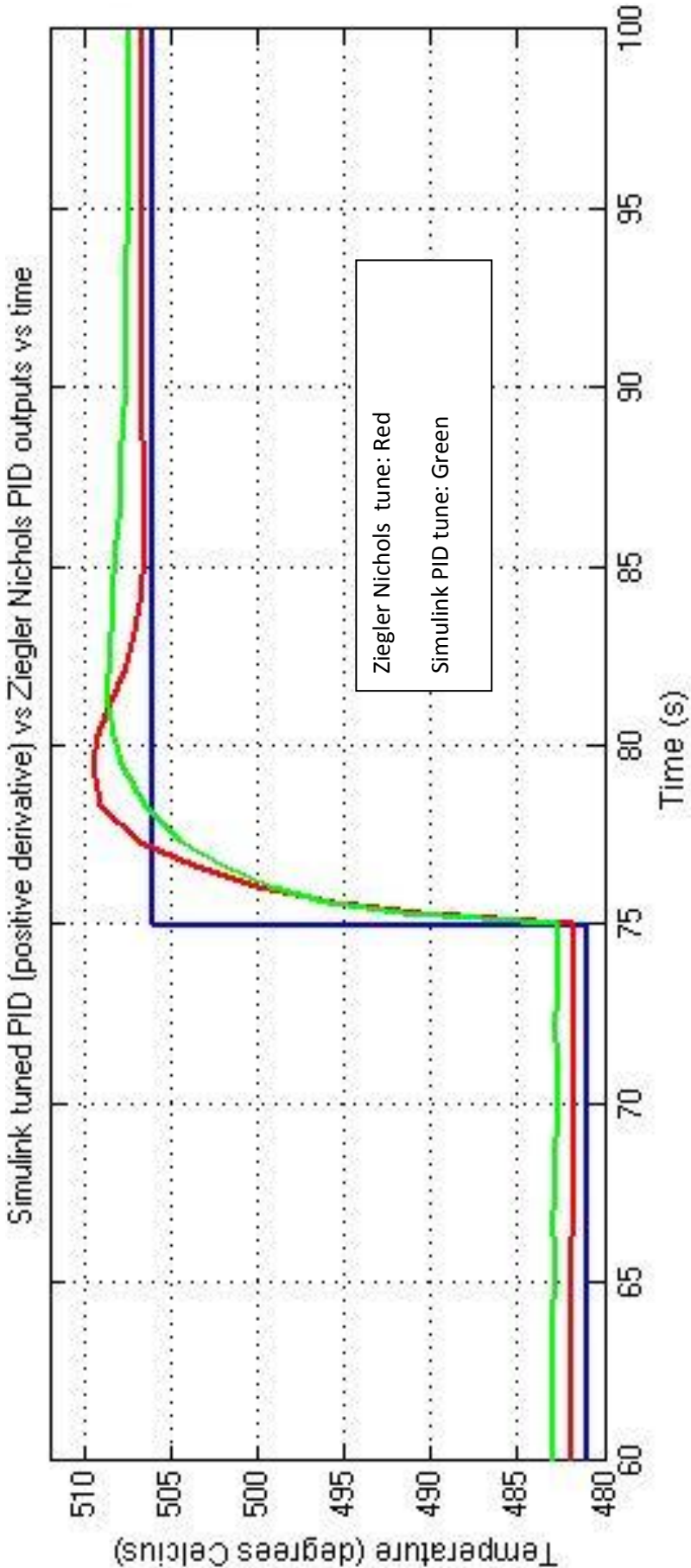
Appendix K- Matlab Simulink PID tune



Appendix K- Matlab Simulink PID tune







Appendix L- Statistical t-tests

t tests (comparing 4.1 and 4.2)					
yield 1			yield 2		
t-Test: Two-Sample Assuming Equal Variances			t-Test: Two-Sample Assuming Equal Variances		
	<i>Variable 1</i>	<i>Variable 2</i>		<i>Variable 1</i>	<i>Variable 2</i>
Mean	146.69	142.553	Mean	146.733	150.274
Variance	0.53975	3.38641	Variance	24.8612	0.740383
Observations	3	3	Observations	3	3
Pooled Variance	1.96308		Pooled Variance	12.8008	
Hypothesized Mean Difference	0		Hypothesized Mean Difference	0	
df	4		df	4	
t Stat	3.6157		t Stat	-1.21225	
P(T<=t) one-tail	0.01122		P(T<=t) one-tail	0.14606	
t Critical one-tail	2.13185		t Critical one-tail	2.13185	
P(T<=t) two-tail	0.02244		P(T<=t) two-tail	0.29212	
t Critical two-tail	2.77645		t Critical two-tail	2.77645	
yield 3			yield 4		
t-Test: Two-Sample Assuming Equal Variances			t-Test: Two-Sample Assuming Equal Variances		
	<i>Variable 1</i>	<i>Variable 2</i>		<i>Variable 1</i>	<i>Variable 2</i>
Mean	145.871	149.331	Mean	141.1	147.7887
Variance	1.78094	3.83269	Variance	3.23882	2.19835
Observations	3	3	Observations	3	3
Pooled Variance	2.80682		Pooled Variance	2.71859	
Hypothesized Mean Difference	0		Hypothesized Mean Difference	0	
df	4		df	4	
t Stat	-2.52963		t Stat	-4.96861	
P(T<=t) one-tail	0.03235		P(T<=t) one-tail	0.00383	
t Critical one-tail	2.13185		t Critical one-tail	2.13185	
P(T<=t) two-tail	0.06469		P(T<=t) two-tail	0.00766	
t Critical two-tail	2.77645		t Critical two-tail	2.77645	

Appendix L- Statistical t-tests

ultimate 1			ultimate 2		
t-Test: Two-Sample Assuming Equal Variances			t-Test: Two-Sample Assuming Equal Variances		
	<i>Variable 1</i>	<i>Variable 2</i>		<i>Variable 1</i>	<i>Variable 2</i>
Mean	232.03	230.13	Mean	232.52	234.24
Variance	7.1559	2.7004	Variance	11.5371	0.2677
Observations	3	3	Observations	3	3
Pooled Variance	4.92815		Pooled Variance	5.9024	
Hypothesized Mean Difference	0		Hypothesized Mean Difference	0	
df	4		df	4	
t Stat	1.04823		t Stat	-0.86708	
P(T<=t) one-tail	0.17684		P(T<=t) one-tail	0.21741	
t Critical one-tail	2.13185		t Critical one-tail	2.13185	
P(T<=t) two-tail	0.35369		P(T<=t) two-tail	0.43482	
t Critical two-tail	2.77645		t Critical two-tail	2.77645	
ultimate 3			ultimate 4		
t-Test: Two-Sample Assuming Equal Variances			t-Test: Two-Sample Assuming Equal Variances		
	<i>Variable 1</i>	<i>Variable 2</i>		<i>Variable 1</i>	<i>Variable 2</i>
Mean	230.273	234.95	Mean	227.707	230.8367
Variance	0.78703	0.3469	Variance	1.13013	3.494433
Observations	3	3	Observations	3	3
Pooled Variance	0.56697		Pooled Variance	2.31228	
Hypothesized Mean Difference	0		Hypothesized Mean Difference	0	
df	4		df	4	
t Stat	-7.60682		t Stat	-2.52098	
P(T<=t) one-tail	0.0008		P(T<=t) one-tail	0.03264	
t Critical one-tail	2.13185		t Critical one-tail	2.13185	
P(T<=t) two-tail	0.0016		P(T<=t) two-tail	0.06529	
t Critical two-tail	2.77645		t Critical two-tail	2.77645	

Appendix L- Statistical t-tests

t-Test: Two-Sample Assuming Equal Variances

	<i>standard deviations of 4.1 yield</i>	<i>standard deviations of 4.2 yield</i>
Mean	3.070942735	3.670922025
Variance	2.091544868	0.71287331
Observations	3	3
Pooled Variance	1.402209089	
Hypothesized Mean Difference	0	
df	4	
t Stat	-0.620548172	
P(T<=t) one-tail	0.284252603	
t Critical one-tail	2.131846786	
P(T<=t) two-tail	0.568505207	
t Critical two-tail	2.776445105	

t-Test: Two-Sample Assuming Equal Variances

	<i>standard deviations of 4.1 ultimate</i>	<i>standard deviations of 4.2 ultimate</i>
Mean	2.22301058	2.679940826
Variance	2.59746511	0.036621591
Observations	3	3
Pooled Variance	1.31704335	
Hypothesized Mean Difference	0	
df	4	
t Stat	-0.487635709	
P(T<=t) one-tail	0.32566394	
t Critical one-tail	2.131846786	
P(T<=t) two-tail	0.65132788	
t Critical two-tail	2.776445105	
